Puerto Rawson

Sustainable Port Expansion: Conceptual Design and Coastal Impact Analysis

CEGM3000: Multidisciplinary Project

MDP366



Delft University of Technology

TU Delft

Puerto Rawson

Sustainable Port Expansion: Conceptual Design and Coastal Impact Analysis

by

MDP366

Student Name	Student Number
Jeroen van Dulst	4856163
Julian van Elderen	4770951
Michiel Hendriks	4909364
Jessy Luijpers	4934199
Sjoerd van der Lugt	4921763
Thomas Neesen	5170508

Supervisor	Dr. Asst. Prof. J.A. Álvarez Antolínez
Supervisor	Ir. S.R. Iglesias
Supervisor	Ir. P. Arecco
Supervisor	Prof.dr.ir. E. Schlangen
Supervisor	Dr. Asst. Prof. H. Hendrikse
Project Duration:	September, 2024 - November, 2024
Faculty:	Faculty of Civil Engineering and Geosciences, Delft

Cover: Aerial picture of Playa Unión taken by Rodrigo Bastida Arias

TU Delft

Abstract

The erosion problem along Playá Union presents significant challenges for future port expansion at Puerto Rawson. This research seeks to address the question of *how to achieve a sustainable and durable port expansion, while minimizing environmental impacts, particularly concerning sediment imbalance along the coastline?*

Using 30 years of wave data, both normal and extreme wave conditions are simulated with SWAN, a numerical based wave model. Conceptual port expansion designs are developed, resulting in a final design with an integrated fully dimensioned breakwater. Based on visual inspections, data, and research, a new cement mixture is proposed for the breakwater armour units. A Life Cycle Assessment evaluates the environmental impact, while the effect on alongshore sediment transport is assessed using the SWAN model outcomes and the CERC formula.

Visual inspection of the current breakwaters lead to a 6.3% reduction in material use in the new breakwater through reuse of armour units. Furthermore, the proposed cement mixture integrates porphyry quarry waste as the coarse aggregate, a choice also supported by prior research in sustainability. With the new End-of-Life approaches added, the total shadow costs are reduced by 22%. The hydrodynamical analysis and model result in extreme wave heights up to 3.98 m at the toe of the breakwater. By applying a neural network and a k-means algorithm on the wave data, five regular wave conditions are run in the SWAN model. The alongshore sediment transport is impacted by new breakwater concepts. Relying solely on the breakwater layout to counteract erosion north of the port, however, does not prove to be a viable approach. Based on design criteria and aspirations, the final conceptual design proposes the removal of the existing southern breakwater, while retaining sufficient space for future port expansion. The breakwater, integrated in the final design, is dimensioned based on standard design principles.

To conclude, the data and model provide valuable insights into the coastal dynamics around Puerto Rawson. The proposed concrete mixture, along with the End-of-Life solutions, minimize environmental impact and enhance durability of the armour units. The sustainable breakwater design, effectively integrated into Puerto Rawson, accommodates for future port expansions.

Preface

This report presents the outcomes of a multidisciplinary project, carried out by a group of six students from Delft University of Technology. Over the past ten weeks, we have deeply engaged with the project, gaining substantial knowledge and practical insight into the fields of port, coastal, and sustainable engineering. This report is aimed at readers interested in innovative approaches to coastal management and port expansion.

As part of our second-year master's program, we were given the opportunity to undertake an international project. Bringing together our diverse expertise across several Civil Engineering disciplines; Structural Engineering, Hydraulic Engineering, and Hydraulic and Offshore Structures. The project was conducted in collaboration with the Facultad de Ingeniería of Universidad de Buenos Aires (UBA FIUBA).

The support of Pablo Arecco and Sebastián Iglesias, who warmly welcomed us to work on this challenging project in Argentina was essential. With their help, we connected with Centro Argentino de Ingenieros (CAI), and Universidad Nacional de la Patagonia San Juan Bosco (UNPSJB), who generously provided us with a workspace. After months of preparation, we are pleased to present the final report of our research.

Special thanks are due to our supervisors José Antolinez, Hayo Hendrikse, Erik Schlangen, Sebastián Iglesias, and Pablo Arecco. Their invaluable guidance, insight, and encouragement enabled the project to progress substantially. We are also grateful to our professional advisors, Ramiro de Gracia, Ramiro Amor Grassi, and Bruno Maggiolo, for their insightful feedback and expertise during project meetings. We also extend our thanks to experts Henk Jonkers, Gozde Ozerkan, Leda Cotti, Hugo Donini, and Gabriel Kaless, whose knowledge and support significantly enriched our work. Last but certainly not least our appreciation goes to Rodrigo Bastida Arias, Leandro Foletto, and Cynthia Gélvez, of the Puerto Rawson Port Directorate, who provided essential data and guided us through the port facilities.

We are equally thankful to our friends in Buenos Aires and Trelew who introduced us to Argentine culture and shared memorable moments with us. Special mentions go to Ramiro de Gracia, Diego Walker, Fernando Iglesias, Alfredo Ychardo, Valentin Vidal, and their families for their kindness and hospitality.

Finally, this project would not have been possible without financial support from the TU Delft FAST Fund and the Hydraulic Department's Lamminga Fund. Their generous funding allowed us to pursue this unique and rewarding experience abroad.

We hope this report contributes to meaningful insights into the fields of coastal- and port engineering and reflects the collaborative efforts and shared expertise that made this project possible.

MDP366
Buenos Aires, November 2024

Disclaimer

This report has been made by master students in Civil Engineering at Delft University of Technology as part of their academic coursework. It presents student-level research of the given case study and reflects their understanding and application of modelling, analysis, and design principles, taught during their studies. While every effort has been made to ensure the accuracy and thoroughness of the methodologies applied, it should be noted that calculations, assumptions, and conclusions herein were made with limited resources, time constraints, and access to data, all within an educational setting.

This report and its findings are intended solely for educational purposes. It is not meant to serve as a professional reference or to be directly applied in real-world engineering, construction, or design projects without thorough validation by experienced practitioners. The authors, supervisors, and involved universities, do not assume any responsibility or liability for actions taken or decisions made based on the contents of the document.

Contents

Abstract i

Preface ii

Disclaimer iii

Nomenclature xv

1 Introduction 1

2 Methodology 3
2.1 Overall methodology . . . 3
2.2 Dimensioning of breakwater within conceptual design . . . 4
2.3 Hydraulic conditions analysis and modelling . . . 5
2.4 Concrete analysis and quantification . . . 6

3 Site study 7
3.1 Site description . . . 7
3.1.1 Site introduction . . . 7
3.1.2 Erosion and sedimentation issues . . . 8
3.1.3 Port expansion ambitions . . . 10
3.1.4 Restinga . . . 10
3.2 Current state of breakwaters . . . 10
3.2.1 Visual inspection . . . 10
3.2.2 Visual inspection results . . . 12
3.2.3 End-of-Life methods and visual inspection conclusions . . . 14

4 Analysis 16
4.1 Design analysis . . . 16
4.1.1 Return Period . . . 16
4.1.2 Classification of breakwater . . . 17
4.1.3 Failure mechanisms . . . 17
4.2 Hydrodynamical analysis . . . 19
4.2.1 General information data . . . 19
4.2.2 Wind analysis . . . 20
4.2.3 Wave analysis . . . 20
4.2.4 Extreme value analysis . . . 22
4.2.5 Water level analysis . . . 23
4.3 Self-Organizing Maps for regular conditions . . . 24
4.3.1 Neural network (n=400) . . . 24
4.3.2 K-means (k=12) . . . 25
4.4 Structural analysis . . . 26
4.4.1 Structural technical reports . . . 26
4.4.2 Initial specifications . . . 26
4.4.3 Rebound number tests . . . 27
4.4.4 New cement mixture . . . 29

5 Wave model and sediment transport 30
5.1 Model type . . . 30
5.2 From site to model . . . 31
5.2.1 Bathymetry . . . 31
5.2.2 Coarse and fine grid . . . 32

5.3 Model configurations . . . 33
5.3.1 Normal conditions . . . 33
5.3.2 Extreme conditions . . . 33
5.4 Output parameters . . . 33
5.4.1 Wave transformations . . . 33
5.4.2 Sediment transport formulation . . . 34
5.5 Reference runs . . . 35
5.5.1 Wave transformation . . . 35
5.5.2 Sediment transport . . . 36

6 Conceptual port expansion designs 38
6.1 Design objectives . . . 38
6.1.1 Design criteria . . . 38
6.1.2 Design aspirations . . . 39
6.2 Conceptual designs . . . 40
6.2.1 Supplementary conceptual designs . . . 40
6.2.2 Final design . . . 41

7 Results 44
7.1 Bathymetry near port . . . 44
7.2 Normal conditions . . . 45
7.2.1 Wave transformation . . . 45
7.2.2 Sediment transport . . . 45
7.3 Extreme conditions . . . 49

8 Dimensioning of breakwater 50
8.1 Sections . . . 51
8.2 Armour layer . . . 52
8.2.1 The Accropode II unit . . . 52
8.2.2 Dimensioning the armour unit . . . 53
8.3 Core and underlayer . . . 54
8.3.1 Core layer . . . 54
8.3.2 Underlayer . . . 54
8.3.3 Erosion, stability, and permeability checks . . . 55
8.4 Toe Dimensioning . . . 56
8.5 Crest dimensions . . . 57
8.6 Rear-side stability . . . 58
8.7 Breakwater roundhead . . . 59
8.8 Technical drawings . . . 59
8.9 Cement mixture comparison and proposal . . . 61
8.10 Concrete quantification . . . 62
8.10.1 Concrete volume determination . . . 62
8.10.2 Quantification of the current Accropodes . . . 62
8.10.3 Quantification of the new Accropodes . . . 63

9 Concrete sustainability 64
9.1 Goal definition . . . 64
9.2 Scope definition . . . 64
9.3 Interpretation . . . 66

10 Discussion 68
10.1 Feasibility . . . 68
10.2 Uncertainties . . . 69
10.2.1 Data . . . 69
10.2.2 Wave model and sediment transport . . . 69
10.2.3 Conceptual design . . . 70
10.2.4 Concrete . . . 71

11 Conclusion 72

12 Recommendations **74**

References **75**

Appendices **79**

A Visual inspection photos **80**
A.1 Accropodes: reference unit . . . 81
A.2 Accropodes: on the breakwater . . . 81

B Concrete volume determination **88**

C Visual inspection results **91**

D Failure mechanisms **94**

E Data analysis **97**
E.1 Wind analysis . . . 97
E.1.1 General . . . 98
E.1.2 Trend . . . 99
E.1.3 Seasonal . . . 99
E.2 Wave analysis . . . 100
E.2.1 Statistics . . . 100
E.2.2 Timeseries . . . 100
E.2.3 Waveroses . . . 101
E.2.4 Trends . . . 102
E.2.5 Seasons . . . 102
E.2.6 T_p analysis . . . 103
E.2.7 Wave vs wind direction . . . 104
E.3 Extreme Value Analysis . . . 105
E.3.1 General . . . 105
E.3.2 Peak over threshold (SWH, SHWW, SHTS) . . . 105
E.3.3 EVA (SWH) . . . 107
E.4 Self-Organizing Maps (SOM) . . . 109
E.4.1 Neural Network (*n* = 400) . . . 109
E.4.2 K-means (*k* = 12) . . . 111

F Proposed cement mixture studies **113**

G Initial cement mixture studies **117**

H Original granulometry **119**

I Rebound number test results **124**

J Wave model and sediment transport - extra information **125**
J.1 Model types and SWAN . . . 125
J.2 Boundary conditions . . . 126
J.3 Model configuration - extended . . . 126
J.3.1 Normal conditions - extended . . . 126
J.3.2 Extreme conditions - extended . . . 127
J.3.3 Other settings . . . 127
J.4 Sediment transport application . . . 128

K Results normal conditions **129**
K.1 Wave transformations . . . 129
K.1.1 Reference situation . . . 130
K.1.2 Concept 1 . . . 131
K.1.3 Concept 2 . . . 132
K.1.4 Concept 3 . . . 133
K.2 Longshore sediment transport . . . 133

L Results extreme conditions **135**
L.1 Wave transformations 135
L.2 Near port wave height results 136

M Dimensions of Accropodes **138**

N Supplementary conceptual designs **139**
N.1 Conceptual design 1 139
N.2 Conceptual design 2 141

O Accroberm II toe unit **143**

P Mix design proportions **144**

Q Life Cycle Assessment **145**
Q.1 Life Cycle Inventory Analysis 145
Q.2 Life Cycle Impact Assessment 150

List of Figures

2.1 Flowchart of the overall methodology . . . 3
2.2 Flow chart for the methodology of dimensioning breakwater in conceptual port expansion design. . . . 4
2.3 Flow chart of the methodology for analysis and modelling of hydraulic conditions . . . 5
2.4 Flow chart of the methodology for concrete analysis and quantification . . . 6

3.1 Location of Port of Rawson and Playa Unión [30]. . . . 8
3.2 Terminology and layout of Puerto Rawson and Playa Unión [30]. . . . 9
3.3 Aerial view of affected coast at Playa Unión [22]. . . . 9
3.4 Old southern breakwater at low water level. Several Akmon units are missing. . . . 11
3.5 Schematic 3D representation of an Akmon armour unit [51]. . . . 11
3.6 Schematic 3D representation of an Accropode armour unit [51]. . . . 11
3.7 Cross-section of the new southern breakwater, divided into three zone. Zone A: green zone, or crown zone; Zone B: yellow zone, or splash zone; Zone C: red zone, or submerged zone. Cross-section from the Port Directorate [62] . . . 12
3.8 Exposed pebble aggregate on an Accropode, after a corner piece has crumbled off. . . . 13

4.1 Schematic overview of rubble mound breakwater cross-section. [65] . . . 17
4.2 Locations of data sources from recent studies/current study . . . 19
4.3 Timeseries of w_{10} over 30 years, featuring the mean and 1000-point moving average. . 20
4.4 Windrose illustrating wind speed, direction, and frequency . . . 20
4.5 Timeseries of SWH over 30 years, featuring the mean and 1000-point moving average. 21
4.6 Plot of SWH over direction (θ_{waves}) the wave originate from, using the ERA5-data. . . . 21
4.7 Waveroses for SWH (a), SHWW (b), and SHTS (c) derived from ERA5-data (1993-2023). Each waverose illustrates the wave height, wave direction and frequency. . . . 21
4.8 Timeseries of SWH. The POT method identified extreme events, indicated in the figure. The threshold is 4.10 m and the declustering time is 12 hours. . . . 22
4.9 Return period plot of SWH, showing data and the fitted GPD curve with a 95 % confidence interval. This illustrates the SWH values associated with RT. . . . 22
4.10 SLR change in water level under different scenarios, near Rawson [49] . . . 23
4.11 Self-Organizing Map (SOM) representing 378 wave conditions analysed through a neural network. Each cell illustrates the relationship between H_s, T_p, θ, and frequency (*f*). Colour gradients indicate the respective values of H_s, *f*, and T_p, allowing for a visual interpretation of the clustering and distribution of wave conditions. . . . 24
4.12 Scatter plots for each combination of variables (H_s, T_p, θ). The 12 clusters are illustrated with squares, with all neurons belonging to a cluster coloured identically. . . . 25
4.13 Self-Organizing Map (SOM) representing 12 wave conditions analysed through k-means. Each cell illustrates the relationship between H_s, T_p, θ, and frequency (*f*). Colour gradients indicate the respective values of H_s, *f*, and T_p, allowing for a visual interpretation of the clustering and distribution of wave conditions. . . . 25
4.14 Current granulometry. There are 64 thin coloured lines, each representing a sample. The thick blue lines represent the boundaries of the design areas [15]. The dark blue and light blue areas respectively represent the design areas I and II, in which a cement mixture is optimally designed for workability and water requirements. . . . 27
4.15 A sclerometer. . . . 28
4.16 Test positions on an Accropode, schematic [51]. . . . 28
4.17 Granulometry of Mrs. Cotti's mixture. The red line represents the mixture, whereas the dark- and light blue areas again represent the design areas, as stated in the Betonpocket [15]. . . . 29

5.1 Survey points from 2010 and 2014 at Puerto Rawson 31
5.2 Created bathymetry of the area 32
5.3 Significant wave height transformation under normal conditions setting 1 for the reference situation. I) The large coarse grid; II) The small fine grid near the port 35
5.4 Bulk alongshore sediment volumes for each segment in all settings in the reference situation. Added with the calculated factorized sediment volume according to the frequency of retrieved normal conditions. 36
5.5 Reference situation longshore sediment transport gradients between cross-sections, blue indicates sedimentation, red erosion. I) Satellite image of the coastline of Puerto Rawson, north on the right [30]; II) The automatically defined coastline with colour gradients of erosion/sedimentation, north on the right III); The magnitudes of longshore sediment transport Q_s in m^3/s in the cross-sections with colour gradients of erosion/sedimentation 37

6.1 Schematisation of the supplementary conceptual designs and their important lay-out dimensions; left: *conceptual design 1*; right: *conceptual design 2* 41
6.2 Schematic drawing of *conceptual design 3* 42

7.1 SWAN input bathymetry for the reference and the three designs concepts in own coordinate system. I) Large and small input grid visualized, as well as zoomed view grid on the port; II) Input bathymetry view on port in reference situation; III) Input bathymetry view on port for concept 1; IV) Input bathymetry view on port for concept 2; V) Input bathymetry view on port for concept 1 44
7.2 Concept 1: longshore sediment transport gradients between cross-sections, blue indicates sedimentation, red erosion. I) Satellite image of the coastline of Puerto Rawson, with BW orientation, north on the right [30]; II) The automatically defined coastline with colour gradients of erosion/sedimentation, north on the right; III) The magnitudes of longshore sediment transport Q_s in m^3/s in the cross-sections with colour gradients of erosion/sedimentation 46
7.3 Concept 2: longshore sediment transport gradients between cross-sections, blue indicates sedimentation, red erosion. I) Satellite image of the coastline of Puerto Rawson, with BW orientation, north on the right [30]; II) The automatically defined coastline with colour gradients of erosion/sedimentation, north on the right; III) The magnitudes of longshore sediment transport Q_s in m^3/s in the cross-sections with colour gradients of erosion/sedimentation 47
7.4 Concept 3: longshore sediment transport gradients between cross-sections, blue indicates sedimentation, red erosion. I) Satellite image of the coastline of Puerto Rawson, with BW orientation, north on the right [30]; II) The automatically defined coastline with colour gradients of erosion/sedimentation, north on the right; III) The magnitudes of longshore sediment transport Q_s in m^3/s in the cross-sections with colour gradients of erosion/sedimentation 48

8.1 Cross-section schematization of a rubble mound breakwater with the dimensions parameters; B = crest width; B_{core} = core width; R_c = crest height; h_t = seaward toe level; h_l = leeward shoulder level; α = slope angle; t_a = armour layer thickness; t_u = underlayer thickness; B_t = seaward toe width; S_s = seaward shoulder width; S_l = leeward shoulder width. [65] 50
8.2 Locations A, B, and C for the cross-sections 51
8.3 Bathymetry along crest length of breakwater; specified: cross-sectional locations along breakwater 52
8.4 Three technical drawing of cross-section along designed breakwater at locations marked in Figure 8.2. I) Cross section at location A; II) Cross section at location B; III) Cross section at location C 60

9.1 Total shadow costs of the three main stages of the LCA, visualised. The x-axis represents the costs in Euros, in millions. 66
9.2 Shadow costs of the aggregates and EoL only, visualised. The x-axis represents the costs in Euros, in millions. 67

A.1 Drawing of the new northern breakwater. The numbers denote the locations of where the photos were taken. The diagonally striped area is covered by Accropodes [62]. . . . 80
A.2 Photo of reference unit - 1 . . . 81
A.3 Photo of reference unit - 2 . . . 81
A.4 Photo of reference unit - 3 . . . 81
A.5 Photo of reference unit - 4 . . . 81
A.6 Photo of unit A0 . . . 81
A.7 Photo of unit A40 - 1 . . . 81
A.8 Photo of unit A40 - 2 . . . 82
A.9 Photo of unit A80 - 1 . . . 82
A.10 Photo of unit A80 - 2 . . . 82
A.11 Photo of unit A120 - 1 . . . 82
A.12 Photo of unit A120 - 2 . . . 82
A.13 Photo of unit A160 - 1 . . . 82
A.14 Photo of unit A160 - 2 . . . 83
A.15 Photo of unit A218 - N . . . 83
A.16 Photo of unit A218 - S - 1 . . . 83
A.17 Photo of unit A218 - S - 2 . . . 83
A.18 Photo of unit A218 - S - 3 . . . 83
A.19 Photo of unit A221 . . . 83
A.20 Photo of unit B0 . . . 84
A.21 Photo of unit B40 - 1 . . . 84
A.22 Photo of unit B40 - 2 . . . 84
A.23 Photo of unit B80 - 1 . . . 84
A.24 Photo of unit B80 - 2 . . . 84
A.25 Photo of unit B120 . . . 84
A.26 Photo of unit B160 - 1 . . . 85
A.27 Photo of unit B160 - 2 . . . 85
A.28 Photo of unit B218 - N . . . 85
A.29 Photo of unit B218 - S . . . 85
A.30 Photo of unit B221 . . . 85
A.31 Photo of unit C0 . . . 85
A.32 Photo of unit C40 . . . 86
A.33 Photo of unit C80 - 1 . . . 86
A.34 Photo of unit C80 - 2 . . . 86
A.35 Photo of unit C120 . . . 86
A.36 Photo of unit C160 . . . 86
A.37 Photo of unit C218 - N . . . 86
A.38 Photo of unit C218 - S . . . 87
A.39 Photo of unit C221 - 1 . . . 87
A.40 Photo of unit C221 - 2 . . . 87

B.1 Division of the New Southern breakwater. The light green, light blue, and light orange areas respectively denote the northern, centre, and southern strips. The dashed lines denote boundaries between sections, where each section employs another type of Accropode. . . . 89
B.2 Division of the northern breakwater. . . . 89
B.3 New Southern breakwater - zone division . . . 90

C.1 Illustration of damage results of new northern breakwater . . . 92
C.2 Illustration of damage results of new norhtern breakwater - head . . . 92

E.1 Wind data analysis with (a) timeseries wind and (b) wind magnitude over direction. . . . 98
E.2 Windrose . . . 98
E.3 Windroses Seasons . . . 99
E.4 Wave data analysis with (a) timeseries SWH and (b) SWH over direction. . . . 100
E.5 Wave data analysis with (a) timeseries SHWW and (b) SHWW over direction. . . . 101

E.6 Wave data analysis with (a) timeseries SHTS and (b) SHTS over direction. 101
E.7 Wave rose plots for wave data analysis with (a) SWH, (b) SHWW, and (c) SHTS. 101
E.8 SWH seasonal waveroses 102
E.9 SHWW seasonal waveroses 102
E.10 SHTS seasonal waveroses 103
E.11 T_p time series 103
E.12 T_p vs SWH, SHWW and SHTS 104
E.13 Direction of the waves of the wind direction 104
E.14 Extreme Value Analysis: (a) Probability of non-exceedance and (b) Probability Density Function (PDF). 105
E.15 Peak Over Threshold (POT) timeseries for wave data: (a) SWH, (b) SHWW, and (c) SHTS.105
E.16 Peak Over Threshold (POT) analysis by direction for wave data: (a) SWH, (b) SHWW, and (c) SHTS. 106
E.17 Poisson distribution analysis for wave data: (a) SWH, (b) SHWW, and (c) SHTS. 106
E.18 GPD fit and QQ-plot analysis for SWH. 107
E.19 Return period plot of SWH, showing data and the fitted GPD curve with a 95 % confidence interval. This illustrates the SWH values associated with RT 107
E.20 Comparison of SWH extremes against (a) TP and (b) W10. 108
E.21 SWH extremes vs wave direction 108
E.22 Boxplots of the neurons over H_s, T_p, and θ_{waves} 109
E.23 Scatter plot of the neurons and their corresponding won datapoints over the variables H_s, T_p, and θ. 110
E.24 Self-Organizing Map (SOM) representing 378 wave conditions analysed through a neural network. Each cell illustrates the relationship between H_s, T_p, θ, and frequency (*f*). Colour gradients indicate the respective values of H_s, *f*, and T_p, allowing for a visual interpretation of the clustering and distribution of wave conditions 110
E.25 Scatter plot of the clusters and their corresponding won neurons over the variables H_s, T_p, and θ_{waves} 111
E.26 Self-Organizing Map (SOM) representing 12 wave conditions analysed through k-means. Each cell illustrates the relationship between H_s, T_p, θ, and frequency (*f*). Colour gradients indicate the respective values of H_s, *f*, and T_p, allowing for a visual interpretation of the clustering and distribution of wave conditions. 111

F.1 Granulometry of the porphyry waste aggregate 114
F.2 Granulometry graph of mixture 5. The thick blue lines represent the boundaries of the design areas [15]. The dark blue and light blue areas represent the design areas I and II, in which a cement mixture is optimally designed for workability and water requirements.116

H.1 Current granulometry. There are 64 thin coloured lines, each representing a sample. The thick blue lines represent the boundaries of the design areas [15]. The dark blue and light blue areas respectively represent the design areas I and II, in which a cement mixture is optimally designed for workability and water requirements. 121

K.1 Wave transformation results, H_s and wave direction under normal conditions for the reference situation small grid. I) H_s small grid offshore setting 1; II) Wave direction small grid offshore setting 1; III) H_s small grid offshore setting 2; IV) Wave direction small grid offshore setting 2; V) H_s small grid offshore setting 3; VI) Wave direction small grid offshore setting 3; VII) H_s small grid offshore setting 4; $VIII$) Wave direction small grid offshore setting 4; IX) H_s small grid offshore setting 5; X) Wave direction small grid offshore setting 5; XI) Schematic of port reference situation 130
K.2 Wave transformation results, H_s and wave direction under normal conditions for concept 1 small grid. I) H_s small grid offshore setting 1; II) Wave direction small grid offshore setting 1; III) H_s small grid offshore setting 2; IV) Wave direction small grid offshore setting 2; V) H_s small grid offshore setting 3; VI) Wave direction small grid offshore setting 3; VII) H_s small grid offshore setting 4; $VIII$) Wave direction small grid offshore setting 4; IX) H_s small grid offshore setting 5; X) Wave direction small grid offshore setting 5; XI) Schematic of port for concept 1 131

K.3 Wave transformation results, H_s and wave direction under normal conditions for concept 2 small grid. I) H_s small grid offshore setting 1; II) Wave direction small grid offshore setting 1; III) H_s small grid offshore setting 2; IV) Wave direction small grid offshore setting 2; V) H_s small grid offshore setting 3; VI) Wave direction small grid offshore setting 3; VII) H_s small grid offshore setting 4; $VIII$) Wave direction small grid offshore setting 4; IX) H_s small grid offshore setting 5; X) Wave direction small grid offshore setting 5; XI) Schematic of port for concept 2 132
K.4 Wave transformation results, H_s and wave direction under normal conditions for concept 3 small grid. I) H_s small grid offshore setting 1; II) Wave direction small grid offshore setting 1; III) H_s small grid offshore setting 2; IV) Wave direction small grid offshore setting 2; V) H_s small grid offshore setting 3; VI) Wave direction small grid offshore setting 3; VII) H_s small grid offshore setting 4; $VIII$) Wave direction small grid offshore setting 4; IX) H_s small grid offshore setting 5; X) Wave direction small grid offshore setting 5; XI) Schematic of port for concept 3 133
K.5 Bulk alongshore sediment volumes for each segment in all settings for all designs and the reference. Added with the calculated factorized sediment volume according to the frequency of retrieved normal conditions. I) Reference situation; II) Concept 1; III) Concept 2; IV) Concept 3 134

L.1 Wave transformation results, H_s and wave direction under extreme conditions for concept 3 small and large grid. I) H_s large grid SSW offshore conditions; II) Wave direction large grid SSW offshore conditions; III) H_s large grid S offshore conditions; IV) Wave direction large grid S offshore conditions; V) H_s small grid SSW offshore conditions; VI) Wave direction small grid SSW offshore conditions; VII) H_s small grid S offshore conditions; $VIII$) Wave direction small grid S offshore conditions; IX) H_s large grid SSE offshore conditions; X) Wave direction large grid SSE offshore conditions; XI) H_s large grid SE offshore conditions; XII) Wave direction large grid SE offshore conditions; $XIII$) H_s small grid SSE offshore conditions; XIV) Wave direction small grid SSE offshore conditions; XV) H_s small grid SE offshore conditions; XVI) Wave direction small grid SE offshore conditions 136
L.2 H_s near port for concept 3 under 4 extreme conditions. I) SSW offshore conditions; II) S offshore conditions; III) SSE offshore conditions; IV) SE offshore conditions 137

N.1 Schematic drawing of conceptual design 1 139
N.2 Schematic drawing of concept design 2 141

O.1 Accroberm II toe unit placement [1]. 143
O.2 Accroberm II unit in toe berm position [1]. 143

Q.1 LCA process tree - current method 147
Q.2 LCA process tree - proposed method 148
Q.3 BoMP of the current method 149
Q.4 BoMP of the proposed method 149
Q.5 Total shadow costs of the LCA, monetized and quantified. The ratio between the current and the proposed method is included. 150

List of Tables

1 Table of terms . . . xv
2 Table of abbreviations . . . xvi

3.1 Boundary conditions for Phase I and II port expansion . . . 10
3.2 Soil properties of the restinga [13]. . . . 10
3.3 Percentage of units per zone and their future purpose . . . 15

4.1 Failure mechanisms overview . . . 18
4.2 Overview of researches and used data for hydrodynamic analyses . . . 19
4.3 Statistical overview of wind magnitude (w_{10}) . . . 20
4.5 Statistical overview of SWH, SHWWW, SHTS, and T_p . . . 21
4.7 Significant wave heights and corresponding return periods based on extreme value analysis. . . . 22
4.9 Wave parameters and corresponding return periods based on extreme value analysis. . . . 22
4.11 Tidal levels for Puerto Rawson [28] [67] . . . 23
4.12 Some properties of the current cement mixture . . . 26
4.13 Summary of sample distribution . . . 27
4.14 Sclerometer tests, summarized . . . 28
4.15 Some properties of Mrs. Cotti's cement mixture . . . 29

5.1 Offshore normal settings used in model runs . . . 33
5.2 Offshore extreme settings with 100-year return period . . . 33

6.1 Pros and cons of *conceptual design 3* . . . 42

7.1 Results extreme conditions from four offshore directions for concept 3, parameters at the toe. . . . 49

8.1 Parameters for all cross-sectional locations of design; CS = "Cross-section" * Note: not evaluated, but assumed to be the same as CS-C . . . 51
8.2 Dimensions of armour units per cross-section . . . 53
8.3 Grading input core parameters for all cross-sections . . . 54
8.4 Grading input Underlayer . . . 54
8.5 Properties of underlayer: $HM_A\ 300 - 1000$ [32] . . . 55
8.6 Results of toe dimensioning parameters . . . 57
8.7 Results of crest dimensions . . . 58
8.8 Dimensions of rear-side stability parameters . . . 58
8.9 Mix design properties, current mixture vs. proposed mixture . . . 61
8.10 Concrete volume per zone . . . 63
8.11 End-of-Life solutions and their assigned concrete volume . . . 63
8.12 Concrete quantification results . . . 63

9.1 Requirements and criteria for several functional properties . . . 65

B.1 Total Accropode unit amount and volume . . . 88
B.2 Accropode distribution and percentages - northern breakwater . . . 90
B.3 Accropode distribution and percentages - new southern breakwater . . . 90
B.4 Concrete volume per zone subdivision . . . 90

C.1 Damage scale explanation . . . 92
C.2 Complete visual inspection . . . 93

E.1 ERA5 variables . . . 97
E.2 Basic statistics of w_{10} . . . 98
E.4 Basic statistics of w_{10} over 30 years . . . 99
E.7 Basic statistics of w_{10} over the seasons . . . 99
E.8 Basic statistics for SWH, SHWW, and SHTS . . . 100
E.11 Mean waveheights over 30 years for SWH, SHWW, and SHTS . . . 102
E.13 Mean waveheights over the seasons for SWH, SHWW, and SHTS . . . 102
E.15 Basic statistics of T_p . . . 103
E.16 Test Results of Poisson Fit . . . 106
E.19 Return periods of SWH, SHWW and SHTS based on EVA . . . 107
E.20 Return Periods for Significant Wave Height and Associated Parameters . . . 108
E.22 Parameter values of the 12 clusters following the k-means algorithm over the 378 neurons. 112

F.1 Important properties of porphyry waste and river pebble . . . 114
F.2 Aggregate percentages of the tested cement mixtures . . . 115
F.3 Granulometry relevant values of mixture 5 . . . 115
F.4 Granulometry values of mixture 5 . . . 116
F.5 Mrs. Cotti's proposed cement mixtures . . . 116

G.1 Studies for the current cement mixture . . . 118

H.1 All granulometry data of the current mixture . . . 119
H.2 Table H.1 continued . . . 120
H.3 All granulometry samples and their coefficients . . . 122
H.4 Table H.3 continued . . . 123

I.1 All sclerometer results . . . 124

J.1 Offshore normal settings used in model runs . . . 126
J.2 Offshore extreme settings with 100 year return period . . . 127

L.1 Results extreme conditions from four offshore directions for concept 3, parameters at the toe . . . 137

M.1 Dimensions of both the original Accropode I [41] and the Accropode II units [1]. . . . 138
M.2 Thickness checks . . . 138

N.1 Pros and cons of concept design 1 . . . 140
N.2 Pros and cons of conceptual design 2 . . . 142

P.1 Initial cement mixture proportions . . . 144
P.2 Proposed cement mixture proportions . . . 144

Nomenclature

This report includes references to individuals closely involved with the project. When the text refers to *supervisors*, it specifically denotes the supervisors from TU Delft. Additionally, the term *stakeholders* is used to indicate relevant supervisors from Argentina, who provided input throughout the project via weekly meetings with the project team.

The terms ACCROPODE™, ACCROPODE™ II, and ACCROBERM™ II are registered trademarks and are used in this report for descriptive purposes only. All rights to the trademark are owned by the *Concrete Layer Innovations* (CLI). [1]

The terms and abbreviations are given in Table 1 and Table 2, respectively.

Table 1: Table of terms

Abbreviation	Definition
Spring	September, October, November
Summer	December, January, February
Autumn	March, April, May
Winter	June, July, August
ACCROPODE™ I	Accropode(s) armour unit
ACCROPODE™ II	Accropode(s) II armour unit
ACCROBERM™ II	Accroberm II unit

Table 2: Table of abbreviations

Abbreviation	Definition
ASR	Alkali-Silica Reaction
BoMP	Bill of Materials and Processes
CERC	Coastal Engineering Research Council
CPC	Portland Composite Cement
CPN	Portland Normal Cement
CPP	Portland Pozzolanic Cement
DyOPSA	Dragados y Obras Portuarias S.A.
EoL	End-of-Life
EPD	Environmental Product Declaration
EVA	Extreme Value Analysis
HAT	Highest Astronomical Tide
ISO	International Organisation for Standardisation
ITH	Instituto Technólogico del Hormigo S.A.
LABIEVI	Laboratorio de Investigaciones y Ensayos Viales
LAT	Lowest Astronomical Tide
LCA	Life Cycle Assessment
LCI	Life Cycle Inventory Analysis
LCIA	Life Cycle Impact Assessment
MHW	Mean High Water level
MLW	Mean Low Water level
MSL	Mean Sea Level
NEN	Nederlandse Norm
PCR S.A.	Petroquímica Comodoro Rivadavia S.A.
PIANC	World Association for Waterborne Transport Infrastructure
The Port Directorate	Dirección General de Puerto Rawson
RCA	Recycled Coarse Aggregate
SHN	Servicio de Hidrografia Naval
SLR	Sea Level Rise
SLS	Serviceability Limit State
SOM	Self-Orginazing Map
std	standard deviation
SWAN	Simulating WAves Nearshore
UBA	Universidad de Buenos Aires
ULS	Ultimate Limit State
UNPSJB	Universidad Nacional de la Patagonia San Juan Bosco
w/c ratio	Water-to-cement ratio

1

Introduction

Ports disrupt natural sediment flows along coastlines, resulting in serious challenges through erosion or sediment build-up along shorelines. This effect, combined with sea level rise and more frequent extreme weather events, creates an urgent need to rethink port infrastructure. Additionally, the pressure of globalization and expanding international trade requires ports to expand, leading to more disruptions of coastal systems. Port expansions often involve new breakwaters and large dredging operations, which alter hydrodynamics and affect sediment transport. Future resilient port design involves balancing the conflicting interests of commercial needs and coastal preservation.

The port of Rawson (Puerto Rawson) located in Chubut, Argentina, is one of many examples that is currently not equipped for future challenges. Constructed several decades ago, the port underwent major renovations starting in 2001, including breakwater extensions and dredging efforts to enhance port operability. However, the breakwaters have interrupted the natural coastal sediment transport, causing sedimentation to the south and severe erosion north of the port. The rapid coastal retreat at Playa Unión has adverse effects on the local community, including loss of recreational area and potential of flooding. Moreover, the current port layout lacks sufficient space for future development, therefore limiting the region's economic growth opportunities. This affects not only the residents of Puerto Rawson, but also industries relying on the port for trade and export, particularly the fishing industry. Failing to address these problems could result in long-term coastal damage and lost economic opportunities for the whole area. Therefore, redesigning Puerto Rawson and addressing sediment transport issues is vital for supporting the prosperity of local communities and businesses

The primary objective of this report is to develop feasible solutions that enhance the capacity of the port while also examining their impact on sediment transport. This is pursued through a series of supplementary goals that are designed to support the primary objective. These goals include determining the layout and dimensions for new breakwater(s), determining the sea state conditions, and assessing the alongshore sediment transport. Additionally, the report evaluates the current condition of concrete armour units of the existing breakwaters and proposes a more suitable concrete mixture for future construction, ensuring that the planned expansion is more sustainable and durable. The scope of the report is focused exclusively on the external aspects of the port, particularly the breakwaters and their environmental impact and impact on sediment transport. The design of the internal port layout and facilities is outside the scope of this project.

The main research question this report aims to answer is:

How can a sustainable and durable port expansion at Puerto Rawson be realised, while minimizing its environmental impact, particularly in relation to sediment imbalance along the coast?

Sub-questions to guide the investigation:

1. What is a feasible conceptual design that aligns with the objectives of future port expansion?
2. What are the nearshore extreme wave conditions?
3. How do different breakwater layouts influence longshore sediment transport?
4. What are the dimensions of the breakwater introduced in the conceptual port expansion design?
5. What improvements in concrete mixture design enhance the sustainability and durability of the new breakwater?

These research questions are directly linked to the identified problem of sediment imbalance caused by the existing port layout, as outlined in the problem statement. Addressing these questions helps to determine how the port expansion can be achieved sustainably, while minimizing its impact on coastal erosion and sedimentation issues.

This report is organized to lead the reader through a comprehensive exploration of hydraulic and structural assessments, relevant to Puerto Rawson and the region around it. The methodology in Chapter 2 outlines the approach for hydraulic and structural analysis, followed by Chapter 3, which provides a detailed site study of the surrounding area and the current breakwaters. Chapter 4 delves into hydrodynamic and structural assessments, particularly the sea states. Chapter 5 explains the modelling of wave transformation and sediment transport. Chapter 6 introduces conceptual design options, including layouts for port expansion and a new cement mixture proposal. Chapter 7 presents the findings under normal and extreme sea conditions, while Chapter 8 focuses on finalizing the breakwater design dimensions and quantifications. Chapter 9 evaluates concrete sustainability through a life cycle assessment. In Chapter 10, uncertainties in the design are discussed, leading to the concluding insights in Chapter 11, which summarizes key findings. Finally, Chapter 12 provides recommendations for future improvements.

2

Methodology

This chapter outlines the methodology employed in this research. The overall approach to addressing the research and sub-questions is first presented. In the following sections, the specific sub-approaches are discussed in detail. The dimensioning of the breakwater within the conceptual design, hydraulic conditions analysis and modelling, and concrete analysis and quantification all come to play.

2.1. Overall methodology

The aim of this methodology is to propose a sustainable and durable port expansion in Rawson.

The project methodology is illustrated in Figure 2.1, which outlines three distinct yet interconnected pathways that guide the transformation from a problem description to a final design proposal. These pathways are identified as: hydraulic conditions analysis and modelling (*green*), breakwater dimensioning within the conceptual port expansion design (*blue*), and concrete analysis and quantification (*orange*). Each pathway is essential in progressing from the initial framework, through analysis and design, to impact assessment, forming the basis for the final design proposal.

The three multidisciplinary pathways come together in the final design proposal. The final breakwater design includes, among other, a detailed dimensioning of the structure. The sustainability study, along with a new proposed cement mixture, aims to reduce the environmental impact of the breakwater. Additionally, the design should be integrated into the layout of Puerto Rawson, while also considering its impact on longshore sediment transport. This analysis will help assess the breakwater's effect on the erosion problem at Playa Unión.

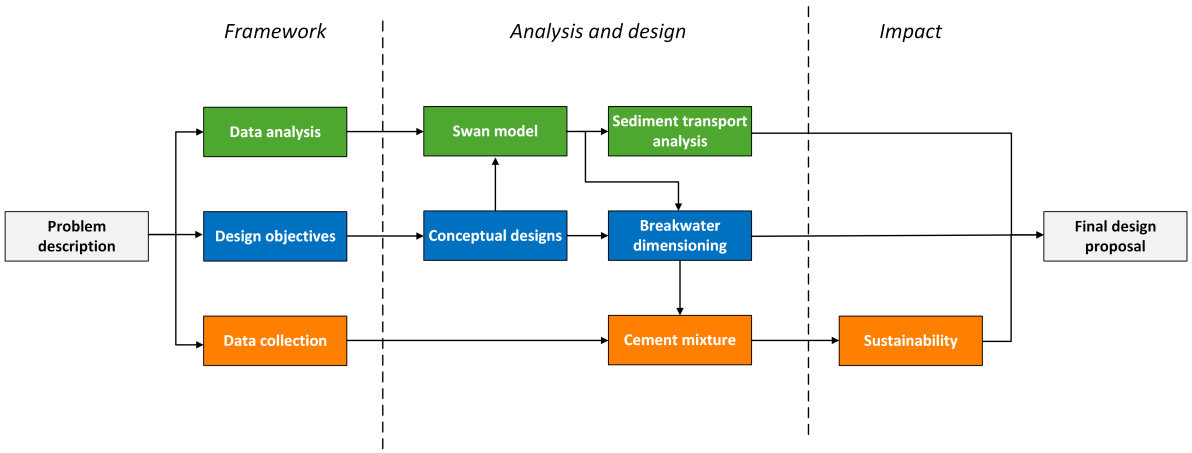


Figure 2.1: Flowchart of the overall methodology

2.2. Dimensioning of breakwater within conceptual design

The goal of this part of the methodology is to dimension a new breakwater within a developed conceptual design of a port expansion. The methodology addresses the key question: *What is a feasible conceptual port expansion design, and what are the dimensions of the incorporated breakwater configuration?* Figure 2.2 visualises the methodology in the way of a flow chart, with further explanation per step listed below.

1. At first design objectives are established as the basis for developing the conceptual designs.
   (a) Design criteria are set, guided by PIANC guidelines for safe port entrances, which represent essential standards that must be met to ensure the design's viability.
   (b) Design aspirations are set to ensure the designs include project-specific ambitions, categorized within the domains of *sediment transport analysis*, *environmental impact* and *space for future port operations*.
2. Subsequently, three conceptual port expansion designs are developed: two supplementary designs and one final design. The bathymetry models of all three designs are used as input for the SWAN model, mentioned in Section 2.3.
   (a) The supplementary designs are not intended as optimal design solutions, but to serve conceptual designs that emphasize a specific design aspiration.
   (b) The final design serves as the foundation for subsequent dimensioning of the breakwater.
3. A design analysis of the breakwater is performed, including the determination of the parameters *return period* and *design life*. Moreover, the failure mechanisms of the breakwater are listed and boundary conditions for the ULS and SLS are defined.
4. Finally, a definitive breakwater design is dimensioned, incorporating input from the design analysis, extreme nearshore conditions generated by the SWAN-model, and the breakwater's positioning based on the conceptual port design. Subsequently, the breakwater dimensions are used for the concrete quantification outlined in Section 2.4.

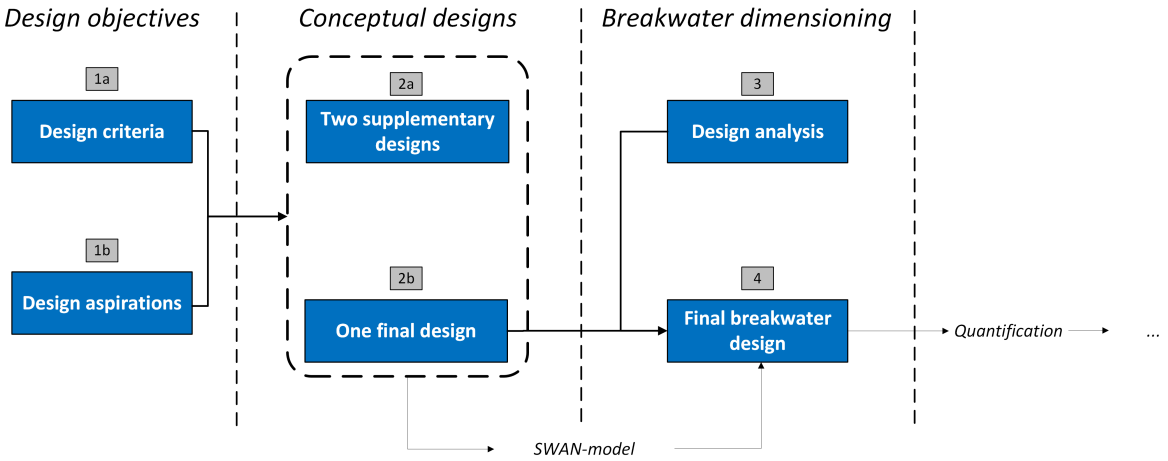


Figure 2.2: Flow chart for the methodology of dimensioning breakwater in conceptual port expansion design.

2.3. Hydraulic conditions analysis and modelling

The goal of the methodology for analysing and modelling hydraulic conditions is twofold: (1) to provide nearshore extreme wave conditions for the breakwater design, and (2) to analyse sediment transport along the Puerto Rawson coast. The methodology addresses the key question: *What are the prevailing sea state conditions, and how do they influence coastal sediment transport?* Figure 2.3 visualises the methodology, with further details explained below.

1. A dataset of 30 years hourly ERA5-data, including wind and wave climate variables, forms the basis for the data analysis.
2. The goal of this branch is to identify nearshore conditions for the dimensioning of the final breakwater design.
   (a) An Extreme Value Analysis (EVA) is used to determine offshore extreme conditions (H_s, T_p, θ_{waves}, w_{10}, θ_{wind}) — along with the associated return periods (RT).
   (b) These extreme conditions are then transformed nearshore using a SWAN (2D) model.
3. The goal of this branch is to analyse the sediment transport (erosion/sedimentation) along the coast of Puerto Rawson for multiple breakwater designs.
   (a) Machine learning algorithms are used to reduce the dataset to 10 representative off-shore conditions (H_s, T_p, θ_{waves}).
   (b) These regular conditions are then transformed from off-shore to nearshore conditions using a SWAN (2D) model.
   (c) The results of SWAN are then used to analyse the sediment transport along the coast of Puerto Rawson for multiple breakwater designs. This analysis is based on the CERC-formula.

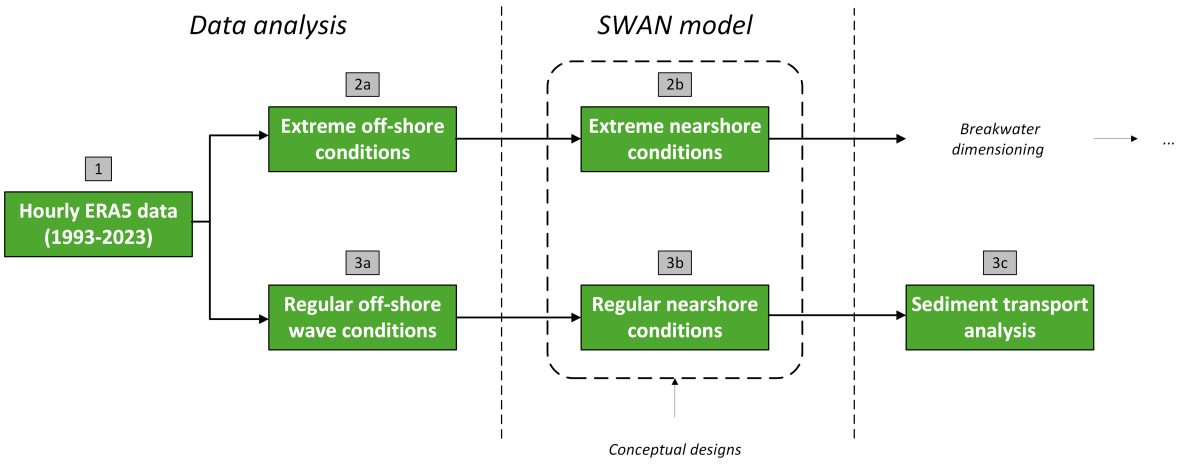


Figure 2.3: Flow chart of the methodology for analysis and modelling of hydraulic conditions

2.4. Concrete analysis and quantification

The goal of the methodology for the structural concrete analysis is to propose a more durable and sustainable concrete mixture, compared to the current mixture. The methodology addresses the key question: *What improvements in concrete mixture design can enhance the sustainability and durability of the new breakwater?* The methodology is visualised in Figure 2.4 and is explained below in further detail.

1. Inspections, both visual and structural, are conducted, to analyse the state of the concrete Accropodes of the current breakwater. This is needed for the final mix design.
2. The goal of this branch is to collect sufficient data, to eventually determine the proportions of the current cement mixture.
   (a) At first, initial data is gathered from the *Dirección General de Puerto Rawson* (Port Directorate of Rawson).
   (b) With this data, the current cement mixture is sought after, which is needed for the final mix design.
3. The next branches' goal is to propose a new cement mixture, which is both more durable and more sustainable than the current mixture.
   (a) Research is conducted into creating a new cement mixture.
   (b) The new cement mixture is proposed and validated using the relevant standards.
4. The fourth branch is to propose a final mix design, using the information gathered from collecting data.
   (a) Using the data from the inspection, together with the current- and proposed cement mixture, a new final mix design is introduced. By comparing structural aspects of both designs, a mix design is chosen.
   (b) Using this final mix design and the concrete volume from the breakwater design, everything is quantified and checked for availability.
5. Finally, a comparative Life Cycle Assessment (LCA) is conducted, to assess the sustainability of the current- and final mix design. By calculating the shadow costs of each stage, the sustainability can be monitized and compared.

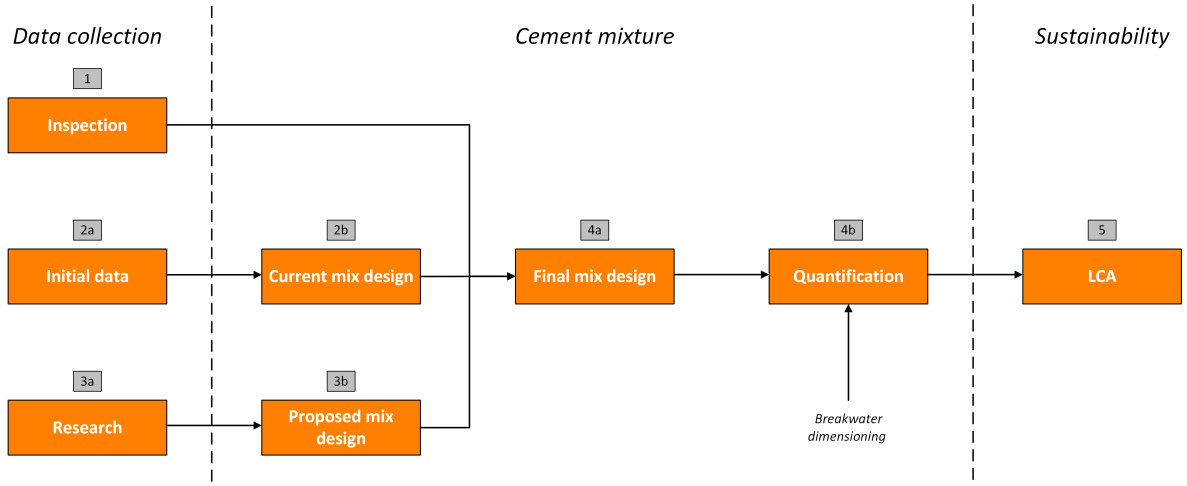


Figure 2.4: Flow chart of the methodology for concrete analysis and quantification

3

Site study

This chapter introduces the project site by giving a clear visualization of the area and a description of the port. It shows the close by town of Playa Unión and zooms out to discuss the flaws and limitations of the coastal system. Besides, a visual inspection of the armour units is done. This lays the foundation for later analyses on cement mixtures through discussing the flaws and limitations observed in the current port design.

3.1. Site description

The site description provides an overview of the historical development of the Puerto Rawson, highlighting the consequential coastal erosion impact of the port on Playa Unión. Furthermore, this section explains key terminology for this report. The site description also explores potential future expansion plans for the port and includes a brief overview of the unique restinga along the coast.

Notably, the site description in this report focuses exclusively on topics considered essential to the objectives of this project. A more comprehensive site description, including details on the geology of the area, the fishing industry, the local ecosystem, and a stakeholder analysis can be found in the MP341 report from 2023 [47].

3.1.1. Site introduction

This project focuses on Puerto Rawson and Playa Unión, situated at the mouth of the Chubut River in Chubut province, Argentina. The locations are marked in Figure 3.1. As of 2024, Puerto Rawson serves as a critical fishing port for the region, driven by rising demand for seafood products. The fleet consists of smaller vessels, both publicly and privately owned, targeting key fish stocks such as shrimp, squid, and hake [78].

To accommodate the growing demand for these products, the port has undergone significant expansion. The number of quays along the Chubut River's mouth has steadily increased with infrastructure developments. The latest quay wall extension was completed in 2002 on the northern river bank, and in 2024, construction of a new quay wall started on the southern riverbank, both enhancing the operational capacity of the port [12]. Future expansion plans are also under consideration and are discussed further in Subsection 3.1.3.

A complete historical overview of the development of Puerto Rawson and Playa Unión is given by Donini [29]. The development of the port started in the 1960s and 1970s. Construction of the old breakwaters protected the area near the river mouth, eliminating the need to sail up river to the town of Rawson. Between 1960 and 1963, the initial northern breakwater — now referred to as the *old northern breakwater* — was constructed using concrete sheet piles. A decade later, between 1972 and 1974, the first southern breakwater, now known as the *old southern breakwater*, was built using Akmon armour blocks.

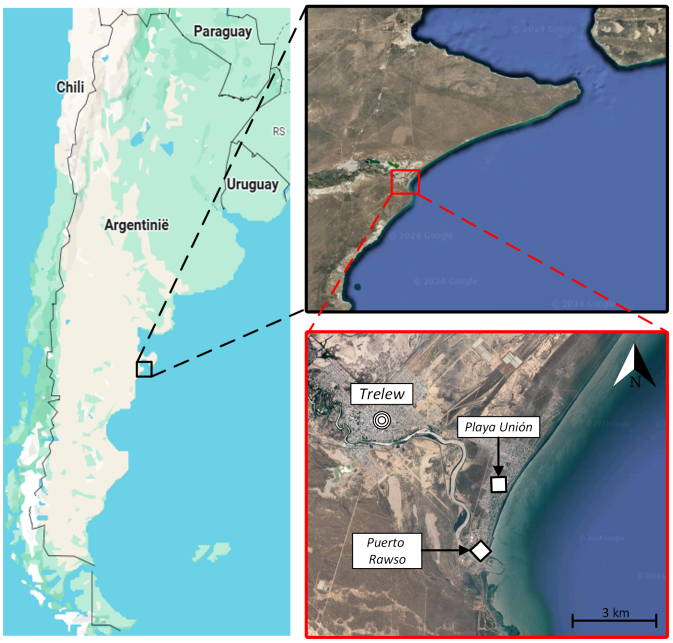


Figure 3.1: Location of Port of Rawson and Playa Unión [30].

Before these breakwaters were constructed, the coast of Playa Unión was close to equilibrium, i.e. no erosion and sedimentation issues. However, as the port wanted to grow in the following decades and the old breakwaters did not function properly, further infrastructure was needed. In 2002, the southern breakwater was extended with a breakwater made of Accropode armour units, forming the *new southern breakwater*. Similarly, in 2003, the northern breakwater was expanded using the same Accropode armour units, now referred to as the *new northern breakwater*.

The breakwaters that are currently in place are identified by four distinct names: the *old northern*, *old southern*, *new northern*, and *new southern* breakwaters. The specific locations and are illustrated in Figure 3.2.

Previous studies on the coast of Playa Unión and Puerto Rawson have analysed local wind and wave climate. Two of the most recent studies in the area were done by the National University of Córdoba in 2022, and the *Instituto del Agua* (INA) in 2009 [22] [6]. At Puerto Rawson, a predominant wind blows offshore, from land to sea. However, the strongest winds originate from the ocean, predominantly from the south, with maximum wind speeds reaching 20 $\mathrm{m/s}$ [22]. Due to the strong off-shore wind climate, only 35% of wind-generated-waves reach the coast, while ocean swells reach the coast almost in full. In the coastal area, the maximum significant wave height is 4.13 m, with 75% of waves below 1.49 m and 50% below 1.03 m. The largest waves predominantly come from the SE and SSE, with a smaller portion of waves from the NE [6].

3.1.2. Erosion and sedimentation issues

North of the port lies Playa Unión. Due to the construction of the breakwaters, the coast of Playa Unión has eroded in the areas directly north of the port [29]. Construction of both the old and new breakwaters influence the longshore transport. The breakwaters obstruct longshore sediment transport, and the construction of the new breakwaters block river sediments from flowing out of the inner port. The areas of sedimentation and erosion are marked in Figure 3.2. It is important to highlight that north of Playa Unión sedimentation picks up again. This is north of the areas marked with erosion in Figure 3.2.

The coastal erosion along Playa Unión has been well-documented, with significant shoreline retreat occurring over the past decades. Notable erosion episodes include periods between 1976 and 1996, as well as 2002, when a severe storm caused substantial damage to shoreline infrastructure. Through the construction of a groyne on Playa Unión, referred to as *short breakwater*, sediment loss from the area just north of the port was tried to be limited. The groyne was constructed between 2012 and 2016,



Figure 3.2: Terminology and layout of Puerto Rawson and Playa Unión [30].

and has further altered sediment transport patterns, exacerbating erosion in some areas while causing sediment build-up in others [18]. In response, authorities attempted additional coastal protection measures, such as deploying sandbags and barriers to limit the coast retreat. The protective measurements and severity of the coastal retreat can be seen in Figure 3.3.

In addition to these structural measures, the port authority initiated a dredging campaign in Puerto Rawson, aiming to redistribute sediment accumulated in the port along the beach at Playa Unión. However, the dredged material contained organic matter and clay, which gave the water a dark colour. This led to a termination of the project by the mayor of Rawson, who feared the discolouration indicated water toxicity, forcing the dredging campaign to stop prematurely [61]. This incident caused significant concern for the port authority, putting future dredging efforts at risk.



Figure 3.3: Aerial view of affected coast at Playa Unión [22].

3.1.3. Port expansion ambitions

As discussed in Subsection 3.1.1, the port of Rawson is growing and the plan is to expand further in the area south of the southern breakwater. According to the stakeholders, such plans foresee an initial expansion (Phase I) focussing on increasing throughput of fish. Additionally, the scope includes a larger throughput (Phase II), and both phases include project cargo for onshore wind turbines. The boundary conditions for the port expansion are displayed in Table 3.1.

Table 3.1: Boundary conditions for Phase I and II port expansion

Category	Unit	Phase I (2030)	Phase II (2040)
Shrimp	[tons/year]	100,000	200,000
Squid	[tons/year]	50,000	100,000
Hake	[tons/year]	50,000	100,000
Others	[tons/year]	-	100,000
Containers	[TEU]	20,000	60,000
Design vessel	[−]	Madrid Trader	Panamax
Wind cargo	[turbines/year]	50	50

3.1.4. Restinga

The coastal area of Chubut features tidal flats that are shaped by the interaction of marine and fluvial processes. Coastal features like tidal flats are often referred to as a *restinga* in Argentina. The soil composition of the restinga includes tuffaceous claystone [9]. The restinga extends along the broader coast of Chubut; however, in this report, *restinga* refers specifically to the area outlined in Figure 3.2.

Research on the soil composition of the restinga is conducted by Serman y Asociados s.a. [13]. The depth profile of the restinga can be specified by two sections along the depth. The first section of the restinga is 2.4 m thick and consists of four distinct soil layers: silts and subordinate clays, medium sands with silt, sandy silts, and sandy gravels. Under the top layers lies a resistant tuffaceous substrate, a volcanic stone which is rich in silt and clay. The exact depth to which the tuff layer extends is unknown. Research on the soil composition of the restinga wav done through triaxial tests and the found mechanical properties is displayed in Table 3.2.

Table 3.2: Soil properties of the restinga [13].

Description	γ_{sat} [$\mathrm{Kn/m^3}$]	C_u [kPa]	ϕ [°]
Gravel and sandy clays	20	0	30
Tuffaceous claystone	17	45	26

3.2. Current state of breakwaters

An assessment of the current state of the breakwaters is conducted. The breakwaters contain concrete armour units to provide stability. Potential sustainable and economical improvements can be made to the cement mixture of the armour units, based on visual inspection. These improvements can significantly lower the total environmental impact of a new concrete mixture, and thus of the new breakwater.

3.2.1. Visual inspection

The breakwater consists of unreinforced concrete Akmon and Accropode units, shown in respectively Figure 3.5 and Figure 3.6. The Akmon units are present in the old southern breakwater. Designed in 1962 (before the Accropode), the Akmon has a simpler shape and interlocking is limited [48]. The Akmon units have degraded to the point that they do not provide stability, with some units missing, as seen in Figure 3.4. Next to that, they are completely submerged at high water level which leads to a loss of functionality of this structure. The degradation of the Accropodes is assessed by conducting a

field research. Photos were taken and subsequently compared, to assess the extent of the damage to these units, these are found in Appendix A. The breakwater is divided into parts, both along its length and over its cross-section. The division of the cross-section can be seen in Figure 3.7 and is further substantiated below:

- To divide the breakwater over its complete length, it is possible to check where the breakwater has sustained the most damage with respect to the incoming waves;
- The cross-section is divided to check the degradation of the Accropodes, regarding low and high tide. The units that are fully submerged during high water level (zone C, submerged zone), are compared to the units that are always dry (zone A, crown zone);
- The units that are semi-submerged during high water level and completely dry during low tide complete the set (zone B, splash zone). These are thus positioned between zone A and C.

The division of the cross-section can be seen in Figure 3.7. Note that this is a cross-section of the new southern breakwater, the new northern breakwater only has Accropodes on one side of the breakwater. From this figure, it is also clear that there are more Accropodes in zone C, than there are in zone A and B. A more detailed description is found in Appendix B.



Figure 3.4: Old southern breakwater at low water level. Several Akmon units are missing.

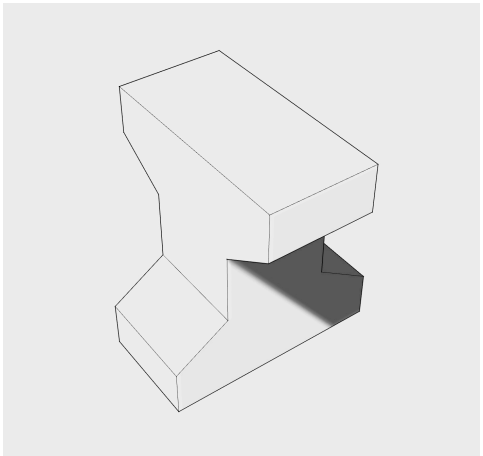


Figure 3.5: Schematic 3D representation of an Akmon armour unit [51].

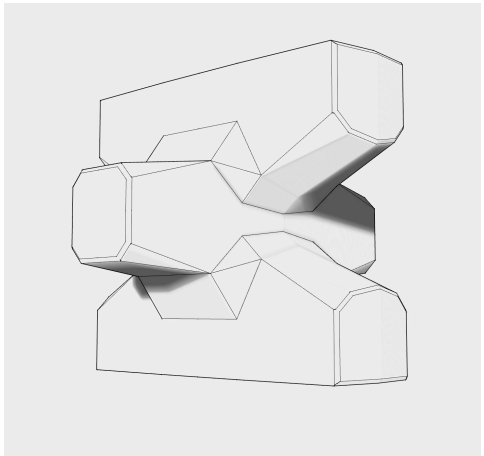


Figure 3.6: Schematic 3D representation of an Accropode armour unit [51].

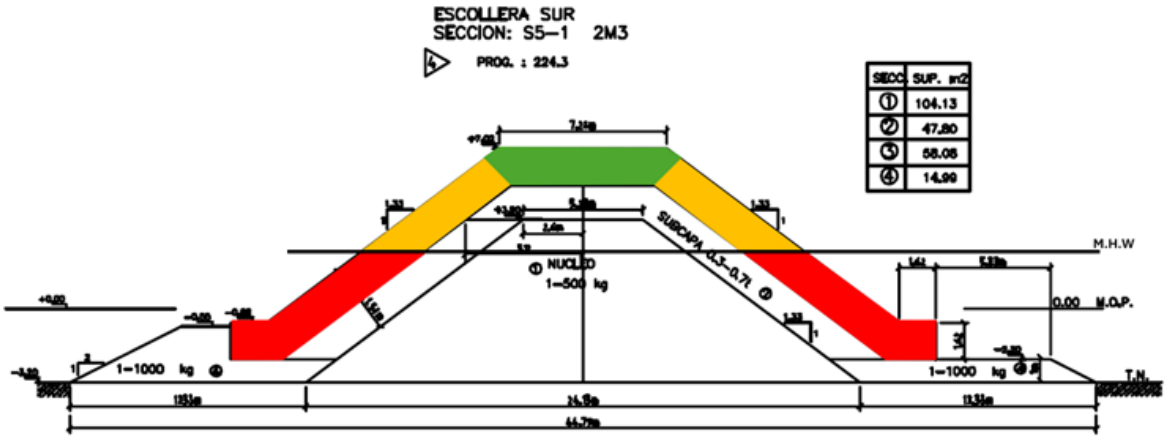


Figure 3.7: Cross-section of the new southern breakwater, divided into three zone. Zone A: green zone, or crown zone; Zone B: yellow zone, or splash zone; Zone C: red zone, or submerged zone. Cross-section from the Port Directorate [62]

As a reference, photos are also taken of an undamaged Accropode. In front of the Port Directorate office, a fully intact unit is positioned, which is not impacted by the seawater. It was however susceptible to the sun, rain and wind throughout its service life. This unit functions as a reference unit, since the only major difference between the Accropodes of the breakwater and the one on land is the influence of the seawater. The reference Accropode has been painted grey; thus the damage to the paint is not considered in this report. Photos of the reference unit are found in Section A.1.

3.2.2. Visual inspection results

The complete damage sheet is found in Appendix C. The units with the most observed damage are those in zone C, while the units in zone A show the least amount of damage. The Accropodes in zone B show the most variety in damage. Next to the visual damage assessment, it is also important to assess which factors caused the damages. Damage that is connected to metals in the concrete are disregarded, since the concrete is unreinforced.

- Firstly, it can be noted that almost all of the concrete units are missing small fragments, mostly at corners and edges. These are damages that occurred when placed during construction of the breakwater;
- The Alkali-Silica Reaction (ASR) is a common type of damage to concrete, which is caused by the reaction between the cement paste and most aggregate types [69]. Internal swelling occurs, which subsequently leads to cracking and spalling, after which a gel is formed and will seep out of these cracks. In this case, the gel could not be observed, most probably because the concrete units are located in a windy environment. Next to that, it is also possible that the gel has been washed away by seawater;
- Concrete carbonation occurs when concrete is exposed to carbon dioxide. This type of damage is not directly visible, but it does influence the strength of the concrete, which is assessed in Subsection 4.4.3;
- Small surface cracks which occur during demoulding and temperature differences are early age concrete cracks. The mix composition, exposure environment, curing conditions, as well as other factors, all have an influence on these cracks [68]. The Port Directorate mentioned these cracks, too [62].

It cannot be determined, by visual inspection only, which cracks originated from which specific cause. For this, destructive concrete tests need to be conducted. This was however not allowed by the Port Directorate. This has a significant consequence in the determination of the End-of-Life (EoL) purposes for the Accropodes. The fact that there are cracks and sometimes discolouration around these cracks could indicate that one or more internal processes of the concrete have started. This could signal a deeper deterioration within the concrete and the aggregates, which can potentially lead to a shorter service life in their new function.

The aggregates used in the cement mixture for the Accropodes are relatively large, as shown in Figure 3.8. These aggregates are pebbles collected from the riverbeds of the Chubut River [62]. The Accropode in Figure 3.8 is nearly perfectly fractured along the surfaces of the pebbles. This occurred due to the pebbles' very smooth surface and the constant pressure exerted by flowing water. The smooth surface negatively impacts the bonding strength between the cement and the aggregate [63].



Figure 3.8: Exposed pebble aggregate on an Accropode, after a corner piece has crumbled off.

3.2.3. End-of-Life methods and visual inspection conclusions

To conclude this section, percentages are given to each zone, to denote how many of the Accropodes in the respective zone can be used for sustainable purposes; this is discussed in more detail in Chapter 9. In this stage, it is sufficient to report the percentage of Accropodes that can be either reused, repurposed, or recycled. These solutions follow a circular economy approach based on the 10R model [25] and are to be called the EoL solutions. Within this model, reuse in the new breakwater is the most preferred option (R3), followed by repurposing as artificial reefs (R7), recycling into new aggregates (R8), and finally landfill disposal.

Reusing Accropodes is the preferred EoL option from both an environmental and economic standpoint. It reduces the need for new unit manufacturing, making the construction process of the new breakwater more cost-effective and sustainable. For this option, units with sufficient structural integrity are required. Most of the concrete units from the crown zone (zone A) are suitable, as these units have experienced minimal to no deterioration due to less exposure to seawater. Consequently, they are only integrated into the crown zone of the new breakwater, where similar conditions reduce the likelihood of deterioration and help assure the structural integrity of the future breakwater.

The second option involves *repurposing* Accropodes as artificial reefs, where structural integrity is not a requirement. Concrete parts with visible cracks, broken sections, or other significant damages are still useful for these ecological applications, ensuring that the materials continue to serve a valuable environmental function [14]. Units from zone B that exhibit cracking as well as some of the units from zone C are allocated to artificial reefs, as their condition disqualifies them from reuse in the new breakwater or recycling into new aggregates. Although surface cracks may suggest internal damage that prevents their use in construction, this does not affect how well they function in marine environments. In fact, these cracks and holes offer surfaces for marine vegetation to grow, enhancing the ecological role of the structures. This approach not only maximizes the ecological benefits of these materials by transforming them into artificial reefs, but also reduces waste while fostering marine biodiversity and providing a foundation for ecosystems to thrive.

The third EoL option for the Accropodes involves crushing it into *Recycled* Coarse Aggregates (RCA). However, only concrete that does not contain excessive cracks is suitable for RCA. These compromise the concrete's physical and chemical properties, resulting in weak aggregates that may perform inadequately in new applications [27]. This option is reserved for units that are not robust enough for direct application in the new breakwater. They are particularly sourced from the splash zone (zone B), where they may have been subjected to more aggressive conditions (e.g. frequent water exposure), yet remain free from significant surface cracks. It is thus possible to ensure that the recycled aggregates retain the necessary properties for use in new concrete applications, promoting sustainable construction practices.

The fourth and final option is to dispose the Accropodes to a *landfill*. This option is only reserved for the units that show the most damage. These units are completely broken, lost all of their structural integrity and strength, or are fully saturated due to the seawater. Almost all of the Accropodes that have to go to a landfill are from zone C, as well as all the Akmon units.

The percentages are an approximation, since only a limited amount of photos are taken and only at the northern breakwater. It is nearly impossible to inspect each Accropode in the given time frame and without professional guidance. This means that the photos that were taken of Accropodes in a zone, are a generalisation of that specific zone. Furthermore, it is assumed that the Accropodes of the new northern breakwater are representative of all the Accropodes of both breakwaters. That means that the units of the new southern breakwater have the same damage degradation as the units of the new northern breakwater. This assumption is necessary, since the new southern breakwater is inaccessible. The percentages are based on the visual inspection and are shown in Table 3.3. The following guidelines are made for these percentages:

- Accropodes that only have crumble damage, and nothing else, are reused. These are units with a damage score of 1;
- Accropodes that have a damage score of 5 are completely broken and have no structural integrity and strength left. These units are taken to the landfill, since they can no longer fulfil any other purpose;
- Accropodes that have cracks in them and discolouration are to be repurposed or brought to a landfill, due to the unknown internal processes in the concrete. However, it is expected that some units can still be recycled.

Table 3.3: Percentage of units per zone and their future purpose

Zone	Description	Percentage [%]
A	Reuse	80
	Repurpose	20
	Recycle	0
	Landfill	0
B	Reuse	10
	Repurpose	60
	Recycle	20
	Landfill	10
C	Reuse	0
	Repurpose	30
	Recycle	0
	Landfill	70

The recyclability of the concrete poses an interesting discussion. Since the cause of the cracks are unknown, the recyclability is unknown as well. It is thus uncertain if any Accropodes can be recycled at all. The proposed solution is to test the Accropodes that will be repurposed as artificial reefs, using destructive testing. By drilling a core into the concrete (coring) and collecting the dust samples, chemical analyses can be carried out. In a laboratory, these samples can be examined and assessed for multiple processes, such as chloride ingress [66]. This proposed solution will however take a lot of time and funding, since each Accropode has to be tested for, individually. Based on this, three-quarters of the units are planned for use in artificial reefs, and one-fourth is anticipated to be recyclable.

4

Analysis

This chapter provides a comprehensive analysis of the critical factors influencing the design and performance of the breakwater. It starts with an analysis of return periods, structural classifications, and failure mechanisms. An evaluation of hydrodynamic conditions follows, focusing on the wind and wave climate. Additionally, regular wave conditions are assessed using self-organization. The longshore sediment transport is later analysed using these regular conditions. Then the current cement mixture used in the breakwater is evaluated, and a new mixture is proposed. Together, these analyses form the technical basis for the dimensioning of the breakwater.

4.1. Design analysis

The design analysis of the breakwater is realised through an examination of critical design choices like return period, breakwater classification, and failure mechanisms, all contribute to achieving both serviceability and ultimate limit state requirements in the design phases of 6 and Chapter 8.

4.1.1. Return Period

The Design Life of the breakwater is determined to be 50 years, since this is typical choice for breakwaters [77]. For the majority of ULS considered in this analysis, a return period (RT) of 100 years is established, which is typical for breakwaters [72]. This corresponds to an annual probability of failure of 1% for the identified failure modes, indicating the chance that the breakwater could fail due to extreme loading conditions in any given year.

Using this information, the cumulative failure probability is calculated for the entire design life (DL) of the structure. The mathematical formulation for this calculation is presented in Equation 4.1.

$$P_{f,DL} = 1 - \left(1 - \frac{1}{RT}\right)^{\frac{1}{DL}} \tag{4.1}$$

$$R_{t,DL} = 1 - P_{f,DL} \tag{4.2}$$

Substituting the values for DL and RT into Equation 4.1 shows that the failure probability over the Design Life of the structure is 39.5%. This means that there is a significant likelihood that the breakwater encounters conditions leading to failure at least once during its intended lifespan.

In addition, the reliability of the structure is also determined using Equation 4.2. After applying the calculations, the reliability of the breakwater is 60.5%. This implies that there is a 60.5% probability that the structure is not exposed to the extreme design conditions throughout its 50-year design life.

4.1.2. Classification of breakwater

The breakwater classification, along with a range of associated stability numbers, is essential for establishing specific design assumptions related to failure criteria discussed later in this chapter. Similar to the existing northern and southern breakwaters, the design of the new breakwater incorporates a rouble mound with large interlocking concrete armour blocks. Since the concrete blocks achieve their strength through interlocking, only minimal movement of the blocks is permitted. This restriction means that the breakwater cannot reshape, and any damage is defined by the displacement of armour units. As a result, the breakwater is classified as a conventional, statically stable rubble mound breakwater [65].

Figure 4.1 shows a schematic cross-section of such a rubble mound breakwater, highlighting its essential components. The concrete units form an armour layer on a sloped surface, which dissipates energy of incoming waves. Toe and scour protection at the base prevent erosion caused by wave action and currents. Filter and underlayer materials allow drainage while preventing the finer materials in the core from washing out, ensuring internal stability. Finally, rear-side stability refers to the lee side of the breakwater, and is designed to withstand forces from overtopping and from wave impact in the port.

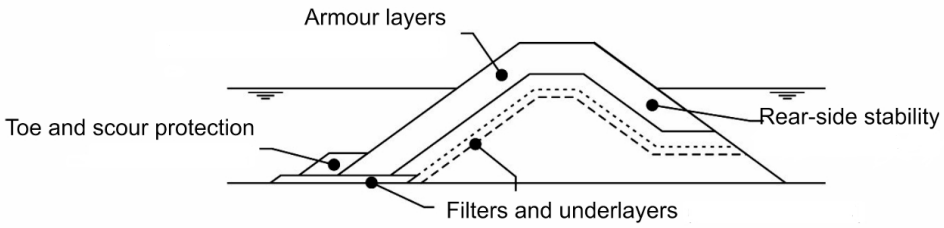


Figure 4.1: Schematic overview of rubble mound breakwater cross-section. [65]

The overall stability of the armour layer is quantified by the stability number, N_s, using Equation 4.3. According to Rock Manual [65], structures with large armour units are represented by a small N_s. For a conventional rubble mound breakwater classification, a typical range of the value for N_s is from 1 to 4 [65].

$$N_s = \frac{H_s}{\Delta D_n} \tag{4.3}$$

Where:

H_s : Significant wave height at the toe $[\mathrm{m}]$;
Δ : Relative density $[\mathrm{kg/m^3}]$;
D_n : Nominal diameter $[\mathrm{m}]$

4.1.3. Failure mechanisms

In this section, a brief analysis of the possible failure mechanisms is presented. This analysis is fundamental for ensuring structural integrity and supporting effective designs. Additionally, this section aims to explain the influence of specific parameters on the design process. Finally, this section summarizes all relevant failure mechanisms. A more thorough analysis is located in Appendix D, which covers also the less relevant failure mechanisms and goes into the choices and assumptions made in the analysis.

Failure can occur after trespassing two types of limits, namely the SLS and ULS are taken into account. SLS refers to the performance of the structure under normal conditions and outlines the essential function. Exceeding the SLS indicates that the structure is not operating as planned, even though it might not result in damage or failure, e.g. too much overtopping that could damage the vessels in the port while the breakwater is not damaged. ULS refers to a structure's capacity to withstand extreme loading conditions. The structure may get damaged or even collapse if the ULS is exceeded.

The Rock Manual [65] introduces nine different types of Failure mechanisms. An analysis on the failure mechanism is conducted and is displayed in Appendix D. Table 4.1 summarizes the relevant failure mechanism for this project and displays the according criteria for SLS and ULS.

Table 4.1: Failure mechanisms overview

Failure mechanism	Limit state	Description	Criterium	Return period
Overtopping	ULS	No damage to breakwater	$q = 10\,\mathrm{l/m/s}$	100 years
	SLS	No damage to vessel	$q = 1\,\mathrm{l/m/s}$	1 year
Rock stability	ULS	Intermediate damage	$D_{15,\mathrm{f}}/D_{15,\mathrm{b}} < 5$	100 years
	SLS	Start of damage	$D_{15,\mathrm{f}}/D_{15,\mathrm{b}} < 2$	1 year
Armour stability	ULS	No damage	$N_{od} = 0$	100 years
	SLS	No damage	$N_{od} = 0$	1 year
Toe stability	ULS	Acceptable damage	$N_{od} = 2$	100 years
	SLS	Almost no damage	$N_{od} = 0.5$	1 year
Migration of sublayers	ULS	No erosion of sublayers	$D_{15,\mathrm{b}}/D_{15,\mathrm{f}} < 1$	100 years
Transmission	SLS	Limited wave height in port	N/A	1 year

4.2. Hydrodynamical analysis

The goal of the hydrodynamic analysis is to gain insight into the wind and wave climate along the coast of Puerto Rawson. This analysis is based on ERA5-data, covering the period from 1993 to 2023 (Subsection 4.2.1). The wind and wave analysis provide an understanding of the region's hydrodynamical climate. Next, an Extreme Value Analysis (EVA) is performed to assess extreme wave conditions. Finally, the tidal regime, wind set-up, and sea-level rise are considered in the water level analysis.

Previous studies on the coast of Playa Unión and Puerto Rawson have been done. One of the most recent studies was done by the National University of Córdoba in 2022. The aim of the Córdoba research was to analyze the current situation of Playa Unión and evaluate the key physical processes involved in the coastal dynamics. It proposed short- and medium-term measures to minimize the effects of local and general erosion in the area. This research conducted a statistical analysis using ERA5-data 1990 to 2020 and defining extreme events for various return periods [22].

Another study was done by engineering consultancy firm Serman, by order of the local contracter Industrias Bass. This research aims to evaluate, from a nautical perspective, the modifications in the access channel and port area that would be necessary for future feeder-type container ships to enter the port [67]. For the wave climate, the firm relied on a a research of *Instituto Nacional del Agua* (INA) of 2009. The data used by this research ranged from a period from 01/01/1996 to 31/12/2005, using ARGOS data [6].

As a hydrodynamical analysis was done in both researches, they serve as comparison studies for this analysis. The data collection locations from the Córdoba and INA research are shown in Figure 4.2. The complete hydrodynamical analysis can be found in Appendix E.

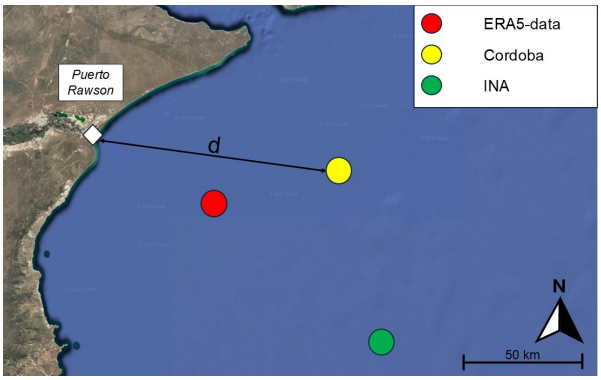


Figure 4.2: Locations of data sources from recent studies/current study

Table 4.2: Overview of researches and used data for hydrodynamic analyses

Research	d [km]	Data source	Data period
Córdoba	90	ERA5	1990-2020
INA	127	ARGOS	1996-2005
MDP	49	ERA5	1993-2023

4.2.1. General information data

The ERA5-dataset is produced by the Copernicus Climate Change Service at the European Centre for Medium-Range Weather Forecasts (ECMWF). It combines a variety of observations from satellites and weather stations with numerical weather predictions, and offers hourly estimates of climate variables for the atmosphere, land, and oceans. Covering the period from 1940 to the present, the ERA5-dataset provides global coverage on a 31 km grid [31]. The retrieved dataset is 30 years, starting at 01/01/1993 00:00 until 12/12/2023 23:00. The retrieved variables are given in Table E.1. The location from which the ERA5-data is extracted (Lat: 43°30'00.0"S, Long: 64°30'00.0"W) is visualized in Figure 4.2. Although every model has inherent assumptions and uncertainties, ERA5 offers a highly detailed and comprehensive dataset. However, this analysis uses a large dataset, which helps to partially mitigate the impact of uncertainties.

An important aspect of ERA5-data and the following analyses is that wind and wave directions follow the nautical convention. This means that the direction is specified as the point from which the wind or waves originate, measured clockwise from the North (N = 0 °or 360 °, E = 90 °, S = 180 °, W = 270 °).

4.2.2. Wind analysis

In this section, a wind analysis is conducted at the offshore location using the previous defined ERA5-data. The objective of this analysis is to gain insights into the wind's magnitude, direction, and general patterns. The data provides the u- and v-components of the wind, which represent wind velocities 10 meters above the water surface. It is assumed that these wind speeds approximate those directly above the waves, though in reality, the magnitude is reduced due to surface friction and turbulence effects near the water surface. To determine the total wind speed (w_{10}) and direction (θ_{wind}), the Pythagorean theorem was applied to the u- and v-components of the wind. The data was systematically analysed using the following steps: statistical analysis, timeseries computation, windrose analysis, seasonal analysis, and long-term trend analysis. The complete wind analysis is provided in section E.1, while the most important results are provided in this section.

Table 4.3: Statistical overview of wind magnitude (w_{10})

Statistics	mean	std	min.	25%	50%	75%	max.
W_{10} [m/s]	7.51	3.14	0.03	5.23	7.41	9.68	23.64

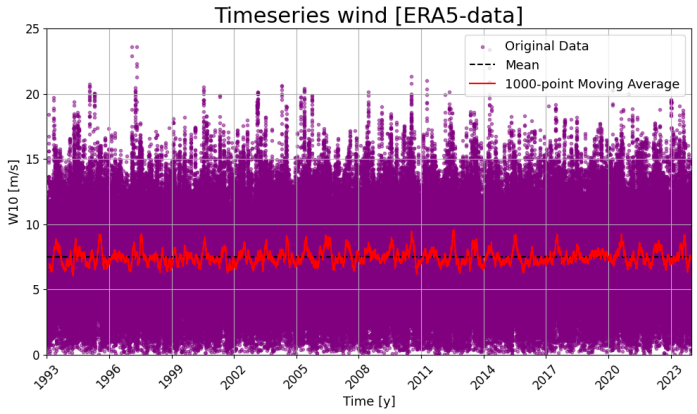


Figure 4.3: Timeseries of w_{10} over 30 years, featuring the mean and 1000-point moving average.

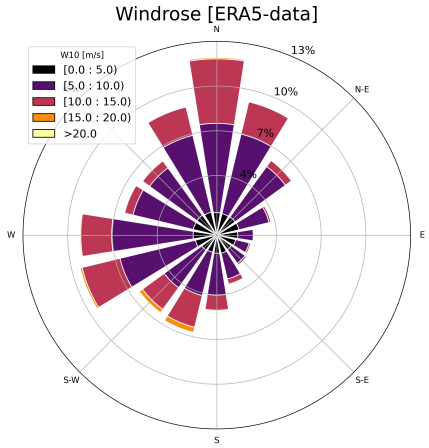


Figure 4.4: Windrose illustrating wind speed, direction, and frequency

The mean wind speed is presented in Table 4.4 and illustrated in Figure 4.3, which also incorporates a moving average. This moving average serves as an initial indicator for the trend analysis revealing that, aside from the oscillatory patterns indicative of seasonal variations, there is no long-term trend. In Figure 4.4, the wind direction ranges from SSW to NNE, dominated by wind from W and N. This observation is consistent with windroses from Córdoba, INA, as well as findings from field observations, all indicating a strong local offshore wind. Furthermore, by plotting w_{10} over θ_{wind}, valuable insights on the direction of the wind (and its maxima) are obtained in (Figure E.1b). It is concluded that (almost) all w_{10} are larger than 18 $[\mathrm{m/s}]$ come from S to SE. Apparently, the wind predominantly originates from land, during extreme conditions or storms, the wind shifts to originate from sea, particularly from the S to SE direction. A trend analysis that is conducted showed no trends over the 30 years of data. A similar analysis is conducted to assess differences in wind climate between the seasons. Apart from higher eastern wind-speeds during winter, no significant differences w found (see Table E.7).

4.2.3. Wave analysis

The objective of this analysis is to gain insights into the wave climate offshore near Puerto Rawson. The ERA5-data offered different types of data on wave height: the Significant height of combined wind waves and swell (SWH), the significant Height of Wind Waves (SHWW), and the Significant Height of Total Swell (SHTS). To understand the contributions of swell and wind to the total significant wave height, the wave analysis is threefold. The complete wave analysis can be found in section E.2, while the most important results are given in this section.

Table 4.5: Statistical overview of SWH, SHWWW, SHTS, and T_p

Statistics	units	mean	std	min.	25 %	50 %	75 %	max.
SWH	[m]	1.40	0.63	0.32	0.97	1.26	1.68	7.17
SHWW	[m]	0.79	0.72	0.00	0.24	0.60	1.15	6.88
SHTS	[m]	1.01	0.44	0.05	0.71	0.93	1.22	4.60
T_p	[s]	7.83	2.35	2.62	5.81	7.71	9.75	18.87

Table 4.6 shows that the SWH parameter results in the largest wave heights. The maximum wave height for SHTS is significantly smaller than SWH and SHWW. Figure 4.5 shows the timeseries of SWH over 30 years, while Figure 4.6 shows SWH over the wave direction (θ_{waves}). The moving average shows seasonal fluctuation, long term trend, which also applies for SHTS and SHWW. For SWH, extreme wave heights predominantly approach from SE to SSW, from SE to S for SHTS, and from SSE to SW for SHWW. This supports the observation in Subsection 4.2.2 that, while winds usually originate from land, they shift to come from the sea during storms or extreme conditions. As a result, extreme wind driven waves (SHWW) tend to come from the south during storm events.

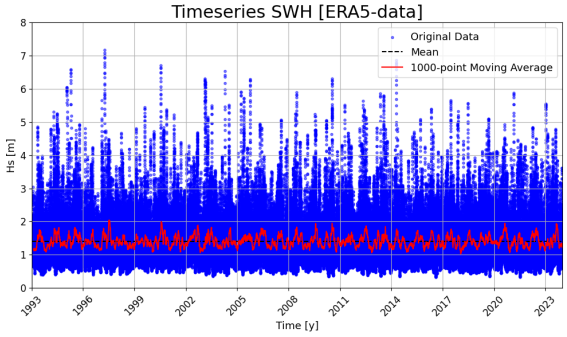


Figure 4.5: Timeseries of SWH over 30 years, featuring the mean and 1000-point moving average.

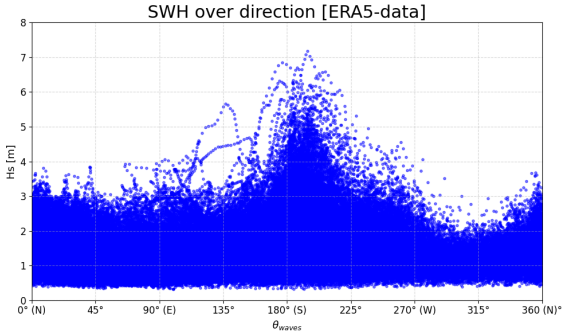
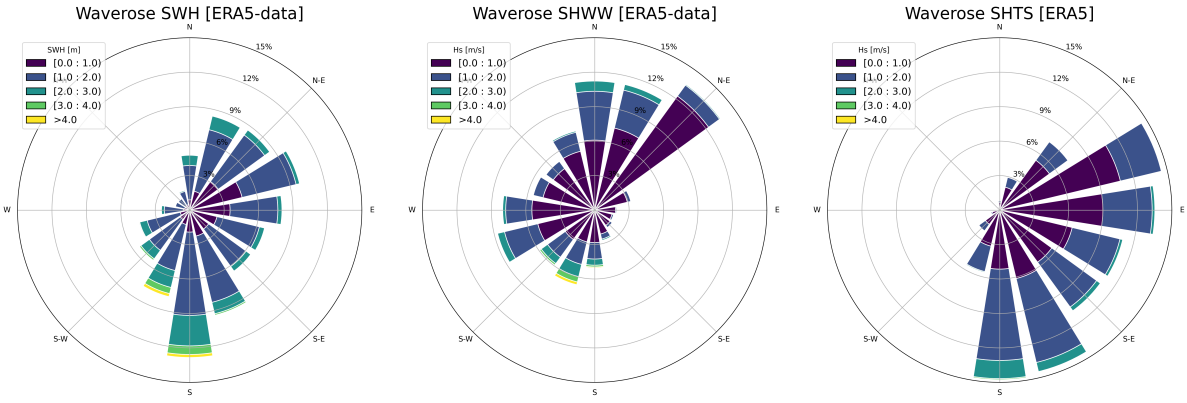


Figure 4.6: Plot of SWH over direction (θ_{waves}) the wave originate from, using the ERA5-data.

The waveroses for SWH, SHWW, and SHTS are shown in Figure 4.7. This gives a good impression of the build up of SWH. The waveroses of SHWW (b) and SHTS (c) are completely opposite in direction. The waverose of SHWW clearly indicates the dominant offshore wind direction, comparable to the windrose (Figure 4.4). The waverose of SHTS shows the incoming direction of swell waves from open sea, ranging from ENE to S. For each parameter, a trend- and seasonal analysis is performed, which showed no significant differences over time or between seasons.



(a) Waverose SWH **(b)** Waverose SHWW **(c)** Waverose SHTS

Figure 4.7: Waveroses for SWH (a), SHWW (b), and SHTS (c) derived from ERA5-data (1993-2023). Each waverose illustrates the wave height, wave direction and frequency.

4.2.4. Extreme value analysis

An extreme value analysis (EVA) is performed on all three wave heights (SWH, SHWW, SHTS) to find the extreme wave heights with corresponding return periods. These values are used as input for the SWAN model (Chapter 5) to find the extreme nearshore wave heights after the transformation of the waves over the bathymetry. For each parameter, the complete EVA can be found in section E.3. In this section, the most relevant conclusions and results are given.

For the EVA, both Peak over Threshold (POT) and Block Maxima (BM) are viable approaches to identify extremes. Given the size and the long timespan of the data, the POT approach is used as it allows to extract multiple extremes in a timespan (e.g. a month). The extremes selected by the POT-method are visualized in Figure 4.8, ranging from SWH = 4.10 m to SWH = 7.17 m. A declustering time of 12 hours is used, as it effectively separates individual extreme storms, ensuring statistical independence. The threshold is optimized using the Chi-Square test. Virtually all extremes come from the SE to SSW. After fitting a General Pareto Distribution (GPD) (which is complementary to the POT method) over the extreme wave heights and validating the fit, the return period over wave height is plotted (Figure 4.9). The bootstrap method is used to compute the 95 % confidence interval.

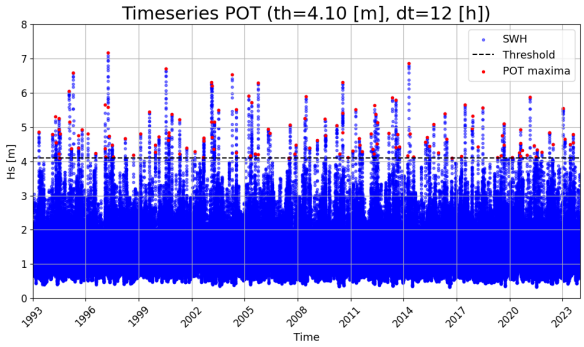


Figure 4.8: Timeseries of SWH. The POT method identified extreme events, indicated in the figure. The threshold is 4.10 m and the declustering time is 12 hours.

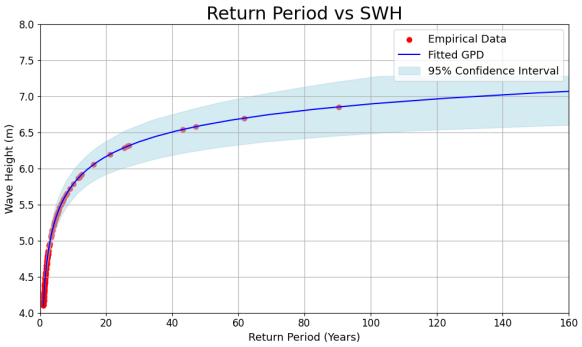


Figure 4.9: Return period plot of SWH, showing data and the fitted GPD curve with a 95 % confidence interval. This illustrates the SWH values associated with RT.

After conducting the EVA on SWH, correlations are assessed between extreme events and other variables, including T_p, w_{10}, and θ_{wind}. During storm events, wind and wave directions are found to be closely aligned, i.e. coming from the same direction. Linear regression provides a good fit for SWH against T_p and w_{10}. This enables the estimation of corresponding values for these parameters at return periods, presented in Table 4.10. Eventually, the EVA of SWH results in the largest extremes. Based on the wave analysis, the storms are assumed to originate from SE to SSW.

Table 4.7: Significant wave heights and corresponding return periods based on extreme value analysis.

Return Period [y]	SWH [m]	SHWW [m]	SHTS [m]
5	5.35	5.03	3.25
10	5.78	5.49	3.44
50	6.61	6.40	3.85
75	6.78	6.60	3.95
100	6.90	6.74	4.01
150	7.05	6.91	4.10

Table 4.9: Wave parameters and corresponding return periods based on extreme value analysis.

Return Period SWH [y]	H_s [m]	T_p [s]	w_{10} [m/s]
5	5.35	10.33	17.63
10	5.78	10.65	18.44
50	6.61	11.24	19.97
75	6.78	11.37	20.29
100	6.90	11.45	20.51
150	7.05	11.56	20.79

4.2.5. Water level analysis

A water level analysis determines the relevant water heights under different conditions. The SHN, established by the *Servicio de Hidrografia Naval*, serves as a standard reference level for nautical safety in Argentina. This reference corresponds to the *reduction plane*, or the lower limit of the mean low tide [50].

The tidal regime along this section of the Argentine coast is semi-diurnal [26], meaning there are two high tides and two low tides each day. The tidal amplitude fluctuates between 1 and 2.5 meters [28]. The most important tidal levels are listed in Table 4.11 [28] [67].

For regular conditions, the Mean Sea Level (MSL) value is used. However, when assuming extreme conditions, this level is insufficient. The selected design high water level for extreme conditions comprises three components, the Mean High Water level (MHW), wind set-up, and Sea Level Rise (SLR). These values are +4.52 m SHN (MHW), 0.3 m, and 0.36 m (SLR), respectively. Combining these components results in a design high water level of +5.18 m SHN, which is used as extreme condition input for the wave transformation model. This approach assumes the simultaneous occurrence of these three factors, adopting a conservative stance in the design process.

The SLR value of 0.36 m is based on the predicted SSP2-4.5 climate scenario for 2080, given a 50-year design life [49]. While this scenario is deemed appropriate for the current design stage, it does not involve inherent uncertainties. Figure 4.10 illustrates three climate scenarios and the corresponding SLR projections for the Rawson area. In future use of this water level analysis, it is recommended to reassess the selected SLR value. Finally, it is noted that wave set-up and set-down near the breakwater have not yet been included in this calculation, as these effects can only be determined after running a wave transformation model.

Table 4.11: Tidal levels for Puerto Rawson [28] [67]

Tidal abbreviation	LAT	MLW	MSL	MHW	HAT
Level in m SHN	+0.04	+0.96	+2.75	+4.52	+5.40

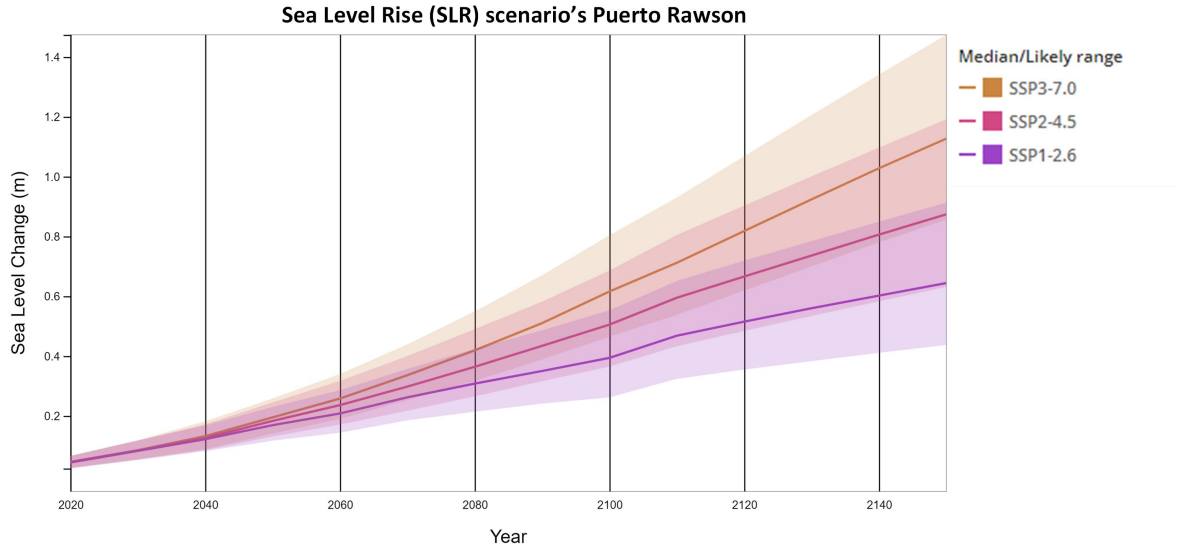


Figure 4.10: SLR change in water level under different scenarios, near Rawson [49]

4.3. Self-Organizing Maps for regular conditions

The objective of this analysis is to reduce the dataset (30 years of hourly wind and wave data) to ~10 conditions that represent the data. These are considered as representative regular wave conditions, and are used for assessing sediment transport for each breakwater concept (chapter 7). Neural networks and clustering algorithms are used to achieve this. To increase computational efficiency, the dataset is narrowed down to the most relevant parameters for sediment computation: H_s, T_p, and θ_{waves}. The longshore sediment transportation is discussed in chapter 5.

Neural networks and k-means clustering are effective tools for analysing large datasets. These machine learning algorithms provide the model with flexibility by allowing it to learn from the data itself, resulting in an accurate representation of clusters [40]. This approach provides a better representation of the data than by simply selecting average conditions or retrieving random conditions. The dataset is first represented using a neural network of 400 neurons, as shown in Figure 4.11. After representing the data with the neurons, k-means clustering is applied to the neurons, resulting in 12 combinations of wave conditions (Figure 4.13). This approach is preferred since k-means is sensitive to outliers and performs better when clusters are similar in size [39]. The results are provided in this section, with the complete analysis in Appendix section E.4.

4.3.1. Neural network (n=400)

For the neural network application, the Python library MiniSom was used. This unsupervised neural network is set up with a 20 by 20 grid, learning rate, and a Gaussian neighbourhood function [36]. The network is trained iteratively, resulting in 383 active neurons and 17 empty neurons. Empty neurons are neurons that did not win any data point during the training process. After a statistical analysis, 5 neurons are discarded due to unrealistically high variance (std_θ > 100°). In the end, the neural network results in 378 neurons, representing an equal amount of unique combinations of H_s, T_p, and θ_{waves}. The neurons are visualized in Figure 4.11. The frequency, indicated by a background blue gradient, represents the number of data points each neuron won. However, a higher frequency does not necessarily mean these are *more representative* regular conditions. Counter-intuitively, conditions with the highest frequency correspond to outlier regions in the data, such as waves coming from the west. Generally in the figure, one can see the dominant wave direction of wave coming from E to S. Furthermore, as noted in the wave analysis section, the neural network highlights that storms originate from the SE to SSW directions, as indicated by the cells with filled black circles.

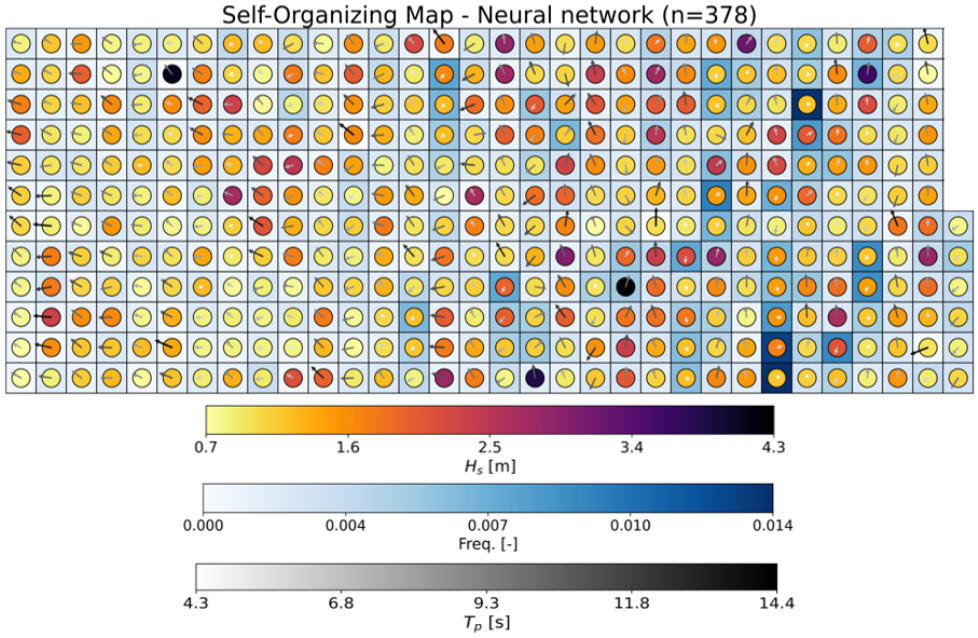


Figure 4.11: Self-Organizing Map (SOM) representing 378 wave conditions analysed through a neural network. Each cell illustrates the relationship between H_s, T_p, θ, and frequency (*f*). Colour gradients indicate the respective values of H_s, *f*, and T_p, allowing for a visual interpretation of the clustering and distribution of wave conditions.

4.3.2. K-means (k=12)

Ideally, all 378 conditions computed by the neural network are used in the model to evaluate sediment transport. This is however not possible due to time constraints. By applying k-means, these 378 neurons are grouped into 12 clusters (*k* = 12) based on similarities in H_s, T_p, and θ_{waves}. The objective of k-means is to minimize the variance within clusters, i.e. minimizing the distance between points within the same cluster [74]. K-means is a fast and straightforward algorithm, but it is sensitive to outliers which can skew results. This effect is reduced by first applying the neural network on the dataset. Alternative methods such as Density-Based Spatial Clustering of Application with Noise (DBSCAN), Gaussian Mixture Model (GMM), and agglomerative clusters are also tested. Despite these tests, k-means produced the best visual representation of the 378 neurons. The k-clusters and the neurons each cluster represents are visualized in Figure 4.12.

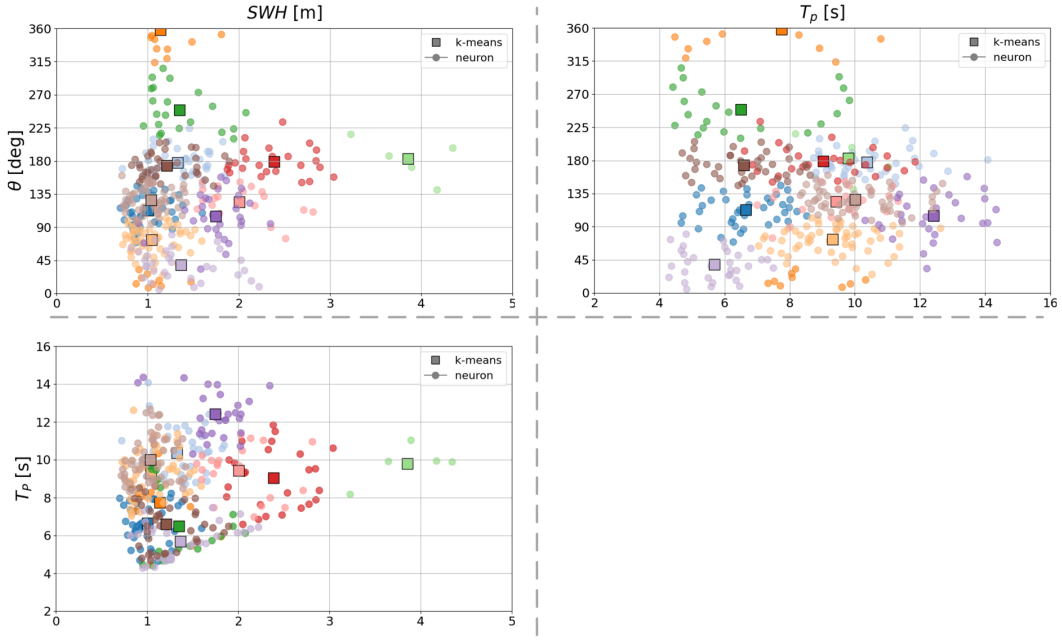


Figure 4.12: Scatter plots for each combination of variables (H_s, T_p, θ). The 12 clusters are illustrated with squares, with all neurons belonging to a cluster coloured identically.

The 12 clusters are shown in Figure 4.13, illustrating regular conditions coming from S to ENE. The exact values for H_s, T_p, θ, and *f*, are given in the Table E.22. It is notable that cell VII represents swell waves, characterized by a high peak period (T_p), arriving from the open sea. Among the 12 conditions, two clusters are highlighted in red: cell XII represents extreme wave conditions coming from the south, while cell IX indicates offshore wind-driven waves heading east, which do not reach Puerto Rawson. Contrary to the neural network, the cluster frequency does reflect the likelihood of occurrence. Lower frequencies indicate rare events, while higher frequencies represent more regular conditions.

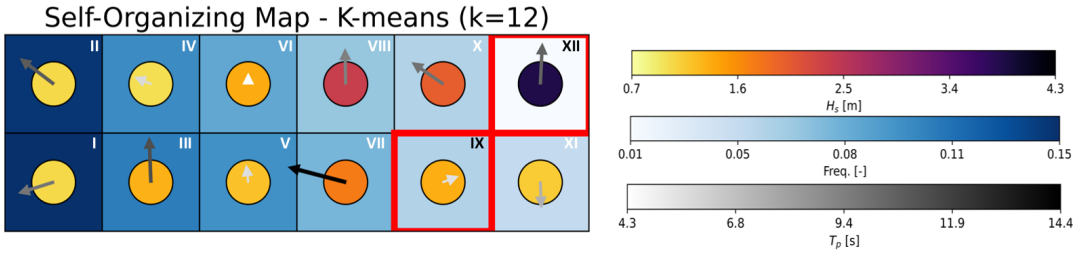


Figure 4.13: Self-Organizing Map (SOM) representing 12 wave conditions analysed through k-means. Each cell illustrates the relationship between H_s, T_p, θ, and frequency (*f*). Colour gradients indicate the respective values of H_s, *f*, and T_p, allowing for a visual interpretation of the clustering and distribution of wave conditions.

4.4. Structural analysis

In this section, a structural analysis is conducted on the current cement mixture of the Accropodes. By exposing the potential structural weaknesses of the current mixture, a new mixture is proposed, based on research. Granulometry analyses and sclerometer tests aid in the determination of the strengths and weaknesses of not only the current, but also of the proposed mixture.

4.4.1. Structural technical reports

Former concrete and construction materials professor Ing. L. Cotti de La Lastra conducted research into the use of porphyry quarry waste as an aggregate for concrete. In her research, Mrs. Cotti proposed a cement mixture, using waste material from porphyry quarrying. With slump tests, compressive strength tests, ASR tests and more, the mixture is in accordance with the Argentinian concrete standards [42]. Next to that, the collection of this waste is a far more sustainable process, than the collection of pebbles from the banks of Chubut river. Finally, the study compares these river pebbles to the porphyry waste aggregates, on their physical properties and granulometry in several cement mixtures. The research is summarized in Appendix F [23].

The Port Directorate released documents regarding the current breakwater (2002-2004). These documents contain information about the cement mixture used, including its granulometry. Furthermore, the complete build-up of the breakwater is provided, including, but not limited to, Accropode volumes and drawings [62].

Dragados y Obras Portuarias S.A. (DyOPSA), the company that was responsible for the construction of the breakwater, instructed both Instituto Technológico del Hormigon S.A. (ITH) and Laboratorio de Investigaciones y Ensayos Viales (LABIEVI) of the UNPSJB to conduct studies and experiments regarding the cement mixture (2001). The results are found in Appendix G [59].

4.4.2. Initial specifications

To gain an understanding of the concrete used in the Accropodes of the current breakwater, it is essential to elaborate on its composition and initial specifications. This subsection offers an overview of the mix proportions and physical properties. By examining these aspects, the concrete characteristics are understood.

The mix proportions and physical properties of the mixture used for construction are given in Table 4.12.

Table 4.12: Some properties of the current cement mixture

Property / content	Unit	Value
w/c ratio	[−]	0.42
Total water content	[L]	160
CPP	[kg]	380
Natural fine aggregate, Sand Chubut river	[kg]	740
Natural coarse aggregate, Pebble Chubut river	[kg]	1090
Plasticizer	[L]	1.13
28 days compressive strength	[MPa]	33.5
Slump	[cm]	5.0
ASR, accelerated mortar bar expansion test	[%]	0.086
Wet density	[kg/m^3]	2408
Dry density	[kg/m^3]	2288

In Figure 3.8, the current coarse aggregate is exposed. This aggregate is too large to use effectively in a cement mixture. To get a clear and concise answer to this hypothesis, research into the granulometry of the current concrete mixture is to be conducted. The granulometry is compared to the design criteria as stated in the Betonpocket [15] and the criteria given in NEN-EN-ISO 14688-2:2019 [57]. Appendix H

contains all the granulometry data of the current mixture. In the same appendix, the data is reviewed and processed accordingly.

Figure 4.14 shows the current granulometry data. The coloured lines depict all of the 64 granulometry samples. On the x-axis are the opening sizes (apertures) of the sieves used in millimetres, based on a log-scale. On the y-axis, the amount of aggregate that has passed said sieves is shown in percentages. Using this information and the shape of the diagrams, one can determine what kind of aggregate has passed through the sieves, i.e. the aggregate distribution.

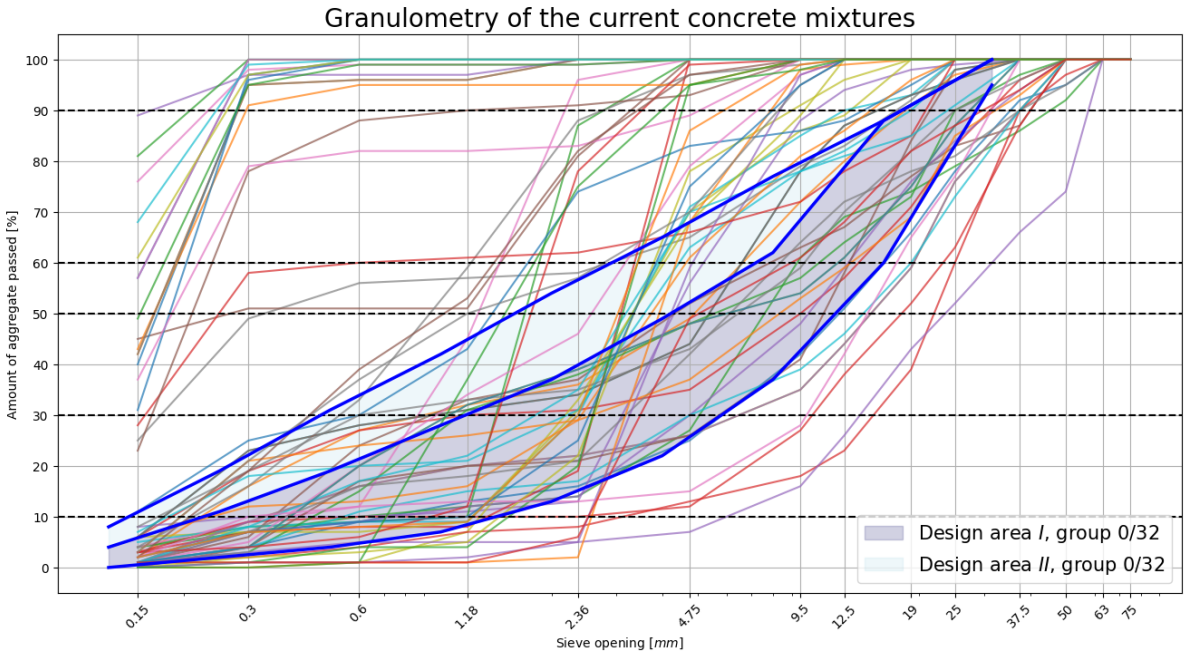


Figure 4.14: Current granulometry. There are 64 thin coloured lines, each representing a sample. The thick blue lines represent the boundaries of the design areas [15]. The dark blue and light blue areas respectively represent the design areas I and II, in which a cement mixture is optimally designed for workability and water requirements.

Table 2 from NEN-EN-ISO 14688-2:2019 gives information on the shape and grading of the distribution, based on C_U and C_C. These results are found in Table 4.13. The table indicates that only 4 of the 64 samples are well graded, whereas 27 samples did not fit any distribution at all.

Table 4.13: Summary of sample distribution

Type of distribution	Times found
Uniformly graded	19
Badly graded	4
Moderately graded	3
Well graded	4
Discontinuously graded	7
NONE	27

4.4.3. Rebound number tests

Next to the granulometry analysis, rebound number tests are also carried out. This test makes use of the Schmidthammer (or sclerometer, see Figure 4.15) which has a spring-loaded hammer mass, which, when released, strikes a plunger in contact with the surface to be tested. The mass rebounds, and the distance from the plunger to the mass is measured, which is the so-called rebound number.

This rebound number indicates the residual strength of the surface of the concrete specimen. Generally speaking, the lower the rebound number, the lower the compressive strength, and vice versa.

The same test locations are used as stated in Subsection 3.2.1 and Appendix C. According to the NEN-EN 12504-2:2021, the surface area of the concrete test subject is to be free of water, dust, and other loose materials for a sclerometer test. The Accropodes at the bottom of the breakwater only showed up at low water level for a short while. Next to that, these units were covered in vegetation, which could not be cleaned in time before flood. Therefore, the Accropodes in zone C were not tested. This means that there are 14 test locations left for the sclerometer tests, all in accordance with the code [53]. Each Accropode was tested on two different positions, which are to be called the 'leg' and the 'body', as shown in Figure 4.16. Appendix I contains all of the sclerometer test results; which are summarized in Table 4.14.



Figure 4.15: A sclerometer.

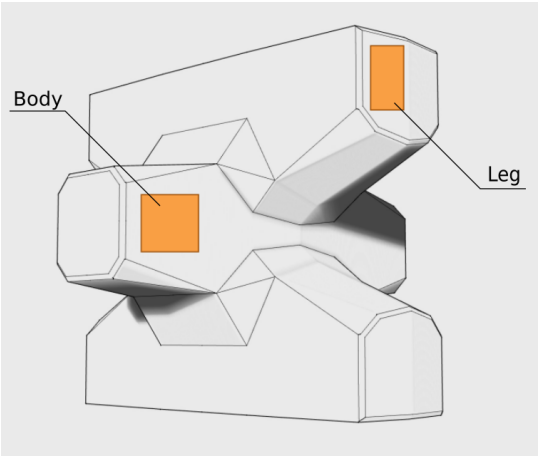


Figure 4.16: Test positions on an Accropode, schematic [51].

Table 4.14: Sclerometer tests, summarized

Accropode location	Test location on Accropode	Median of the rebound number [–]
Zone A	Body	46
Zone A	Leg	47
Zone B	Body	43
Zone B	Leg	45

From Table 4.14, one can see that the median rebound numbers of zone A are a little higher than those of zone B. This difference is explained by the fact that the Accropodes in zone A are more prone to carbonation, which has a strong influence on the rebound number. This number could be higher by up to 50 %, compared to uncarbonated concrete [5]. Carbonation can only take place when the concrete is exposed directly to carbon-dioxide. When concrete is underwater, this cannot happen, and thus the rebound number is to be lower as well.

Regarding the age and carbonation of said Accropodes, there is evidence that the rebound number is not appropriate to assess the (residual) strength of the concrete. The Accropodes were built and placed in the years 2001, 2002 and 2003, which means that the units are over 20 years old [62]. In these 20+ years, the concrete has significantly affected by salt, water, wind, carbon-dioxide, and temperature changes. For this reason, the concrete is only tested for its homogeneity [19][20][24].

Although the rebound numbers are a bit higher in zone A than they are in zone B, they do not differ that much from one another, and the values for the body and the leg are similarly close. Concluding, the concrete is still homogeneous.

4.4.4. New cement mixture

The observed degradation of the current breakwater, combined with the aspiration for creating a more sustainable breakwater, underscores the necessity of a new proposed mix design. Appendix F gives detailed information on studies conducted by Ing. L. Cotti de la Lastra [23]. In Section 8.9, a comparison with the current mix design based on physical performance is provided, while Chapter 9 assesses its environmental impact through a comparable LCA.

The proposed mix design integrates porphyry quarry waste as the coarse aggregate, drawing on data that highlights its physical properties in concrete, as well as its reduced environmental impact compared to the use of river pebbles. The proposed mixture largely maintains the composition of the current mix while integrating this more sustainable aggregate. The granulometry of these mixtures is also examined, to ensure its viability.

In Table 4.15, the mix proportions and physical properties of the best-performing cement mixture are summarised. The final granulometry of the mixture is shown in Figure 4.17. From this figure, it is clear that this is a well graded and balanced mixture: the red line, which represent the proposed mixture, is almost fully encompassed by design area I. Furthermore, when using C_U, C_C, and the same distribution criteria as for the current mixture's granulometry, the mixture classifies as 'Well graded'.

Table 4.15: Some properties of Mrs. Cotti's cement mixture

Property / content	Unit	Value
w/c ratio	[−]	0.45
Total water content	[L]	157.5
CPP	[kg]	350
Natural fine aggregate, Aridos Fontana	[kg]	804
Natural coarse aggregate, porphyry waste	[kg]	955
Plasticizer	[%]	0.7
Air entrapment	[%]	0.05
28 days compressive strength	[MPa]	41
Slump	[cm]	11.0
ASR, accelerated mortar bar expansion test	[%]	0.10
Wet density	[kg/m^3]	2345
Dry density	[kg/m^3]	2228

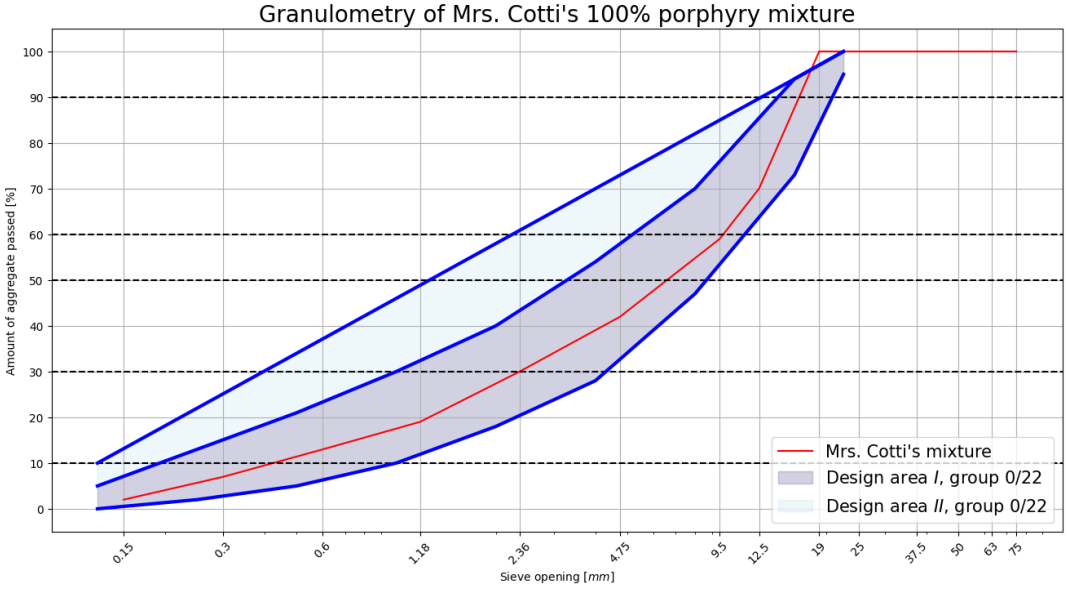


Figure 4.17: Granulometry of Mrs. Cotti's mixture. The red line represents the mixture, whereas the dark- and light blue areas again represent the design areas, as stated in the Betonpocket [15].

5

Wave model and sediment transport

Coastal modelling is a powerful tool for analysing and predicting how interventions, such as breakwaters, influence coastal dynamics. Coastal modelling is also used for transforming hydrodynamic conditions from offshore to nearshore.

In this chapter, the model selected for this study is discussed. It explains how the coast of Puerto Rawson is implemented in the model. Subsequently, the model configurations are discussed. An explanation of possible outcome parameters follows, after which sediment transport calculations are explained. Finally, reference runs are conducted and analysed to gain insight into the erosion problem in the study area.

Inner port hydrodynamics fall outside the scope of this research. Additionally, sediment discharge from the Chubut River is not accounted for in this study. While both factors influence coastal development near Rawson, incorporating them into the wave model and sediment transport calculations increases the complexity beyond the scope of this project. Particularly given the limited time frame of this research.

5.1. Model type

Selecting an appropriate model type is crucial for accurately analysing wave transformation, coastal erosion, and sediment transport. The use of models in this area is restricted due to limited and sometimes unreliable data on hydrodynamics, topography, and morphodynamics. Coastal models vary widely in complexity and application, with some more suited for certain data availability or specific environmental scenarios.

Section J describes multiple possible models used for wave transformations and sediment transport calibrations. In this report, the SWAN (Simulating WAves Nearshore) model is used. SWAN is a phased averaged wave model, solving the wave energy balance equation. The main advantages of SWAN the model are described in Section J.1. SWAN is used in a stationary 2D horizontal (2DH) mode, due to the lack of continuous hydrodynamic data, which prevents the use of non-stationary simulations. The model requires a well-defined bathymetric grid, upon which the hydrodynamic boundary conditions (wave height, period, and direction) are applied. These conditions are transformed across the computational grid, enabling output at any point within the model domain. The use of SWAN provides a comprehensive understanding of wave behaviour along the coast of Puerto Rawson.

The strength in handling complex bathymetries and computational efficiency of SWAN in transforming offshore wave conditions to nearshore, makes SWAN the ideal choice for the scope of this study. Furthermore, the capability to operate in nested grid setups provides enhanced resolution in areas of interest. This is particularly valuable, as wave transformations near structures require precise calculations (in this case breakwaters).

5.2. From site to model

After selecting SWAN as the model for Puerto Rawson, the next step is to integrate the site data into the model. The specific attributes of the site are described in Section 3.1. Upcoming section discusses the build-up of the input bathymetry and its integration within the computational grid. The implementation of the boundary conditions is explained in Section J.2.

5.2.1. Bathymetry

Bathymetric surveys of the foreshore at Puerto Rawson and Playa Unión were conducted in 2010 and 2014. In 2010, multiple cross-sections were taken both north and south of the harbour entrance. Additional surveys in 2014 included the inner port and portions of the existing breakwater. The surveys produced a dataset of coordinates and corresponding bottom depths in SHN, forming the basis for the bathymetric profile used in the SWAN model. However, the combined surveys cover only approximately 14 km of coastline, with a maximum offshore reach of 5 km. Figure 5.1 shows the location of these surveys relative to Puerto Rawson.

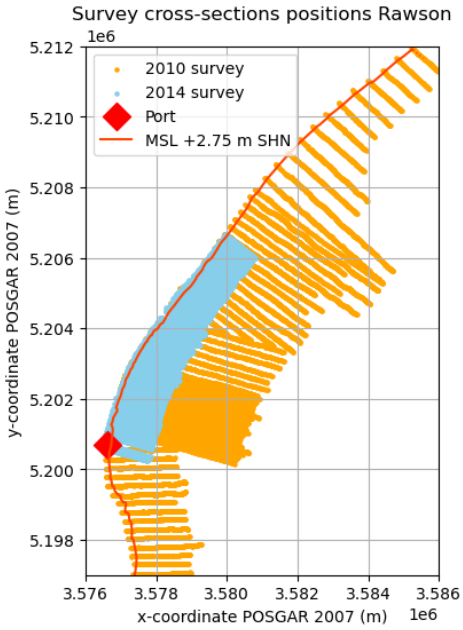


Figure 5.1: Survey points from 2010 and 2014 at Puerto Rawson

For accurate wave transformation modelling from offshore to nearshore conditions, a larger area is needed. Therefore, the survey data was supplemented with a GEBCO gridded bathymetry dataset. GEBCO is a global terrain model with a 15 arc-second grid interval (equivalent to 330 m at Puerto Rawon) [35]. The GEBCO dataset is merged with the survey results while ensuring consistency in coordinate and reference systems (SHN). The local coordinate system used is the EPSG:5345 POSGAR 2007 / Argentina 3. This system is used for engineering purposes and topographic mapping in Argentina [33]. After aligning the GEBCO data with the SHN reference system, a new bathymetric grid is created with 10 m spacing in both x- and y-directions. The data points are interpolated onto this refined grid, yielding the bathymetry file, illustrated in Figure 5.2. This figure shows the wider area, including the river valley of Chubut, the coastline, the hills in the south-west, and the gently sloping foreshore. The location of Puerto Rawson is again highlighted in this figure. This file serves as the primary input into SWAN, though spatial resolution and computational efficiency considerations are addressed in following sections.

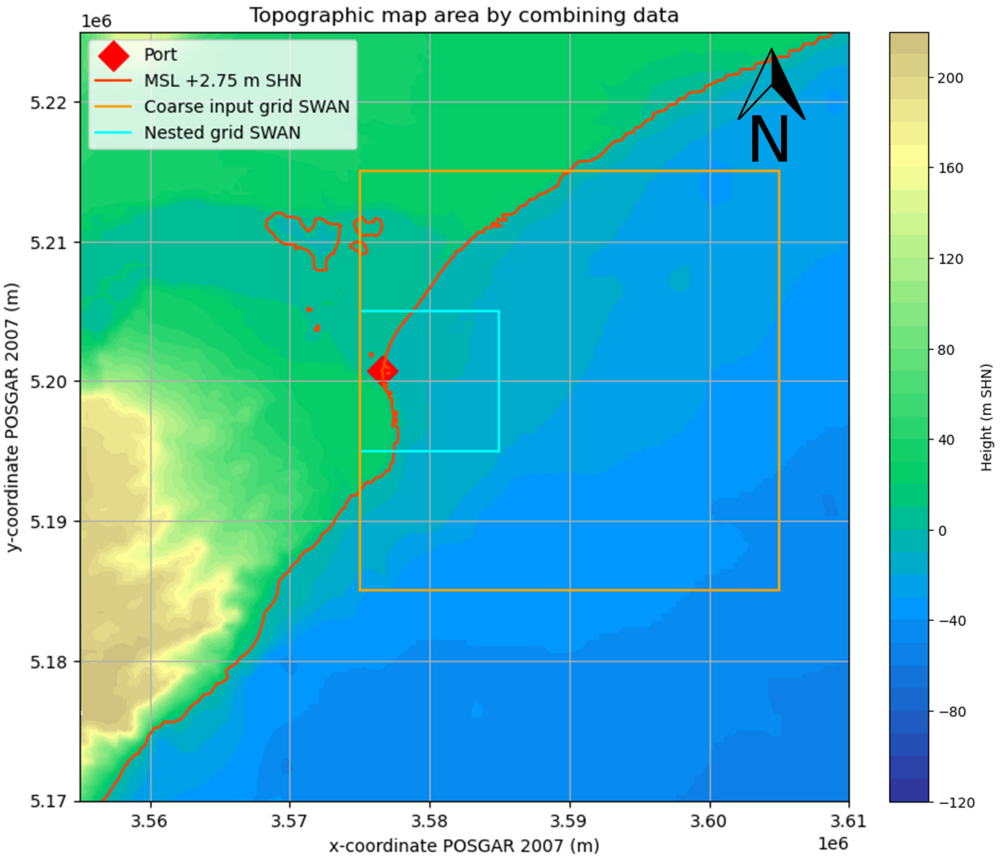


Figure 5.2: Created bathymetry of the area

5.2.2. Coarse and fine grid

Not all bathymetric data shown in Figure 5.2 is required in the SWAN model; including excessive land and sea areas would slow down computations, without improving accuracy. Additionally, memory limitations of SWAN also necessitate careful grid selection to avoid overflow errors. For optimal balance, the input bathymetry is limited to a 30 km by 30 km grid, shown in orange in Figure 5.2. The harbour entrance of Puerto Rawson is located in the middle left of this grid, extending approximately 15 km north and south, and 28 km westward from the input boundary. Using the interpolated bathymetry resolution of 10 m results in 3,000 meshes in both x- and y-directions for the input bathymetry grid.

To optimize computational speed while retaining the necessary level of detail, test runs are conducted, and the nested grid functionality of SWAN is utilized. This technique involves performing two separate SWAN runs: a large coarse grid run, followed by a small fine grid run. The coarse grid output provides boundary conditions for the fine grid, allowing for more detailed output for the latter. In this study, the coarse computational grid covers the orange grid of Figure 5.2 (30 by 30 km). This grid has a resolution of 60 m. The fine grid, shown in light blue in Figure 5.2, spans 10 km by 10 km, with a resolution of 20 m. The results from the fine grid are used for more in-depth wave transformation analyses and sediment transport calculations. The coarse grid only serves as an intermediary step to transform offshore conditions into more detailed nearshore results.

5.3. Model configurations

In Chapter 4, an analysis of both regular and extreme wave and wind conditions is conducted. Apart from these conditions, additional settings and functions within SWAN can be defined, such as quadruplets, triads, and white-capping. This section provides an overview of the selected conditions. Additional applied model settings are discussed in Section J.3.

5.3.1. Normal conditions

Due to time restraints, only 5 of the 10 relevant regular conditions are chosen, based on their frequency of occurrence as described in Section 4.3. The conditions with the highest frequency are selected and listed in Table 5.1. These conditions are run with the same water level, set at MSL +2.75 m SHN, as described in Subsection 4.2.5. Subsection J.3.1 describes more model configurations for the normal conditions. The wave transformations for regular conditions are used to assess longshore sediment transport. However, uncertainties remain in transport computations, as different formulations can yield results that vary significantly in magnitude [16].

Table 5.1: Offshore normal settings used in model runs

Setting	H_s [m]	T_p [s]	Direction [°N]	Simplified Dir
1	1.04	9.31	73	ENE
2	1.04	10.01	127	SE
3	1.33	10.37	178	S
4	1.01	6.66	113	ESE
5	1.21	6.60	173	S

5.3.2. Extreme conditions

Extreme nearshore conditions are needed for dimensioning the breakwater. The extreme offshore conditions (derived in Subsection 4.2.4) are transformed nearshore using SWAN. Extreme values for a 100-year return period are applied. To capture the directional variability of extreme conditions, four primary directions are considered, to determine the orientation that yields the highest wave height at the toe (SSW, S, SSE, SE). Table 5.2 lists the input settings for these simulations, each modelled at the design high water level of +5.18 m SHN as described in Subsection 4.2.5. Wave set-up and set-down are added to the water level post-transformation. Subsection J.3.2 describes more model configurations for the extreme conditions.

Table 5.2: Offshore extreme settings with 100-year return period

Setting	H_s [m]	T_p [s]	w_{10} [m/s]	Direction [°N]	Simplified Dir.
1	6.90	11.45	20.51	202.5	SSW
2	6.90	11.45	20.51	180	S
3	6.90	11.45	20.51	157.5	SSE
4	6.90	11.45	20.51	135	SE

5.4. Output parameters

The SWAN model is now ready for execution. However, post-processing and additional calculations are required for analysis-ready output. This section outlines the essential parameters and describes the sediment transport formulation. The application of the sediment transport formulation is further discussed in Section J.4.

5.4.1. Wave transformations

Relevant SWAN output parameters for this research include water level, water depth, significant wave height, peak period, mean period, and wave direction. These parameters are retrieved as output from SWAN and undergo post-processing. Not all results are relevant or interesting for examination. It is decided for the normal conditions to only analyse the wave heights and wave directions in the small grid, given in Appendix K. This is also done for the extreme conditions and in part of the small grid,

near the port (Appendix L). Moreover, the formally used local coordinate system is rewritten into a more workable coordinate system. For consistency, the same regular grid is used, however, the origin is translated to the bottom right corner of the large coarse grid. Following SWAN results use the revised coordinate system. In this new coordinate definition, Puerto Rawson is located at the coastline between y-coordinates 15000 till 16000.

5.4.2. Sediment transport formulation

Longshore sediment transport is the net movement of sediment, perpendicular to the shoreline [16]. Gradients in this longshore transport drive erosion and sedimentation. For analysing the impact of structures on structural coastal development, longshore coastal sediment transport magnitudes need to be retrieved. SWAN does not directly compute sediment transport, but the output does facilitate sediment transport calculations. Various methods exist for calculating sediment transport, however, not all of them are applicable. In coastal engineering, bulk transport formulations are often used as they are robust, easy to calibrate, and apply [16]. A bulk formulation represents the total longshore sediment transport over the entire breaker zone. The commonly used longshore transport formulation is the CERC formula. It was developed by the Coastal Engineering Research Council, from which the abbreviation originates. The formula was calibrated using prototype and laboratory measurements [16]. The formula gives the bulk longshore transport due to the action of waves, approaching the coast at an angle. Due to the exclusion of tidal currents, of which no data exist in this case, the formulation is well applicable. The most generic form of the CERC formula, as derived by Komar and Inman [45], is shown in Equation 5.1.

$$S = \frac{K}{\rho g (s-1)(1-p)} (E \cdot n \cdot c)_b \cos(\phi_b) \sin(\phi_b) \tag{5.1}$$

Where:

S : the deposited volume of sediment transported $[\mathrm{m}^3/\mathrm{s}]$
ρ : density of the water $[\mathrm{kg}/\mathrm{m}^3]$
g : gravitational acceleration $[\mathrm{m}/\mathrm{s}^2]$
s : the relative density of the sediment ρ_s/ρ $[-]$
p : porosity $[-]$
K : coefficient $[-]$
E : Wave energy $[\mathrm{J}/\mathrm{m}^2]$
n : the ratio between group and phase velocity $[-]$
c : the wave phase velocity $[\mathrm{m}/\mathrm{s}]$
ϕ : the wave angle of incidence $[-]$
b : subscript referring to the outer edge of the breaker zone $[-]$

In the application used in this research, it is more practical to use different wave parameters, as it is hard to pinpoint the edge of the breaker zone. The CERC formulation can be rewritten in deep water wave parameters, when assuming wave refraction over shore-parallel contours [10]. This form is shown in Equation 5.2 [10]. It is noted here, that the sediment properties and densities are all implemented in the K_2 coefficient. Next to that the sediment transport is dependent on the angle of incidence of the waves. When simplifying the formulation and investigating the dependence of sediment transport on offshore wave directions, it has been shown that longshore sediment transport is at a maximum with an offshore wave angle of 43° to the shore normal [16]. The overall relation between bulk longshore transport rates and the deep-water wave angle is known as the (S, ϕ) -curve.

$$Q_s = K_2 H_0^{\frac{12}{5}} T^{\frac{1}{5}} \cos(\phi_0 - \theta)^{\frac{6}{5}} \sin(\phi_0 - \theta) \tag{5.2}$$

Where:

Q_s : volume alongshore sediment transport $[\mathrm{m}^3/\mathrm{s}]$
K_2 : empirical constant $[\mathrm{m}^{3/5}\mathrm{s}^{-6/5}]$
H_0 : deep water wave height $[\mathrm{m}]$
T : wave period $[\mathrm{s}]$
ϕ_0 : the deep water wave angle of incidence $[-]$
θ : the shore normal orientation $[-]$

In this research, Equation 5.2 is applied to estimate sediment transport. However, it has several inherent limitations. First, it considers only wave-induced longshore currents, disregarding other factors that drive alongshore currents, such as tides. Second, sediment transport is described as independent of sediment properties, such as grain size and porosity, despite the empirical relationship between K_2 and sediment characteristics. Consequently, this implies that it also overlooks parameters, such as beach slope and associated breaker types. Finally, the equation provides only a bulk value for longshore sediment transport within the breaker zone, without enabling identification of the cross-shore location of sediment transport [16]. In applying Equation 5.2, the significant wave height ($H_{0,s}$) is used. The typical value of K_2 equals ~0.34 $\mathrm{m}^{3/5}\mathrm{s}^{-6/5}$ for root-mean-square wave heights $H_{0,rms}$. However, it is assumed that $H_{0,s} \approx 1.4 H_{0,rms}$ [34]. Thus, K_2 equals ~0.15 $\mathrm{m}^{3/5}\mathrm{s}^{-6/5}$ when using $H_{0,s}$ [11]. The application of this formula with the SWAN results is described in SectionJ.4.

5.5. Reference runs

This section presents selected results from the reference run, to illustrate the model's output under normal conditions, giving insight in the current longshore sediment transport patterns. The reference run only employs normal wave conditions, which helps clarify the existing issues of erosion and sedimentation along the coastline.

5.5.1. Wave transformation

The wave transformation results under normal conditions for one setting are illustrated in Figure 5.3. The figure shows the large grid (I) and small grid (II) for setting 1 conditions. Setting 1 applies an offshore ENE wave direction, causing pronounced wave refraction as the waves approach the shore. Within the small grid, the wave direction shifts almost completely to the east, i.e. perpendicular to the coastline. Due to energy dissipation, the wave heights decrease slightly as they approach the shore, but increase again due to shoaling, before eventually breaking near the coastline. To facilitate comparison between normal conditions outcomes, the wave height magnitudes H_s in the colour bar are standardized. Images like Figure 5.3, showing wave height and direction, are also displayed in Appendix K and Appendix L.

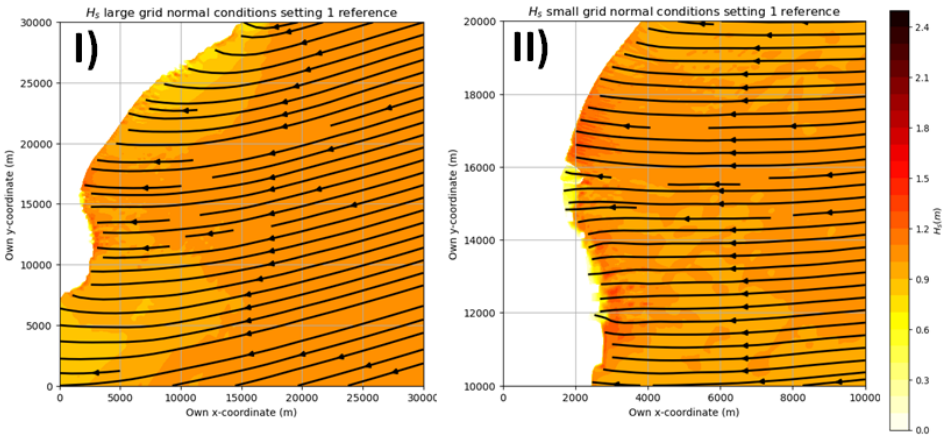


Figure 5.3: Significant wave height transformation under normal conditions setting 1 for the reference situation. I) The large coarse grid; II) The small fine grid near the port

5.5.2. Sediment transport

The results shown in Figure 5.4 display the magnitude of longshore sediment transport (Q_s) for each of the five normal condition settings, as reported in Table 5.1. Varying results for each setting are observed, as expected, given the differences in wave height, direction, and period.

Generally, a higher H_s input leads to greater absolute Q_s values, demonstrated by settings 3 and 5. Here, positive Q_s values indicate transport northwards, while negative Q_s values indicate transport southwards. For setting 1, with an ENE offshore wave direction, mostly negative Q_s values reflect this north-to-south transport. A detailed analysis of Figure 5.4 is challenging, especially when investigating structural coastal erosion or sedimentation. Therefore, the results from all settings are combined in one overall bulk alongshore sediment volume. This is achieved by multiplying each setting with its derived frequency in Section 4.3, and summing them. Dividing the sum of the sediment volume by the sum of the five frequencies (equal to 0.601), returns a factorized volume. This is a representation of the sediment transport volumes for all conditions, similar to a weighted average. This result is visualized by the black dots and lines in Figure 5.4. It shows that the total sediment transport is only positive, thus going from south to north.

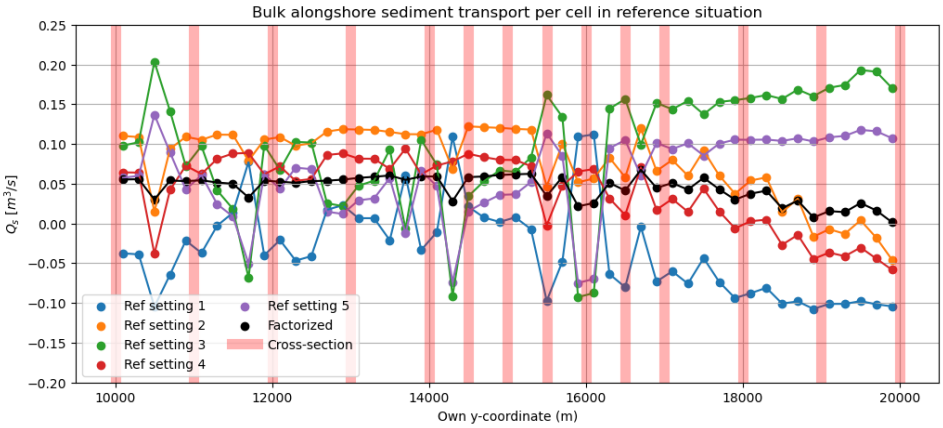


Figure 5.4: Bulk alongshore sediment volumes for each segment in all settings in the reference situation. Added with the calculated factorized sediment volume according to the frequency of retrieved normal conditions.

Still, reviewing Q_s values across the entire coastline is challenging at a resolution of 200 meters. To gain better insight in sediment transport, cross-sections (CS) are placed at intervals of 1000 meters along the coastline, and at 500 meters near the port (shown in Figure 5.4). This provides a total of 14 cross-sections, used in the erosion and sedimentation analysis. Structural erosion or sedimentation occurs due to longshore transport gradients [16]. The coastline is divided into 13 sections, with erosion occurring where sediment outflow exceeds inflow, and sedimentation where inflow exceeds outflow. The transport gradient - derived by subtracting the inflow at the southern CS from the outflow at the northern CS - yields either a positive value (erosion) or a negative value (sedimentation). Figure 5.5 displays these computed results.

Figure 5.5 comprises three parts. The top section shows a satellite image of the 10 km coastal stretch near Puerto Rawson [30]. The middle section shows the coastline as defined by the model, with a blocky resolution of 20 m, that reflects intertidal areas complicating precise definition under MSL. The bottom section plots Q_s values at each defined cross-section. Blue and red colours represent sedimentation and erosion gradients between cross-sections, respectively. The existing breakwaters are evident in the transport gradient anomalies (darker colours), and coastline orientation impacts the transport gradients, as anticipated from Equation 5.2. Chapter 7 revisits these sediment transport gradients for different design alternatives, in the same format.

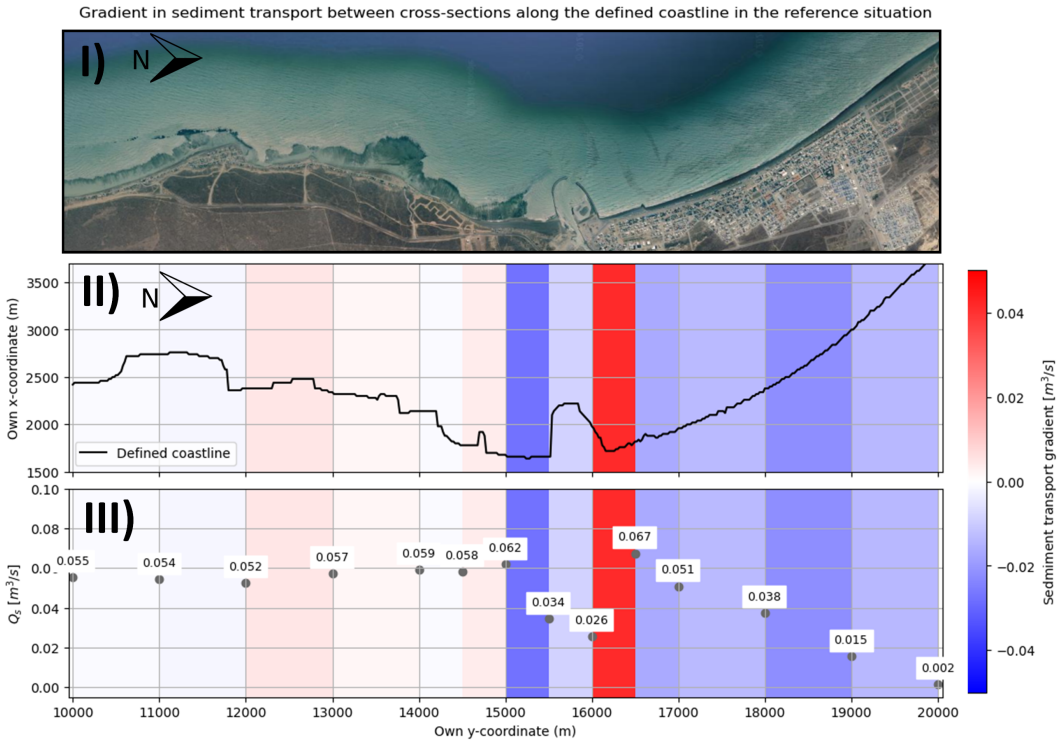


Figure 5.5: Reference situation longshore sediment transport gradients between cross-sections, blue indicates sedimentation, red erosion. I) Satellite image of the coastline of Puerto Rawson, north on the right [30]; II) The automatically defined coastline with colour gradients of erosion/sedimentation, north on the right III); The magnitudes of longshore sediment transport Q_s in m^3/s in the cross-sections with colour gradients of erosion/sedimentation

In comparison with the current erosion and sedimentation problems discussed in Section 3.1, several conclusions on the model emerge. From south to north (left to right in Figure 5.5), the first 5 km of coastline experiences minimal sedimentation and erosion. In this southern portion, slight sedimentation is followed by minimal erosion, likely due to the coastline's orientation change. This general pattern aligns with field observation, though the model may not capture the exact magnitudes. Strong sedimentation (dark blue) appears near the southern breakwater, extending nearly perpendicular to the coast. This is in agreement with the field observations described in Section 3.1. As the coastline progresses past the port entrance, significant erosion (dark red) is noted around the northern breakwater, shifting to sedimentation near $y = 16500$. While this sedimentation pattern aligns with field observations, in reality, the erosion occurs up to 1 to 1.5 km north of the breakwater. The reason for this is that the model may inadequately represent the groyne's effect on sediment transport. Particularly in its role as an obstacle that induces erosion in its lee, and leads to sedimentation windward. In the final coastal stretch, sedimentation aligns with site observations.

Sediment transport results are often contextualized against established transport volumes per year. At $y = 15000$, Q_s values translate to a northward net transport of approximately 1,950,000 $\mathrm{m}^3/\mathrm{year}$. While this is high, the CERC-based sediment transport formula used (Equation 5.2) is known to overestimate sediment transport volumes [16]. Alternative formulae might yield lower transport magnitudes, as different sediment transport formulae results often differ by an order of magnitude. This discrepancy highlights the need for calibration using sediment properties, to produce realistic values. Lacking data, this initial result provides only a preliminary estimate. For this research, sediment transport outcomes are thus evaluated qualitatively, with future studies recommended for calibration and validation of the model formulation to enhance accuracy.

6

Conceptual port expansion designs

This part of the report addresses the first research sub-question, outlined in Chapter 1. Conceptual port expansion designs are developed, guided by design criteria and design aspirations. Creating multiple conceptual designs is important, since it is difficult to implement all the design criteria and design aspirations into one single solution. Ultimately, one of the conceptual designs is selected as the final design. This design serves as the foundation for subsequent dimensioning of the breakwater in Chapter 8.

In the first section of this chapter, a list of relevant design objectives is provided. Key variables, including navigational safety and environmental impact, are examined in further detail. The second section introduces the developed conceptual designs, each of which highlights a distinct design objective. Two of the three designs serve as supplementary conceptual designs and are outlined briefly. A more detailed explanation of these two designs is given in Appendix N. Subsequently, the selected final design is elaborated on further in detail, including an evaluation of the advantages and disadvantages.

6.1. Design objectives

The conceptual designs are developed based on a set of distinct design objectives. These objectives can be categorized into design criteria and design aspirations. Design criteria represent standards that must be met to ensure the viability of the design. Design aspirations represent desirable objectives that should be met to follow project-specific ambitions. In line with stakeholder preferences, the objectives emphasize technical aspects over social considerations, to highlight the technical focus of the report.

6.1.1. Design criteria

In order for the design of the port expansion to allow for safe access, it must comply to design criteria related to navigational safety. These criteria apply to the orientation of the access channel relative to the dominant wave height and to the shore normal.

The expansion of the port results in significant changes to the layout, resulting in the need for a re-assessment of the navigational safety both inside as well as outside the port to meet the international safety standards by PIANC [60]. According to the PIANC-guidelines, the orientation of the access channel, shaped by the placement of the breakwaters, must avoid direct alignment with the dominant wave direction. If waves are allowed to pass the breakwaters and enter the port without diffracting, wave energy is not absorbed by a coastal defence structure, which leads to interference and potential damage to the docked vessels. To ensure safety for vessels navigating into the harbour under varying weather conditions, the access channel must be oriented between 30° and 90° relative to the dominant wave direction and to the shore normal. An orientation of 30° is considered optimal, while 90° is suboptimal, as harsh weather conditions could cause vessels to drift off course and therefore require higher vessel speeds in the access channel [79].

Based on these considerations, the following design criteria are defined:

- The angle between the access channel and the dominant wave direction must range from 30° to 90 °.
- Waves coming from the dominant direction (SSE) must not enter the harbour directly.

6.1.2. Design aspirations

Design aspirations are set to ensure the designs include project-specific ambitions. The aspirations are organised into three categories: *sediment transport analysis*, *environmental impact* and *space for future port operations*.

Sediment transport analysis

Incorporating a new breakwater in the overall design of a port expansion allows for an analysis of its impact on longshore sediment transport. One parameter influencing longshore sediment transport is the dominant angle of incoming waves relative to the breakwater orientation. For maximising sediment transport in the longshore bulk formulation, this angle should be 43°, as described in Subsection 5.4.2. This breakwater orientation is expected to increase northward sediment transport, which theoretically leads to a bypass of sediment over the port. If effective, this would reduce the erosion in Playa Unión. In addition, longshore sediment transport near a harbour is affected by the access channel, which functions as a sediment trap. The increased depth of an access channel relative to the surrounding seabed leads to siltation in the channel. This results in the need for regular maintenance dredging, which is a very costly, and thus, undesirable process.

Taking both variables into account, the following design criteria are defined:

- The angle of the breakwater orientation relative to the dominant wave direction (SSE) should be 43°.
- The design should incorporate only one access channel.

Environmental Impact

The environmental footprint of a new breakwater can be substantial, making it desirable to minimize its impact as much as possible. To achieve this, varying initiatives can be taken. At first, the restinga, introduced in Section 3.1, can be incorporated into the design as the foundation of the breakwater, creating a partially nature-based solution of sufficient strength (see Subsection 3.1.4). For the restinga to effectively serve as part of the breakwater foundation, the entire width of the breakwater crest should be positioned on the restinga. However, due to the limited area of the restinga, which restricts design options for orientation of the new breakwater, at least half the length of the breakwater should be supported by the restinga. Secondly, reusing materials from existing breakwaters further reduces material needs, contributing to a more sustainable design. Additionally, connecting the new breakwater to parts of the existing breakwaters not only minimizes material usage, but also decreases construction time, thereby reducing environmental pollution.

Accordingly, with a focus on environmental impact, the following design criteria are defined:

- The restinga should fully support the crest width along at least half of the length of the breakwater.
- The new breakwater design should incorporate reused material of the existing breakwaters.
- The new breakwater design should incorporate parts of the existing breakwaters.

Space for future port operations

The planned expansion of the port is part of a long-term plan of turning the port into an important pillar in the shipping industry for the province of Chubut and the Patagonia region in Argentina. This expansion aims to accommodate larger vessels in the future, including the Madrid Trader and the PanamaX vessels. Working towards this vision, the development of the port is split into two phases: Phase I and Phase II, as introduced in Subsection 3.1.3. Currently, vessels with comparable dimensions to the Madrid Trader are be able to dock safely in the harbour. By 2040, during Phase II, significantly larger vessels, such as the PanamaX, should be able to safely enter the harbour and dock. Providing a safe harbour entrance for vessels of this scale is of importance, and with that international port design guidelines should be followed.

Considering these design standards, the following design criteria are defined and later checked in the design through rules of thumb from PIANC guidelines: [60]

- The harbour basin should have adequate width and length to accommodate a turning basin for the vessels sizes expected in Phase I and Phase II.
- The access channel must be of sufficient width and length to provide a safe entrance for vessels expected in Phase I and Phase II.

6.2. Conceptual designs

The following section presents the three conceptual designs, each designed with a primary focus on a different design objective: *optimal longshore sediment transport*, *feasibility of construction*, and *space for future port operations*, respectively. The following design parameters are incorporated across all three designs:

- Each design excludes any modifications to the new northern breakwater in accordance with the stakeholders.
- The current harbour is expanded to the south across all three designs, as the northern side is restricted by adjacent residential areas, making it unavailable for development.
- Each design incorporates already planned modifications to quay walls of the port and the old northern breakwater.
- The dominant wave direction for regular nearshore conditions is assumed at SSE, or 157.5° from North, based on Córdoba [22] (since results of the report are presented in Chapter 7).
- All designs include a new, straight-lined breakwater, with a possible slight deflection at the eastward end. This alignment helps simplify the design's application in the SWAN model.
- All designs feature a port expansion with new quay walls.

As the three designs are not compared against one another, only one has been developed as the most preferred design by incorporating most of the design objectives. The other two are labelled as *supplementary* to emphasize specific primary design objectives of the project. The purpose of these supplementary designs is not to create an optimal design solution, but to develop a conceptual design that perfectly emphasizes a specific design aspiration. These designs present the potential outcomes of prioritizing a particular design aspiration significantly higher than other project-specific desires. A practical application of such a design is to provide input for sediment transport models, allowing for the analysis of varying impacts based on different layouts. These models are further explained in Section 7.1.

6.2.1. Supplementary conceptual designs

The supplementary conceptual designs are introduced in this subsection as *conceptual design 1* and *conceptual design 2*, highlighting the design objectives of *optimal longshore sediment transport* and *feasibility of construction* respectively. The design objective of *optimal sediment bypass* is selected to identify a port expansion lay-out that includes the optimal breakwater orientation according to longshore sediment transport theory (see Subsection 5.4.2). Additionally, the project objective of *feasibility of construction* (design 2) prioritizes a conceptual design solution in which modifications to both the existing old and new southern breakwater are not permitted.

The designs in this subsection are schematically illustrated by visualizing the lay-out of the design, highlighting each design's relevant contributions to the port expansion. Figure 6.1 shows an aerial view of both *conceptual design 1* (left image) and *conceptual design 2* (right image). Subsequently, this subsection briefly elaborates on both designs. Further details regarding specific design considerations, as well as the presence or absence of other incorporated design aspirations, are outlined inAppendix N.

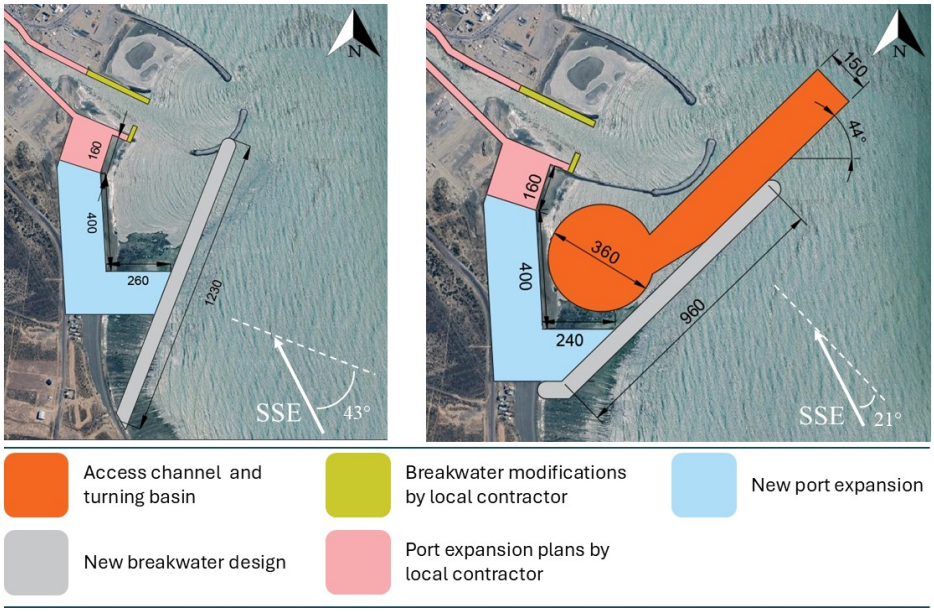


Figure 6.1: Schematisation of the supplementary conceptual designs and their important lay-out dimensions; left: *conceptual design 1*; right: *conceptual design 2*

Conceptual design 1
The first conceptual design is developed with a focus on achieving the optimal breakwater orientation in alignment with longshore sediment transport theory. The design aims to keep the existing breakwater lay-out of the harbour by extending the most seaward part of the new southern breakwater to create a new breakwater. The orientation of the new breakwater is set such that the angle between its shore normal and the dominant wave direction matches the optimal angle of 43° for longshore sediment transport (see Subsection 5.4.2).

Conceptual design 2
The second conceptual design is developed with a focus on the feasibility of construction. Given the uncertainty regarding permits of the local government to modify the existing breakwater configuration, this design serves as a practical alternative in cases where a separate harbour access is required. The design aims to keep the entire existing breakwater lay-out and expand the harbour by adding a separate access channel to the new harbour basin. The conceptual design proposes the new breakwater to be positioned along the edges of the restinga to use the elevated soil layer as a foundation, reducing the need for extensive substructure materials. The structure is then aligned to ensure adequate distance to the southern breakwater, allowing for sufficient width in the access channel to safely accommodate for future vessel sizes.

6.2.2. Final design

The third conceptual design is developed with a focus on space for future port operations. Given the expansion ambitions of the port in the near future, this design serves as a feasible solution to accommodate all expansion requirements. It is presented as the preferred conceptual design in accordance with the stakeholders by integrating nearly all design objectives into a cohesive plan that expands the harbour area to meet realistic future port operations. Figure 6.2 provides a schematic visualization of the conceptual design. It includes the removal of the entire existing southern breakwater and the construction of a new breakwater further seaward along the edge of the restinga. This creates a large harbour basin, which allows for safe entrance and docking to vessels sizes of both Phase I and Phase II. Although the designed turning basin does not have sufficient width and length for safe turning of Phase II vessels, these vessels only visit the port of Rawson a few times per year, during which they are assisted by tugboats to turn outside the breakwaters and safely enter the port.

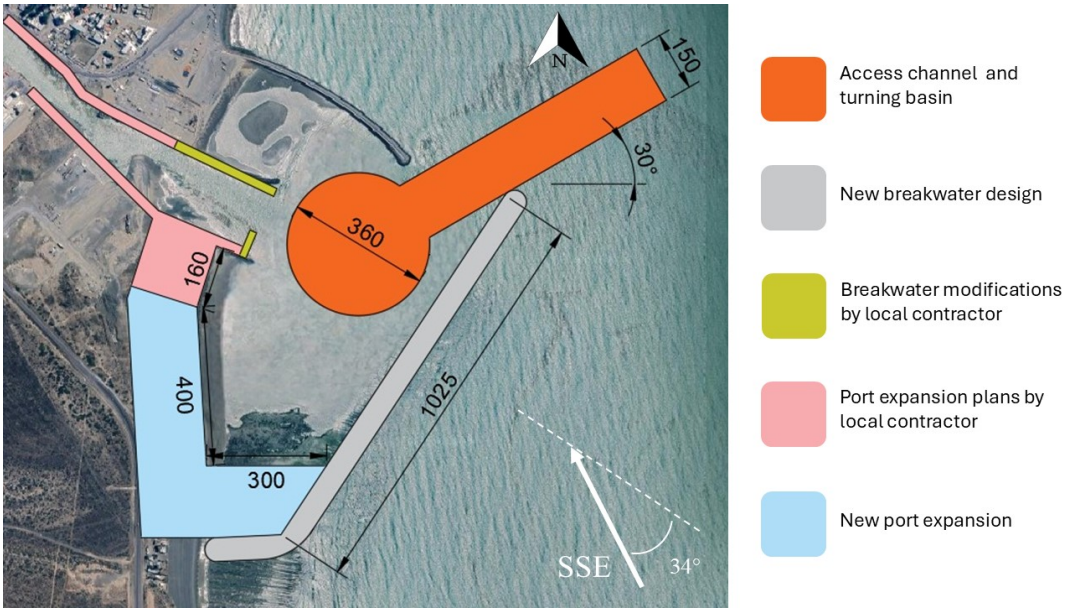


Figure 6.2: Schematic drawing of *conceptual design 3*

Table 6.1 presents the design objectives and their presence or absence in the conceptual design respectively as a *pro* or *con*.

Table 6.1: Pros and cons of *conceptual design 3*

Pros	Cons
Waves coming from the dominant direction (SSE) cannot enter the harbour directly.	The angle of the breakwater orientation relative to the dominant wave direction is not 43°.
The angle between the access channel and the dominant wave direction (SSE) is 90°.	The harbour basin does not have adequate width and length to accommodate a turning basin for the vessels sizes expected in Phase II.
The design incorporates only one access channel.	
The restinga fully supports the crest width along at least half of the length of the breakwater.	
The new breakwater design incorporates reused material of the existing breakwaters.	
The new breakwater design incorporates parts of the existing breakwaters.	
The harbour basin has adequate width and length to accommodate a turning basin for the vessels sizes expected in Phase I.	
The access channel is of sufficient width and length to provide a safe entrance for vessels expected in Phase I and Phase II.	

As shown in Table 6.1, concept 3 does not include a 43° angle of the breakwater orientation relative to the dominant wave direction. Subsection 6.2.1 discussed that implementing this breakwater orientation this far into the sea requires overly excessive material use and is therefore not feasible for this design. However, the conceptual design performs very well by including all other design criteria and aspirations. Considering the dominant wave direction from SSE and refracted nearshore waves from the east, the

breakwaters provide sufficient protection of the port, and the overall lay-out ensures safe access for future vessel sizes. Additionally, the design integrates multiple environmentally friendly and sustainable features. The restinga plays an essential role, supporting at least half of the breakwater along its length, reducing material needs. The entire northern breakwater is preserved in the new design, as its structural integrity is sufficient to remain serviceable for the near future. Furthermore, removal of the southern breakwater allows for the reuse the intact concrete blocks within the crown zone of the new breakwater, as outlined in Subsection 3.2.3.

In addition to the design objectives, other advantages and disadvantages of this design are also evaluated. Firstly, the new harbour basin is sufficiently large to accommodate a potential terminal along the inner slope of the breakwater. Given the port expansion goal to allow larger vessels to enter, this design provides the option for future adaptations, such as the addition of a cruise ship terminal. Conversely, this design is developed with a long-term vision, incorporating dimensions to accommodate vessel sizes and port operations that may not be immediately used in operation. As a result, certain aspects of the design are intentionally extensive, leading to potentially high costs. It should be noted, however, that economic feasibility does not fall in the scope of this report, as the primary objective is to ensure that the design aligns with projected future needs and provides flexibility for port expansion.

In Chapter 7, the bathymetry of this conceptual design, along with that of the supplementary conceptual designs, is applied in the SWAN model to determine the respective nearshore regular wave conditions. These SWAN runs are subsequently used to assess the impact of each breakwater orientation on longshore sediment transport. Finally, only the bathymetry of *conceptual design 3* is used to obtain nearshore extreme wave conditions in Section 7.3. These conditions are then applied to dimension cross-sections along the length of the new breakwater.

7

Results

This chapter presents the outcomes of the SWAN model, its post-processing steps, and sediment transport calculations. First, the input bathymetry used in the model is introduced, detailing adjustments near the port area, to incorporate the proposed design concepts. Thereafter, the results of the model under normal conditions are discussed. The primary focus in assessing the impact of the concepts on the coastal dynamics is analysing the gradient in longshore sediment transport gradients. Finally, the chapter examines the results under extreme conditions for concept 3. This concept is identified as the preferred design. It is thus the only design analysed under these extreme conditions.

7.1. Bathymetry near port

Figure 7.1 presents the input bathymetry, used in the SWAN model, for the reference scenario and each of the three design concepts. The bathymetry is displayed using the updated coordinate system. The figures on the right provide a detailed view of a 2 by 2 km area surrounding the port. Concept 1 (top right; III) and concept 2 (bottom middle; IV) are developed according to the specification in Subsection 6.2.1, while concept 3 (bottom right; V) represents the final design as outlined in Subsection 6.2.2. Additionally, the access channels are incorporated into the bathymetry to achieve a more realistic representation. However, depth adjustments within the inner port are not included, as the focus of this study is on hydrodynamic effects on the seaside of the new breakwater, rather than on conditions within the port itself.

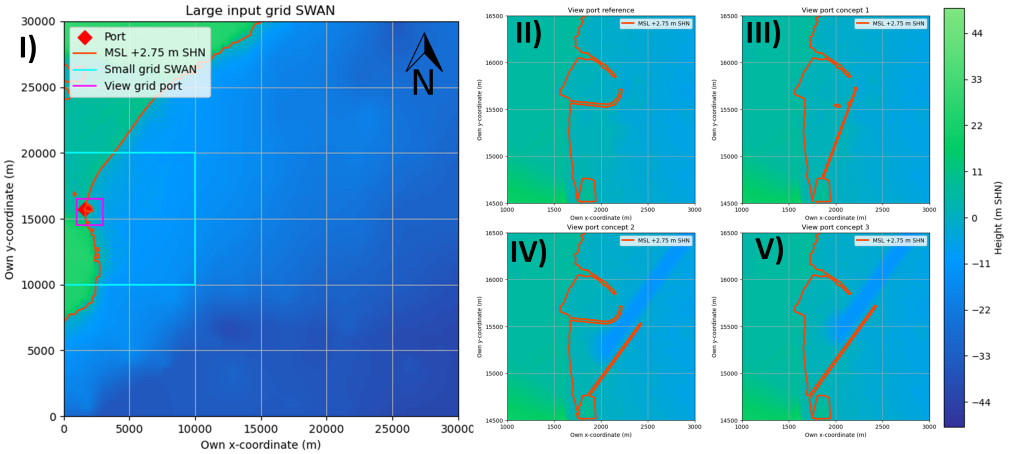


Figure 7.1: SWAN input bathymetry for the reference and the three designs concepts in own coordinate system. I) Large and small input grid visualized, as well as zoomed view grid on the port; II) Input bathymetry view on port in reference situation; III) Input bathymetry view on port for concept 1; IV) Input bathymetry view on port for concept 2; V) Input bathymetry view on port for concept 1

7.2. Normal conditions

This section presents the findings from the model simulations under normal wave conditions, with a focus on the longshore sediment transport gradients. These gradients provide insight into erosion and sedimentation along the coastline. For further details and supplementary figures on normal conditions results, refer to Section K.

7.2.1. Wave transformation

Wave transformation results for each scenario across all five settings are provided in section K.1. No abnormalities or unexpected patterns are observed in the wave transformations, indicating consistent model performance. Overall, it is shown that the nearshore dominant wave direction at Puerto Rawson is SSE. This reaffirms the previously made assumption for the concept designs, discussed in Section 6.2.

7.2.2. Sediment transport

This section outlines the longshore sediment transport gradients along the 10 km stretch of coastline. The figures in this section illustrate the results for concept 1 (Figure 7.2), concept 2 (Figure 7.3), and concept 3 (Figure 7.4). The outcomes of the reference simulation can be found in Figure 5.5 in Subsection 5.5.2. In the latter subsection, the methodology for obtaining and interpreting these results is explained. Next to that, it provides a comparison between the reference model outcomes and field observations on erosion and sedimentation patterns. Intermediate results for bulk longshore sediment volumes, as displayed in Figure 5.4, are given for all three concepts and are elaborated upon in section K.2.

The sediment transport analysis in this study is based on the application of the CERC-formula (Equation 5.2). The coastal orientation across the scenarios varies only where the breakwater designs are implemented (intervention zone). Outside of this zone, across different offshore conditions, the wave transformations (H_s and T_p) remain consistent between the design concepts. As a result, longshore sediment transport volumes outside of the intervention zone remain almost unchanged. Thus, the associated sediment transport gradients are also unaffected. Although this homogeneity is a simplification of actual coastal dynamic processes, it reflects the limitations of the CERC formulations applied here.

Like the reference situation, the design's initial 4.5 km of coastline south of the port continues to exhibit minimal sedimentation and erosion patterns. The most northern section of the 10 km coastal stretch, however, demonstrates a similar sedimentation pattern as previously discussed. The model likely under-represented this section, possibly due to its inability to accurately represent the groyne in this area, as detailed in Subsection 5.5.2. Consequently, sediment transport gradients outside the intervention zone for each design concept are the same as in the reference situation; illustrated by looking at Figures 7.2, 7.3, and 7.4, and comparing them with Figure 5.5.

Therefore, the areas outside the intervention zone are not discussed in further detail. This also suggests that the erosion zone directly north of the northern breakwater will remain consistent across all scenarios. The sediment transport formulation employed here limits the capacity, to quantify transport effects between adjacent sections. This prevents any conclusion about the impact of a new breakwater on erosion in this area to a qualitative level. Consequently, the sediment transport calculations offer no clear indication of increased or decreased erosion within this zone.

For clarity, the satellite images included with the sediment transport gradient figures have been mirrored. In these images, north is to the right, south to the left, and east at the top. This orientation aligns with the model-defined coastline and ensures a consistent view. This modified orientation does not affect the analysis, as longshore sediment transport gradients are typically evaluated as a one-dimensional line along the coast.

The longshore sediment transport gradient in concept 1 differs most significantly from the reference scenario, as illustrated in Figure 7.2. Concept 1 was oriented to optimize sediment transport by aligning the breakwater at a 43° angle to the dominant wave direction. This alignment generates the highest sediment transport volumes in the cross-sections, going through the breakwater design. Notably, sedimentation at the southern connection of the new breakwater to the land is substantially reduced, compared to the reference scenario. Moving northwards, a small erosion zone appears along the midsection of the breakwater. At the port entrance, these initially high transport rates drop significantly, leading to increased sedimentation in this area.

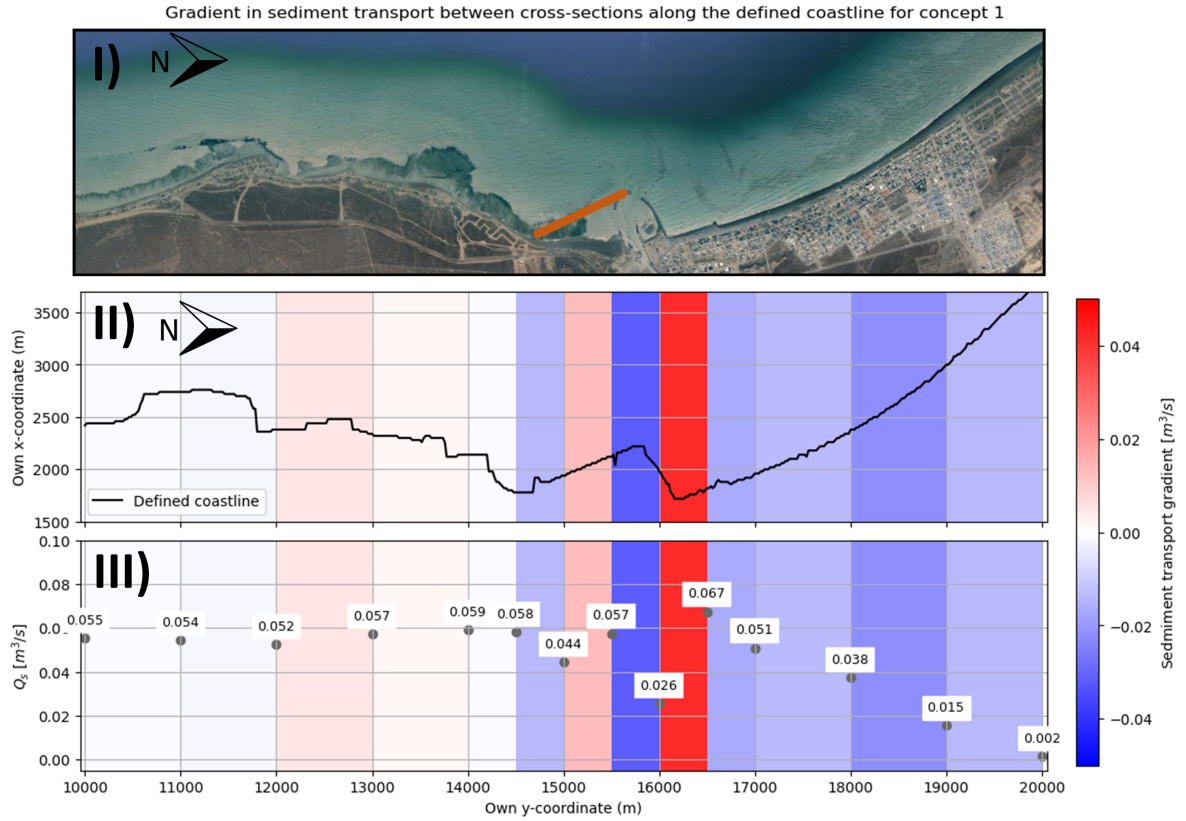


Figure 7.2: Concept 1: longshore sediment transport gradients between cross-sections, blue indicates sedimentation, red erosion. I) Satellite image of the coastline of Puerto Rawson, with BW orientation, north on the right [30]; II) The automatically defined coastline with colour gradients of erosion/sedimentation, north on the right; III) The magnitudes of longshore sediment transport Q_s in m^3/s in the cross-sections with colour gradients of erosion/sedimentation

If implemented, this concept would include a deep access channel at the port entrance, acting as a sediment trap for longshore sediment transport. The increased depth would reduce wave-induced forces near the bed, thereby limiting sediment (re)suspension and transport [16]. Combined with the modelled sedimentation near the port entrance, this would likely lead to rapid siltation of the access channel. This is an undesirable outcome for port operations. Therefore, while concept 1 maximizes sediment transport volumes along the breakwater, the extent to which sediment would reach the northern stretch of coast (erosion zone) remains uncertain.

In the scenario of concept 2, illustrated in Figure 7.3, a different sedimentation pattern emerges. The sediment transport volumes decrease, relative to the reference scenario, producing significant sedimentation along the southern (landward) side of the new breakwater. A zone of erosion then appears around the breakwater's midsection. Given the lower sediment transport volumes near the port entrance, sedimentation in this zone remains minimal.

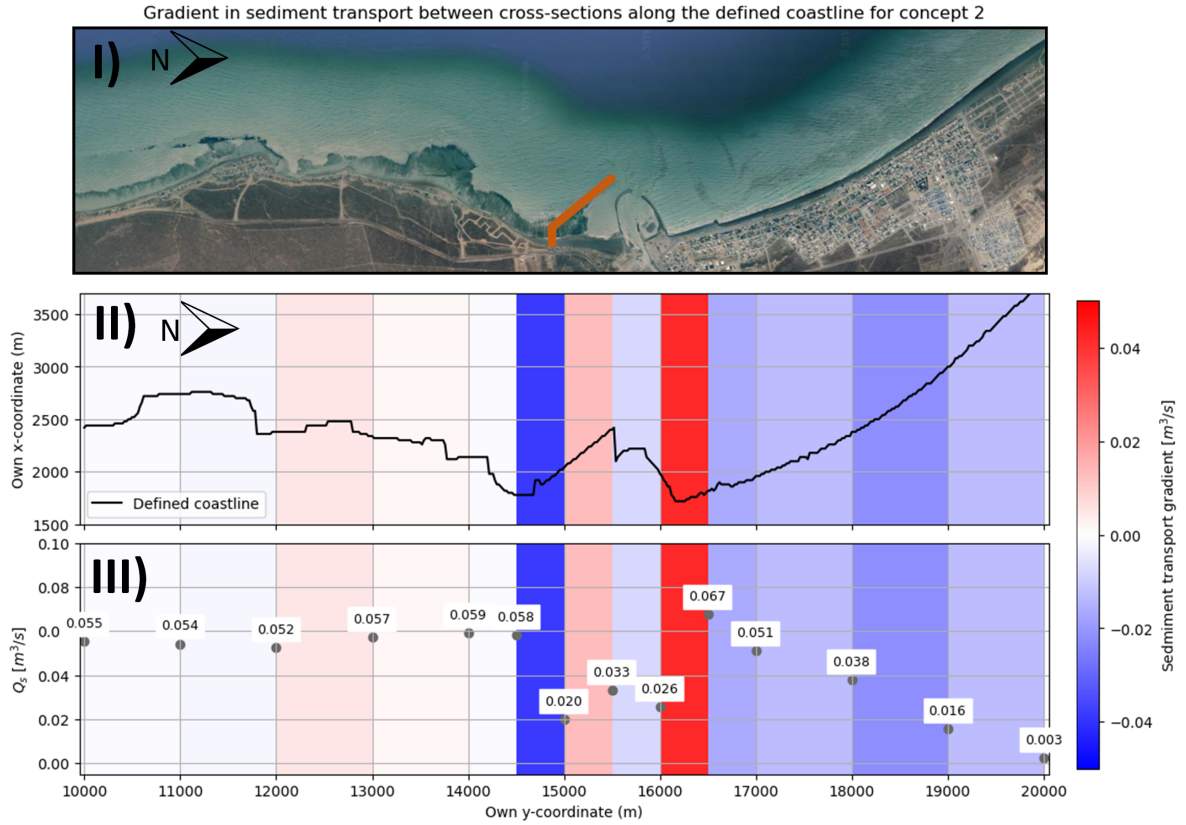


Figure 7.3: Concept 2: longshore sediment transport gradients between cross-sections, blue indicates sedimentation, red erosion. I) Satellite image of the coastline of Puerto Rawson, with BW orientation, north on the right [30]; II) The automatically defined coastline with colour gradients of erosion/sedimentation, north on the right; III) The magnitudes of longshore sediment transport Q_s in m^3/s in the cross-sections with colour gradients of erosion/sedimentation

The implementation of this concept incorporates two access channels. As previously noted with concept 1, similar challenges arise regarding sediment transport across these two channels. Although the modelled sedimentation at the entrance is reduced compared to concept 1, the existence of two access channels complicates sediment transport even further. This setup therefore also increases the likelihood of access channel siltation, thereby hindering port operations.

Concept 3, as shown in Figure 7.4, intensifies the effects observed in concept 2. Sediment transport volumes in the breakwaters cross-sections are further reduced. This leads to the same strong sedimentation on the southern (landward) side of the breakwater. In the midsection, the gradient approaches zero, indicating neither erosion or sedimentation (shown in white). Near the port entrance, the previously noted sedimentation effects for each scenario, change to slight erosion.

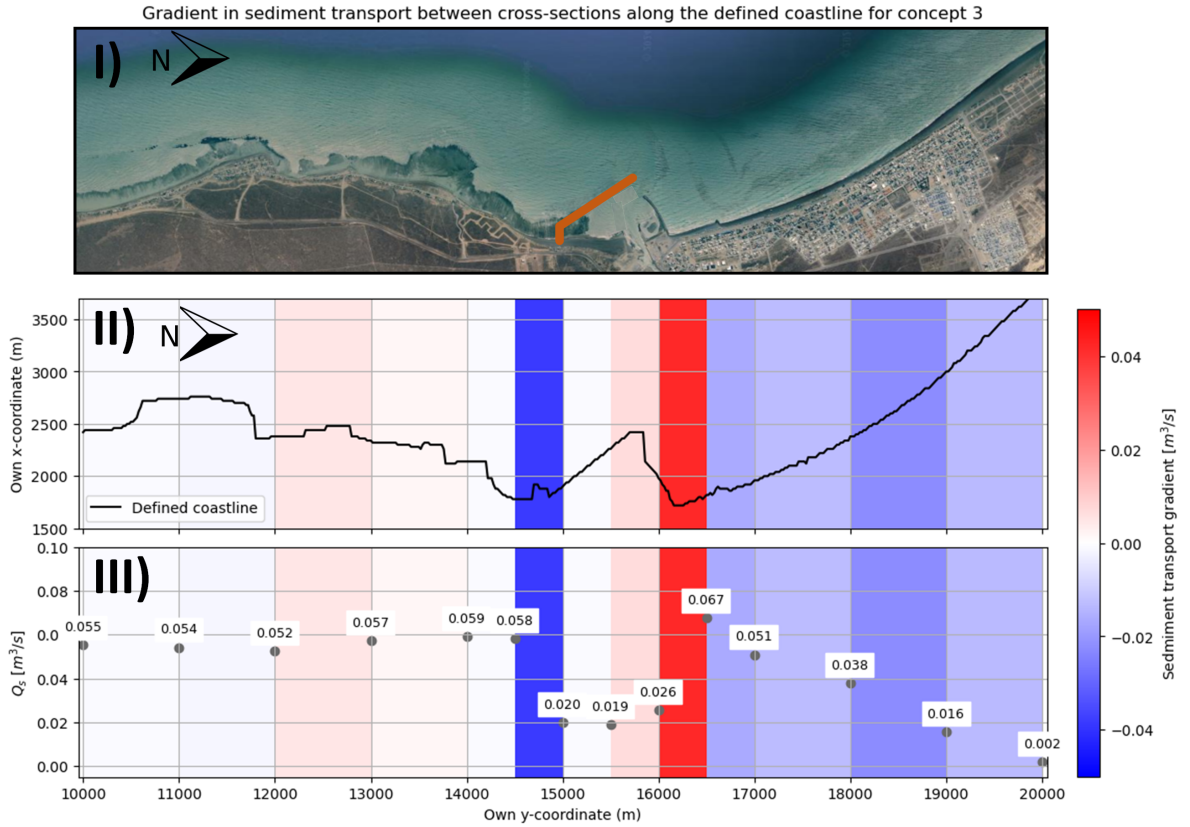


Figure 7.4: Concept 3: longshore sediment transport gradients between cross-sections, blue indicates sedimentation, red erosion. I) Satellite image of the coastline of Puerto Rawson, with BW orientation, north on the right [30]; II) The automatically defined coastline with colour gradients of erosion/sedimentation, north on the right; III) The magnitudes of longshore sediment transport Q_s in m^3/s in the cross-sections with colour gradients of erosion/sedimentation

The implementation of concept 3 includes a single access channel, which is preferable over 2 access channels, from a sediment transport perspective. Modelled sediment transport results indicate no sedimentation near the port entrance, and even show slight erosion in this area. Consequently, this concept is expected to result in minimal access channel siltation. Comparing these mechanisms to concept 1 and 2, results in concept 3 being the preferred design.

Uncertainty remains across all concepts, regarding the extent to which sediment would reach the northern coastal stretch (erosion zone). This uncertainty is partly due to the presence of the access channel. It is also influenced by the model's limitations, in accurately calculating and defining sediment transport around obstacles, such as a breakwater. It is thus unclear which concept would most effectively mitigate erosion north of the port. However, in the model results, both concepts 2 and 3 trap significant sediment volumes south of the proposed breakwater. This concentrated sedimentation presents a potential opportunity. With sediment accumulating in a defined section, dredging could be conducted efficiently in this area. The dredged material, from this area south of the breakwater, can be used to nourish the eroded coast at Playa Union. This could counteract the ongoing erosion problem.

7.3. Extreme conditions

This section presents the findings from simulations conducted under extreme offshore conditions. For these simulations, four offshore wave conditions are modelled, each varying solely in wave direction, as outlined in Table 5.2. These extreme scenarios represent conditions with a 100-year return period. They are applied exclusively to concept 3, as this design was determined to be the most appropriate solution. The results of the extreme condition simulations are used for the dimensioning of the breakwater.

Wave transformation results for each setting, under these extreme conditions, are available in section L.1. As with the normal conditions, no irregularities or unexpected patterns are observed in the wave transformations, indicating stable model performance.

For breakwater dimensioning, the primary interest lies in the hydrodynamic parameters at the toe of the breakwater's offshore limit. This is where the structure encounters the most severe wave forces. To establish which offshore wave direction produces the governing (normative) conditions, near-port wave heights are examined for each setting. This is shown in Section L.2. Table 7.1 presents an overview of wave heights, periods, wave directions, and water levels associated with each setting. The results clearly indicate that the southeast offshore wave direction (setting 4) yields the highest wave heights at the toe of the breakwater. Thus, this setting is identified as the normative condition. Consequently, the parameters associated with setting 4 are applied, in further dimensioning of concept 3.

Additionally, wave setup at the toe of the breakwater is included in the water level analysis. This setup effect is combined with the baseline water depth to calculate the total water depth at the toe. This is presented in the last column of Table 7.1.

Table 7.1: Results extreme conditions from four offshore directions for concept 3, parameters at the toe.

Setting	**Offshore direction**	H_s [m]	T_p [s]	T_{m01} [s]	**Direction [°N]**	**Wave set-up** [m]	**Water depth** [m]
1	SSW	2.87	11.64	6.68	138.4	0.031	8.651
2	S	3.47	11.64	7.41	133.2	0.054	8.674
3	SSE	3.81	11.64	7.91	125.2	0.091	8.711
4	SE	3.98	11.64	8.21	117.2	0.126	8.746

8

Dimensioning of breakwater

To protect the designed port expansion from incoming extreme wave conditions, a detailed study into the structural design of a new coastal defense structure is conducted. The objective of this study is to develop a rubble mound breakwater cross-section design. This design must protect the port, while allowing port operations to continue under safe and controlled marine conditions.

This chapter outlines the stepwise design process for the cross-sections of the breakwater, beginning with the determination of the dimensions for respectively the armour layer, core and underlayer. This is followed up by the dimensioning of the toe, and ultimately, the application of the wave overtopping formula to define the crest dimensions. An overview of all relevant breakwater dimensions is given in Figure 8.1. Subsequently, this chapter provides an insight into the design of the roundhead, includes a technical drawing of the cross-section of the breakwater, and quantifies the volume of the armour units used in the armour layer of the breakwater.

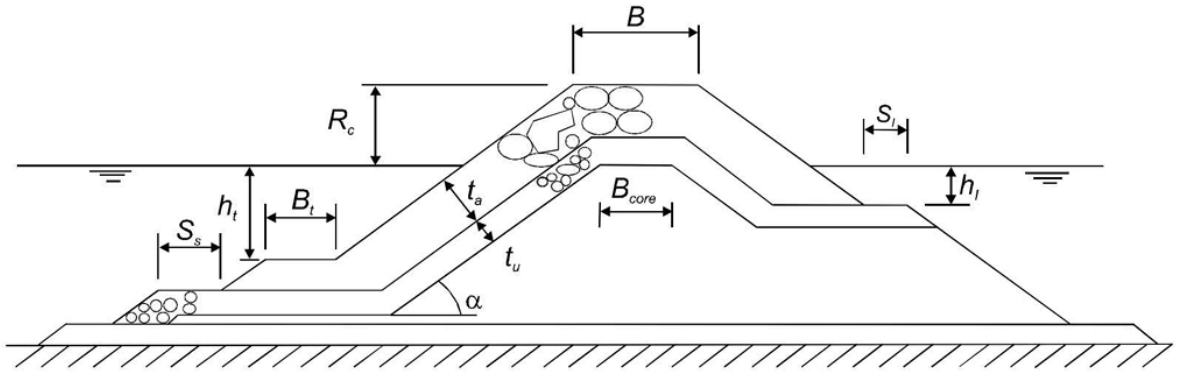


Figure 8.1: Cross-section schematization of a rubble mound breakwater with the dimensions parameters; B = crest width; B_{core} = core width; R_c = crest height; h_t = seaward toe level; h_l = leeward shoulder level; α = slope angle; t_a = armour layer thickness; t_u = underlayer thickness; B_t = seaward toe width; S_s = seaward shoulder width; S_l = leeward shoulder width. [65]

Throughout this chapter, specific key parameters are applied consistently to all the cross-sections that are introduced in section 8.1. An overview of these parameters is provided in Table 8.1.

Table 8.1: Parameters for all cross-sectional locations of design; CS = "Cross-section"
* Note: not evaluated, but assumed to be the same as CS-C

Parameter	Symbol	Unit	CS - A	CS - B	CS - C
Design water level	DWL	[m SHN]	+5.31	+5.31	+5.31
Water depth at toe	d	[m]	3.47	4.14	8.75
Significant wave height	H_s , H_{m0}	[m]	2.00	3.00	3.98
Angle of attack	$DirN$	[°]	117.2*	117.2*	117.2
Density concrete	ρ_c	[kg/m^3]	2228	2228	2228
Relative density concrete	Δ_c	[kg/m^3]	1.17	1.17	1.17
Density rock	ρ_r	[kg/m^3]	1640	1640	1640
Relative density rock	Δ_r	[kg/m^3]	0.60	0.60	0.60

8.1. Sections

The breakwater dimensions are calculated for three different cross-sections along the length of the entire breakwater and mark the area of the sections that divide the breakwater. The sections and cross-sectional locations are introduced in Figure 8.2. As the significant wave height decreases along the breakwater in shallower waters, parameters such as crest height, armour layer thickness, and toe dimensions must be adjusted to accommodate the dampened wave conditions effectively. Designing the structure solely for the most extreme conditions would result in an over dimensioned design with excessive material use. In Figure 8.3, the bathymetry along the length of the structure is visualized with three vertical lines representing the cross-sections. Each cross-section marks the start and end of a section of the breakwater. Each section features the same armour unit size, toe dimensions, and crown width, with crown height being the only parameter that varies across sections due to differences in water depth. Notably, cross-section A applies to all of section 1, cross-section B to section 2, and cross-section C to section 3.



Figure 8.2: Locations A, B, and C for the cross-sections

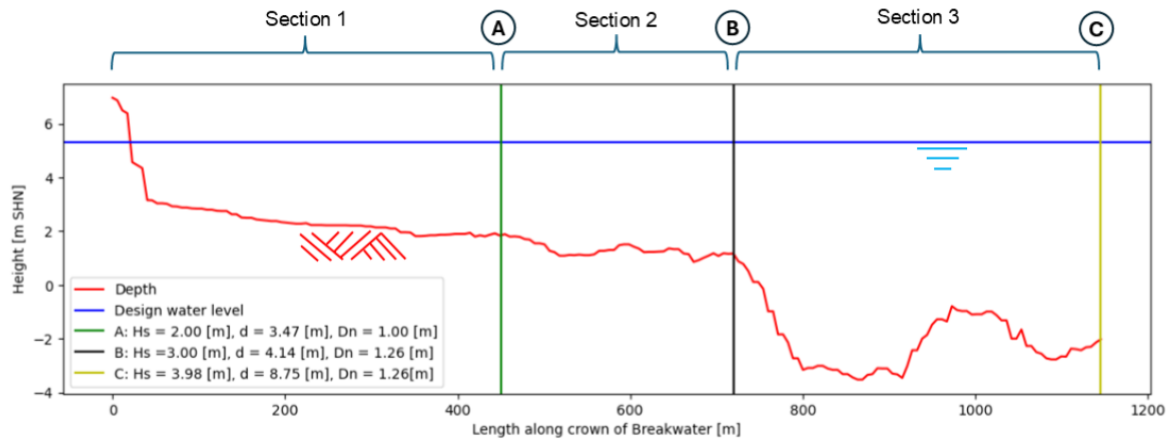


Figure 8.3: Bathymetry along crest length of breakwater; specified: cross-sectional locations along breakwater

8.2. Armour layer

The primary function of the armour layer is to absorb and dissipate energy from incoming waves, effectively protecting the substructure of the breakwater. In this design, the armour layer consists of randomly placed concrete armour units. These units provide wave resistance through their significant weight and interlocking arrangement, which prevents the structure from shifting or eroding under sustained wave action. In this section, the required dimensions of the armour layer are determined. As the armour stability can vary under different conditions, it must be noted that complex physical model tests are recommended to validate the configuration of this layer.

8.2.1. The Accropode II unit

Accropodes are used for certain existing breakwaters at port of Rawson. Using similar armour in the new breakwater configuration allows for the reuse of undamaged Accropodes from the removed southern breakwater. This decision is made in accordance with the stakeholders. To ensure structural integrity, the Accropodes are designed for zero movement, with even minor damage levels (below 5%) deemed unacceptable [65].

In the current breakwater, the original version of the Accropode is applied, whereas the upgraded Accropode II is used for the new breakwater design. The latter is preferred because of its improved strength and stability relative to the first [1]. Subsection 3.2.3 introduces that the reuse of the Accropodes is limited to the crown of the designed breakwater. The improved Accropode II fills the remainder of the crown and covers the armour layer on both slopes of the breakwater.

However, as both Accropode types have different dimensions, precise interlocking is not feasible. The CLI report [1] outlines that transitions between different unit types result in a grid loss in the armour layer, which requires attention. As the reused Accropodes are applied only in the crown, the grid loss is limited compared to a transition on the slope side. To ensure a smooth transition, the volumes of the two unit types must not differ more than 30% in order to avoid variations in armour thickness. However, this condition is never violated, as all armour units within a specific section have the same volume per unit. Subsequently, the difference in armour thickness should be less then one-sixth of the Accropode II unit height [1]. The dimensions of both Accropode types, along with the transition check, are provided in Appendix M. Based on this appendix, it is concluded that using both types of Accropode units in the crown of the breakwater is feasible.

8.2.2. Dimensioning the armour unit

Before determining the appropriate volume of Accropodes per cross-section of the breakwater, the required minimum nominal diameter is calculated. This is achieved by considering the damage number of the armour unit. The damage to randomly placed units are measured using two metrics: [65]

- N_{od}: The number of displaced units along a defined strip of breakwater with a width matching the nominal unit diameter D_n;
- N_d: The number of displaced units relative to the total number of units within a defined section around the design water level (typically within ±1.5 H_s [65]).

For both Accropode types, start of damage begins at $N_{od} = 0$, and failure of the structure at $N_{od} = 0.5$ [65]. Equation 8.1 and Equation 8.2 show the the stability formulas. Given the fact that an Accropode is not able to move, these equations have already implemented a safety factor of 1.5 [76].

$$\frac{H_s}{\Delta D_n} = 2.5 \text{ , for start of damage } N_{od} = 0 \tag{8.1}$$

$$\frac{H_s}{\Delta D_n} = 2.7 \text{, for failure } N_{od} = 0.5 \tag{8.2}$$

As concluded in Chapter 7, the design wave height for the structure is 3.98 m. The required nominal diameter of the Accropode II is determined using Equation 8.1 [65].

Under wave breaking conditions, the stability number N_s ranges from 2.3 at the breakwater head to 2.5 along the trunk section, as noted in [65]. These values correspond to a slope of 1:1.33, and it is noteworthy that a more gentle slope (i.e. greater than 1:2) does not enhance stability.

The minimum nominal diameter of the armour units is derived through Equation 8.1. When cubed, results in the minimal volume, $V_{a,min}$, as shown in Equation 8.3. Subsequently, the mass of each unit, M_a, is determined through Equation 8.4. A summary of all calculated values is presented in Table 8.2.

$$V_{a,min} = D_n^3 \tag{8.3}$$

Where:

$V_{a,min}$: Minimal volume of the armour unit.
D_n : Nominal diameter of the armour unit.

$$M_a = \rho_c \cdot V_a \tag{8.4}$$

Where:

M_a : Mass of the armour unit;
ρ_c : Density of the concrete used for the unit. Assumed to be 2228 $\mathrm{kg/m^3}$, as discussed in Section 8.9;
V_a : Design volume of the unit, rounded up from $V_{a,min}$.

Table 8.2: Dimensions of armour units per cross-section

Parameter	Symbol	Unit	CS - A	CS - B	CS - C
Minimum nominal diameter of armour unit	$D_{n,min}$	[m]	0.68	1.02	1.18
Minimal volume of armour unit	$V_{a,min}$	[$\mathrm{m^3}$]	0.31	1.06	1.67
Design volume of armour unit	V_a	[$\mathrm{m^3}$]	1.0	2.0	2.0
Design mass of armour unit	M_a	[kg]	2228	4456	4456
Design nominal diameter of armour unit	D_n	[m]	1.0	1.26	1.26
Armour layer thickness	t_a	[m]	1.36	1.71	1.71

8.3. Core and underlayer

The substructure of a breakwater consist of an underlayer, optional filter layer(s), and a core. During the design phase, accurately predicting the exact rock grading for the material poses challenges and requires several assumptions. Standardized rock gradings often have wide size ranges, and core material is typically ungraded, causing uncertainties in the analysis of the layer dimensions. To mitigate these challenges, the standardized rock grading that most closely aligns with the design requirements for the underlayer supporting the Accropodes is selected. It is assumed that this rock grading is available for this project. Additionally, the specifications for commonly used quarry run material for the core are also assumed.

8.3.1. Core layer

The core is primarily used for volume-filling purposes and, as such, do not require a specific characteristic size, such as M_{50}. As the maximum particle size is generally specified, the minimum sizes should be controlled as well [65]. For this design, the core layer is assumed to consist of standard quarry run material with a mass range of 1–500 kg. To validate the design, the parameters D_{15} and D_{85} of the quarry run material are required. However, since core materials are often non-graded, an assumed grading is applied in this design, as presented in Table 8.3.

Table 8.3: Grading input core parameters for all cross-sections

Parameter	Symbol	Unit	Core
Density of the core	ρ_c	[$\mathrm{kg/m^3}$]	1570
Minimal mass of core	$M_{min,c}$	[kg]	0.50
Maximal mass of core	$M_{max,c}$	[kg]	3350
Range of median weight	$W_{c,50}$	[kg]	100
Median sieve diameter	$d_{c,50}$	[cm]	40.0
15th percentile	$d_{c,15}$	[cm]	21.8
85th percentile	$d_{c,85}$	[cm]	60.7

8.3.2. Underlayer

Rubble mound breakwaters are constructed with an underlayer, and where necessary, filter layers to prevent erosion of the core material and ensure the overall stability of the structure [65]. The underlayer is positioned directly beneath the armour layer, while filter layers are placed between the underlayer and the core. In this specific design, it is determined in subsection 8.3.3 that an additional filter layer is not required since core and underlayer are already stable. Consequently, the term *filter layer* is not mentioned further on in the report and the term *underlayer* is used instead.

The required properties for the underlayer of Accropode II units are derived using Rock Manual [65]. The following rules of thumb are applied for these derivations, where M_a is the mass of the armour unit:

- $M_{50,u} \approx 0.10 \cdot M_a$;
- $M_{min,u} \approx 0.07 \cdot M_a$;
- $M_{max,u} \approx 0.14 \cdot M_a$.

As a result, the required mass ranges for the underlayer can be derived, as shown in Table 8.4.

Table 8.4: Grading input Underlayer

Parameter	Symbol	Unit	CS - A	CS - B	CS - C
Nominal mass of underlayer	$M_{50,u}$	[kg]	223	446	446
Minimal mass of underlayer	$M_{min,u}$	[kg]	156	312	312
Maximal mass of underlayer	$M_{max,u}$	[kg]	312	624	624

Since the exact grading remains uncertain, the closest standardized grading is used — in this case, HM_A 300-1000 [32]. The corresponding properties of this standard grading are displayed in Table 8.5.

Table 8.5: Properties of underlayer: $HM_A\ 300 - 1000$ [32]

Parameter	Symbol	Unit	Underlayer
Density of the underlayer	ρ_u	[$\mathrm{kg/m^3}$]	1640
Range of median weight	$W_{u,50}$	[kg]	450 - 690
Median sieve diameter	$d_{u,50}$	[cm]	65 - 75
15th percentile	$d_{u,15}$	[cm]	46 - 57
85th percentile	$d_{u,85}$	[cm]	61 - 69
85th / 15th percentile	$d_{u,85}$ / d_{15}	[-]	1.4
Nominal diameter	$d_{u,n50}$	[cm]	59
Layer thickness	t_u	[cm]	88

8.3.3. Erosion, stability, and permeability checks

This subsection covers the checks for erosion, stability, and permeability, ensuring the structure can withstand hydraulic forces without degrading. These checks confirm that the selected materials provide sufficient resistance to erosion and remain stable under operational conditions, while also maintaining adequate permeability for water to flow through the structure.

With regard to internal erosion, this design utilizes standardized grading for the underlayer that have been pre-assessed for erosion resistance, and are therefore considered appropriate. Subsequently, the stability of the interface between the underlayer and the core is evaluated. This is done by comparing the rock diameters of the 15th percentile of the underlayer grading to the 85th percentile of the core grading, according to Equation 8.5. If validated, there is no need for a filter layer between the underlayer and the core. For this check, the worst-case scenario is assumed for the underlayer. For the underlayer value the maximum value for the 15th percentile is selected from Table 8.5; thus, $d_{u,15} = 57.0$ cm. Similarly, the core layer value is selected as $d_{c,85} = 60.7$ cm (Table 8.3).

$$d_{u,15}/d_{c,85} < 5 \tag{8.5}$$

From Equation 8.5 follows: $57.0/60.7 = 0.94 < 5$. Thus, these two gradings are valid, ensuring that no internal erosion occurs between the underlayer and the core.

Ultimately, the permeability of the entire breakwater must be addressed, as a permeable structure maintains the integrity of the sublayers and prevents internal erosion or migration of particles. Based on Rock Manual [65], permeability can be assessed through Equation 8.6. For this check, the worst-case scenario is assumed for the underlayer, by selecting the minimum value of $d_{u,15} = 46.0$cm from Table 8.5. Similarly, the value for the rock diameter of the 15th percentile of the core grading is selected as $d_{c,15} = 20.8$ cm.

From Equation 8.6 follows: $46.0/20.8 = 2.2 > 1$, thus these two gradings are valid, ensure the structure is permeable.

$$d_{u,15}/d_{u,15} > 1 \tag{8.6}$$

From Equation 8.6 follows: $46/20.8 = 2.2 > 1$; Thus, these two gradings are valid. This ensures the permeability of the breakwater, allowing water to pass freely between layers without washing out the finer materials.

8.4. Toe Dimensioning

A reduction in strength at the base of the slope of the breakwater can trigger sliding of the structure, a failure mechanism introduced in Section 4.1.3. Constructing a standard toe mound at the base of the seaward slope ensures stability for this slope, thereby supporting the structural integrity of the entire breakwater. The toe protection is designed with a single Accropode placed in front of the base, supported by a double layer of rockfill. In order to prevent erosion of the seabed in front of the breakwater, the entire toe mound is placed on an extra filter layer, or anti-scouring mattress. In this section, the depth of the toe crest, h_t, the grading of the rockfill, D_{n50}, and the toe width, B_t, are calculated for each cross-section. The results are shown in Table 8.6.

To determine the nominal median diameter of the armour rocks, D_{n50} [m], used in the rockfill, the stability formula of the toe by Van der Meer et al. [75] is applied in Equation 8.7. This equation gives the relative toe depth as h_t/h and as h_t/D_n. A relatively high toe with a value of $h_t/h < 0.4$ is considered a berm [65], which is not applicable to this design. As a result, Equation 8.7 is applicable for the ranges of:

$$0.4 < h_t/h < 0.9\ , \qquad 3 < h_t/D_{n50} < 25$$

$$\frac{H_s}{\Delta D_{n50}} = \left(2 + 6.2\left(\frac{h_t}{h}\right)^{2.7}\right) N_{od}^{0.15} \tag{8.7}$$

Before calculating D_{n50}, several parameters are determined first. The crest height of the toe, h_t, is assumed to be positioned at 1.5 times the value for H_s below DWL [65]. Moreover, the water depth in front of the toe, h [m], is obtained from Table 8.1 as the depth below DWL. Additionally, the rockfill density, required to calculate the relative density, is assumed equal to the rock density of the underlayer, ρ_u, from Table 8.5. The value of the damage number is taken at $N_{od} = 0.5$, indicating the start of damage, which is advisable to use for design purposes [65]. This damage number is applicable to a standard toe configuration with a thickness of 2 to 3 rocks and a width of 3 to 5 rocks, which is the case for this toe design. With these parameter values, the nominal median diameter of the rocks in the toe is then determined.

After having defined D_{n50}, a final condition needs to be checked. The thickness of this rockfill, t_r, must not exceed that of the used Accropode, t_a, and should be at least two-thirds of the Accropode's height, H_a [1]. This results in the following condition for the rockfill thickness: $\frac{2}{3}H_a < t_r < t_a$. If this condition is not satisfied, the proposed type of standard toe mound is unsuitable for the specific cross-section, and an alternative type of toe mound must be considered.

Ultimately, the standard toe width for rubble mound breakwaters, B_t, is calculated. For sufficient horizontal stability, the rockfill should have a minimum width equal to three times the diameter of the applied armour rocks [65], i.e. $B_t \geq 3D_{n50}$. Additionally, the anti-scouring mattress incorporates a shoulder width, S_s [m], with a minimum value of $S_s = 2$ m [65]. The layer thickness and rock grading of the mattress are taken to be equal to those of the underlayer of the breakwater. All the calculated parameters and checks, mentioned in this section, are shown in Table 8.6.

Table 8.6: Results of toe dimensioning parameters

Description	Parameter	CS - A	CS - B	CS - C
Significant wave height	H_s [m]	1.73	2.07	3.98
Depth of toe crest	h_t [m]	2.60	3.11	5.97
Depth in front of toe	h [m]	3.47	4.14	8.75
Damage number	N_{od} [-]	0.5	0.5	0.5
Relative density	Δ [-]	0.59	0.59	0.59
Nominal diameter of rockfill	D_{n50} [m]	0.673	0.800	1.779
Check relative toe depth 1	0.4 < h_t/h < 0.9	0.75 (Satisfied)	0.75 (Suffices)	0.68 (Suffices)
Check relative toe depth 2	3 < h_t/D_{n50} < 25	3.86 (Satisfied)	3.89 (Suffices)	3.36 (Suffices)
Check thickness of rockfill	$\frac{2}{3}H_a < t_r < t_a$	1.35 (Suffices)	1.6 (Suffices)	3.558 (Fails)
Toe width	B_t [m]	2.02	2.4	-
Seaward shoulder width	S_s [m]	2	2	-

As shown in Table 8.6, cross-section C does not meet the rockfill thickness requirement, as its D_{n50} exceeds the upper limit of the Accropode. As a result, the standard toe mound type is unsuitable for cross-section C. In this case, the CLI report [1] advises to use an Accroberm II toe unit as a replacement for the traditional rockfill in the same toe mound configuration. This is a concrete toe block and its implementation adds to the development of a new ecosystem, contributing to a sustainable design. The dimensions of these units correspond to those of the armour units. As the Accroberm II unit is a substitute to the rockfill, it is advised to set the height of the unit equal to the minimum acceptable thickness for rockfill, i.e. $\frac{2}{3}H_a$. However, this suggested toe type needs more research to validate its feasibility for the design. An illustration of both an example and its application is provided in Appendix O.

8.5. Crest dimensions

The crest dimensions of the breakwater are key variables for the protection of the port. The crest height, R_c, and the crest width, B_c, are defined in order to prevent the waves from overtopping the structure. However, designing for no overtopping results in extreme conservative dimensions. As a result, some overtopping is permitted, in alignment with the design not allowing pedestrian or vehicle access on top of the breakwater. The ULS design value for the maximum allowable discharge of overtopping is set at $q = 10\,\mathrm{l/s/m}$ for $RT = 100$ years, as is introduced in Section 4.1.3.

To determine the crest height and crest width from the maximum allowable overtopping, the wave overtopping formula is applied, as recommended for design and assessment approaches: [77]

$$\frac{q}{\sqrt{g \cdot H_s^3}} = 0.1035 \cdot \exp[-(1.35\frac{R_c}{H_s \cdot \gamma_f \cdot \gamma_\beta})^{1.3}] \tag{8.8}$$

where:

H_s : Significant wave height at the toe of the breakwater (from Table 8.1);

γ_f : Roughness factor of the seaward slope of the structure; For Accropodes: $\gamma_\mathrm{f} = 0.46$ [77]

γ_β : Influence of oblique waves; $\gamma = 1 - 0.0063|\beta|$, with $\beta = 6.8°$

Given that the crest design of the breakwater does not include secondary function requirements, i.e. no road or crown wall on top of the breakwater. Therefore, the crest width, B_c, can be designed at a minimum value of $B_{c,min} = 3 \cdot D_{n50}$ [65]. Considering that similar armour units are applied on the crest as on the seaward slope, the required stone grading is already defined in Subsection 8.2.2. Below the calculated crest dimensions per cross-section are presented.

Table 8.7: Results of crest dimensions

Description	Parameter	Unit	CS - A	CS - B	CS - C
Crest height	R_c	[m]	1.95	3.23	4.56
Crown height	h_c	[m SHN]	7.26	8.54	9.87
Crest width	B_c	[m]	3.00	3.78	3.78

8.6. Rear-side stability

To finalize the cross-section dimensions of the breakwater's trunk section, parameters for the rear-side are determined. Similar to the sea side, the lee side includes a toe mound with a depth, h_l, and a shoulder width, S_l (as shown in Figure 8.1). These two parameters ensure the stability of the inner slope, which consists of single armour layer equalling the front slope and the breakwater crest. The rear-side stability is impacted by specific hydraulic forces at each cross-sectional location. These forces include water volumes from structure overtopping and wave disturbances within the harbour caused by diffraction, reflection, or in port wind-driven waves.

Considering the ULS values for water volumes overtopping the crest of the structure, the rear side needs a strong design [77]. Using similar armour units as the sea side slope of the breakwater provides sufficient strength and stability for the inner slope to withstand forces from overtopping waves.

Regarding wave disturbance, modelling the diffracted and reflected waves inside the harbour basins falls out of the scope of this project. Wind waves can be assumed as non-threatening to the stability of the inner slope, as the harbour basin dimensions do not allow for significant wave development due to wind. An assumption is made to take the bow waves of the largest vessels entering the harbour as the most extreme values for wave disturbance within the harbour basin.

To accurately determine the stability of the inner slope, multiple laboratory-scale physical tests should be conducted to evaluate the impact of overtopping waves. Moreover, modelling of diffracted, reflected, and incident waves within the harbour basin is needed for a more comprehensive understanding of the wave forces affecting the inner slope. Further research into both experimental and modelling analyses is advised for future reports to better understand the inner slope's stability of this breakwater.

In the breakwater design for this project, the Accropode armour unit is selected to adequately protect the stability of the inner slope. This conservative choice of armour size for the rear-side of the breakwater eliminates the need for additional rockfill at the toe mound. The interlocking Accropodes provide sufficient stability to withstand the minimal wave forces present within the harbour basin. To mitigate potential erosion at the base of the inner slope, a scour mattress, equal to that used at the seaward toe (see Section 8.4), is included for added protection. For the shoulder width a value of S_l = 0.5t_u is considered practical for design purposes [65]. The value for the underlayer thickness (t_u) can be found in Table 8.5. The final results of the rear-side stability parameters are presented in Table 8.8.

Table 8.8: Dimensions of rear-side stability parameters

Description	Parameter	Unit	CS - A	CS - B	CS - C
Depth in front of toe	d_l	[m]	3.47	4.14	8.75
Lee side toe depth	h_l	[m]	2.59	3.26	7.87
Lee side shoulder width	S_l	[m]	0.44	0.44	0.44

8.7. Breakwater roundhead

Having determined all the essential dimensions of the trunk section of the breakwater, only the roundhead of the breakwater remains to be designed. A detailed design is out of the scope of this project. As a result, this section provides a brief overview of the stability of the roundhead and the criterion for its radius.

The roundhead, located at the seaward end of the trunk section, is often positioned in deeper waters and experiences more extreme hydraulic conditions compared to the trunk. Particularly, as waves break at this location, it is subjected to large velocities and wave forces. As a result, the stability criteria of the trunk section do not directly apply to the roundhead. To obtain equivalent stability, the mass of the armour units is to be increased, or alternatively, the the slope is reduced [65]. These adjustments are not quantified, as they vary with each breakwater configuration.

In addition, the interlocking grid of armour units is the weakest at the breakwater head, as the grid pattern differs significantly from the pattern used in the trunk section. Not only is the placement of armour units at the head associated with larger gaps in the armour layer, but the curvature of the underlayer also badly impacts the interlocking pattern and thereby the stability of the roundhead.

In order to minimize the curvature of the underlayer and additionally prevent a significant reduction in interlocking, the radius of the breakwater's roundhead at DWL for single-layer armour units, e.g. Accropodes, should be at least three times the design wave height: [65]

$$R \geq 3H_{s,d}\,[m] \tag{8.9}$$

Where R is the radius of the roundhead and $H_{s,d}$ is the design significant wave height at the toe. This criterion ensures sufficient stability of the roundhead by maintaining the interlocking of the armour units.

8.8. Technical drawings

Technical drawings of the breakwater at cross-sections A, B, and C are presented in Figure 8.4. These illustrations provide a detailed view of the structural design at each cross-section, incorporating all the dimensions and specifications established in the preceding sections of this chapter. By visualizing the breakwater at multiple points, these drawings offer insight into the variation in structural elements across its length and highlight critical design considerations, such as material thickness, slope angles, and foundation depth. These drawings serve as a comprehensive reference for understanding the cross-sectional structure.

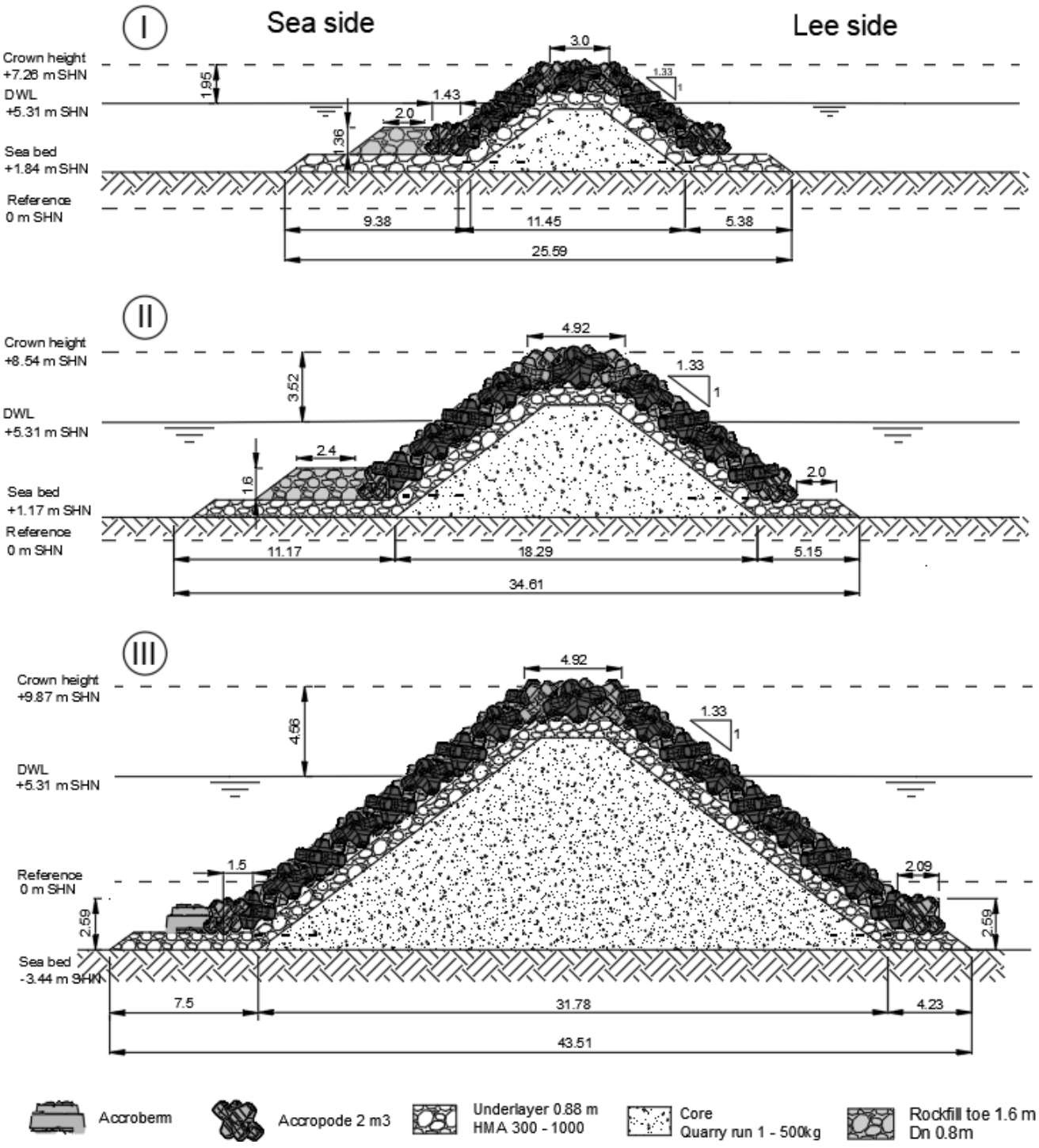


Figure 8.4: Three technical drawing of cross-section along designed breakwater at locations marked in Figure 8.2. I) Cross section at location A; II) Cross section at location B; III) Cross section at location C

8.9. Cement mixture comparison and proposal

In this section, a cement mixture is chosen to integrate in the new Accropodes. To substantiate this decision, a comparison is made between the current mixture and the proposed mixture. This is presented in Table 8.9. The values of the current mixture are taken from Appendix G, whereas the proposed mixture is cement mixture 5 from Appendix F.

Table 8.9: Mix design properties, current mixture vs. proposed mixture

Property	Unit	Current	Proposed
w/c ratio	$[-]$	0.42	0.45
Total water content	$[\mathrm{L}]$	160.0	157.5
CPP	$[\mathrm{kg}]$	380	350
Natural fine aggregate, sand (Chubut river)	$[\mathrm{kg}]$	740	-
Natural fine aggregate, sand (Aridos Fontana)	$[\mathrm{kg}]$	-	804
Natural coarse aggregate, pebble (Chubut river)	$[\mathrm{kg}]$	1095	-
Natural coarse aggregate, porphyry waste	$[\mathrm{kg}]$	-	955
Plasticizer	$[\mathrm{L}]$	1.130	0.804
Air entrapment	$[\mathrm{L}]$	-	0.057
Wet density	$[\mathrm{kg/m^3}]$	2408	2345
Dry density	$[\mathrm{kg/m^3}]$	2288	2228
28 days compressive strength	$[\mathrm{MPa}]$	33.5	41.0
Slump	$[\mathrm{cm}]$	5.0	11.0
ASR accelerated extension 16 days	[%]	0.09	0.10

Using the values from this table, several checks are performed and evaluated, which are listed below:

- According to NEN 8005:2022, the maximum allowable w/c ratio for concrete of environmental class $XF3$ is 0.5. Both mixtures suffice [52];
- The minimum required cement content is 300 $\mathrm{kg/m^3}$. Again, both mixtures suffice [52];
- Since the coarse porphyry aggregate is angular and rough-textured, the bonding strength with the cement is enhanced, compared to the bonding strength of the pebbles. [63];
- The dry densities of both mixtures are between 2200-2300 $\mathrm{kg/m^3}$. They can thus both be classified as *normal weight concrete* [15];
- The compressive strength of the proposed mixture is considerably higher than that of the current mixture. This generally means that the concrete is mechanically stronger;
- The slump test of the proposed mixture is more than twice the slump of the current mixture, resulting in a relatively increased workability, compared to the current mixture. It is concluded that the proposed mixture is easier to pour and to work with;
- Although the ASR percentage is higher in the proposed mixture, it does not exceed the specified maximum of 0.10 % [58].

To conclude, both mixtures show minimal differences, and both suffice to the relevant codes. However, the proposed mixture is shown to be more useful, since this mixture has an improved workability and compressive strength, compared to the current mixture. Next to that, Figure 3.8 confirms that the current pebbles are too large and too smooth for optimal concrete performance. Considering these factors, the proposed mixture is selected to integrate into the breakwater design.

8.10. Concrete quantification

The final section of this chapter focuses on the quantification of the Accropodes. Firstly, the volume of the required Accropodes in the newly designed breakwater is calculated. Subsequently, the Accropodes, currently positioned in the new southern breakwater, are quantified. This approach is taken to quantify the units used for the EoL solutions in the new breakwater. Finally, the required amount of raw materials and other concrete components are determined.

8.10.1. Concrete volume determination

A deterministic approach is proposed for the quantification of the Accropodes in the new breakwater, and the corresponding concrete volume [1]. This approach multiplies theoretical surface area, on which the Accropodes are distributed, with a concrete consumption coefficient. Each cross-section contains a so-called neutral fibre, a line through the centre of the armour layer. The length of the neutral line is calculated as twice the slope length, with the addition of three times the block width at the crown and one and a half times the block width at each toe. The neutral fibre is calculated for a theoretical value, however, can only contain whole blocks. Therefore two additional block widths have been taken into account for conservative measures. This results in eight block widths for toe, crown, and conservative measure. Integrating these neutral fibres over the length over the breakwater, results in the theoretical surface area. Finally, when multiplied by the concrete consumption coefficient, the volume is determined. This approach is captured in Equation 8.10.

$$V_c = C_{cc} \int_0^{L_{BW}} \left\{ 2 \cdot \frac{h_c - h}{\sin \alpha} + 8 \cdot D_v \right\} dx \tag{8.10}$$

Where:

V_c : Concrete volume [m^3]
C_{cc} : Concrete consumption coefficient [$\mathrm{m}^3/\mathrm{m}^2$]
L_{BW} : Length of the breakwater [m]
h_c : Crown height [m]
h : Water depth [m]
α : Slope [$^\circ$]
D_v : Horizontal width armour unit [m]

Using this formula, it is determined that the required concrete volume of the entire breakwater is 32,710 m^3.

8.10.2. Quantification of the current Accropodes

It is essential to elaborate on the feasibility of constructing the new breakwater, especially with the proposed sustainable concrete mixture and reuse of old Accropodes. Initial data from the Rawson Port Directorate provides a combined total volume for both the northern and southern breakwaters, detailing the volumes of three different sizes of Accropodes (1 m^3, 2 m^3, and 3 m^3) [62]. Since only the southern breakwater is of interest (Subsection 6.2.2), an estimation is made which employs a simplified calculation method based on the top-view and cross-sectional drawings of the breakwater [62]. The total volume of concrete in this section is calculated to be 9,150 m^3, assumptions and methods for this calculation are to be found in Appendix B.

Using the same subdivision of the breakwaters as shown in Figure 3.7, specific volumes are allocated to each zone, see Table 8.10.

Table 8.10: Concrete volume per zone

Zone	Volume [m^3]
Zone A	2300
Zone B	2300
Zone C	4550
Total	9150

From the previous subsection, it is determined that 32,710 m^3 of concrete is required for the new breakwater. This volume is however not the total amount of concrete to be made, since EoL solutions are applied to this project. Reusing the Accropodes of the new southern breakwater reduces the total amount of concrete needed. The total volume of concrete Accropodes to be produced thus depends on three factors: the volume of concrete needed for the new breakwater, the quantity of concrete units available for reuse, and the availability of materials for the production of the Accropodes. Furthermore, the data generated from the quantification of Accropodes and their EoL options contribute to the LCA, providing critical insights into the environmental impact of the new breakwater project.

8.10.3. Quantification of the new Accropodes

Table 8.11 denotes the EoL solutions and how much concrete is allocated to each of those solutions, in m^3. The calculation of the total volume is based on the percentages of the Accropodes per zone, as determined in Subsection 3.2.3. These are subsequently multiplied by the volumes determined in the previous subsection.

Table 8.11: End-of-Life solutions and their assigned concrete volume

End-of-Life solution	Zone A [%]	Zone B [%]	Zone C [%]	Total volume [m^3]
Reuse	80	10	-	2070
Repurpose	20	60	30	3205
Recycle	-	20	-	460
Landfill	-	10	70	3415

The new breakwater requires 32,710 m^3, as stated in Table 8.12. Subtracting the reused Accropodes from this volume yields 30,640 m^3, which corresponds to a reduction of 6.3 %. This is the total volume of the required concrete, by applying the the proposed mix design. Using Table P.2 from Appendix P, the total amount of (raw) materials needed for the new breakwater can be determined and are shown in Table 8.12. These values are also used in the LCA (Chapter 9).

Table 8.12: Concrete quantification results

Component	Amount [m^3]
Water	4991
CPP	3518
Fine aggregate	9927
Porphyry waste	12057
Plasticizer	26
Air entrainer	2

9

Concrete sustainability

A sustainability analysis is conducted to asses the viability of the proposed cement mixture and EoL solutions. Using a Life Cycle Assessment (LCA), this analysis broadens the focus to include the monetization of environmental impacts, allowing for a comprehensive evaluation of overall sustainability. Two scenarios are compared: one where the proposed cement mixture and sustainable EoL strategies are used, and another which makes use of the current mixture in combination with the landfill solution.

The LCA is structured and conducted according to various NEN norms, including NEN-EN 15804+A2 [54] [55] [56], and consists of four key phases:

- Goal and scope definition;
- Life Cycle Inventory Analysis (LCI);
- Life Cycle Impact Assessment (LCIA);
- Interpretation.

First, the goal and scope are defined in the following sections. The LCI and LCIA are presented in Appendix Q. The interpretation of the results obtained in these phases are summarized at the end of this chapter.

9.1. Goal definition

The LCA study aims to evaluate the environmental impact and possible advantages of using the proposed concrete mixture and EoL solutions. This is done by comparing two different approaches for constructing the new breakwater. The first approach involves demolishing the old breakwater and transporting all the concrete to a landfill, while constructing new Accropodes using the same concrete mixture as the current units. This approach is hereafter defined as the current method. The second approach explores the use of the proposed concrete mixture which incorporates a more sustainably sourced aggregate, i.e. porphyry waste. It assesses four different EoL options, described in Subsection 3.2.3. This approach is hereafter defined as the proposed method. The assessment focuses solely on the construction and EoL stages, excluding the operation stage.

9.2. Scope definition

In the scope of an LCA, the functional unit provides a reference for comparing environmental impacts. Here, the functional unit is defined as the Accropodes, used in both the existing and the new breakwater. This facilitates an examination of the EoL solutions, while also considering the advantages of using the proposed cement mixture. The construction of the entire breakwater involves more materials and processes than just those related to the Accropodes (e.g. the construction of the breakwater's armour layer). Nevertheless, these components are excluded from the functional unit of this study, since it is assumed that they are mostly the same for both methods. The results therefore remain comparable to one another, and the environmental impact of the entire breakwater system can still be assessed.

Both the functional units of the current method and the proposed method are evaluated to determine if they meet their functional requirements effectively. The functional requirements are specified in Section 4.1 , Chapter 8. The functional properties of the Accropodes under both methods are comparable and meet the requirements, as outlined in Table 9.1.

Table 9.1: Requirements and criteria for several functional properties

Functional properties	Unit	Current method	Proposed method	Requirement
Accropode unit volume	$[\mathrm{m}^3]$	1, 2, and 3	1 and 2	1 and 2
Concrete density	$[\mathrm{kg/m}^3]$	2288	2228	2200 - 2600
Concrete compressive strength	$[\mathrm{MPa}]$	33.5	41.0	30.0
Breakwater lifetime	$[\mathrm{y}]$	50	50	50

The system boundaries of both methods include:

- The deconstruction of the old breakwater (EoL stage C1 – C4);
- The remaining value of the old breakwater elements (D).
- The manufacturing of new Accropodes (manufacturing stage A1 - A3);
- The construction of the new breakwater (construction stage A4 – A5);

The life cycle inventory data is sourced from ENVIRONDEC, an online database for EDP's [3]. Other LCA data, including, but not limited to, product- and process-specific data, is obtained via TU Delft experts [44]. The analysis applies a scoring and evaluation method to assess environmental impacts across several categories, which are taken from NEN-EN 15804+A2 [54].

Conducting this study in Argentina poses challenges due to the lack of representative Environmental Product Declarations (EPD's). While efforts are made to use representative up-to-date information, obtaining such data is difficult. Data from comparable products and processes are used from countries in Europe and Brazil. However, since a comparative LCA is conducted, the relative difference in total shadow costs is analysed, not their absolute values. The comparison is done solely to state which process generates a lower environmental impact, the exact prices do not matter. By using data from other countries and continents in both methods, the difference in costs stays the same.

The LCA is reviewed to ensure the data quality and results are both relevant and accurate. However, some stages have been simplified. Detailed processes (e.g. how many hours a construction worker has to work to place one Accropode) are left out of the study. As a result, the total obtained shadow costs are lower than in reality. By leaving out these detailed processes in both methods, the difference in total costs stay the same. It is thus concluded that both methods are appropriate to compare.

Although the defined functional unit and system boundary provide a robust framework for evaluating the environmental impacts, it does not encompass all potential effects. Particularly those related to the broader scope of people, planet, and profit, which are difficult or even impossible to monetize [7]. The most significant factors that are outside the scope of this assessment are outlined below:

- The porphyry quarries, located in proximity to roads, present considerable safety hazards. Numerous documented incidents of vehicles veering into quarry ditches, highlight the risks they pose to the surrounding community [23];
- Porphyry quarries disrupt the landscape, leaving visible scars and waste, that diminish regional aesthetic value [23];
- Rehabilitation processes of the quarries are not possible with porphyry waste present. These rehabilitation processes are necessary to resolve the problem of desertification which is a big problem in the Chubut region [23];
- The LCA does not account for the impact on flora and fauna, resulting from the extraction of pebbles from the riverbed [17][64];
- The disruption of natural sediment transport by river pebble extraction [17][64];

9.3. Interpretation

The results give a monetization in terms of shadow costs for the two methods, in Euros. A concise interpretation of the results is visualized, in Figure 9.1 and Figure 9.2. In section Q.2 the underlying values are incorporated in Figure Q.5.

When analysing Figure 9.1, comparing the various life stages of both methods, several conclusions can be drawn. The total shadow costs of the project, using the proposed method, are reduced by 22%, compared to the current method. This reduction is mainly attributed to the use of more sustainable coarse aggregates and EoL solutions.

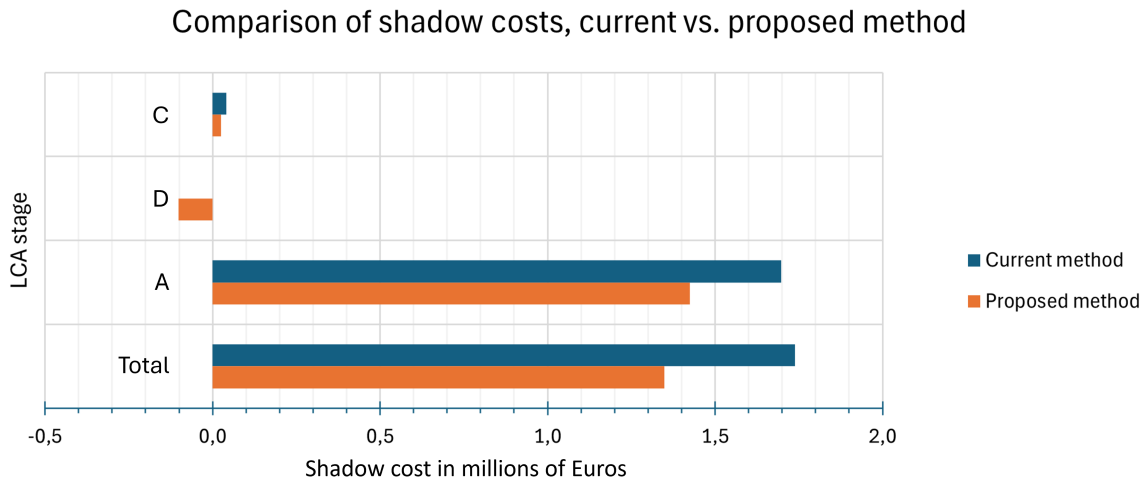


Figure 9.1: Total shadow costs of the three main stages of the LCA, visualised. The x-axis represents the costs in Euros, in millions.

The LCA aims to evaluate whether the proposed EoL solutions and the proposed cement mixture improve the project's overall sustainability. Figure 9.2 illustrates a comparison between the current and proposed methods, regarding the use of aggregates and EoL strategies. The total costs associated to the aggregates decrease by a factor of almost 4.4. Although transporting porphyry aggregates from the quarries to the construction site leads to transport impacts, the overall shadow costs remain lower than that of the locally sourced pebble aggregates. Additionally, the shadow costs for the EoL stages (stage C) and the residual value (stage D) for the proposed method accumulate to a negative shadow cost. These result from the residual value of the EoL solutions and indicate a positive environmental impact.

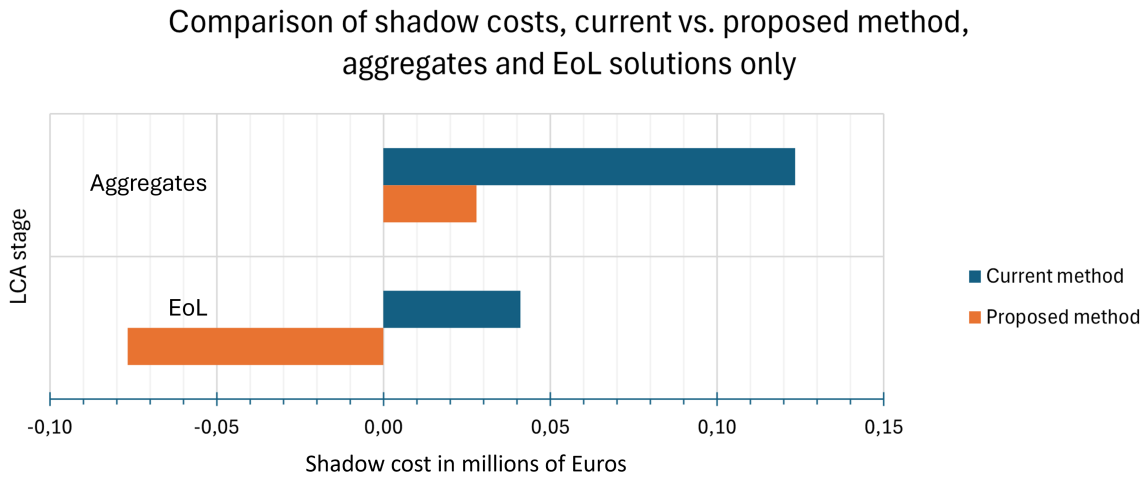


Figure 9.2: Shadow costs of the aggregates and EoL only, visualised. The x-axis represents the costs in Euros, in millions.

Based on the results of the LCIA, it can be concluded that incorporating both the proposed cement mixture, which uses porphyry quarry waste as a coarse aggregate, and the EoL solutions contribute to a construction process with reduced environmental impact.

Nevertheless, there is potential for further improvement in terms of sustainability. The shadow costs associated with CPP (the incorporated cement) still make up over 90 % of the total project shadow costs. This significant contribution indicates that the exploration of an alternative, more sustainable cement could yield benefits, in terms of additional overall project sustainability.

10

Discussion

This chapter explores the implications of the report's findings by examining not only the feasibility of the project, but also key uncertainties in the analysis. First, the feasibility of the project and the breakwater design are evaluated. Next, the discussion addresses the most significant uncertainties, offering an overview of factors that affect the reliability and applicability of the results.

10.1. Feasibility

For the port to be financially feasible, its operations, such as dredging, should remain within manageable limits. As outlined in Subsection 7.2.2, the extent to which sediment is transported to the northern coastal stretch (the erosion zone) remains unknown in this research. The model does not account for the interaction between the port water body and the ocean, leaving the extent of siltation within the harbour undetermined. It is known that concept 3 traps relatively more sediment south of the port, which in turn increases erosion to the north. The entrapment of sediment south of the port reduces siltation within the port, minimizing its impact on port operations. To still address the erosion problem, a strategy involving the dredging of the concentrated sedimentation zone, south of the proposed breakwater, is suggested. The dredged material could then be relocated to nourish the eroded coastal area at Playa Unión. This operation would require regular repetition. However, it is more financially feasible to dredge sediment in the sedimentation zone rather than allow it to flow into the harbour. Allowing sediment to accumulate in the harbour would result in widespread siltation, which would impact port operations and become a more costly alternative.

In addition to maintenance dredging, the access channel and inner port require dredging through hard, rocky material, which presents technical challenges and adds to overall costs. An examination by port experts is necessary to assess the feasibility of the to-be-dredged access channel, in conjunction with the proposed port layout.

Extending the port to the south requires cooperation between the landowner and the owner of the breakwater (the local government). Both parties must first agree on the plans before the government can issue permits. Additionally, the landowner will need to secure funding for the project. Given the current economic situation in Argentina, securing the necessary funding for such a large project is challenging.

10.2. Uncertainties

In addition to evaluating the overall feasibility of this project, uncertainties in this report persist concerning data accuracy, wave modelling, sediment transport calculations, design specifications, and concrete analysis. Each of these uncertainties is briefly discussed in the following sections.

10.2.1. Data

This subsection highlights two primary areas of uncertainty: the analysis of ERA5-data and the SOM approach to the data.

ERA5 data analysis

ERA5 data, while comprehensive, is based on model assimilation and reanalysis, which introduces inaccuracies, especially near coastlines. Additionally, the data analysis relies on a single offshore extraction point, located 50 km south-east of Puerto Rawson. Including extraction points to the east and north-east of Puerto Rawson could provide deeper insights into the offshore wind and wave climate. This would be similar to the approach used in the Córdoba study [22]. Furthermore, there is considerable uncertainty in the EVA, especially when estimating extreme events with a return period of 100 years. The EVA relies heavily on extrapolation, which amplifies any underlying data or model uncertainties.

SOM analysis

In the SOM analysis, three uncertainties need to be addressed. Firstly, the selection of neurons and clusters is not conducted using established methods, such as the Elbow Method or cross-validation. Instead, the number of clusters (k = 12) is predetermined, due to time constraints for the longshore sediment transport analysis. Secondly, validation and calibration of both the neural network and k-means clustering are not performed, which affects the reliability of the results. Finally, rigorous downscaling and significant simplification of the data are applied, which leads to loss of information.

10.2.2. Wave model and sediment transport

Key uncertainties related to the wave model and the evaluation of its results are listed below. While additional uncertainties exist, the following are deemed the most significant for consideration.

Model assumptions and simplifications

SWAN, like other numerical models, operates on a series of assumptions and simplifications to approximate complex physical processes. These involve approximations in wave transformations and hydrodynamic interactions. Although such simplifications are necessary for computational efficiency, they inevitably introduce uncertainties in the outcome of the model. It is essential to acknowledge that a full replication of all physical processes is not possible, leading to an inherent degree of approximation and associated uncertainty.

Uncertainty due to numerical approximations

The numerical methods employed in SWAN to solve hydrodynamic and wave equations further contribute to model uncertainties. Elements such as grid size and choice of specific numerical schemes can all impact the accuracy of simulations. For instance, using a finer grid can yield more detailed results, though it requires higher computational resources. Therefore, a trade-off between the two always needs to be made.

Boundary conditions and stationarity

The boundary conditions and choice of stationary simulations, such as the defined position for offshore conditions, are made based on assumptions. Any simplification within these inputs can propagate through the model, influencing the reliability of the results. For instance, wave interactions, near boundaries from different input parameters. This can partly be mitigated by choosing the grid and generating outcomes, such that these are further away from the boundaries.

Sediment transport calculation

As outlined in Chapter 5, numerous assumptions were necessary in calculating sediment transport, due to limited data availability and time constraints within this study. It is essential to reiterate that these results should be interpreted qualitatively rather than quantitatively. The use of the CERC formulation provides a preliminary assessment of sediment transport. However, it does not comprehensively account for all morphodynamic and hydrodynamic processes involved. The representation of sediment properties is particularly limited, underscoring the need for further research to achieve a more accurate evaluation of the local coastal dynamics.

10.2.3. Conceptual design

This subsection outlines the key assumptions and uncertainties involved in the conceptual design of the port expansion.

Breakwater removal

It is assumed that the removal of the entire southern breakwater can be integrated into the design. However, it remains uncertain whether modifications to the existing breakwater configuration are permitted by the local authorities, as the breakwater is owned by a different party from the one facilitating the port expansion. This introduces potential challenges, that could negatively impact the project's progress. If no adjustments to the southern breakwater are allowed, concept 2 would serve as a practical alternative.

Panamax

It is assumed that Panamax-class vessels are able to turn outside the port area before being assisted through the port entrance. Through consultations with stakeholders, it was determined that turning Panamax vessels outside the port is an acceptable solution. Moreover, as these vessels only arrive a few times per year, finding a suitable weather window is feasible.

Access channel configuration

The alignment of the access channel in the final conceptual design is 90 degrees, with respect to the dominant wave direction (SSE). According to PIANC guidelines, this is classified as a suboptimal situation, as harsh weather conditions could cause vessels to drift off course, therefore requiring higher vessel speeds in the access channel. This in turn results in a longer breaking zone, which should be integrated into the design to ensure navigational safety.

Bathymetry

The most recent bathymetric surveys of the seabed were conducted in 2010 and 2014, and these measurements have been fused with GEBCO data to form the bathymetry used in this research. While inherent measurement uncertainties exist in both data sets, it is uncertain whether the current bathymetry of the restinga still matches the used data. Given the dynamic nature of coastal areas, the bathymetry is likely to have altered. This uncertainty affects the accuracy of the model as well as the final conceptual design.

Quantification

There are inherent uncertainties in the approach, used to calculate the concrete volumes of the proposed breakwater. The calculation method assumes that multiplying the surface area by a consumption factor yields the necessary concrete volume. However, the actual quantity may vary, as the design specifies the use of individual concrete blocks and a particular crown height, potentially leading to a requirement for more blocks than initially estimated. Furthermore, the roundhead of the breakwater is not included in the calculation, which would likely result in an increase of total concrete volume. Beyond these calculation uncertainties, the placement of Accropodes in a random arrangement can also cause the required quantity to vary.

Optimal armour unit

This report presents a proposed design for the breakwater as part of the port expansion. Following consultations with stakeholders, it was decided to use the Accropode armour unit in this design. Since only one design option is developed, alternative armour units are not analysed. It is possible that alternative armour units could result in a design requiring fewer materials.

10.2.4. Concrete

The uncertainties regarding concrete can be subdivided into the three branches of the structural methodology: inspection (data collection), the cement mixture, and sustainability. These are discussed in detail below.

Inspection

The observations from the visual inspections conducted at the new northern breakwater are assumed to be applicable to the new southern breakwater, although the rate of degradation may differ. Additionally, visual inspection alone is inadequate for evaluating degradation caused by internal mechanisms, which leads to discrepancies between the observed and actual condition of the Accropodes. Consequently, the classification into EoL solutions may not accurately reflect the true state of the Accropodes, leading to potential errors in the associated percentages.

Cement mixture

The proposed mixture is solely based on the research of Mrs. Cotti, summarized in Appendix F [23]. While this provides a solid foundation, relying on a single research without conducting additional tests limits the applicability and performance of the mixture under project specific conditions.

Sustainability

The calculation of shadow costs for the materials and processes studied in Section Q.2 relies on data from Brazil and Europe, as Argentinian data was unavailable. Furthermore, not all construction processes have been accounted for, and the environmental impact of porphyry aggregate extraction is assumed to be zero. This means that, while this may influence the absolute value of the total shadow costs, its impact on the comparative analysis between the current and proposed methods is limited.

11

Conclusion

In this chapter, the five sub-questions presented are answered. Through these answers, the main research question is addressed.

1. What is a feasible conceptual design that aligns with the objectives of future port expansion?

After having incorporated the design criteria and design aspirations, a representable and feasible conceptual design of a port expansion is established and shown in Figure 6.2. Given the expansion ambitions of the port in the near future, this design serves as a comprehensive plan that expands the harbour area to meet realistic future port operations.

2. What are the nearshore extreme wave conditions?

An extreme value analysis of 30 years of offshore data reveals that storms predominantly approach from the south-east, with H_s = 6.90 m for a 100-year return period. When implementing these results in the SWAN model, they indicate nearshore storm conditions with H_s = 3.98 m.

3. How do different breakwater layouts influence longshore sediment transport?

The runs of the SWAN model, combined with the CERC formula, show varying longshore sediment transport outcomes, based on different port breakwater layouts. Concept 1, with a 43° angle between the waves and breakwater, maximizes alongshore sediment transport. In contrast, other angles (concepts 2 and 3) cause sediment accumulation in front/south of the port. However, to ensure effective port operations, a design with a greater sediment-blocking angle is preferred, combined with maintenance dredging. The dredged sediment can then be deposited on the eroded coastline to the north as nourishment.

4. What are the dimensions of the breakwater introduced in the conceptual port expansion design?

The design results are captured in three drawings of different cross-sections of the conceptual designs. These drawings give further inside into the dimensions of the breakwater and can be found in Figure 8.4. The design incorporates Accropode armour units of 1 m^3 and 2 m^3, and in some areas an Accroberm toe is required. The total amount of concrete required for this design is 32710 m^3.

5. What improvements in concrete mixture design can enhance the sustainability and durability of the new breakwater?

The proposed cement mixture design, which integrates porphyry waste as a replacement for river pebble aggregates, offers improved physical properties and durability. By enhancing this mixture, using sustainable EoL solutions in the proposed construction method, the project achieves greater sustainability, expressed in lower total shadow costs.

These research questions are directly linked to the identified problem of sediment imbalance caused by the existing port layout, as outlined in the problem statement. Addressing these questions will help determine how the port expansion can be achieved sustainably, while minimizing its impact on coastal erosion and sedimentation issues.

The main research question this report aims to answer is:

How can a sustainable and durable port expansion at Puerto Rawson be realised, while minimizing its environmental impact, particularly in relation to sediment imbalance along the coast?

By integrating insights from multiple disciplines for the examination of the port design aspects, such as a breakwater, new possibilities are explored and innovative solutions are developed. The data and model provide valuable insights into the coastal dynamics around Puerto Rawson. The proposed concrete mixture, along with the End-of-Life solutions, minimize environmental impact and enhance durability of the armour units. This sustainable breakwater design, effectively integrated into Puerto Rawson, accommodates for future port expansions.

12

Recommendations

Based on the findings and analyses presented in this report, the following recommendations are proposed to address key challenges and optimize the project's outcomes.

The coast of Playa Unión currently faces significant erosion issues. Even if port expansion is executed immediately, the findings indicate that this would not effectively resolve the erosion problem without additional regular dredging and nourishment plans. Therefore, it is recommended to decouple the objectives of mitigating coastal erosion and expanding the port, approaching them as distinct challenges. Addressing the erosion problem demands further research into coastal protection measures, such as groynes or foreshore nourishments. However, once the port expansion is implemented, the concentrated sediment deposition zone south of the port could serve as a strategic dredging site. Sediment collected here could be regularly redistributed through maintenance nourishments. A well-planned maintenance strategy could offer a feasible long-term solution for the Playa Unión coastline.

It is recommended that the development of a new cement mixture does not rely solely on literature research, but also involves the creation and testing of various mixtures. In these studies, the potential use of porphyry waste as a fine aggregate could also be explored. Additional tests, such as core sampling for ASR reactivity, are needed to assess deterioration processes more accurately. To decrease environmental impact, future studies could consider using cement with a lower environmental impact. In these studies, a more robust LCA can be achieved by integrating country-specific EPD's, and extending the scope to the entire breakwater system. Finally, a construction plan could ensure Accropode reuse in the new crown, maintaining port functionality by completing the new breakwater before dismantling the old.

For future studies, it is recommended to explore multiple design variants and evaluate them using a Multi-Criteria Analysis (MCA), with particular attention to material usage to reduce both costs and environmental impact. Additionally, alternative armour units should be assessed, as they may reduce the demand for raw materials. Other areas for further investigation include optimizing maintenance dredging, analysing wave reflection in the port, and studying the access channel's effects on longshore sediment transport.

To realize the economic potential of Puerto Rawson and the Chubut province, a collaborative approach among key stakeholders — such as landowners, local government, and the fishing community — is essential. By uniting efforts, stakeholders can work towards a port design that addresses both economic and environmental needs. Additionally, implementing an effective maintenance strategy is crucial, not only to enhance port efficiency but also to mitigate erosion at Playa Unión. Together, these efforts can lay the foundation for sustainable regional growth.

References

[1] Concrete Layer Innovations (CLI). *ACCROBERM II Design Guidelines*. Version V03, Published in February 2023. Concrete Layer Innovations. 2023.

[2] Servicio Meteorológico Nacional (SMN). *Estadísticas Climatológicas Normales - período 1991-2020*. Tech. rep. Relevant data found in rows 662 to 669. Servicio Meteorológico Nacional, 2023. URL: https://ssl.smn.gob.ar/dpd/observaciones/estadisticas_normales_9120.zip.

[3] EPD International AB. URL: https://www.environdec.com/home.

[4] Harbour used for transport of Accropodes by boat to artificial reef projects near Puerto Madryn. Calculations of transportation distances in Appendix Q are based on the location of the harbour. URL: https://appm.com.ar/.

[5] International Atomic Energy Agency. "Guidebook on non-destructive testing of concrete structures". In: *Training Course Series* 17 (2002).

[6] Instituto Nacional del Agua. *ESTUDIO MEDIANTE MODELACION MATEMATICA DEL CLIMA DE OLAS EN EL PUERTO DE RAWSON*. Tech. rep. INA Laboratorio de Hidraulica, 2009.

[7] Hanan Alhaddi et al. "Triple bottom line and sustainability: A literature review". In: *Business and Management studies* 1.2 (2015), pp. 6–10.

[8] Jose-Henrique Alves and Michael Banner. "Performance of a Saturation-Based Dissipation-Rate Source Term in Modeling the Fetch-Limited Evolution of Wind Waves". In: *Journal of Physical Oceanography - J. Phys. Oceanogr.* 33.6 (2003), pp. 1274–1298. DOI: 10.1175/1520-0485(2003)033<1274:POASDS>2.0.CO;2. URL: https://doi.org/10.1175/1520-0485(2003)033%3C1274:POASDS%3E2.0.CO;2.

[9] A. Ardolino, J. L. Panza, and E. Ylláñez. *Geological Sheet 4566 I Garayalde, Chubut Province.* Site study. 2003.

[10] A. D. Ashton and A. B. Murray. "High-angle wave instability and emergent shoreline shapes: 1. Modeling of sand waves, flying spits, and capes". In: *Journal of Geophysical Research* 111 (2006), F04011. DOI: 10.1029/2005JF000422. URL: https://doi.org/10.1029/2005JF000422.

[11] A. D. Ashton and A. B. Murray. "High-angle wave instability and emergent shoreline shapes: 2. Wave climate analysis and comparisons to nature". In: *Journal of Geophysical Research* 111 (2006), F04012. DOI: 10.1029/2005JF000423. URL: https://doi.org/10.1029/2005JF000423.

[12] Serman y Asociados s.a. *19-014-IB-PR-EN-IF-101-Informe Final-A-0B-SAC: NAUTICO MUELLES CORPORACION PUERTO RAWSON*. Tech. rep. Industrias Bass, 2019.

[13] Serman y Asociados s.a. *Dimensionado de espigón interior en Puerto Rawson*. Tech. rep. Industrias Bass, 2021.

[14] Mark Baine. "Artificial reefs: a review of their design, application, management and performance". In: *Ocean & Coastal Management* 44.3-4 (2001), pp. 241–259. DOI: https://doi.org/10.1016/S0964-5691(01)00048-5.

[15] Betonhuis. *Betonpocket 2020*. 2021.

[16] J. Bosboom and M. J. F. Stive. *Coastal Dynamics*. 1.2. Delft, The Netherlands: Delft University of Technology, TUDelft Open, Jan. 2023. ISBN: 978-94-6366-370-0. DOI: 10.5074/T.2021.001. URL: https://doi.org/10.5074/T.2021.001.

[17] Siamak Boudaghpour and Seyyed Arman Hashemi Monfared. "Environmental effects of irregular extracting of gravel from river beds". In: *Proceedings of the 3rd IASME/WSEAS international conference on Energy & Environment*. 2008, pp. 213–218. DOI: https://dl.acm.org/doi/abs/10.5555/1576758.1576795.

[18] F. Brágoli and H.J. Donini. *Impacto del puerto en la dinámica costera de Playa Unión*. Site study.

[19] Philip Jun Celerinos et al. “An assessment of rebound hammer test in estimating the concrete compressive strength in seawater”. In: *Res. Eng. Struct. Mater.* (2023), pp. 947–967. DOI: http://dx.doi.org/10.17515/resm2023.712me0321.

[20] PJ Celerinos et al. “Influence of seawater exposure at the splash zone on the reliability of the rebound hammer test in estimating concrete compressive strength”. In: *Res. Eng. Struct. Mater.* (2024). DOI: http://dx.doi.org/10.17515/resm2024.120me1211rs.

[21] A Waste separation, treatment, and final disposal plant. This plant is used for the landfill of Accropodes from the old breakwater. Calculations of transportation distances in Appendix Q are based on the location of the plant. URL: https://consorciogirsu.com.ar/.

[22] Universidad Nacional de Córdoba. *ESTUDIO DE LA DINÁMICA COSTERA DE PLAYA UNIÓN Y PROPUESTA DE PROTECCIÓN PARA LA COSTANERA, PROVINCIA DE CHUBUT*. Tech. rep. FACULTAD DE CIENCIAS EXACTAS, FÍSICAS Y NATURALES LABORATORIO DE HIDRÁULICA, 2022.

[23] Leda Cotti de la Lastra. “Aporte al Desarrollo sustentable en la Patagonia Argentina a partir de la utilización del material de descarte de la industria del pórfido como agregado en hormigón”. Summary can be found in Appendix F.

[24] Bart Craeye, Patricija Kara De Maeijer, and Neel Renne. “Effect of carbonation on non-destructive strength and durability assessment of limestone based concrete”. In: *Proceedings of the International Conference on Non-destructive Evaluation of Concrete in Nuclear Applications*. 2023.

[25] Jacqueline Cramer. “Circulaire economie: van visie naar realisatie”. In: *Utrecht Sustainability Institute* (2015).

[26] J. L. Davies and K. M. Clayton. *Geographical Variation in Coastal Development*. 2nd. Longman Publishing Group, 1980. ISBN: 9780582484344.

[27] Farid Debieb et al. “Mechanical and durability properties of concrete using contaminated recycled aggregates”. In: *Cement and Concrete Composites* 32.6 (2010), pp. 421–426. ISSN: 0958-9465. DOI: https://doi.org/10.1016/j.cemconcomp.2010.03.004.

[28] H. J. Donini. “Los procesos de erosión costera en Playa Unión desde 1963: análisis retrospectivo e incidencias de las obras portuarias y de protección ejecutadas”. MA thesis. Universidad Nacional de la Patagonia San Juan Bosco, 2021.

[29] H.J. Donini. *Los procesos de erosión costera en Playa Unión*. Site study. 2022.

[30] Google Earth. *Google Earth*. Accessed: 2024-10-09. 2024. URL: https://www.google.com/earth.

[31] ECMWF. *ERA5: data documentation*. 2024. URL: https://confluence.ecmwf.int/display/CKB/ERA5%3A+data+documentation (visited on 09/30/2024).

[32] EN13383-1. *European norm: Armourstona - Part 1: Specification*. European committee for standardization. 2013. URL: https://nobelcert.com/DataFiles/FreeUpload/EN%2013383-1-2013.pdf.

[33] EPSG.io. *EPSG:5345 - Projected Coordinate System*. Accessed: 2024-09-10. 2024. URL: https://epsg.io/5345.

[34] J. Fredsøe and R. Deigaard. “Mechanics of Coastal Sediment Transport”. In: *Journal of fluid mechanics* (1992), p. 369. DOI: 10.1017/S0022112095212187. URL: https://doi.org/10.1017/S0022112095212187.

[35] GEBCO. *GEBCO Gridded Bathymetry Data*. Accessed: 2024-09-08. 2024. URL: https://www.gebco.net/data_and_products/gridded_bathymetry_data/.

[36] GitHub. *minisom*. 2024. URL: https://github.com/JustGlowing/minisom (visited on 10/29/2024).

[37] K. Hasselmann et al. “Measurements of wind-wave growth and swell decay during the Joint North Sea Wave Project (JONSWAP)”. In: *Ergänzungsheft zur Deutschen Hydrographischen Zeitschrift, Reihe A(8), No. 12* (1973), 95 pp. DOI: 10.12691/ajme-5-2-1. URL: https://doi.org/10.12691/ajme-5-2-1.

[38] L. H. Holthuijsen. *Waves in Oceanic and Coastal Waters*. Cambridge University Press, 2007. DOI: 10.1017/CBO9780511618536. URL: https://doi.org/10.1017/CBO9780511618536.

[39] IBM. *What is a k-means clustering?* 2024. URL: https://www.ibm.com/topics/k-means-clustering (visited on 10/29/2024).

[40] IBM. *What is a Neural Network?* 2024. URL: https://www.ibm.com/topics/neural-networks (visited on 10/29/2024).

[41] Concrete Layer Innovations. *ACCROPODE™ Basic Specifications Version D*. Tech. rep. Limited validity, contact CLI. Concrete Layer Innovations (CLI), 2015.

[42] Centro de Investigación de los Reglamentos Nacionales de Seguridad para las Obras Civiles (CIRSOC). *Reglamento Argentino de estructuras de hormigón*. July 2005.

[43] IRAM. *1674: Agregados determinación de la reactividad alcalina potencial método acelerado de la barra de mortero*. 1997.

[44] H.M. Jonkers and N.G. Ozerkan. These are the files which are used in Appendix Q, in the determination of the shadow costs.

[45] P. D. Komar and D. L. Inman. "Longshore sand transport on beaches". In: *Journal of Geophysical Research* 75.30 (1970), pp. 5914–5927. DOI: 10.1029/JC075i030p05914. URL: https://doi.org/10.1029/JC075i030p05914.

[46] Povindar Kumar Metha and Paulo Monteiro. *Concrete: Microstructure, Properties, and Materials*. McGraw-Hill Publishing, 2006.

[47] MP341. *Possible integrated coastal interventions in Playa Unión and Puerto Rawson*. Study assignment MP341. TU Delft, 2023.

[48] Markus Muttray and Bas Reedijk. "Design of concrete armour layers". In: *Hansa International Maritime Journal* 6 (2009), pp. 111–118. URL: https://www.researchgate.net/profile/Bas-Reedijk/publication/275960407_Design_of_Concrete_Armour_Layers/links/554b8c450cf21ed213594b1a/Design-of-Concrete-Armour-Layers.pdf.

[49] NASA. *IPCC AR6 Sea Level Projection Tool*. Accessed: 2024-09-17. 2024. URL: https://sealevel.nasa.gov/ipcc-ar6-sea-level-projection-tool.

[50] Servicio De Hidrografía Naval. *Hidrografía Naval*. Accessed: 2024-09-20. 2024. URL: http://www.hidro.gov.ar/.

[51] Cameron Nelson. website used for the figures of the schematic Akmon and Accropode units (Figure 3.5 and Figure 3.6). URL: https://www.cameronnelson.net/pages/tetrapods.php.

[52] NEN. *8005: Dutch supplement to NEN-EN 206: Concrete - Specification, performance, production and conformity*. 2022.

[53] NEN-EN. *12504-2: Testing concrete in structures - Part 2: Non-destructive testing - Determination of rebound number*. 2012.

[54] NEN-EN. *15804+A2: Sustainability of construction works - Environmental product declarations - Core rules for the product category of construction products*. 2019.

[55] NEN-EN-ISO. *14040: Environmental management - Life cycle assessment - Principles and framework*. 2006.

[56] NEN-EN-ISO. *14044: Environmental management - Life cycle assessment - Requirements and guidelines*. 2006.

[57] NEN-EN-ISO. *14688-2:2019 + 8991:2020: Geotechnical investigation and testing - Identification and classification of soil - Part 2: Principles for a classification*. 2020.

[58] TG Nijland, WA de Bruijn, and JBH Jansen. "Preventie van betonschade door ASR reactie: Toelichting op CUR-Aanbeveling 89". In: *Cement* 54 (2002), p. 85.

[59] Dragos y Obras Portuarias S.A. "Estudio de las proportiones de hormigones informe tecnico". This is the unpublished technical document of DyOPSA, with tests and results of the current concrete mixture, conducted by ITH and LABIEVI. A summary of the studies is found in Appendix G. Also contains the granulometry of the current mixtures, these are found in Appendix H. 2001.

[60] PIANC. *Master plans for the development of existing ports*. MarCom Report 158. PIANC, 2014.

[61] PortalPortuario. “Argentina: Company in charge of dredging”. In: *PortalPortuario* (2023).

[62] Dirección General de Puerto Rawson. “Supervisión de la Obra: Remodelación de PUERTO RAWSON - 1 ° Etapa”. Technical information about the construction of the breakwaters. 2001.

[63] G Appa Rao and BK Raghu Prasad. “Influence of the roughness of aggregate surface on the interface bond strength”. In: *Cement and Concrete Research* 32.2 (2002), pp. 253–257. DOI: https://doi.org/10.1016/S0008-8846(01)00668-8.

[64] ES Rentier and LH Cammeraat. “The environmental impacts of river sand mining”. In: *Science of the Total environment* 838 (2022). DOI: https://doi.org/10.1016/j.scitotenv.2022.155877.

[65] Construction Industry Research and Information Association (CIRIA). *The Rock Manual: Physical Processes and Design Tools*. CIRIA C683. Construction Industry Research and Information Association. 2007. URL: https://www.ciria.org.

[66] Maria S Ribeiro, João Lage, and Arlindo Gonçalves. “Chloride assessment in structures. Influences of sampling and test location”. In: *Cement and Concrete Research* 117 (2019), pp. 82–90. DOI: https://doi.org/10.1016/j.cemconres.2019.01.002.

[67] Serman & asociadios S.A. *ESTUDIO NÁUTICO MUELLES CORPORACIÓN PUERTO RAWSON*. Tech. rep. Serman & asociadios S.A., Oct. 2019.

[68] Md Safiuddin et al. “Early-age cracking in concrete: Causes, consequences, remedial measures, and recommendations”. In: *Applied Sciences* 8.10 (2018), p. 1730. DOI: https://doi.org/10.3390/app8101730.

[69] R Narayan Swamy et al. *The alkali-silica reaction in concrete*. Tech. rep. Blackie Glasgow, 1992.

[70] SWAN Team. *SWAN - Simulating WAves Nearshore*. Version 41.51. Accessed: 2024-09-12. 2024. URL: https://swanmodel.sourceforge.io/.

[71] SWAN Team. *SWAN User Manual*. Version 41.51. Homepage: http://www.swan.tudelft.nl. Delft University of Technology, Faculty of Civil Engineering and Geosciences, Environmental Fluid Mechanics Section. P.O. Box 5048, 2600 GA Delft, The Netherlands, 2024.

[72] D. Todd, A Blanksby, and J. Schepis. “Verification of design life exposure and performance of a berm breakwater”. In: *Coastal engineering* (2012).

[73] Tremix s.r.l. is a company dedicated to the production of premixed concrete for construction projects. The old Accropodes are crushed at this plant into RCA. Calculations of transportation distances in Appendix Q are based on the location of the plant. URL: https://www.tremixsrl.com.ar/.

[74] Modeling Uncertainty and Data for Engineers. *Feedforward Neural Networks*. Tech. rep. Technical University of Delft, 2023.

[75] J. W. Van der Meer, K. D’Angremond, and E. Gerding. *Toe Structure Stability of Rubble Mound Breakwaters*. Ed. by J. E. Clifford. London: Thomas Telford, 1995.

[76] J.W. Van der Meer. “Stability of cubes, tetrapods and Accropode”. In: *Design of Breakwaters ’88*. Eastbourne, 4-6 May. London: Thomas Telford, 1988, pp. 71–88.

[77] J.W. Van der Meer et al. *Manual on Wave Overtopping of Sea Defences and Related Structures*. 2nd. www.overtopping-manual.com, 2018.

[78] del Vecchio. *Caracterización morfodinamica de Playa Unión*. Feasability study 1.EE.696. Ministery of interior, public works, and housing (Argentina), 2018.

[79] H.J. Verheij, P. Taneja, and H.J. de Vriend. *Ports and Waterways – Navigating the Changing World*. Ed. by Mark van Koningsveld. Licensed under CC BY-NC-SA 4.0. Delft, The Netherlands: Delft University of Technology, Hydraulic Engineering, Ports and Waterways, 2023. ISBN: 978-94-6366-443-1. DOI: 10.5074/T.2021.004. URL: https://textbooks.open.tudelft.nl.

[80] J. Wu. “Wind-stress coefficients over sea surface from breeze to hurricane”. In: *Journal of Geophysical Research* 87.C12 (1982), pp. 9704–9706. DOI: 10.1029/JC087iC12p09704. URL: https://doi.org/10.1029/JC087iC12p09704.

[81] L. Yan. *An Improved Wind Input Source Term for Third Generation Ocean Wave Modelling*. Scientific Report WR-87–8. De Bilt, Netherlands: Royal Netherlands Meteorological Institute (KNMI), 1987.

A

Visual inspection photos

This appendix contains the photos made of the Accropodes in Puerto Rawson.

The new northern breakwater has a walkway consisting of concrete slabs, of which there are 221. The unit closest to the shoreline is unit 1 and the unit furthest from the shoreline (at the breakwater head) is unit 221. The Accropodes are only present at the northern side of the breakwater, except for near the head, where the units are engulfing the breakwater from all sides. Since the expectation was that the extent of the damage was worse near the head, more measurements and comparisons have been done here. Figure A.1 denotes the locations of the breakwater where photos have been taken. There are 7 test locations, 3 of which are near the head of the breakwater: 218 N(orth), 218 S(outh) and 221. Therefore, there are 21 photo locations in total, which are named by their location in the cross-section (A, B or C, from Figure 3.7), and their location as viewed from above (0, 40, 80, from Figure A.1). Section A.1 contains the photos of the reference unit in front of the Port Directorate, whereas Section A.2 contains the photos taken on the new northern breakwater.

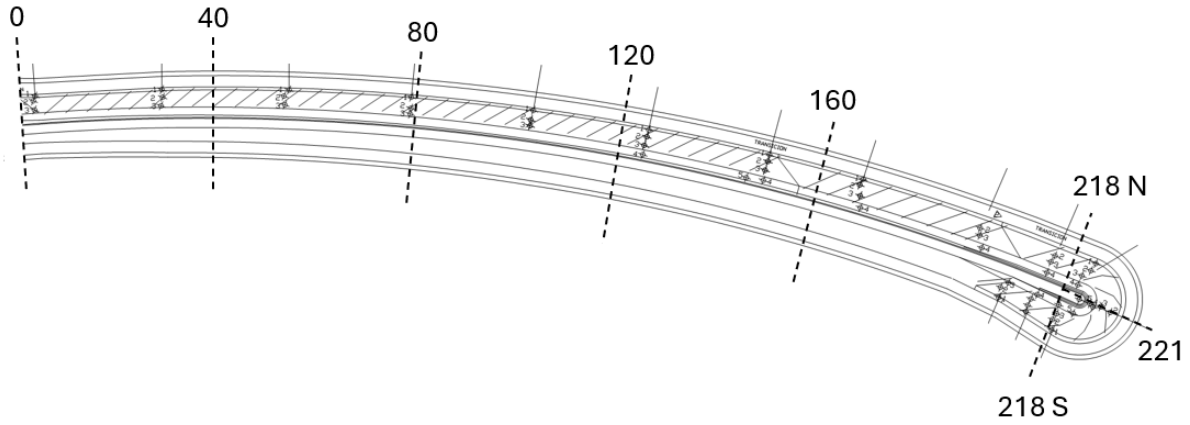


Figure A.1: Drawing of the new northern breakwater. The numbers denote the locations of where the photos were taken. The diagonally striped area is covered by Accropodes [62].

A.1. Accropodes: reference unit



Figure A.2: Photo of reference unit - 1



Figure A.3: Photo of reference unit - 2



Figure A.4: Photo of reference unit - 3



Figure A.5: Photo of reference unit - 4

A.2. Accropodes: on the breakwater



Figure A.6: Photo of unit A0



Figure A.7: Photo of unit A40 - 1



Figure A.8: Photo of unit A40 - 2



Figure A.9: Photo of unit A80 - 1



Figure A.10: Photo of unit A80 - 2



Figure A.11: Photo of unit A120 - 1



Figure A.12: Photo of unit A120 - 2



Figure A.13: Photo of unit A160 - 1



Figure A.14: Photo of unit A160 - 2



Figure A.15: Photo of unit A218 - N



Figure A.16: Photo of unit A218 - S - 1



Figure A.17: Photo of unit A218 - S - 2



Figure A.18: Photo of unit A218 - S - 3



Figure A.19: Photo of unit A221



Figure A.20: Photo of unit B0



Figure A.21: Photo of unit B40 - 1



Figure A.22: Photo of unit B40 - 2



Figure A.23: Photo of unit B80 - 1



Figure A.24: Photo of unit B80 - 2



Figure A.25: Photo of unit B120



Figure A.26: Photo of unit B160 - 1



Figure A.27: Photo of unit B160 - 2



Figure A.28: Photo of unit B218 - N



Figure A.29: Photo of unit B218 - S



Figure A.30: Photo of unit B221



Figure A.31: Photo of unit C0



Figure A.32: Photo of unit C40



Figure A.33: Photo of unit C80 - 1



Figure A.34: Photo of unit C80 - 2



Figure A.35: Photo of unit C120



Figure A.36: Photo of unit C160



Figure A.37: Photo of unit C218 - N



Figure A.38: Photo of unit C218 - S



Figure A.39: Photo of unit C221 - 1



Figure A.40: Photo of unit C221 - 2

B

Concrete volume determination

In this appendix, the volume of the concrete Accropodes in the current southern breakwater is estimated using data (Accropode distributions, top-view drawings, and cross-sectional drawings) from the Rawson Port Directorate [62]. The Accropodes in the northern and southern breakwaters have a combined volume of 14847 m^3. This is the total volume of the three different types of Accropodes used: 1 m^3, 2 m^3, and 3 m^3. In Table B.1 the total amount of units and the corresponding volumes are given per type of Accropode.

Table B.1: Total Accropode unit amount and volume

Accropode type	**Units**	**Volume [m^3]**
1 [m^3]	3180	3180
2 [m^3]	3870	7740
3 [m^3]	1309	3927
Total	8359	14847

In order to estimate the total volume of concrete in the southern breakwater, the northern and southern breakwater are divided into three distinct regions:

- The northern strip (light green);
- The centre strip (light blue);
- The Southern strip (light orange).

This division is visualised in Figure B.1 and Figure B.2. It is assumed that each of these strips contain an equal amount of concrete per unit of length. The figures further highlight sections where different types of Accropodes are used. The section boundaries are specified by dashed lines which run perpendicular to the breakwater's central axis and mark a location in metres. This value refers to the distance along its central axis from the beginning of the breakwater.

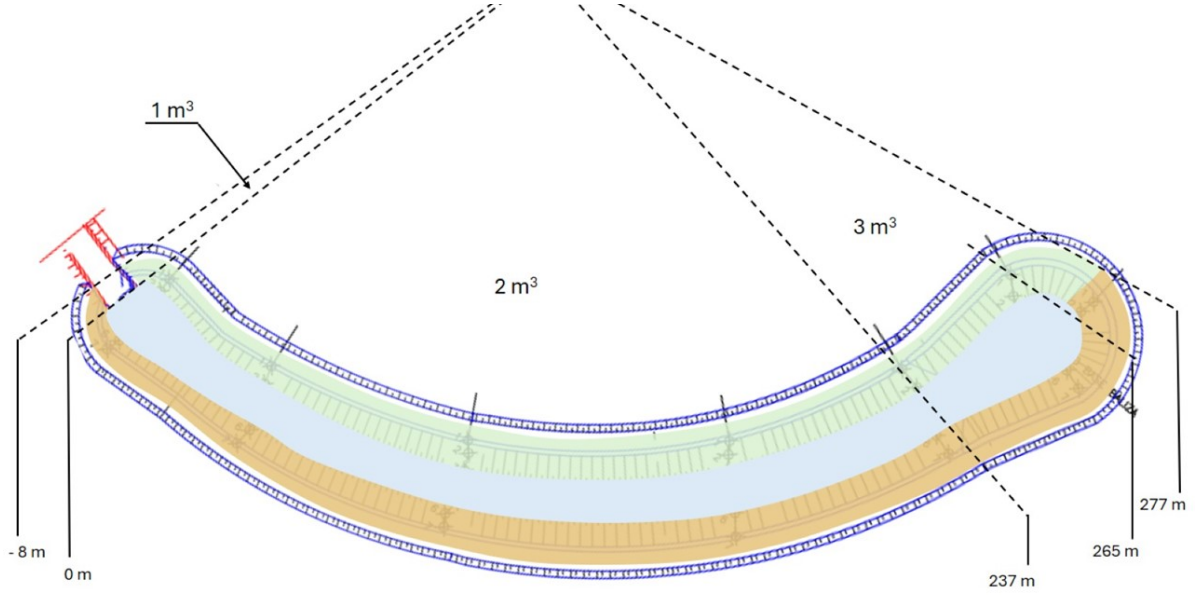


Figure B.1: Division of the New Southern breakwater. The light green, light blue, and light orange areas respectively denote the northern, centre, and southern strips. The dashed lines denote boundaries between sections, where each section employs another type of Accropode.

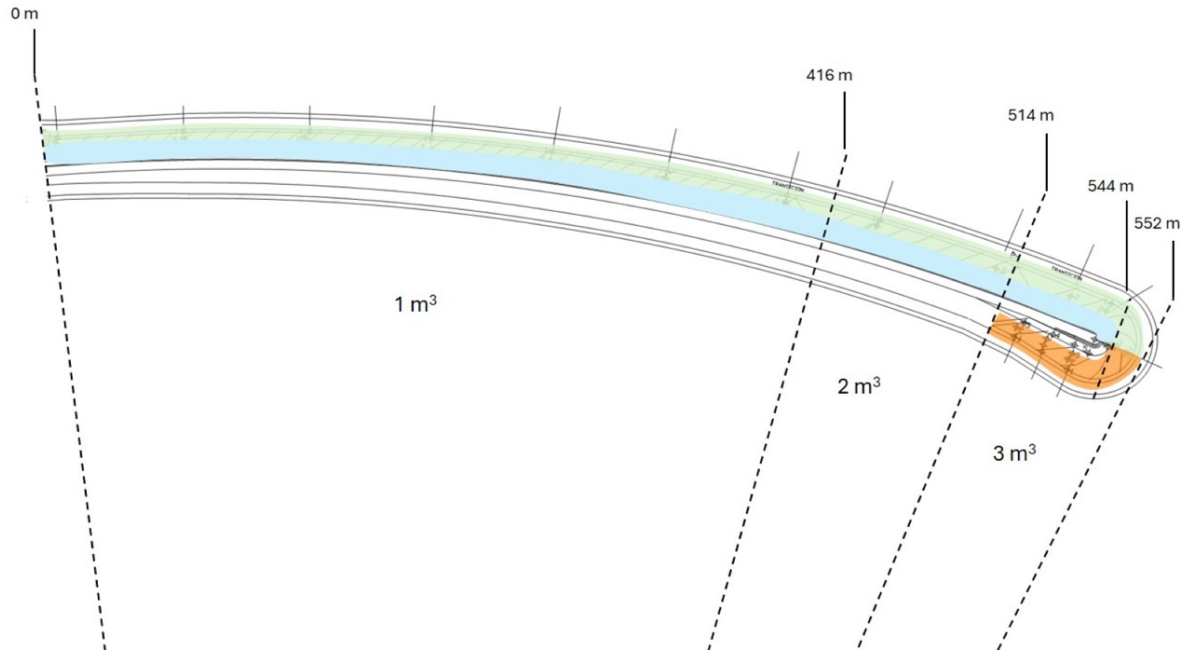


Figure B.2: Division of the northern breakwater.

In Table B.2 and Table B.3, The light green, light blue, and light orange areas respectively denote the northern, centre, and southern strip. The dashed lines denote boundaries between sections, where each section employs another type of Accropode. Using Table B.1 the volume of units for each Accropode type is calculated, and subsequently for both breakwaters as a whole. The relevant quantity is the total volume of concrete units in the southern breakwater, which amounts to 9150 m^3.

Table B.2: Accropode distribution and percentages - northern breakwater

	Northern breakwater					
Accropode type	**Length North [m]**	**Length centre [m]**	**Length South [m]**	**Total length [m]**	**Percentage of total units [%]**	**Volume units [m^3]**
1 [m^3]	416	-	-	416	96.3	3060
2 [m^3]	98	-	-	98	12.1	940
3 [m^3]	38	-	38	96	43.2	1697
Total						**5697**

Table B.3: Accropode distribution and percentages - new southern breakwater

	Southern breakwater					
Accropode type	**Length North [m]**	**Length centre [m]**	**Length South [m]**	**Total length [m]**	**Percentage of total units [%]**	**Volume units [m^3]**
1 [m^3]	8	-	8	16	3.7	120
2 [m^3]	237	237	237	711	87.9	6800
3 [m^3]	36	28	36	176	56.8	2230
Total						**9150**

The cross-section of the breakwater is divided into 3 zones: zone A (submerged zone, red), B (splash-zone, orange), and C (crown zone, green) as illustrated in Figure B.3. The end of the submerged zone is defined by MHW with +4.52 m SHN (2.64 m MOP) defined in Subsection 4.2.5.

Approximately half of the Accropodes are situated in zone C, while both zone A and B contain about a quarter. Based on this, and the total concrete volume of the southern breakwater from Table B.3, the volume per zone is obtained and provided in Table B.4.

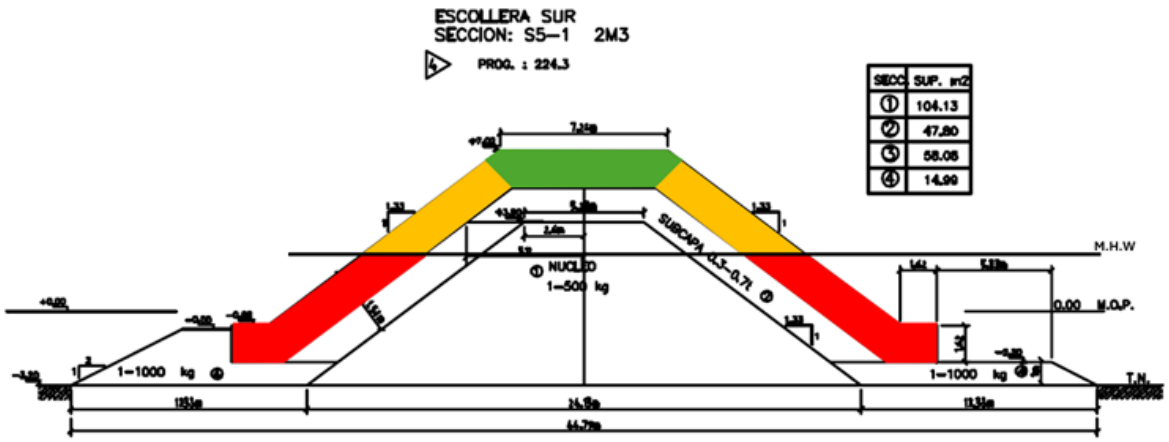


Figure B.3: New Southern breakwater - zone division

Table B.4: Concrete volume per zone subdivision

Zone	**Volume [m^3]**
Zone A	2300
Zone B	2300
Zone C	4550
Total	9150

C

Visual inspection results

This appendix explains the methods, processes, and results of the visual inspection.

The damage from the Accropodes are assessed from a scale of 1 to 5; where 1 denotes minor to no damage, and 5 denotes major damage. The damage assessment is subdivided into five categories:

- *Crumble damage*: This category is assigned to each unit where a small bit of concrete is missing, on a scale from Low to Medium to High (LMH);
- *Cracking damage*: This damage pertains to the amount and size of cracks in the concrete units, if any. Also on the LMH-scale;
- *Discolouration*: Discolouration is also on the LMH-scale, and indicates the extent to which the units have faded from their original colour;
- *Broken*: This damage is applicable to units where big sized concrete pieces are completely detached from its original unit. This damage does not have a scale, the units are only given a simple 'x' if a piece has completely broken off;
- *Vegetation*: Whether or not vegetation can be found on and/or in the concrete units. Mainly applicable to the units that are almost always fully submerged. Again, the units are only assigned an 'x' if vegetation is present;

Note that this damage scale has been made by the researchers of this report, i.e. it is not found in any ISO norms. This approach is used, so that this project has a customised damage assessment approach. In Table C.1, the five damage scores are explained in more detail.

Table C.1: Damage scale explanation

Damage score	Explanation	Example
1	Minor to no damage. Accropodes where small pieces have chipped off and show (almost) no surface damage.	Unit A0 Figure A.6
2	Relatively small damage. Concrete might show cracks, can be slightly discoloured and some pieces may be missing.	Unit B80 Figure A.23
3	Properly damaged. Cracks in the concrete are large enough to go across, or even fully through the unit. The concrete is considerably discoloured and might have lost significant residual strength.	Unit B221 Figure A.30
4	Significantly damaged. Vegetation is found on the concrete and cracks are expending across the Accropode. These cracks are mostly at places, where an arm of the unit might fall off later in their service life.	Unit C218 - S Figure A.38
5	Broken. The Accropode might have lost an arm, vegetation can be found all around the concrete and lots of fragments are missing.	Unit C221 Figure A.39

Table C.2 shows the complete results of the visual inspection. Figure C.1 and Figure C.2 simplify these results for better understanding.

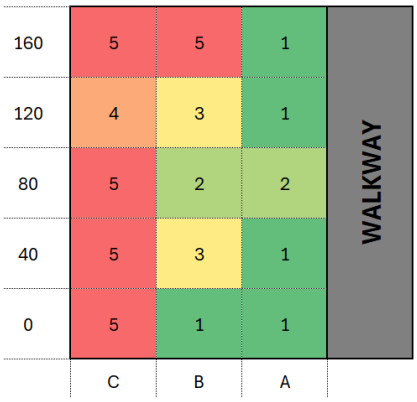


Figure C.1: Illustration of damage results of new northern breakwater

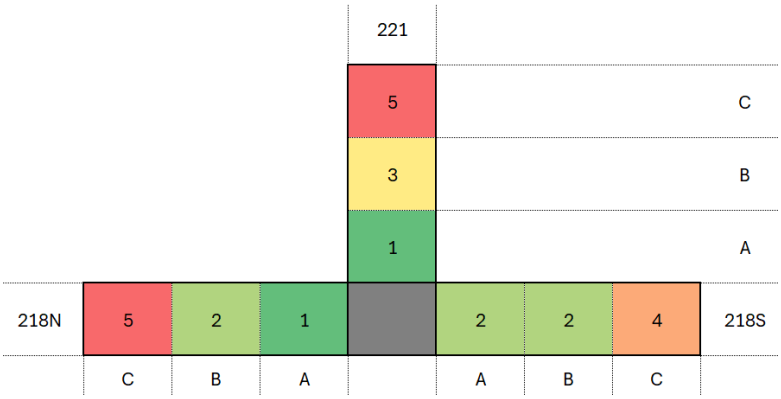


Figure C.2: Illustration of damage results of new norhtern breakwater - head

Table C.2: Complete visual inspection

Zone	#	Sample	Crumbled	Cracking	Discolouration	Broken	Vegetation	TOTAL
A	0	1	L	-	-	-	-	1
A	40	1	L	-	-	-	-	1
A	40	2	L	-	-	-	-	1
A	80	1	L	-	-	-	-	1
A	80	2	M	-	-	-	-	2
A	120	1	L	-	-	-	-	1
A	120	2	L	-	-	-	-	1
A	160	1	L	-	-	-	-	1
A	160	2	L	-	-	-	-	1
A	218N	1	-	L	-	-	-	1
A	218S	1	-	M	L	-	-	2
A	218S	2	-	L	L	-	-	2
A	218S	3	L	-	-	-	-	1
A	221	1	L	-	-	-	-	1
B	0	1	L	-	-	-	-	1
B	40	1	H	M	H	-	-	3
B	40	2	M	-	L	-	-	2
B	80	1	M	-	M	-	-	2
B	80	2	L	-	-	-	-	1
B	120	1	M	-	L	-	-	2
B	160	1	L	M	M	-	-	3
B	160	2	M	H	M	x	x	5
B	218N	1	L	L	M	-	-	2
B	218S	1	L	L	M	-	-	2
B	221	1	L	M	M	-	-	3
C	0	1	M	H	H	x	x	5
C	40	1	H	H	H	x	x	5
C	80	1	M	H	M	-	x	4
C	80	2	H	H	H	-	x	5
C	120	1	H	H	M	-	x	4
C	160	1	H	H	H	x	x	5
C	218N	1	M	H	H	x	x	5
C	218S	1	M	M	H	-	x	4
C	221	1	L	H	H	x	x	5
C	221	2	H	L	H	-	x	4

D

Failure mechanisms

This Appendix contains the failure mechanism analysis from Section 4.1.3. In the report, the most important conclusions of this analysis are given in Table 4.1. This Appendix is based on the theory from the Rock Manual [65].

Overtopping

Overtopping is often the most critical failure mechanism of a breakwater, as it directly impacts its primary function: preventing waves from entering the harbour and causing flooding. High overtopping discharges can result in operational disruption and structural damage in the port. In Puerto Rawson, vehicles and pedestrians are prevented from crossing the structure.

According to the EurOtop Manual [77], the following discharge limits apply:

$$\text{ULS:} \quad q < 10\,\text{l/m/s} \tag{D.1}$$

$$\text{SLS:} \quad q < 1\,\text{l/m/s} \tag{D.2}$$

where q is the overtopping discharge per meter width of the breakwater. The ULS is taken for a conservative condition of $H_{m0} > 5$ m, experienced by a rubble mound breakwater with a rear-side designed for wave overtopping. The SLS ensures safety for smaller boats at $5 - 10$ m from wall at $H_{m0} = 3 - 5$ m. If overtopping exceeds these limits, structural interventions, e.g. increasing the crest height, are necessary to maintain functionality.

Slope Instability

Slope instability occurs when the materials used in the construction cannot maintain the natural or designed slopes. Stability between layers must also meet design criteria to prevent the displacement or collapse of the slope. Meeting the stability criteria is therefore essential:

$$D_{15,\text{filter}} < 5\, D_{85,\text{base}} \tag{D.3}$$

where:

$D_{15,filter}$: the diameter at 15% traversing the filter layer.

$D_{85,base}$: the diameter at 85% passing in the base material.

This ensures that finer particles remain within the protected layer. An unstable slope compromises the entire structure, causing erosion, sliding, or even collapse of the breakwater.

Movement of Armour Layer

The armour layer plays a vital role in dissipating wave energy. For Accropode units, any displacement is unacceptable. The required criterion for zero movement is expressed as:

$$N_{od} = 0 \tag{D.4}$$

where N_{od} is the number of displaced units per defined strip along the breakwater. Zero movement ensures long-term durability, as dislocation of the armour units could lead to rapid deterioration of the structure.

Migration of Sublayers

The migration of sublayers refers to the erosion or displacement of materials between structural layers, which compromises internal stability. Permeability ensures that water can pass freely between layers without washing out the finer materials. This helps maintain the integrity of the sublayers and prevents internal erosion or migration of particles.

$$D_{15,\text{filter}} > D_{15,\text{base}} \tag{D.5}$$

Besides permeability, a structure also has to be well graded to prevent internal erosion. This can be verified by the following criteria:

$$\log(D_{10}/D_0) > \log(D_{20}/D_{10}) \qquad > \log(D_{30}/D_{20}) > etc \tag{D.6}$$

Where:

D_0 : Smallest particle size in the grading $[\mathrm{m}]$
D_{10} : Particle size at which 10% of the material is finer and 90% is coarser $[\mathrm{m}]$
D_{20} : Particle size at which 20% of the material is finer and 80% is coarser $[\mathrm{m}]$
D_{30} : Particle size at which 30% of the material is finer and 70% is coarser $[\mathrm{m}]$

Sliding of the Structure

Sliding occurs when the structure loses resistance against horizontal forces, typically from wave impact. Ensuring a proper toe structure and internal stability is crucial to prevent sliding. The stability against sliding is evaluated by:

$$F_s = \frac{\mu \cdot W}{H} > 1.2 \tag{D.7}$$

where μ is the friction coefficient, W is the weight of the structure, and H is the horizontal wave force. A factor of safety larger than 1.2 ensures that the structure remains stable under design conditions.

Erosion of the Foreshore

Erosion of the foreshore refers to the eroding of sediments in front of the breakwater, which affects wave dynamics and toe stability. However, limited information is available about the material composition of the foreshore in this harbour. As such, a detailed evaluation of the erosion potential is not possible at this stage.

Settlement

Settlement occurs when the foundation of the breakwater sinks or shifts, potentially leading to unevenness and structural instability. In this case, settlement is considered irrelevant, as the site rests on the restinga — a material known for its high strength and stability. Furthermore, there is no available data on the settlement behaviour of a restinga, making further assessment difficult.

Piping

Piping refers to the movement of water through or beneath the breakwater, which erodes foundation materials and undermines the structure. However, since the water level on both sides of the breakwater is nearly equal, the risk of piping is minimal.

Liquefaction

Liquefaction occurs when saturated soils lose strength due to dynamic loading, such as wave action, causing the structure to sink or collapse. This mechanism is unlikely in this case because the subsoil is not composed of fine-grained materials, which are typically prone to liquefaction.

E

Data analysis

This Appendix contains the complete wind analysis, the wave analysis the Extreme Value Analysis, and the Self-Organization analysis. In the report, the most important conclusions of these analyses are given in Chapter 4.

These analysis are based on ERA5-data, produced by the Copernicus Climate Change Service at ECMWF. It combines a variety of observations from satellites and weather stations with numerical weather predictions, and offers hourly estimates of climate variables for the atmosphere, land, and oceans [31]. Covering the period from 1940 to the present, the ERA5-dataset provides global coverage on a 31 km grid. The retrieved dataset was 30 years of hourly ERA5-data, starting at 01-01-1993 00:00:00 until 12-12-2023 23:00. The location of the extraction point is 49 km offhsore of Puerto Rawson (Lat: 43 °30'00.0"S, Long: 64 °30'00.0"W). Important to note is that ERA5-data and the analyses follow the nautical convention for direction. This means the direction is specified as the point from which the wind or wave originate from, measured clockwise from North (N= 0 °or 360 °, E = 90 °, S = 180 °, W = 270 °). The retrieved variables from ERA5 are given in Table E.1.

Variables	Description	Unit
u_{10}	10m u-component of wind	$[\mathrm{m/s}]$
v_{10}	10m v-component of wind	$[\mathrm{m/s}]$
$\overline{\theta}$	Mean wave direction	$^\circ$
$\overline{T}$	Mean wave period	$[\mathrm{s}]$
$H_{s,total}$	Significant height of combined wind waves and swell	$[\mathrm{m}]$
$H_{s,wind}$	Significant height of wind waves	$[\mathrm{m}]$
$H_{s,swell}$	Significant height of swell waves	$[\mathrm{m}]$
H_{max}	Maximum individual wave height	$[\mathrm{m}]$
θ_{total}	Mean direction of combined wind waves and swell	$^\circ$
θ_{wind}	Mean direction of wind waves	$^\circ$
θ_{swell}	Mean direction of swell waves	$^\circ$
T_p	Peak wave period	$[\mathrm{s}]$

Table E.1: ERA5 variables

E.1. Wind analysis

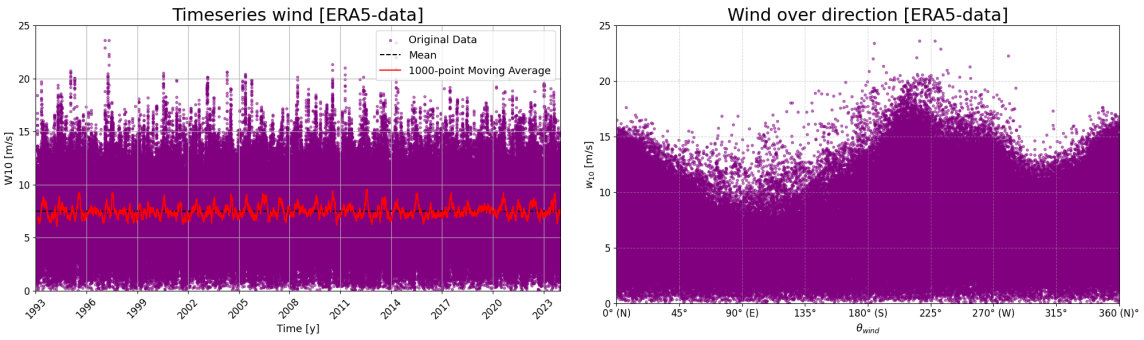
The objective of this analysis is to gain insight into the wind's magnitude, direction, and general patterns. The ERA5-data provides the u- and v- components of the wind, which represents wind velocities 10 meters above the water surface. It is assumed that these wind speeds approximate those directly above the wave, though in reality the magnitude is reduced due to surface friction and turbulence effects near the water surface. To determine the total wind speed (w_{10}) and direction (θ_{wind}), the Pythagorean theorem was applied to the u- and v-components of the wind.

E.1.1. General

Table E.3 gives the basic statistics of the wind magnitude. Figure E.1 gives the timeseries of w_{10} and the plot of w_{10} over the direction. Figure E.1a visualizes the mean wind speed over the years. The 1000-point moving average shows an oscillatory motion over the years, but no long term upward or downward trend. Figure E.1b shows that most extreme wind magnitudes (w_{10} > 15 $\mathrm{m/s}$) come from SSE to SSW.

Table E.2: Basic statistics of w_{10}

Statistics	mean	std	min.	25 %	50 %	75 %	max.
w_{10} [$\mathrm{m/s}$]	7.51	3.14	0.03	5.23	7.41	9.68	23.64



(a) Timeseries wind

(b) Wind magnitude of direction

Figure E.1: Wind data analysis with (a) timeseries wind and (b) wind magnitude over direction.

Figure E.2 gives the windrose off-shore of Puerto Rawson. The wind direction ranges from SSW to NNE, dominated by wind from W and N. This indicates a strong local offshore wind. From the windrose in combination with Figure E.1b, it is concluded that while the wind predominantly originates from land, during extreme conditions or storms, it shifts to originate from sea.

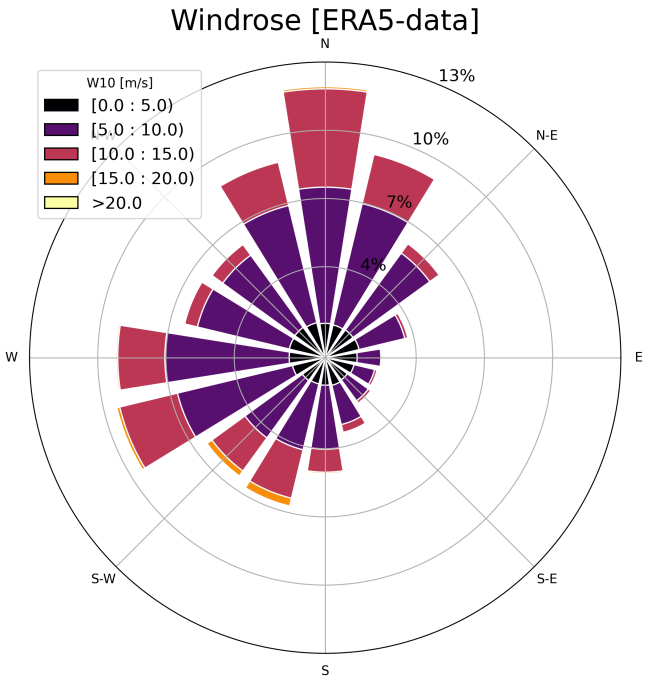


Figure E.2: Windrose

E.1.2. Trend

The goal of performing a trend analysis on 30 years of wind data is to identify long-term patterns and potential changes in wind parameters. The data is split into three 10-year periods. The basic statistics of the period are given in Table E.5. Although there are some slight differences over the phases, no long term trend is detected.

Table E.4: Basic statistics of w_{10} over 30 years

Statistics w_{10} **[**$\mathrm{m/s}$**]**	mean	std	min.	25 %	50 %	75 %	max.
Phase 1 (1993-2003)	7.41	3.12	0.03	5.16	7.30	9.53	23.64
Phase 2 (2003-2013)	7.60	3.17	0.04	5.30	7.53	9.76	21.33
Phase 3 (2003-2023)	7.50	3.13	0.05	5.21	7.40	9.65	23.42

E.1.3. Seasonal

The goal of the seasonal wind analysis is to identify and understand patterns and variations in wind speed and direction over the seasons. The basic statistics of the seasons are given in Table E.7, and the windroses of each season are given in Figure E.3. Winter exhibits the strongest winds, while spring has the weakest, though seasonal variability is generally modest. In winter winds predominantly originate from the land (WSW–NNW), while in other seasons, this shifts to a dominance of N–NNE winds.

Table E.7: Basic statistics of w_{10} over the seasons

Statistics w_{10} **[**$\mathrm{m/s}$**]**	mean	std	min.	25 %	50 %	75 %	max.
Winter	7.99	3.21	0.03	5.69	7.91	10.17	21.33
Spring	7.17	3.00	0.04	4.97	7.09	9.24	19.87
Summer	7.29	3.06	0.06	5.08	7.21	9.36	23.64
Autumn	7.56	3.22	0.04	5.22	7.44	9.79	23.61

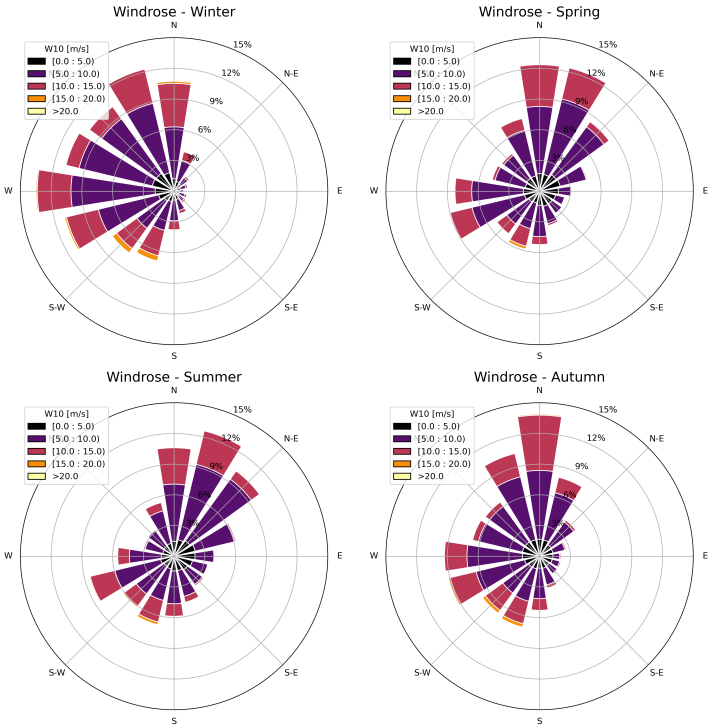


Figure E.3: Windroses Seasons

E.2. Wave analysis

The objective of this analysis is to gain insights into the wave's magnitude, direction, and general patterns. The ERA5-data offers different types of data on significant wave height: the Significant height of combined wind waves and swell (**SWH**), the Significant Height of Wind Waves (**SHWW**), and the Significant Height of Total Swell (**SHTS**). To understand the contributions of swell and wind to the total significant wave height, the wave analysis is threefold.

E.2.1. Statistics

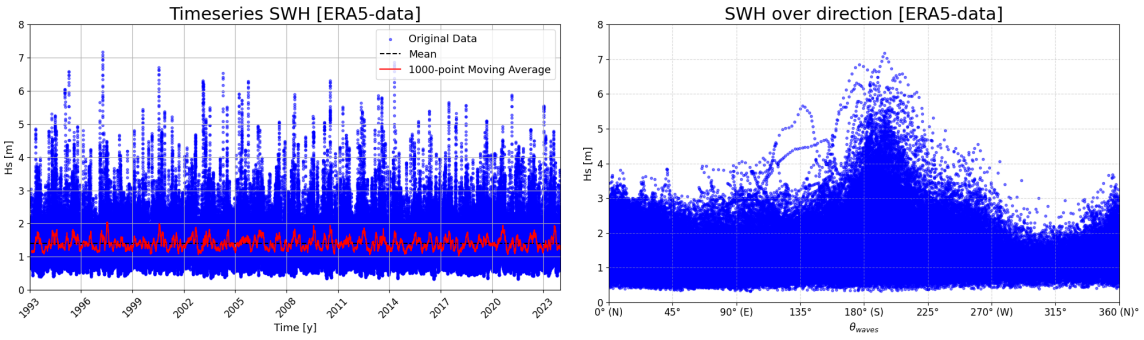
Table E.9 contains the basic statistics of the different wave heights. It is clear that SWH results in the largest wave heights, although the maximum value of SWH and SHWW do not differ that much. SHTS result in the smallest significant wave heights. Interestingly, SHWW has a minimum of 0.00, indicating no wind-driven waves when there is no wind.

Table E.8: Basic statistics for SWH, SHWW, and SHTS

Statistics [m]	mean	std	min.	25 %	50 %	75 %	max.
SWH	1.40	0.63	0.32	0.97	1.26	1.68	7.17
SHWW	0.79	0.72	0.00	0.24	0.60	1.15	6.88
SHTS	1.01	0.44	0.05	0.71	0.93	1.22	4.60

E.2.2. Timeseries

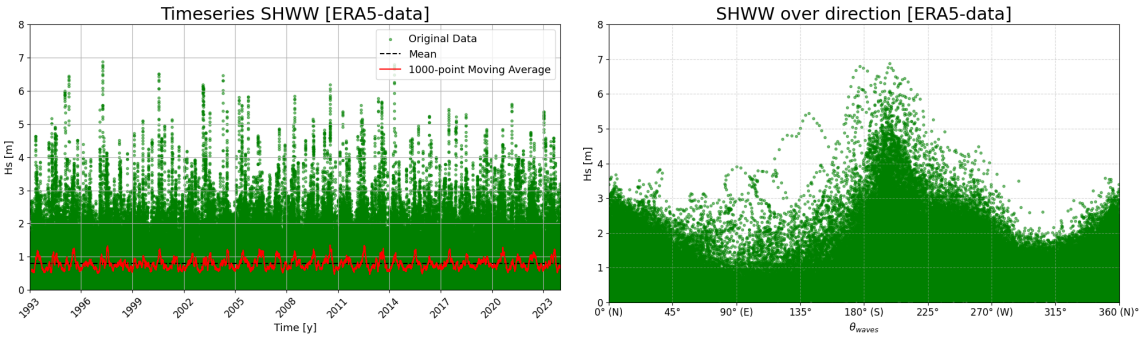
The timeseries of SWH, SHWW, and SHTS, along with wave height over wave direction, provide an insight into wave patterns. The timeseries of the wave heights over time and over direction are given in Figure E.4, Figure E.5, and Figure E.6. The moving averages do indicate an oscillatory motion over time, but no long-term trend. For SWH, extreme wave heights predominantly come from SSE-SSW, from SEE-SW for SHWW, and from SE-S for SHTS. Although the latter exhibits a less pronounced peak compared to SWH and SHWW.



(a) Timeseries SWH

(b) SWH over direction

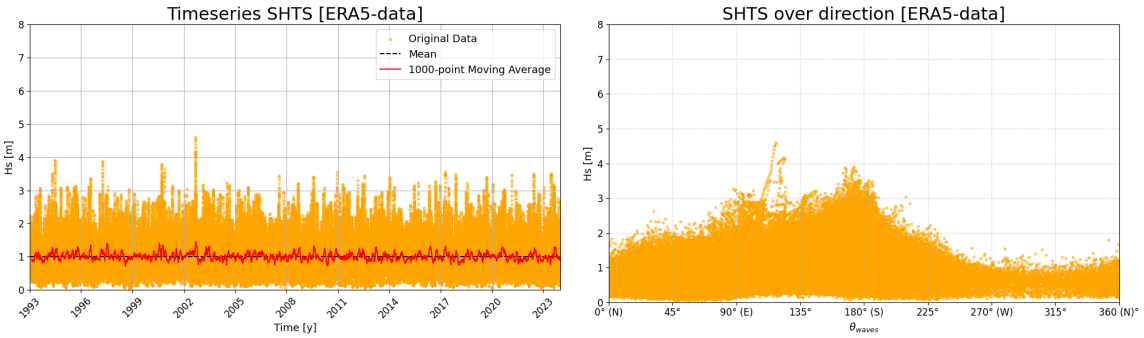
Figure E.4: Wave data analysis with (a) timeseries SWH and (b) SWH over direction.



(a) Timeseries SHWW

(b) SHWW over direction

Figure E.5: Wave data analysis with (a) timeseries SHWW and (b) SHWW over direction.



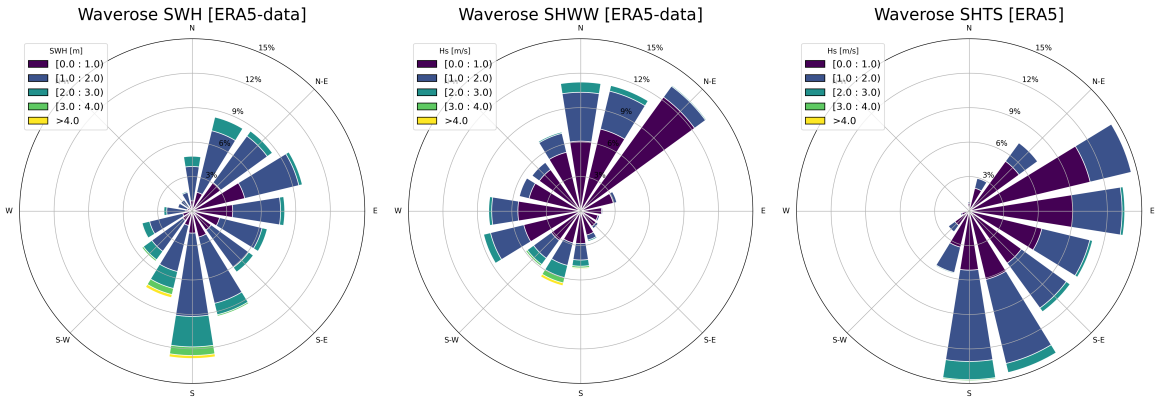
(a) Timeseries SHTS

(b) SHTS over direction

Figure E.6: Wave data analysis with (a) timeseries SHTS and (b) SHTS over direction.

E.2.3. Waveroses

In this section, the waveroses for SWH, SHWW, and SHTS are visualized in Figure E.7. The waveroses for SHWW and SHTS are completely opposite, with SHWW reflecting the dominant offshore wind at Puerto Rawson. In contrast, the waverose for SHTS shows incoming swell waves from the open sea, ranging from ENE to S. The SWH waverose is less distinct than those of SHWW and SHTS, but it does indicate the primary direction of incoming storms, which is from the south.



(a) SWH wind rose

(b) SHWW wind rose

(c) SHTS wind rose

Figure E.7: Wave rose plots for wave data analysis with (a) SWH, (b) SHWW, and (c) SHTS.

E.2.4. Trends

The goal of performing a trend analysis on 30 years of wave data is to identify long-term patterns and potential changes in wave parameters. The data is split into three 10-year periods. The basic statistics of the period are given in Table E.11. Although there are some slight differences over the phases, no long term trends are detected.

Table E.11: Mean waveheights over 30 years for SWH, SHWW, and SHTS

Mean waveheights [m]	SWH	SHWW	SHTS
Phase 1 - (1993-2003)	1.40	0.77	1.03
Phase 2 - (2003-2013)	1.41	0.81	1.00
Phase 3 - (2013-2023)	1.39	0.79	1.00

E.2.5. Seasons

The goal of seasonal wave analysis is to identify and understand patterns and variations in wave parameters. The basic statistics of the seasons are given in Table E.13, and the windroses of each season are given in Figures E.8, E.9, and E.10. As expected, the largest wave heights occur during winter. SHW and SHWW exhibit some seasonal variability. In contrast, SHTS remains relatively constant, indicating a constant swells from open sea.

Table E.13: Mean waveheights over the seasons for SWH, SHWW, and SHTS

Mean waveheights [m]	SWH	SHWW	SHTS
Winter	1.53	0.94	1.03
Spring	1.32	0.68	1.00
Summer	1.32	0.70	0.98
Autumn	1.44	0.83	1.02

The windrose for SWH shows more extreme (yellow) bars during winter compared to other seasons. Additionally, SHWW follows the same pattern as the wind described in Section E.1, with predominant land-based winds (WSW–NNW) in winter and a shift to N–NNE winds in other seasons. Furthermore, the consistency of SHTS over the years is reflected in the similar waveroses observed across the seasons.

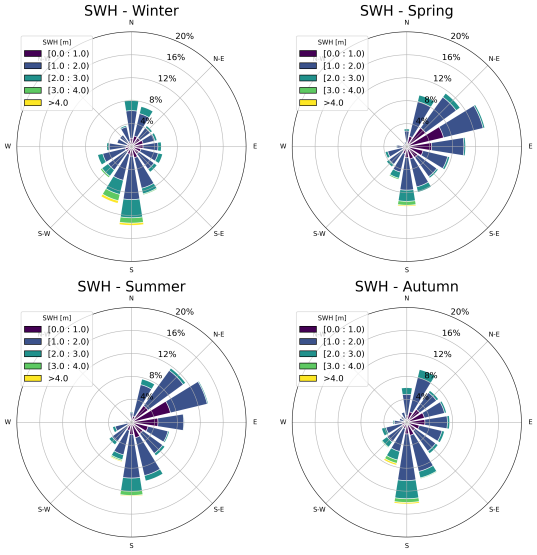


Figure E.8: SWH seasonal waveroses

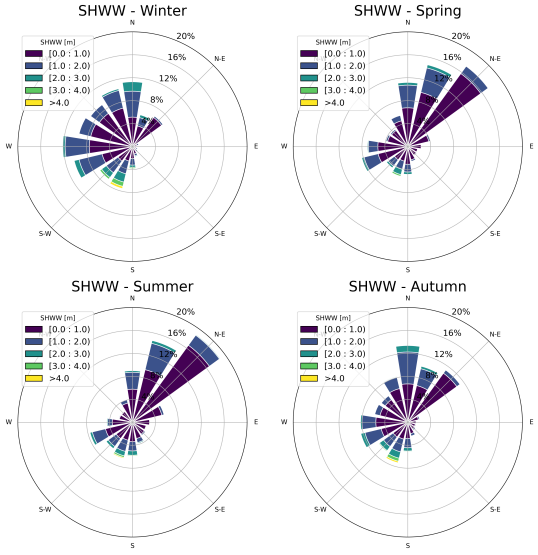


Figure E.9: SHWW seasonal waveroses

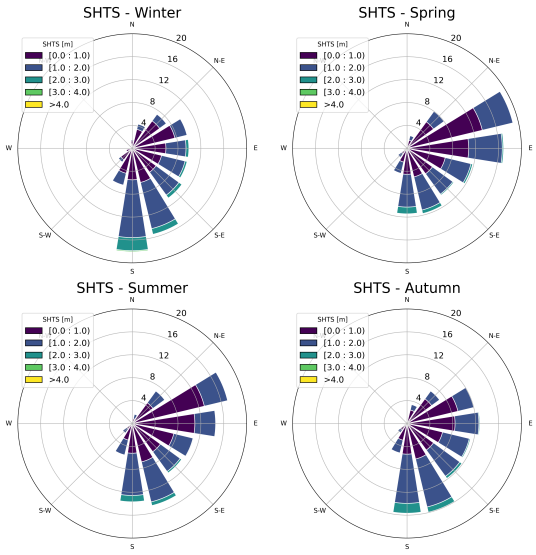


Figure E.10: SHTS seasonal waveroses

E.2.6. T_p analysis

The goal of this analysis is gain insight into the peak period (T_p) of the ERA5-data. The basic statistics are computed in Table E.15. The mean of this table and the moving average are also incorporated in Figure E.11. Furthermore, T_p is computed over each wave height (SWH, SHWW and SHTS) in Figure E.12. One can clearly see the bounds of the data dictated by wave steepness, resulting in white-capping on the open sea. A large waveheight wave height in combination with a very small period, is not possible due to steepness (e.g. SWH = 6 m and T_p = 5 s).

Table E.15: Basic statistics of T_p

Statistics	mean	std	min.	25%	50%	75%	max.
T_p [s]	7.83	2.35	2.62	5.81	7.71	9.75	18.87

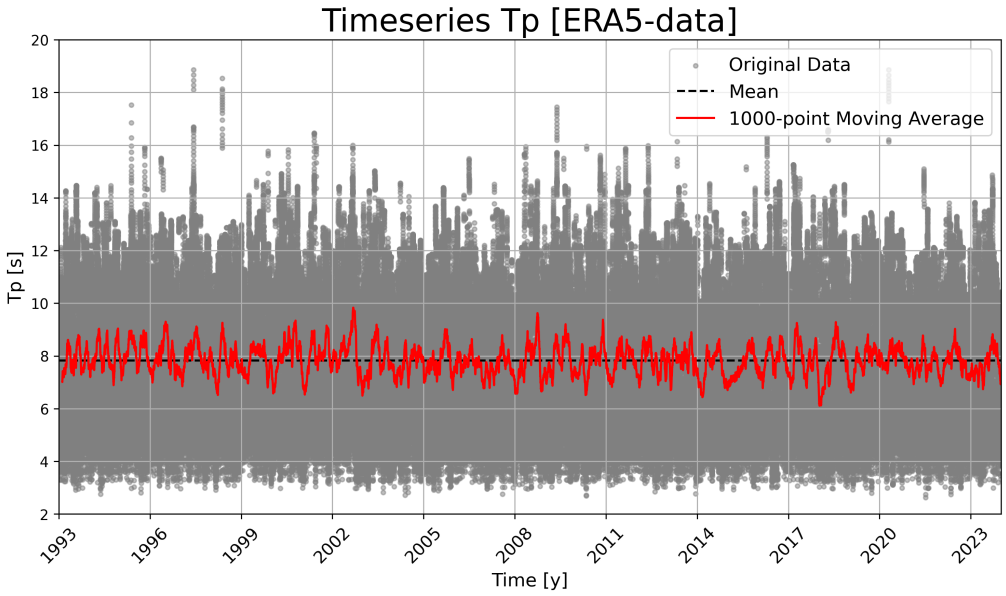


Figure E.11: T_p time series

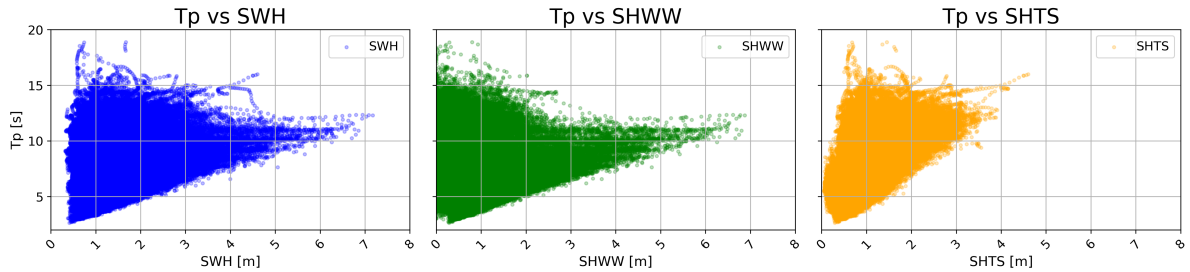


Figure E.12: T_p vs SWH, SHWW and SHTS

E.2.7. Wave vs wind direction

The goal of this section is to gain insight into the correlation between wind and wave direction, as visualized for SWH, SHWW, and SHTS in Figure E.13. A notable difference is observed in the scatter plots for SHWW compared to the other two waveheights. As expected, there is a strong correlation between wind direction and wave direction, indicated by the y = x line. However, for waves coming from NNE, no correlation is found with the wind direction. SWH and SHTS show a weaker visual correlation between the two variables. However, they do align in areas with limited data, specifically when waves come from the W and winds come from the E.

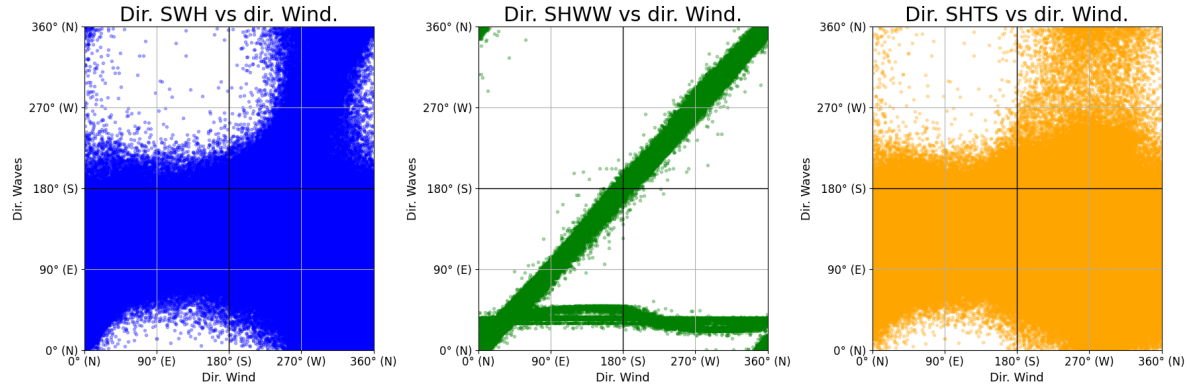


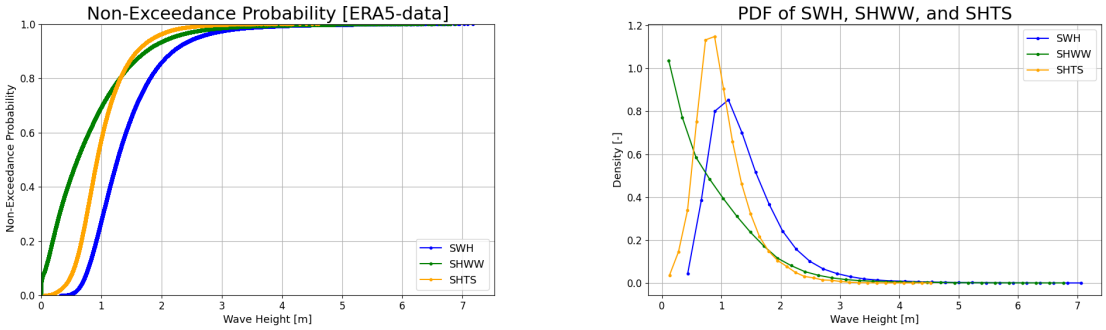
Figure E.13: Direction of the waves of the wind direction

E.3. Extreme Value Analysis

An extreme value analysis (EVA) was performed on all three wave heights (SWH, SHWW, SHTS) to find the extreme wave heights with corresponding return period. These values are used as input for the SWAN model (Chapter 5) to find the extreme nearshore wave heights after wave transformation over the bathymetry.

E.3.1. General

To understand the wave height distributions, the non-exceedance probability and probability density function (PDF) are plotted for each wave height in Figure E.14. These plots indicate that SWH is most likely to produce the largest extremes. However, to ensure comprehensive analysis, the extreme value analysis (EVA) was performed for all three wave heights. The PDF of SHTS exceeds a density of 1, which is acceptable as long as the area under the curve equals 1, which is the case.



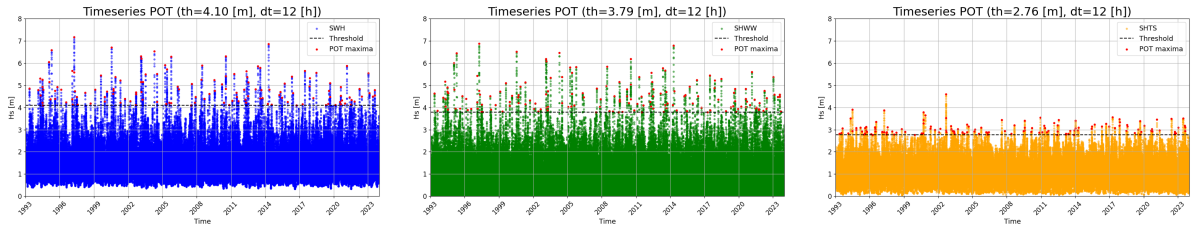
(a) Probability of non-exceedance

(b) Probability Density Function (PDF)

Figure E.14: Extreme Value Analysis: (a) Probability of non-exceedance and (b) Probability Density Function (PDF).

E.3.2. Peak over threshold (SWH, SHWW, SHTS)

For the EVA, both Peak over Threshold (POT) and Block Maxima (BM) were viable approaches to identify extremes. Given the size and the long timespan of the data, the POT approach was used as it allows to extract multiple extremes in a timespan (e.g. a month). The threshold (th) defines which observations are considered extreme. The declustering time (dt) is used to identify and separate independent extreme events from clusters of peaks in the data. The choice of these paremeters is validated by (1) plotting a Poisson distribution over the extremes and (2) perform a χ^2-test. Using this validation process as an iteration, optimal values for the threshold were found. The POT over the timeseries for SWH, SHWW, and SHTS is visualized in Figure E.15. To gain insights in where these extreme wave heights originate from, the extremes are also plotted over the wave direction in Figure E.16. The Poisson validation is visualized in Figure E.17 and the χ^2-test is given in Table E.17. The χ^2-test measures how much the observed data deviates from the expected data under the null hypothesis, while the p-value assesses the significance of that deviation [74]. P-values close to 1 suggests that the POT fits the data well. The χ^2 values range between 1.61 and 2.53, indicating that the observed values are close to the expected values.

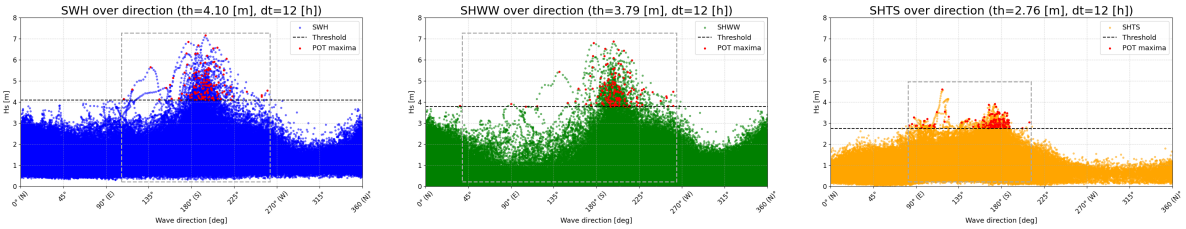


(a) Timeseries POT SWH

(b) Timeseries POT SHWW

(c) Timeseries POT SHTS

Figure E.15: Peak Over Threshold (POT) timeseries for wave data: (a) SWH, (b) SHWW, and (c) SHTS.



(a) Direction POT SWH **(b)** Direction POT SHWW **(c)** Direction POT SHTS

Figure E.16: Peak Over Threshold (POT) analysis by direction for wave data: (a) SWH, (b) SHWW, and (c) SHTS.



(a) Poisson distribution SWH **(b)** Poisson distribution SHWW **(c)** Poisson distribution SHTS

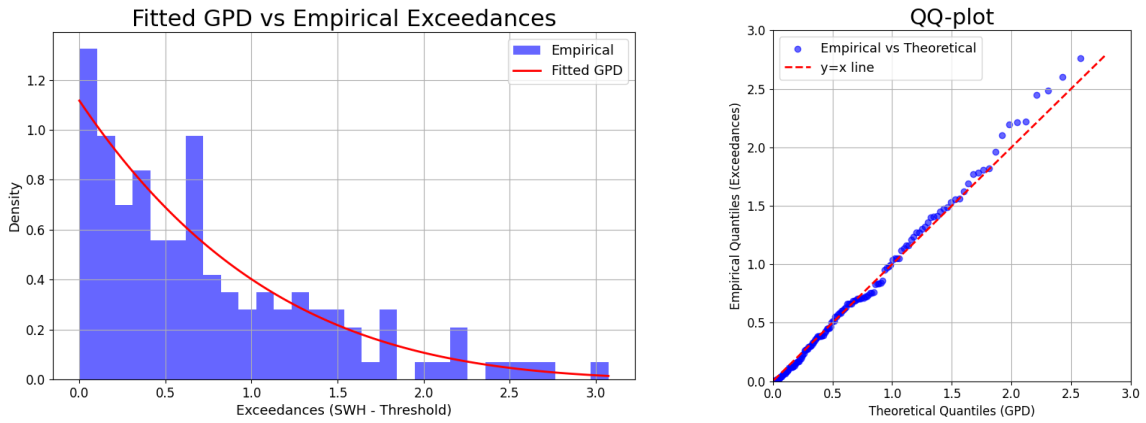
Figure E.17: Poisson distribution analysis for wave data: (a) SWH, (b) SHWW, and (c) SHTS.

Table E.16: Test Results of Poisson Fit

Test Poisson Fit	Chi-Square	P-value
SWH	1.97	0.98
SHWW	2.53	0.93
SHTS	1.61	0.98

E.3.3. EVA (SWH)

The Generalized Pareto Distribution (GPD) was fitted to the exceedances of SWH (Figure E.18a). A quantile-quantile (QQ) plot was used to assess the goodness of fit (Figure E.18b). This plot confirmed a good fit between the empirical and predicted extremes. A plot of SWH against return periods was created incorporating the bootstrap method to estimate confidence a 95 % confidence interval (Figure E.19). This analysis was also done for SHWW and SHTS, finally resulting in Table E.19.



(a) GPD fit SWH

(b) QQ-plot SWH

Figure E.18: GPD fit and QQ-plot analysis for SWH.

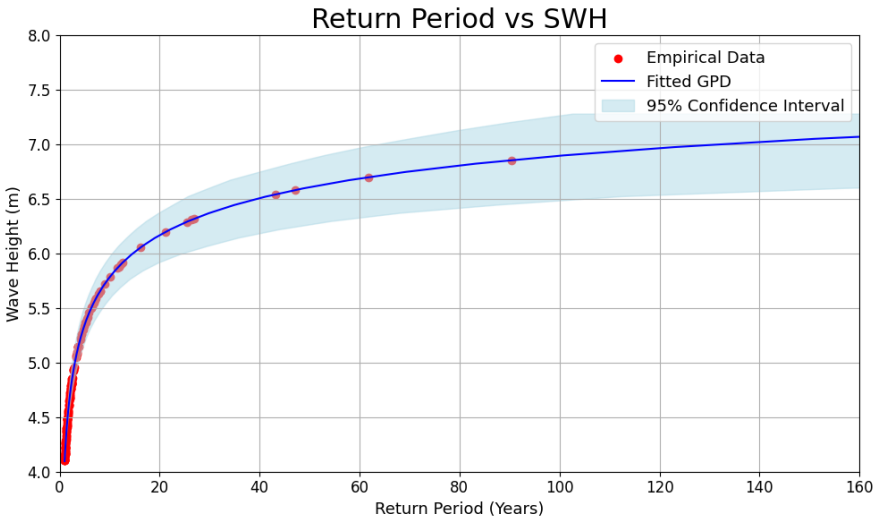


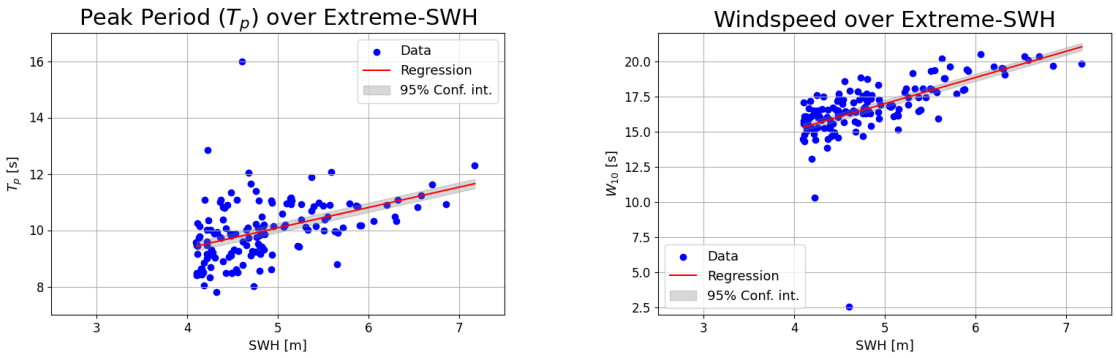
Figure E.19: Return period plot of SWH, showing data and the fitted GPD curve with a 95 % confidence interval. This illustrates the SWH values associated with RT

Table E.19: Return periods of SWH, SHWW and SHTS based on EVA

Return Period SWH [y]	**SWH** [m]	**SHWW** [m]	**SHTS** [m]
5	5.35	5.03	3.25
10	5.78	5.49	3.44
50	6.61	6.40	3.85
75	6.78	6.60	3.95
100	6.90	6.74	4.01
150	7.05	6.91	4.10

Corresponding T_p and w_{10}

After conducting the EVA on SWH, correlations were assessed between extreme events and other variables, including peak wave period (T_p), 10-meter wind speed (w_10), and wind direction (θ_{wind}). Linear regression provided a good fit for SWH against T_p and w_{10} (Figure E.20a and Figure E.20b). This enabled the estimation of corresponding values for these parameters at return periods, which can be found in Table E.20. During storm events, wind and wave directions were found to be closely aligned, coming from the same direction. This is visualized in Figure E.21.



(a) SWH extremes vs TP

(b) SWH extremes vs W10

Figure E.20: Comparison of SWH extremes against (a) TP and (b) W10.

Table E.20: Return Periods for Significant Wave Height and Associated Parameters

Return Period SWH [y]	H_s [m]	T_p [s]	w_{10} [m/s]
5	5.35	10.33	17.63
10	5.78	10.65	18.44
50	6.61	11.24	19.97
75	6.78	11.37	20.29
100	6.90	11.45	20.51
150	7.05	11.56	20.79

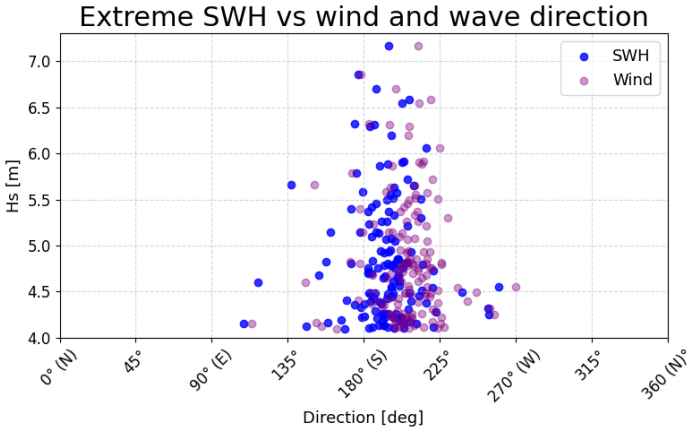


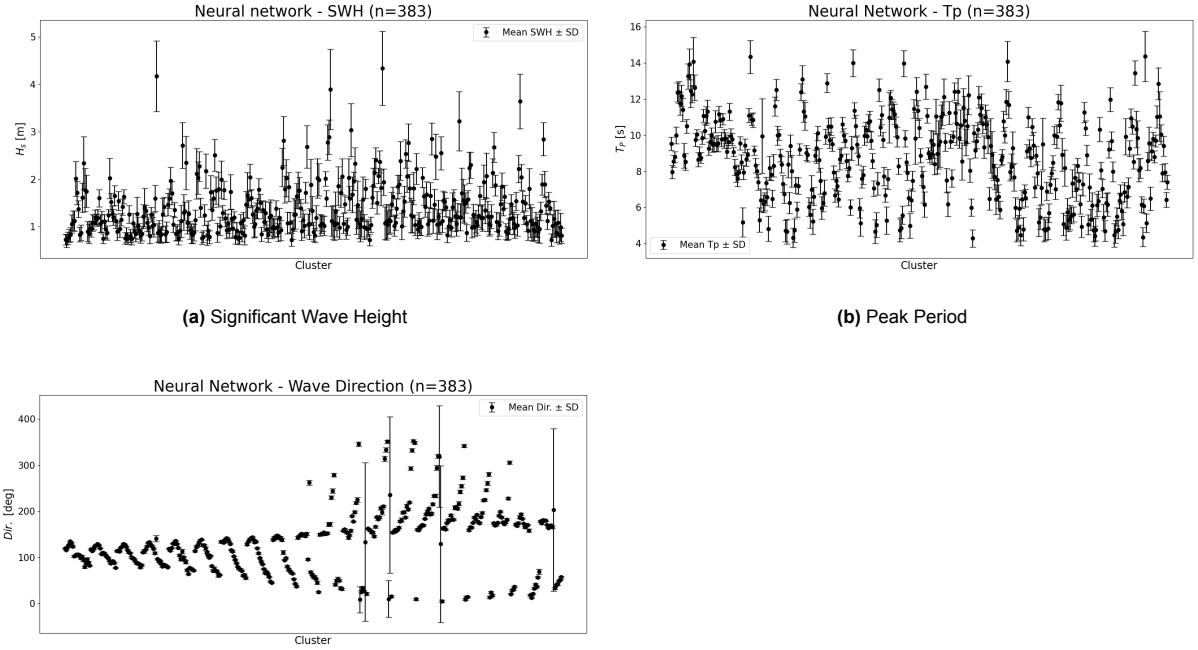
Figure E.21: SWH extremes vs wave direction

E.4. Self-Organizing Maps (SOM)

The goal of this analysis is to reduce the large dataset (30 years of hourly wind and wave data) to ~10 conditions that represent the data. These are considered as representative regular wave conditions and are used for assessing sediment transport for each breakwater concept (Chapter 7). This appendix is complementary to the information given in Section 4.3. The data is first represented by neurons, using a neural network (n=400). This is done using the MiniSom python package [36]. After this, k-means is used on the neurons to find 10 clusters.

E.4.1. Neural Network (n = 400)

As described, the neural network is trained iteratively, resulting in 383 active neurons. The mean values and their box-plot for the parameters (H_s, T_p, θ_{waves}) is given in Figure E.22. As one can see, 5 neurons have an unrealistically high variance (std_θ > 100°) in Figure E.22c. These neurons are discarded, resulting 378 neurons representing unique combinations of H_s, T_p and θ_{waves}.



(a) Significant Wave Height

(b) Peak Period

(c) Mean Direction

Figure E.22: Boxplots of the neurons over H_s, T_p, and θ_{waves}

The neurons and the datapoints each neuron won, are shown in Figure E.23. One can see that the more extreme regions (e.g. H_s > 2.5 m) are represented by fewer neurons than the more dense regions of data (1 m < H_s < 2 m). Overall, the neurons are well spread out over the data. The magnitude of the variables (H_s, T_p, θ_{waves}) is visualized in a Self-Organizing Map (Figure E.24). The frequency (indicated by the background blue gradient) represents the number of data points each neuron won. However, a higher frequency does not mean these are *more representative* regular conditions. Counter-intuitively, conditions with the highest frequency often correspond to outlier regions in the data, such as waves coming from the west. Generally, one can see the dominant wave direction of waves coming from E to S. Furthermore, as observed in the wave analysis in Section E.2, the neural network too represents storms dominantly coming from SSE-SSW.

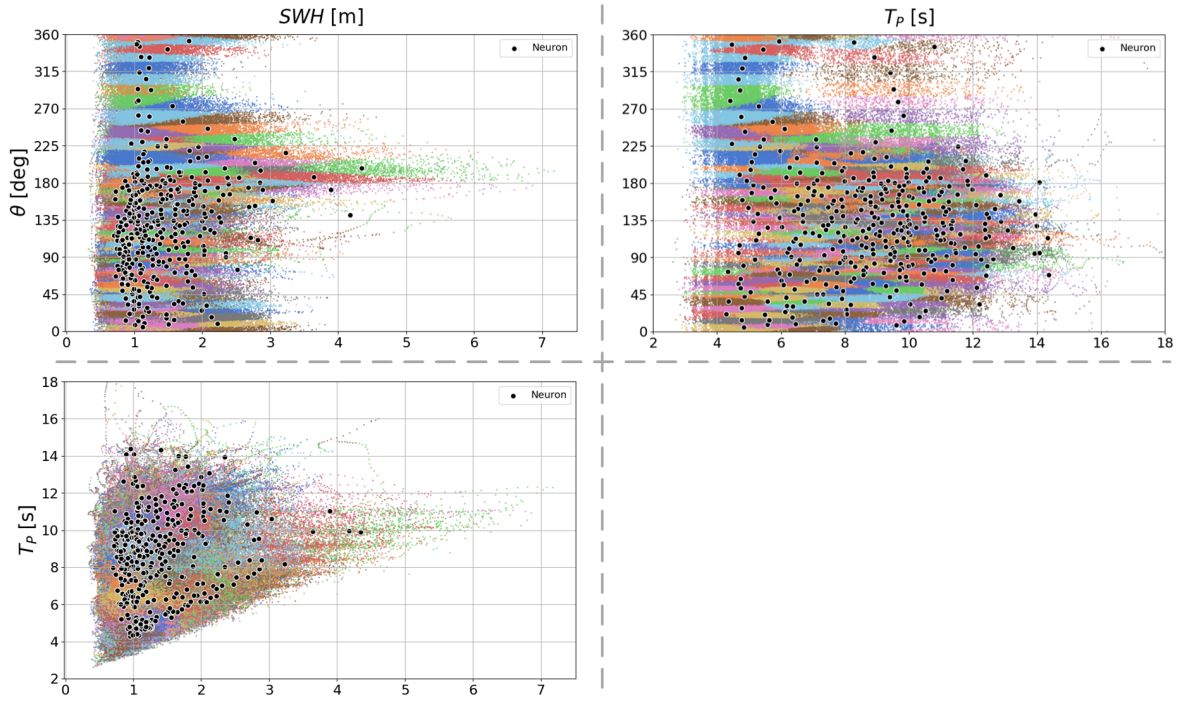


Figure E.23: Scatter plot of the neurons and their corresponding won datapoints over the variables H_s, T_p, and θ.

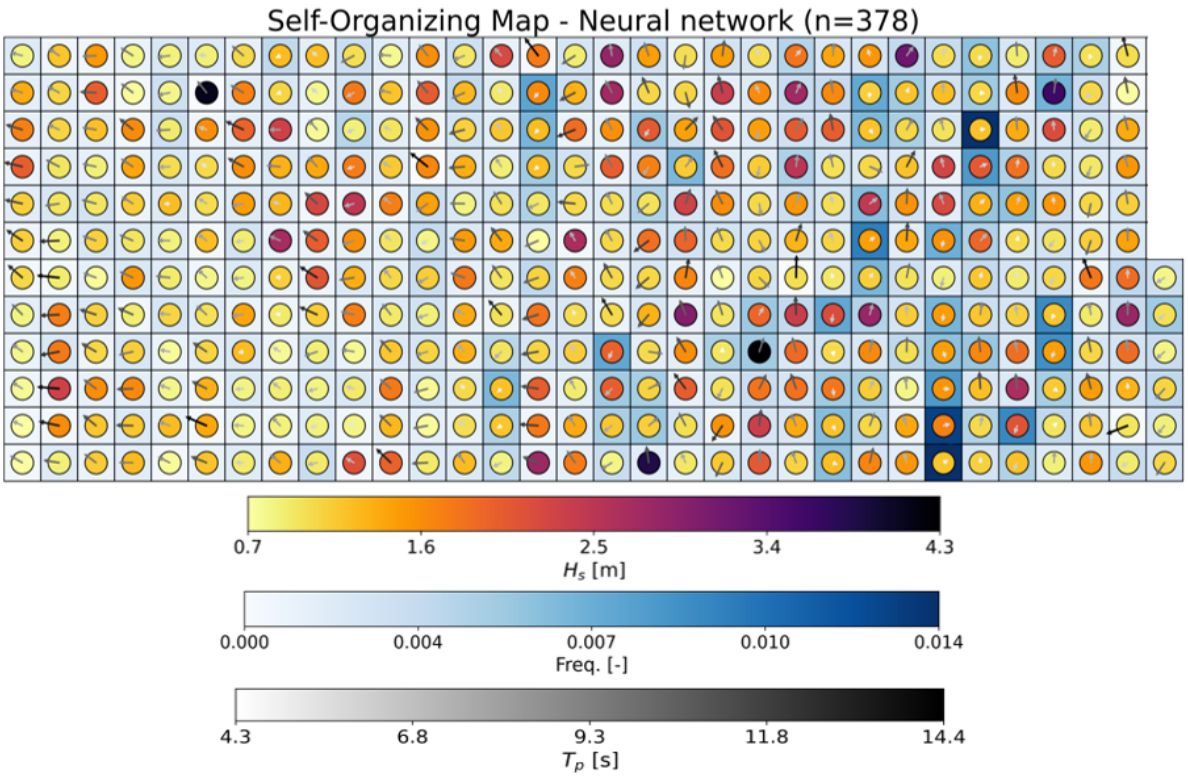


Figure E.24: Self-Organizing Map (SOM) representing 378 wave conditions analysed through a neural network. Each cell illustrates the relationship between H_s, T_p, θ, and frequency (f). Colour gradients indicate the respective values of H_s, f, and T_p, allowing for a visual interpretation of the clustering and distribution of wave conditions

E.4.2. K-means (k = 12)

By applying k-means, the 378 neurons are grouped into 12 cluster (*k* = 12) based on similarities in H_s, T_p, and θ_{waves}. K-means forms clusters by minimizing the sum of squared distances between each data point and the centre of its assigned cluster, also referred to as minimizing within-cluster sum of squares (WCSS). K-means is a fast and straightforward algorithm, but is sensitive to outliers. This effect is reduced by first applying the neural network on the data-set. The k-clusters and the neurons each cluster represents are visualized in Figure E.25. The magnitude of the variables (H_s, T_p, θ_{waves}) is visualized in a Self-Organizing Map (Figure E.26). The exact values of each cluster are also given in Table E.22.

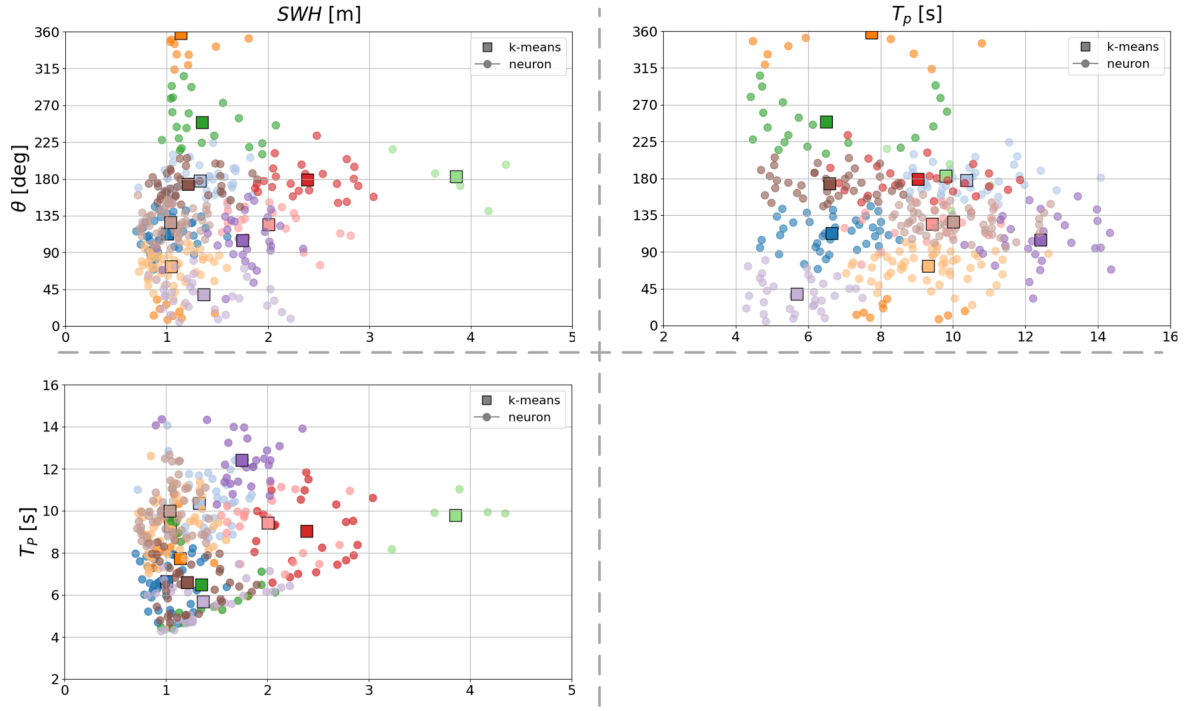


Figure E.25: Scatter plot of the clusters and their corresponding won neurons over the variables H_s, T_p, and θ_{waves}

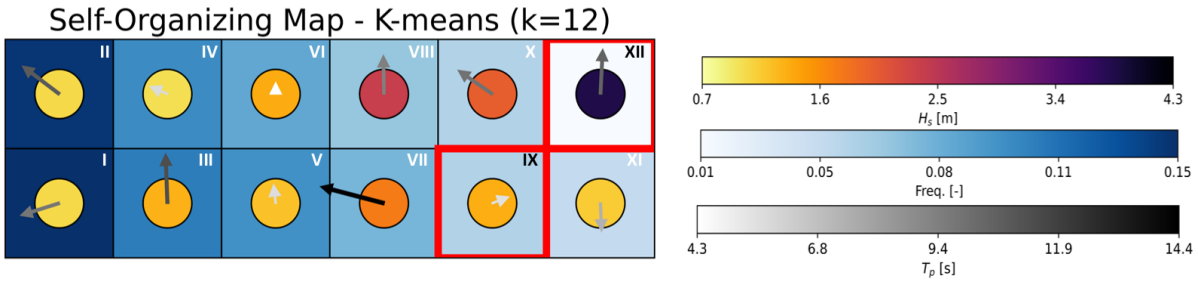


Figure E.26: Self-Organizing Map (SOM) representing 12 wave conditions analysed through k-means. Each cell illustrates the relationship between H_s, T_p, θ, and frequency (*f*). Colour gradients indicate the respective values of H_s, *f*, and T_p, allowing for a visual interpretation of the clustering and distribution of wave conditions.

Table E.22: Parameter values of the 12 clusters following the k-means algorithm over the 378 neurons.

k-means cluster	H_s [m]	T_p [s]	θ [deg]	Dir.	frequency
1	1.04	9.31	73	ENE	0.148
2	1.04	10.01	127	SE	0.146
3	1.33	10.37	178	S	0.108
4	1,01	6.66	113	ESE	0.101
5	1.21	6.60	173	S	0.098
6	1.37	5.69	39	NE	0.085
7	1.75	12.42	105	ESE	0.077
8	2.38	9.03	179	S	0.066
9	1.35	6.50	249	WSW	0.056
10	2.01	9.42	124	SE	0.056
11	1.14	7.75	358	N	0.048
12	3.86	9.79	183	S	0.013

F

Proposed cement mixture studies

This Appendix contains a breakdown of Ing. L. Cotti de la Lastra's research and a general investigation into the physical properties and quarrying of pebble and porphyry [23]. The studied mixture will be referred to as the proposed mixture.

The primary distinction between the current mixture and the proposed mixtures resides in the type of coarse aggregate used. In the current mixture, pebble stone is used. This aggregate is sourced from the banks of the Chubut river, adjacent to the temporary construction site [62]. While this proximity reduces transportation costs, it raises significant concerns about environmental sustainability. According to Mrs. Cotti and several other studies, the extraction of marine and river pebbles lead to significant ecological degradation. The extraction of river pebbles disrupts the local ecosystem, instigates erosion, negatively influences sediment transport processes, and increases turbidity in the river [17][64].

In contrast, the proposed mixture incorporates porphyry quarry waste as the coarse aggregate. Porphyry quarry waste is a by-product of the local mining industry. Companies involved in the extraction of desired porphyry neglect to utilise the waste generated during the extraction process. Currently, there are 36 porphyry quarries with an excess of waste in the region between Puerto Madryn and Puerto Rawson. The waste accumulates to an estimated 80,000 m^3 annually. By incorporating this waste into concrete production, there is no need to extract river pebbles. This practice also aids in rehabilitating the landscape. The neglected quarries often serve as dumping grounds, which causes multiple problems in the region, including severe desertification. This in turn reduces the aesthetic quality of the landscape. Additionally, the ditches that arise from these quarries are located next to roads. Due to insufficient maintenance, safety hazards related to traffic emerge, such as cars veering into these ditches. The use of locally and readily available raw materials promotes a more environmentally sustainable solution.

Both aggregates possess unique properties that influence their suitability for different applications. In Table F.1, key physical properties of porphyry and pebble stone aggregates are compared. The most notable differences are the higher bond strength properties of porphyry and the greater workability of pebble stone.

Table F.1: Important properties of porphyry waste and river pebble

Property	Porphyry quarry waste	Pebble
Origin	Residue rock from quarrying of porphyry	Found naturally along shorelines and river beds
Size classification	Coarse aggregate	Coarse aggregate
Petrographic classification	An igneous volcanic rock, typically a rhyolitic ignimbrite	Primarily composed of sandstone and acid vulcanite
Shape classification	Angular, due to mechanical crushing during quarrying	Rounded, due to natural weathering and water pressure
Texture classification	Rough	Smooth
Workability	Lower workability due to its angular shape, requires plasticizers to improve	Higher workability due to its round shape and smooth texture
Bond strength	Higher bond strength with cement due to its rough texture	Lower bond strength with cement due to its smooth texture
Application	Suitable for high-strength concrete, where bonding strength is essential	Suitable for standard concrete applications where workability is more critical than strength

Mrs. Cotti did not only research the environmental impacts of obtaining the different aggregates, but also conducted extensive laboratory tests, evaluating the performance of different cement mixtures with these aggregates. The research focused on key factors such as compressive strength, workability (slump), and ASR reactivity. The porphyry waste itself is first reviewed on its granulometry, using the same criteria as in Appendix H. The distribution is found in Figure F.1. The blue line is steep, which means that this concerns a uniformly distributed aggregate [15]. This is due to the porphyry waste being from the same quarry and from the same material.

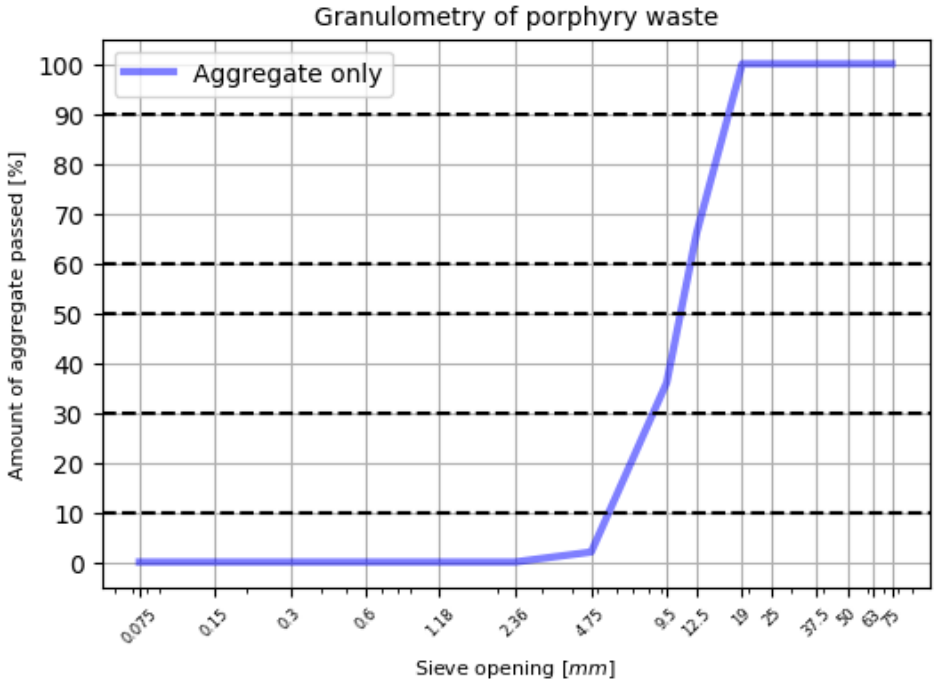


Figure F.1: Granulometry of the porphyry waste aggregate

This coarse aggregate is subsequently incorporated with the fine aggregates and the other components found in a cement mixture, such as water, plasticizers, and air-entrainers. Five cement mixtures are proposed, each of which contain a different amount of pebbles and porphyry. The aggregate percentages of pebbles and porphyry waste per cement mixture are found in Table F.2.

Table F.2: Aggregate percentages of the tested cement mixtures

Cement mixture	Percentage of pebbles [%]	Percentage of porphyry waste used [%]
1	100	0
2	75	25
3	50	50
4 & 5	0	100

First of all, a significant increase in compressive strength is observed, when comparing cement mixtures containing 100 % porphyry aggregate versus those with 100 % pebble stone. After 28 days, the porphyry-based mixture exhibited a 19 % increase in strength, which further improved to 40 % after 56 days. These superior strength properties are largely attributed to the angular shape and rough texture of porphyry, which provide better bonding with the cement mixture[63].

The workability is assessed using the slump test, which initially indicated a decrease in settlement from 11 cm for cement mixture 1, to 6 cm for cement mixture 4. This reduction suggests lower workability in the porphyry-based mixture, which could imply challenges in handling and placing the concrete. To address the workability disadvantage, optimizations in the proportioning of plasticizers and aggregates along with the addition of an air-entraining additive improved the workability. By creating tiny air bubbles that act as frictionless spheres, the air-entrainer facilitates easier handling of the concrete. Moreover, according to climate data [2], the area experiences freezing conditions. The air-entrainer also mitigates possible freeze-thaw damage [46]. From the workability tests of this new mixture, a slump of 11 cm is achieved. This new mixture is the fifth mixture.

ASR is examined, based on the accelerated Mortar Bar Test, also known as the NBRI Method (from the National Building Research Institute), described in the Argentinian code IRAM 1674 [43]. This test evaluates the potential for ASR expansion by exposing mortar bars with different aggregate-cement proportions to high-alkali conditions at 80°C. In this research, the aggregates were tested with two types of cement: Composite Portland Cement (CPC) and CPP. The results offer a comparison of ASR behaviour. CPP consistently exhibited much lower reactivity than CPC. The lower alkali content in CPP minimizes the formation of expansive gels that lead to cracking. It is thus a more suitable choice for the proposed concrete mix design. Furthermore, a comparison between the aggregates revealed that pebble aggregate exhibited a slightly lower expansion rate in the ASR test, of 0.08% after 16 days. The fifth cement mixture showed a slightly higher expansion of 0.10% after 16 days. An aggregate is considered potentially reactive when the 16-day expansion in the accelerated mortar test exceeds 0.10%, thus porphyry waste does not pose any severe ASR risks [58]. Table F.5 shows the five proposed cement mixtures. Cement mixture 5 is used as the proposed mix design.

The sieve values of this mixture are found in Table F.4, and the granulometry relevant values in Table F.3. It is fine-tuned such, that the eventual total aggregate is enveloped by design area I from the Betonpocket [15]. Using C_U and C_C, the mixture classifies as 'Well graded'. The complete granulometry graph is shown in Figure F.2.

Table F.3: Granulometry relevant values of mixture 5

Title	D_{10}	D_{30}	D_{60}	C_U	C_C
Mrs. Cotti's mixture	0.449	2.360	9.773	21.717	1.266

Table F.4: Granulometry values of mixture 5

	Sieve size opening [mm]													
Title	**75**	**63**	**50**	**37.5**	**25**	**19**	**12.5**	**9.5**	**4.75**	**2.56**	**1.18**	**0.6**	**0.3**	**0.15**
Mrs Cotti's mixture	100	100	100	100	100	100	70	59	42	30	19	13	7	2

Table F.5: Mrs. Cotti's proposed cement mixtures

Property / content	Unit	Cement mixture 1	Cement mixture 2	Cement mixture 3	Cement mixture 4	Cement mixture 5
w/c ratio	[–]	0.46	0.46	0.46	0.46	0.45
Total water content	[L]	160.0	160.0	160.0	160.0	157.5
CPP	[kg]	350	350	350	350	350
Natural fine aggregate, sand, Aridos Fontana	[kg]	714	714	714	714	804
Natural coarse aggregate, pebble	[kg]	1088	809	570	0	0
Natural coarse aggregate, porphyry quarry waste	[kg]	0	260	546	1046	955
Plasticizer	[%]	0.25	0.45	0.60	1.00	0.70
Air entrapment	[%]	0.05	0.05	0.05	0.05	0.05
Compressive strength 28 days	[MPa]	31.8	37.8	42.3	44.7	41.0
Compressive strength 56 days	[MPa]	33.5	-	-	-	46.9
Slump	[cm]	11.0	10.0	10.0	6.0	11.0
ASR expansion CPC (16 days)	[%]	0.32	-	-	-	0.36
ASR expansion CPP (16 days)	[%]	0.086	-	-	-	0.10

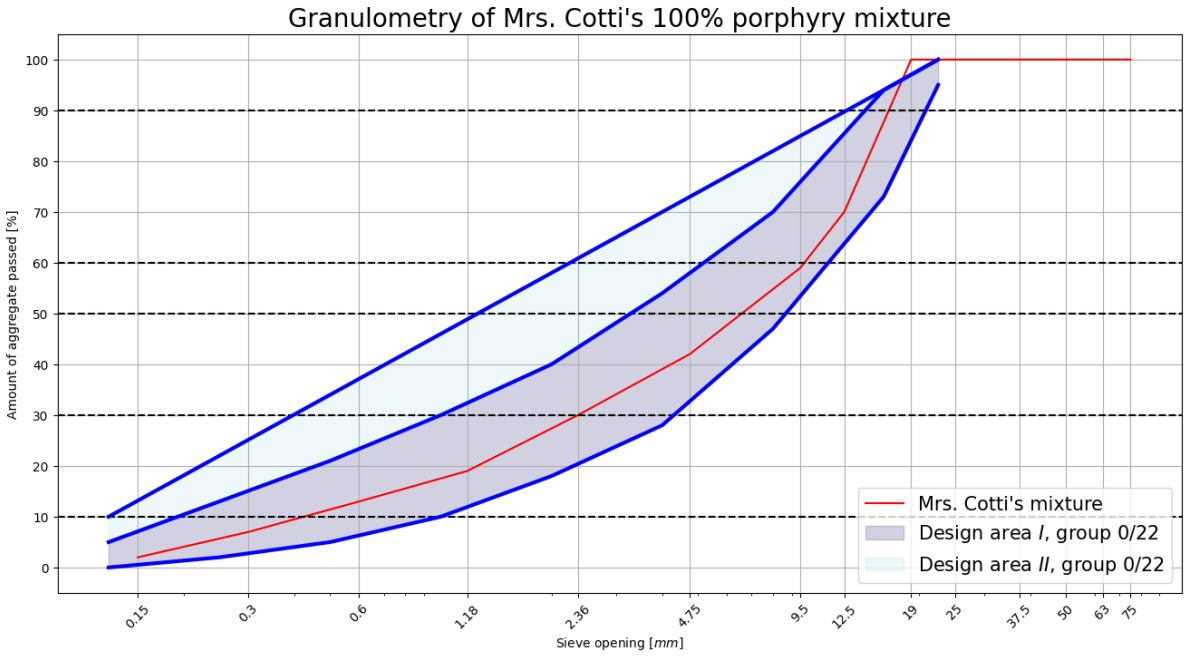


Figure F.2: Granulometry graph of mixture 5. The thick blue lines represent the boundaries of the design areas [15]. The dark blue and light blue areas represent the design areas I and II, in which a cement mixture is optimally designed for workability and water requirements.

G

Initial cement mixture studies

This appendix provides a detailed overview of the studies commissioned by construction company DyOPSYA, which were carried out by ITH and LABIEVI of UNPSJB, concerning the cement mixture used in the breakwater [59].

Initially, two consecutive studies were conducted by ITH. These studies aimed to optimise the concrete mix design and were based on three different formulations that varied the ratios of cement, water, aggregates, and additives. Following the ITH studies, further research was undertaken by LABIEVI at the UNPSJB. This investigation tested four distinct cement mixtures, incorporating various combinations of CPN and CPP. In this study the same mix proportions established in the ITH study were used. The final mixture, resulting from the LABIEVI study, was used for the manufacturing of the Accropodes in the current breakwater.

The concrete comprises of several key materials, including CPP, which was sourced from Petroquímica Comodoro Rivadavia (PCR S.A.). For the construction of the Accropodes, a temporary construction site was built next to the port at the southern side of the Chubut river [62]. The analysed aggregates, coarse and fine, were obtained near this construction site. Furthermore, plasticizer from the company Sika Argentina was used for obtaining the required workability. The key requirements evaluated in the studies included:

- A maximum water-to-cement ratio (w/c ratio) of 0.5;
- A minimum of 350 kg of CPP per cubic metre;
- A minimum measured slump of 4 to 5 cm (as determined by the cone slump test);
- A minimum concrete class of H-25 (or 30 Mpa);
- A maximum accelerated mortar bar extension of 0.10%;
- A maximum aggregate size of 37.5 mm.

All the key requirements are met except for the one related to aggregate size (Subsection 3.2.2).The studies are summarized in Table G.1. A grey row indicates that part of the properties or contents below are part of a group. These are subsequently shown in light gray.

Table G.1: Studies for the current cement mixture

Property / content	Unit	ITH July 2000	ITH August 2000	UNPSJB August 2001
w/c ratio	[–]	0.42	0.42	0.42
Total water content	[L]	160	160	160
CPP	[kg]	380	380	380
Natural fine aggregate	[kg]	740	740	740
Arena Mediana, M1	[kg]	223	-	-
Arena Mediana, M4	[kg]	517	-	-
Arena Zandiana, sur Río Chubut, M5	[kg]	-	740	740
Natural coarse aggregate				
Piedra Zarandeada, M2	[kg]	1090	-	1095
Piedra Zarandeada, sur Río Chubut, M4	[kg]	-	1090	-
Plasticizer	[L]	1.13	1.13	1.13
Slump	[cm]	6.0	5.0	5.0
Initial Setting Time (Vicat Needle)	[min]	-	-	80
Final Setting Time (Vicat Needle)	[min]	-	-	230
Mortar bar expansion test (16 days accelerated test)	[%]	-	-	0.086
Fresh Unit Weight	[kg/m^3]	2440	2390	2396
Dry Unit Weight	[kg/m^3]	2288	-	-
Ambient Temperature	[°C]	16	17	-
Concrete Temperature	[°C]	17	15	-
Mortar compressive strength				
2 days	[MPa]	12.9	17.8	-
7 days	[MPa]	30.8	28.1	-
28 days	[MPa]	44.4	42.4	-
Mortar flexural strength				
2 days	[MPa]	4.0	5.3	-
7 days	[MPa]	7.9	7.9	-
28 days	[MPa]	9.1	10.6	-
Compressive strength				
1 day	[MPa]	4.0	4.6	-
2 days	[MPa]	-	-	17.9
3 days	[MPa]	20.8	18.6	-
7 days	[MPa]	27.6	26.1	29.1
28 days	[MPa]	30.6	31.9	33.5
45 days	[MPa]	33.3	-	-
Alkali content				
Na_2O	[%]	-	-	0.84
K_2O	[%]	-	-	0.46
Total Alkalis (as Na_2O equivalent)	[%]	-	-	1.14

H

Original granulometry

This appendix states the granulometry of the current cement mixture. The data is subsequently processed, using the relevant codes.

There are 16 different granulometry documents, each with four different samples. This means that there are 64 samples in total. The granulometry samples are reported by DyOPSA [59] and are shown in Table H.1 and in Table H.2.

Table H.1: All granulometry data of the current mixture

		Sieve size opening [mm]														
Title	**Sample**	**75**	**63**	**50**	**37.50**	**25**	**19**	**12.50**	**9.50**	**4.75**	**2.56**	**1.18**	**0.60**	**0.30**	**0.15**	**0.075**
2002n12	1	100	100	95	92	78	66	51	42	25	16	13	9	4	1	0
2002n12	2	100	100	100	100	97	91	80	72	49	36	32	27	16	2	0
2002n12	3	100	100	92	86	79	74	69	61	27	14	12	10	7	4	0
2002n12	4	100	100	100	96	83	71	57	50	35	31	30	27	19	6	0
2002n16	1	100	100	100	100	99	98	94	88	56	13	11	10	10	8	0
2002n16	2	100	100	100	87	83	77	67	63	52	37	33	24	6	1	0
2002n16	3	100	100	100	100	100	100	100	100	100	99	99	99	98	76	0
2002n16	4	100	100	100	100	100	92	83	79	65	58	57	56	49	25	0
2002n2	1	100	100	100	90	76	59	44	35	26	22	20	16	9	1	0
2002n2	2	100	100	100	100	96	93	87	78	44	34	31	28	23	6	0
2002n2	3	100	100	100	100	100	100	100	100	100	100	100	100	100	57	0
2002n2	4	100	100	100	100	100	100	100	100	100	100	96	96	95	42	0
2002n21	1	100	100	100	100	100	100	100	100	100	87	10	9	8	4	0
2002n21	2	100	100	100	100	100	100	100	100	100	19	8	8	7	3	0
2002n21	3	100	100	100	100	100	100	100	100	100	100	97	97	97	89	0
2002n21	4	100	100	100	100	100	100	100	100	100	81	51	51	51	45	0
2002n26	1	100	100	100	100	100	100	100	100	100	96	45	12	9	4	0
2002n26	2	100	100	100	100	100	100	100	99	97	88	59	33	16	4	0
2002n26	3	100	100	100	100	100	100	89	86	70	31	9	7	7	6	0
2002n26	4	100	100	100	100	100	93	90	85	71	30	9	9	8	5	0
2002n2s	1	100	100	100	100	100	100	100	100	100	100	100	100	96	40	0
2002n2s	2	100	100	100	100	100	100	100	100	95	95	95	95	91	43	0
2002n2s	3	100	100	100	100	100	100	100	100	100	100	100	100	100	81	0
2002n2s	4	100	100	100	87	63	52	38	27	12	10	10	10	9	3	0
2002n2sur	1	100	100	100	90	76	59	44	35	26	22	20	16	9	1	0
2002n2sur	2	100	100	100	100	96	93	87	78	44	34	31	28	23	6	0
2002n2sur	3	100	100	100	100	100	100	100	100	100	100	100	100	100	57	0
2002n2sur	4	100	100	100	100	100	100	100	100	100	100	96	96	95	42	0

Table H.2: Table H.1 continued

		Sieve size opening [mm]														
Title	**Sample**	**75**	**63**	**50**	**37.50**	**25**	**19**	**12.50**	**9.50**	**4.75**	**2.56**	**1.18**	**0.60**	**0.30**	**0.15**	**0.075**
2002n30	1	100	100	100	100	100	100	100	89	68	33	7	1	1	1	0
2002n30	2	100	100	100	100	98	90	82	78	63	31	21	20	18	7	0
2002n30	3	100	100	100	100	100	95	88	86	83	74	43	30	25	11	0
2002n30	4	100	100	100	100	100	96	86	81	61	29	16	13	12	6	0
2003n12	1	100	100	100	97	90	73	64	57	48	38	31	15	3	1	0
2003n12	2	100	100	97	90	60	39	23	18	13	8	7	4	2	1	0
2003n12	3	100	100	100	94	84	76	59	48	30	14	12	9	7	1	0
2003n12	4	100	100	100	100	98	84	58	41	26	21	20	17	4	0	0
2003n16	1	100	100	100	100	100	100	100	97	79	46	34	20	5	1	0
2003n16	2	100	100	95	90	81	78	72	64	42	21	18	16	7	1	0
2003n16	3	100	100	100	100	87	75	61	54	48	39	32	20	4	1	0
2003n16	4	100	100	100	90	73	60	46	39	30	17	15	11	4	1	0
2003n1sur	1	100	100	100	100	100	100	100	100	100	100	100	100	97	31	0
2003n1sur	2	100	100	100	93	85	69	59	53	37	29	26	24	21	3	0
2003n1sur	3	100	100	100	100	100	100	100	100	100	99	99	99	95	49	0
2003n1sur	4	100	100	100	100	100	85	78	72	66	62	61	60	58	28	0
2003n2	1	100	100	74	66	52	43	26	16	7	5	5	5	3	1	0
2003n2	2	100	100	100	100	100	100	100	100	93	91	90	88	78	23	0
2003n2	3	100	100	100	100	100	100	100	100	89	83	82	82	79	37	0
2003n2	4	100	100	100	96	90	82	70	59	43	35	33	30	19	8	0
2003n21	1	100	100	100	100	100	100	96	91	78	22	5	3	2	0	0
2003n21	2	100	100	100	100	91	85	81	78	70	35	22	17	8	1	0
2003n21	3	100	100	100	100	87	75	61	54	48	39	32	20	4	1	0
2003n21	4	100	100	100	100	100	100	99	98	68	2	1	1	0	0	0
2003n26	1	100	100	100	100	100	100	100	100	95	20	4	4	1	0	0
2003n26	2	100	100	100	100	100	100	100	100	99	78	12	6	4	3	0
2003n26	3	100	100	100	100	100	100	100	97	59	5	2	1	1	0	0
2003n26	4	100	100	100	100	100	100	100	100	97	82	53	39	19	2	0
2003n2	1	100	100	100	100	77	65	42	28	15	13	13	12	10	2	0
2003n2	2	100	100	100	100	100	100	100	95	70	57	50	37	21	3	0
2003n2	3	100	100	100	100	100	100	100	100	100	100	100	100	97	61	0
2003n2	4	100	100	100	100	100	100	100	100	100	100	100	100	99	68	0
2003n30	1	100	100	100	100	100	100	100	95	75	25	10	9	7	2	0
2003n30	2	100	100	100	100	100	100	100	99	86	30	9	8	7	2	0
2003n30	3	100	100	100	100	100	100	100	98	95	75	37	1	0	0	0
2003n30	4	100	100	100	94	87	82	68	61	49	6	1	1	1	1	0

Processing and reviewing the data

The data is reviewed, according to the design criteria stated in the Betonpocket [15], and the criteria given in NEN-EN-ISO 14688-2:2019 [57].

The first design criteria is the environmental class of the concrete, which generally determines the maximum allowable aggregate size. According to the Betonpocket, the Accropodes are to be of environmental class $XF3$. This is explained by the fact that the breakwaters are in a marine environment, and are subjected to dry/wet cycles [15]. Moreover, no other chlorides are present (e.g. road salt), except the seawater itself. This environmental class does not have a maximum aggregate size.

The next design criteria relates to the total aggregate distribution and is dependent on the grain group of the cement mixture, denoted as d/D. They are the smallest and largest nominal aggregates found in the mixture, in mm. The current mixture falls in the grain group $0/32$, however, some aggregates are observed to be bigger than 32 mm (Subsection 3.2.2). One can find two design areas (I and II), between which a cement mixture is optimally designed for workability and water requirement [15].

The granulometry is seen in Figure H.1. The coloured lines depict all of the 64 granulometry samples.

On the x-axis are the opening sizes (apertures) of the sieves used in millimetres and based on a log-scale. On the y-axis, the amount of aggregate that has passed said sieves is shown in percentages. Using this information and the shape of the diagrams, one can determine what kind of aggregates have passed through the sieves, i.e. the aggregate distribution. It is clear that much of the samples do not satisfy the design parameters, i.e. a lot of lines do not find themselves partially or completely within design areas I or II. It is concluded from this figure, that most of the used aggregates are not preferred for a concrete mixture.

It is noted that the tests did contain a 0.075 mm sieve, as per the code, but every sample returned a 0 % passage, as is seen in the rightmost column in Table H.1 and in Table H.2 [57]. DyOPSA reported that there were no tests done for aggregates smaller than 0.075 mm (e.g. a sediment test) [59]. Since this entire column is 0, it has been left out of the results entirely.

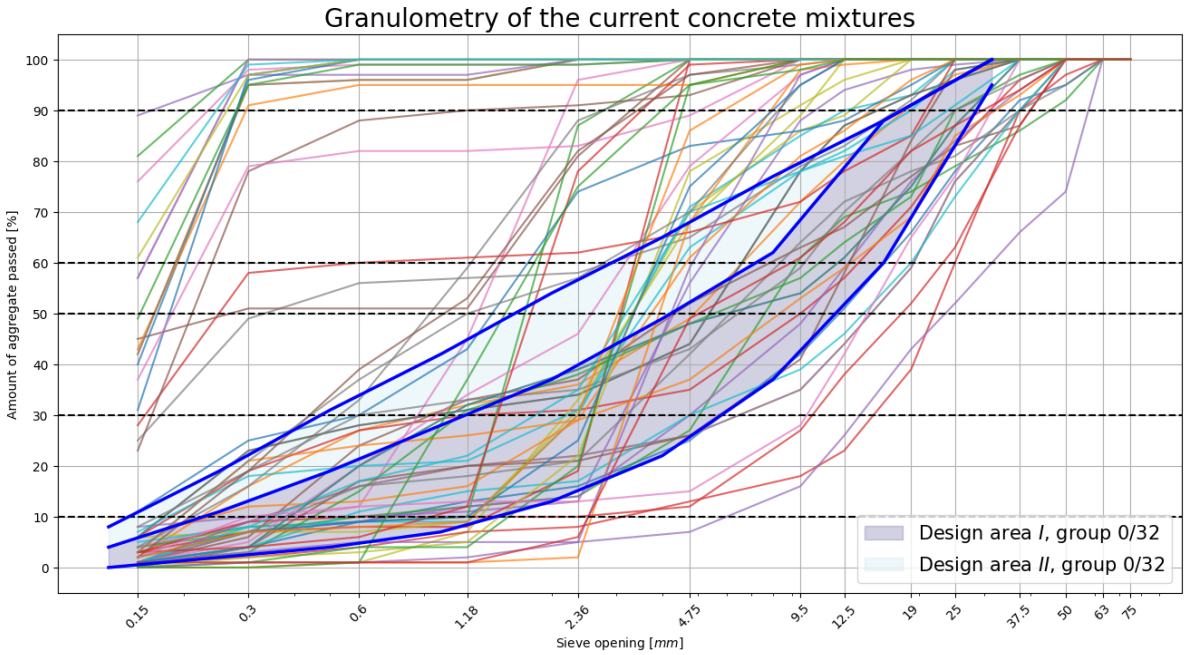


Figure H.1: Current granulometry. There are 64 thin coloured lines, each representing a sample. The thick blue lines represent the boundaries of the design areas [15]. The dark blue and light blue areas respectively represent the design areas I and II, in which a cement mixture is optimally designed for workability and water requirements.

The final relevant design criterium, is calculating the Coefficient of Uniformity C_U, and the Coefficient of Curvature C_C (both dimensionless). These are derived using D_{10}, D_{30}, and D_{60} - the grain sizes at which 10%, 30%, and 60% (in mass percentages) of the total grains are smaller than the specified sizes, all measured in millimetres [57]. Equation H.1 and Equation H.2 show the calculation of these coefficients. The results are shown in Table H.3 and in Table H.4.

$$C_U = \frac{D_{60}}{D_{10}} \qquad \text{(H.1)}$$

$$C_C = \frac{D_{30}^2}{D_{10} \cdot D_{60}} \qquad \text{(H.2)}$$

Table H.3: All granulometry samples and their coefficients

Title	Sample	D_{10} [mm]	D_{30} [mm]	D_{60} [mm]	C_U [–]	C_C [–]
2002n12	1	0.745	6.147	16.400	22.013	3.093
2002n12	2	0.236	0.948	7.022	29.789	0.543
2002n12	3	0.600	5.169	9.360	15.600	4.758
2002n12	4	0.196	1.180	13.893	70.826	0.511
2002n16	1	0.600	3.305	5.344	8.906	3.407
2002n16	2	0.367	0.987	8.205	22.376	0.324
2002n16	3	0.085	0.105	0.134	1.581	0.961
2002n16	4	0.105	0.181	3.043	28.980	0.103
2002n2	1	0.343	6.861	19.353	56.446	7.095
2002n2	2	0.185	0.987	6.985	37.698	0.752
2002n2	3	0.088	0.114	0.160	1.820	0.926
2002n2	4	0.093	0.129	0.201	2.164	0.886
2002n21	1	1.180	1.486	1.946	1.649	0.962
2002n21	2	1.395	2.685	3.570	2.560	1.448
2002n21	3	0.083	0.100	0.126	1.505	0.960
2002n21	4	0.092	0.125	1.534	16.735	0.111
2002n26	1	0.400	0.916	1.527	3.818	1.375
2002n26	2	0.225	0.547	1.221	5.425	1.090
2002n26	3	1.234	2.306	4.137	3.354	1.042
2002n26	4	1.236	2.360	4.109	3.324	1.097
2002n2s	1	0.094	0.131	0.204	2.171	0.903
2002n2s	2	0.092	0.127	0.203	2.197	0.863
2002n2s	3	0.084	0.103	0.131	1.549	0.960
2002n2s	4	2.360	10.318	23.364	9.900	1.931
2002n2sur	1	0.343	6.861	19.353	56.446	7.095
2002n2sur	2	0.185	0.987	6.985	37.698	0.752
2002n2sur	3	0.088	0.114	0.160	1.820	0.926
2002n2sur	4	0.093	0.129	0.201	2.164	0.886
2002n30	1	1.316	2.224	4.204	3.194	0.894
2002n30	2	0.191	2.242	4.526	23.707	5.817
2002n30	3	0.143	0.600	1.827	12.761	1.376
2002n30	4	0.250	2.435	4.675	18.701	5.071

Table H.4: Table H.3 continued

Title	Sample	D_{10} [mm]	D_{30} [mm]	D_{60} [mm]	C_U [–]	C_C [–]
2003n12	1	0.475	1.144	10.786	22.707	0.255
2003n12	2	3.316	15.344	25.000	7.539	2.840
2003n12	3	0.793	4.750	12.882	16.238	2.208
2003n12	4	0.438	6.017	13.000	29.649	6.351
2003n16	1	0.400	1.014	3.374	8.435	0.762
2003n16	2	0.400	3.384	8.636	21.591	3.315
2003n16	3	0.413	1.083	12.071	29.264	0.236
2003n16	4	0.557	4.750	19.000	34.103	2.131
2003n1sur	1	0.099	0.148	0.216	2.177	1.017
2003n1sur	2	0.208	2.659	13.150	63.120	2.580
2003n1sur	3	0.090	0.121	0.186	2.058	0.871
2003n1sur	4	0.102	0.160	0.600	5.895	0.419
2003n2	1	6.333	14.029	32.143	5.075	0.967
2003n2	2	0.108	0.169	0.251	2.332	1.059
2003n2	3	0.095	0.136	0.232	2.437	0.834
2003n2	4	0.177	0.600	9.773	55.128	0.208
2003n21	1	1.527	2.701	3.982	2.607	1.200
2003n21	2	0.367	1.906	4.067	11.092	2.436
2003n21	3	0.413	1.083	12.071	29.264	0.236
2003n21	4	2.650	3.374	4.460	1.683	0.963
2003n26	1	1.623	2.679	3.635	2.240	1.217
2003n26	2	0.987	1.502	2.038	2.066	1.122
2003n26	3	2.581	3.466	4.875	1.889	0.955
2003n26	4	0.221	0.465	1.465	6.641	0.669
2003n2sur	1	0.300	9.929	17.587	58.623	18.684
2003n2sur	2	0.208	0.469	2.912	13.975	0.362
2003n2sur	3	0.087	0.112	0.149	1.704	0.964
2003n2sur	4	0.086	0.108	0.141	1.641	0.962
2003n30	1	1.180	2.599	4.033	3.418	1.419
2003n30	2	1.236	2.360	3.640	2.945	1.238
2003n30	3	0.745	1.067	1.894	2.543	0.807
2003n30	4	2.582	3.694	9.104	3.526	0.580

I

Rebound number test results

Table I.1 contains all of the results of the rebound number tests. The tests are conducted with a sclerometer, in accordance with NEN-EN 12504-2 [53]. The rebound numbers have no unit.

Table I.1: All sclerometer results

		Test number (#)									
Accropode	**LOC**	**1**	**2**	**3**	**4**	**5**	**6**	**7**	**8**	**9**	**Median [–]**
A0	Body	42	46	47	46	44	47	51	48	49	47
	Leg	41	46	46	48	47	44	46	45	46	46
A40	Body	51	51	46	50	47	50	48	46	49	49
	Leg	44	43	58	43	44	46	43	42	44	44
A80	Body	42	46	46	38	46	44	40	44	44	44
	Leg	48	54	45	40	48	46	42	53	46	46
A120	Body	48	44	50	54	47	46	49	44	40	47
	Leg	46	48	48	42	46	48	48	44	40	46
A160	Body	50	45	48	49	47	43	48	45	41	47
	Leg	48	47	47	44	45	45	46	47	42	46
A218N	Body	49	50	40	50	48	45	50	48	38	48
	Leg	51	44	47	48	51	51	50	50	48	50
A218S	Body	50	45	44	44	38	47	43	46	39	44
	Leg	51	43	42	47	46	48	42	43	49	46
A221	Body	50	50	50	50	49	45	44	53	48	50
	Leg	52	44	42	49	45	51	52	46	50	49
B0	Body	40	46	45	48	39	43	45	47	48	45
	Leg	46	41	44	43	45	40	40	43	41	43
B40	Body	40	46	45	48	41	43	45	47	48	45
	Leg	41	44	47	45	40	41	44	42	40	42
B80	Body	47	44	43	40	40	41	45	48	46	44
	Leg	39	42	47	41	39	39	41	43	41	41
B120	Body	45	44	42	45	43	44	46	47	48	45
	Leg	48	43	48	40	41	44	42	44	44	44
B160	Body	48	45	48	43	44	47	44	45	44	45
	Leg	44	41	42	43	41	44	41	46	45	43
B218N	Body	46	51	53	52	55	55	50	49	51	51
	Leg	40	52	40	55	55	48	52	48	48	48
B218S	Body	46	44	44	46	44	44	48	48	48	46
	Leg	50	44	53	42	44	46	44	46	40	44
B221	Body	46	40	40	47	42	43	45	44	43	43
	Leg	45	36	36	46	40	40	46	43	41	41

J

Wave model and sediment transport - extra information

This appendix presents supplementary information in support of Chapter 5. First, the different model types, including SWAN, are discussed. Second, the implementation of the boundary conditions is given. Thereafter, the extended model configurations are discussed. Finally, the sediment transport application in the research is described.

J.1. Model types and SWAN

This section provides an additional explanation of the model types and SWAN, thereby elaborating on Section 5.1.

Coastal models can be divided into several categories. One of which is numerical models. This includes options like Delft3D, XBeach, and SWAN. They provide a robust and adaptable solution for simulating coastal processes but vary in data requirements, scope, and computational intensity. Delft3D, for instance, is a highly versatile model capable of simulating 2D and 3D hydrodynamic flows, waves, sediment transport, and morphology. However, it demands extensive input data and longer computational times, which is not feasible given the current limitations. XBeach, primarily used for simulating storm impacts and rapid coastal changes, also requires detailed morphological data. Due to the data scarcity in this study area, neither Delft3D nor XBeach is suitable.

The SWAN model is selected, as it meets the study's requirements for transforming offshore hydrodynamic conditions to nearshore, while accommodating data limitations. SWAN is a third-generation wave model developed at Delft University of Technology. It is designed to simulate short-crested, wind-generated waves in coastal regions, lakes, and estuaries [70]. It operates by solving the wave action balance equation, which incorporates multiple sources (wind generation, wave growth) and sinks (wave breaking, bottom friction) [71]. SWAN has several advantages that make it suitable for this study. It can simulate wave propagation across different spatial scales, accommodating both 1D and 2D grids. Moreover, it provides multiple operational modes, including stationary and non-stationary simulations, allowing flexibility depending on the available data and the required detail level [71]. In this report, SWAN is used in a stationary 2D horizontal (2DH) mode due to the lack of continuous hydrodynamic data, which prevents the use of non-stationary simulations. The SWAN model requires a well-defined bathymetric grid, upon which the hydrodynamic boundary conditions (wave height, period, and direction) are applied. These conditions are transformed across the computational grid, enabling output at any point within the model domain. By using SWAN, a thorough understanding of wave behaviour is achieved.

Given the scope of this study, the strength in handling complex bathymetry and computational efficiency in transforming offshore wave conditions to nearshore, makes SWAN the ideal choice. Furthermore, the capability to operate in nested grid setups provides enhanced resolution in areas of interest. This

is particularly valuable, as wave transformation near structures requires precise calculations.

J.2. Boundary conditions

This section elaborates on Section 5.2, explaining the boundary conditions in SWAN and how they are implemented in this research.

In SWAN, wave energy leaving the computational domain, or crossing a non-reflective shoreline boundary, is completely absorbed by the boundary conditions [38]. For open boundaries, wave energy entering the domain must be specified. If no boundary conditions are defined, SWAN assumes no wave energy is present, leading to propagation errors [71]. While such erroneous boundary conditions are nearly unavoidable, they propagate into the computational domain, affecting results within triangular zones [38]. Typically, these boundary condition issues are addressed, by aligning the grid parallel to the coastline. This allows to implement deep-water conditions constantly over one boundary. This configuration presumes a uniform depth, considering shore-parallel bathymetric contours. Following this, the lateral boundaries should be placed at a sufficient distance from the region, requiring reliable computational results [38]. However, this strategy does not entirely eliminate the potential for error propagation. Additionally, it was decided not to use a rotated grid for this area, meaning the issue persists.

To mitigate this, a 1D SWAN model run is employed. The offshore extreme and regular wave conditions, as derived in Chapter 4, are assumed to occur in the bottom right (southeast) corner of the computational grid. This corner is also the deepest point in the entire grid, at a level of -41.90 m SHN, therefore being the most appropriate location for assuming the deep water offshore conditions. Applying these conditions from this position, two 1D SWAN runs along the southern and eastern boundary are performed. These results are exported into a boundary spectrum file, for the corresponding large grid resolution. Thereby forming the southern and eastern boundary conditions for the large grid SWAN run. The 1D SWAN results along the southern and eastern boundary are also used as input for the northern and western boundary. The eastern boundary final grid point, in the top right (northeast) of the grid, is the input for the 1D run for the northern boundary. The southern boundary final grid point, in the bottom left (southwest) of the grid, is the input for the 1D run for the western boundary. Again, spectrum files are retrieved, which will be used as input along their respective boundaries in the large grid.

While effective in scenarios with limited data, 1D models carry the risk of underestimating boundary interactions in highly variable bathymetric conditions. Complex coastal geometries may warrant more intricate boundary specifications. Concluding, per offshore condition, regular or extreme, four 1D models will be run for each boundary, and two 2D models will be run for the large and small grids. This approach is assumed most appropriate, considering the duration and available data of this research.

J.3. Model configuration - extended

This section provides extra information on the model configurations, thereby elaborating on Section 5.3. First, the normal and extreme settings are discussed. Thereafter, other settings applied in the model are stated.

J.3.1. Normal conditions - extended

The normal offshore conditions are listed in Table J.1 (Subsection 5.3.1).

Table J.1: Offshore normal settings used in model runs

Setting	H_s [m]	T_p [s]	Direction [°N]	Simplified Dir
1	1.04	9.31	73	ENE
2	1.04	10.01	127	SE
3	1.33	10.37	178	S
4	1.01	6.66	113	ESE
5	1.21	6.60	173	S

The wave transformations for regular conditions are used to assess longshore sediment transport. However, uncertainties remain in transport computations, as different formulations can yield results that vary significantly in magnitude [16]. Consequently, implementing all physical processes within the wave transformation model, does not significantly enhance sediment computation accuracy. Given the elongated effects on computational time, a subset of physical processes is included in the model. These processes, applicable for both regular and extreme conditions, are described in Subsection J.3.3. Three processes are excluded in the normal runs but are activated for the extreme runs.

First of all, wind growth is deactivated. The impact on wave height due to wind growth is limited for normal conditions, as wind speeds and wave heights are low. Secondly white-capping, steepness-induced wave breaking [16], is excluded. Limited white-capping is expected in normal conditions, given the relatively low wave heights. Deactivating white-capping improves computational efficiency without significantly affecting result accuracy. Finally, wave-induced set-up and set-down are also turned off. Their impact on sediment transport calculations would be minimal, given the deep water wave heights used for computations.

J.3.2. Extreme conditions - extended

The extreme offshore conditions are listed in Table J.2 (5.3.2).

Table J.2: Offshore extreme settings with 100 year return period

Setting	H_s [m]	T_p [s]	w_{10} [m/s]	**Direction [°N]**	**Simplified Dir.**
1	6.90	11.45	20.51	202.5	SSW
2	6.90	11.45	20.51	180	S
3	6.90	11.45	20.51	157.5	SSE
4	6.90	11.45	20.51	135	SE

The three processes deactivated under regular condition runs, being wave growth by wind, white-capping, and set-up, are reactivated for extreme conditions, due to their relevance. In extreme conditions, high wind velocities and wave heights require the inclusion of wave growth by wind. This is achieved by aligning wind and wave directions, as concluded by the extreme value analysis. A conservative assumption of constant wind direction and magnitude across the grid is used, due to the lack of data. The input for wind velocities in SWAN is specified as the wind speed at 10 metres above the water surface, aligning with the EVA-derived wind velocities (Subsection 4.2.4). The wind forcing is implemented using the default options in SWAN [71]. For wave growth by wind, this is the method of Yan [81], combined with the wind drag formula according to Wu [80]. Including wind-driven wave growth requires additional dissipation, otherwise, it would lead to unnaturally high wave heights. This dissipative process is white-capping, which allows for the breaking of waves once they become too steep. In default, SWAN implements this using the white-capping calculation method of Alves and Banner [8]. Although both processes increase computational time, they are necessary for accurate extreme conditions modelling. Finally, wave set-up is included due to its substantial impact at the toe of the breakwater. SWAN computes this set-up, and takes it into account for the wave computations [71]. Moreover, a separate output is provided for set-up. This is used to adjust the design high water level accordingly.

J.3.3. Other settings

The remaining settings, relevant to both the normal and extreme conditions, are detailed here. As SWAN operates based on the wave action balance equation, a defined shape for the input spectrum is required [71]. This study employs the JONSWAP spectrum. The JONSWAP spectrum is a mathematical model used to describe the energy distribution of wind-generated waves in a sea state [37]. It builds on the Pierson-Moskowitz spectrum, which describes fully developed seas. However, the JONSWAP spectrum better accounts for less developed and growing seas, therefore being often applied in coastal engineering modelling. For SWAN, the peak enhancement parameter needs to be defined ($\gamma_{JONSWAP}$). The default value of $\gamma_{JONSWAP}$ of 3.3 is used in this research. Additionally, the co-

efficient of directional spreading must be defined. Due to a $cos^m(\theta)$ distribution is assumed in this formulation [71]. The default interpretation as the power of m is chosen, with a magnitude of 2.

The following processes will be accounted for in both conditions. Firstly refraction, which allows for the direction change of the waves. This leads to wave energy convergence in the case of convex depth contours, and divergence in the case of concave depth contours [16]. Depth-induced breaking, vital in nearshore wave modelling, is also implemented using the default breaking parameter γ_{br} of 0.73. This parameter has a relation with the slope of the foreshore. However, it is still used to balance accuracy with computational efficiency.

To improve the computational time and avoid overcomplicating the model, the following processes are not included in the model: quadruplet and triad wave-wave interactions, Bragg and QC scattering, and the infra-gravity energy module. Additionally, due to data limitations, currents, bottom friction, and vegetation and mud effects are excluded. It is recognised that in reality, the effects and processes, finding their origin in these parameters, influence the results of the wave transformations. However, a lack of quantifiable data precludes their inclusion.

J.4. Sediment transport application

The sediment transport formula is defined in Subsection 5.4.2. However, the application of this formula to the SWAN results still needs to be explained. The output of SWAN already offers significant wave height, period, and wave direction for every point in the small computational grid. The shore normal is the only parameter not given as SWAN output. This can be calculated by defining the coastal orientation.

This starts by defining the coastline from the model results. An automated process identifies the coastline as the most offshore point with no wave computations, reflecting land areas above the water. The most offshore point is taken, to make sure the inner port is not defined as coastline, as no longshore sediment transport is possible here. The 10 km stretch of coastline is divided into 50 sections of 200 meters, with each section's coastline orientation determined. This orientation, together with the wave direction, determines the wave incidence angles at each grid point. Offshore conditions needed for the formulation, are assumed to occur 6 km from the coastline, providing inputs for Equation 5.2. From this position, the needed parameters are used as input in the sediment transport formula. This returns the volume of alongshore sediment transport (Q_s) every 20 meters of coastline. There is, however, not much value in having the sediment transport at this resolution. Thus the sediment volume is averaged per 200-meter section, yielding 50 values representing alongshore sediment transport magnitudes along the 10 km coast.

K

Results normal conditions

This appendix presents the outcomes of model simulations conducted under normal offshore conditions. section K.1 The first section details the wave transformation for each normal setting across the reference, concept 1, concept 2, and concept 3 scenarios. Subsequently, the next section provides the results of the bulk alongshore sediment transport calculations for each scenario. Both These results supplement the findings discussed in Section 7.2.

K.1. Wave transformations

The following subsections display the wave transformation results for each scenario under normal offshore conditions. To ensure consistency and facilitate comparison across different settings and scenarios, all figures adhere to a uniform format. Only results from the fine small 10 by 10 km grid are presented.

The figures show wave height and direction for each scenario, with Figure K.1 representing the reference scenario, followed by concept 1 (Figure K.2), concept 2 (Figure K.3), and concept 3 (Figure K.4). In each figure, the different settings are arranged as follows: setting 1 (top left), setting 2 (top right), setting 3 (middle left), setting 4 (middle right), and setting 5 (bottom left). These settings reflect offshore conditions detailed in Table 5.1.

For visual clarity, a schematic of the bathymetry near the port is provided in the bottom right of each figure. All wave height figures share the same colour scale to ensure direct comparability, while wave directions are simplified into main directional categories (e.g. S, SSE, SE) following the nautical convention. The direction magnitudes are, however, displayed according to the Cartesian convention.

K.1.1. Reference situation

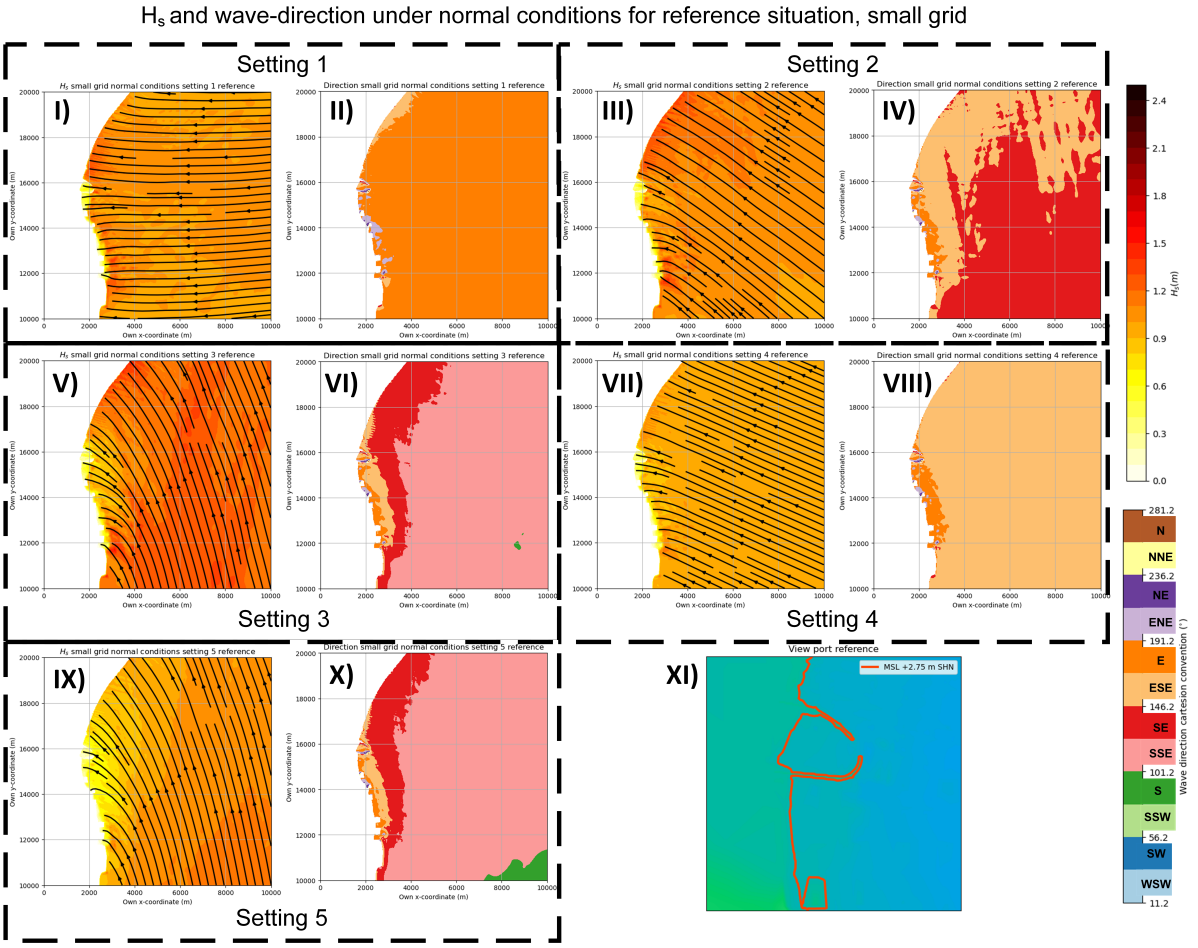


Figure K.1: Wave transformation results, H_s and wave direction under normal conditions for the reference situation small grid. I) H_s small grid offshore setting 1; II) Wave direction small grid offshore setting 1; III) H_s small grid offshore setting 2; IV) Wave direction small grid offshore setting 2; V) H_s small grid offshore setting 3; VI) Wave direction small grid offshore setting 3; VII) H_s small grid offshore setting 4; $VIII$) Wave direction small grid offshore setting 4; IX) H_s small grid offshore setting 5; X) Wave direction small grid offshore setting 5; XI) Schematic of port reference situation

K.1.2. Concept 1

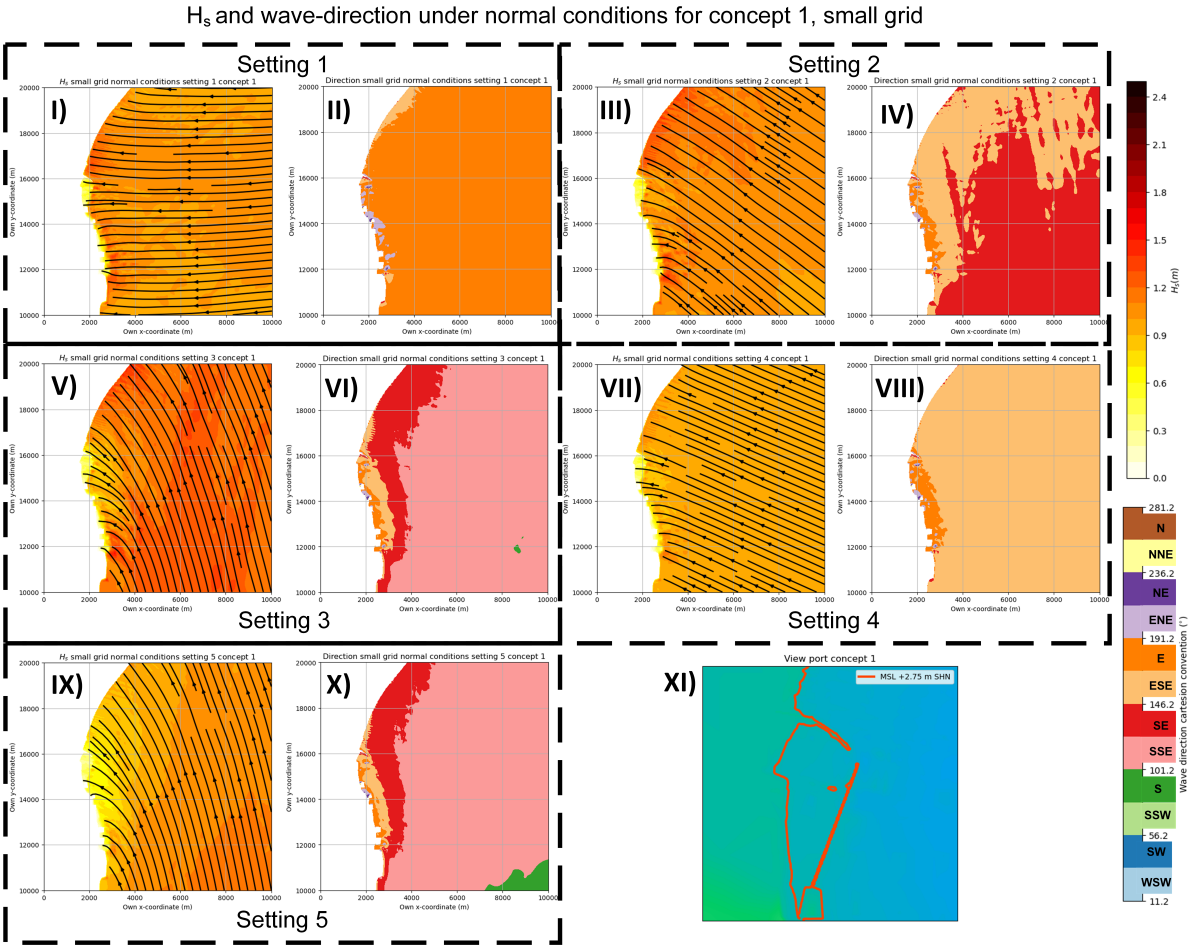


Figure K.2: Wave transformation results, H_s and wave direction under normal conditions for concept 1 small grid. I) H_s small grid offshore setting 1; II) Wave direction small grid offshore setting 1; III) H_s small grid offshore setting 2; IV) Wave direction small grid offshore setting 2; V) H_s small grid offshore setting 3; VI) Wave direction small grid offshore setting 3; VII) H_s small grid offshore setting 4; $VIII$) Wave direction small grid offshore setting 4; IX) H_s small grid offshore setting 5; X) Wave direction small grid offshore setting 5; XI) Schematic of port for concept 1

K.1.3. Concept 2

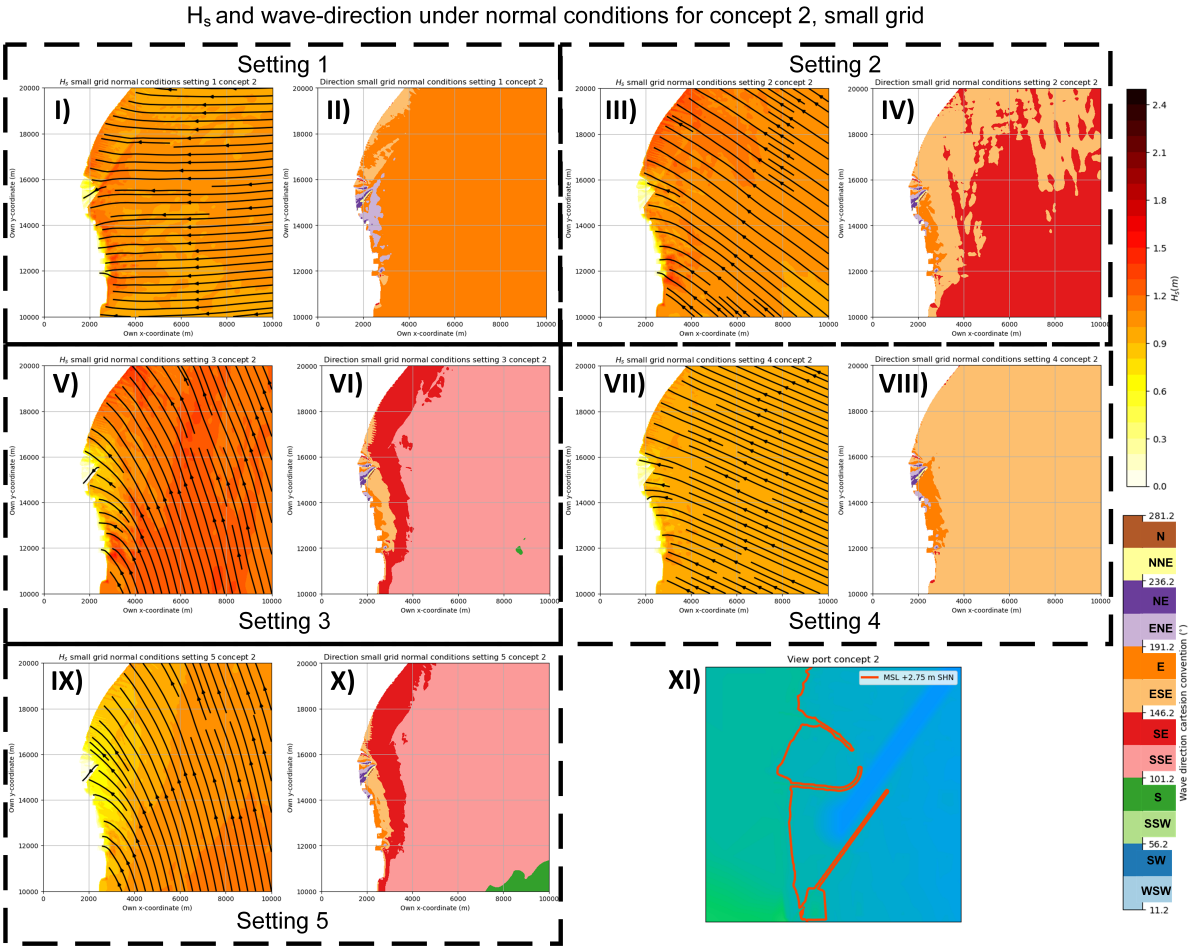


Figure K.3: Wave transformation results, H_s and wave direction under normal conditions for concept 2 small grid. I) H_s small grid offshore setting 1; II) Wave direction small grid offshore setting 1; III) H_s small grid offshore setting 2; IV) Wave direction small grid offshore setting 2; V) H_s small grid offshore setting 3; VI) Wave direction small grid offshore setting 3; VII) H_s small grid offshore setting 4; $VIII$) Wave direction small grid offshore setting 4; IX) H_s small grid offshore setting 5; X) Wave direction small grid offshore setting 5; XI) Schematic of port for concept 2

K.1.4. Concept 3

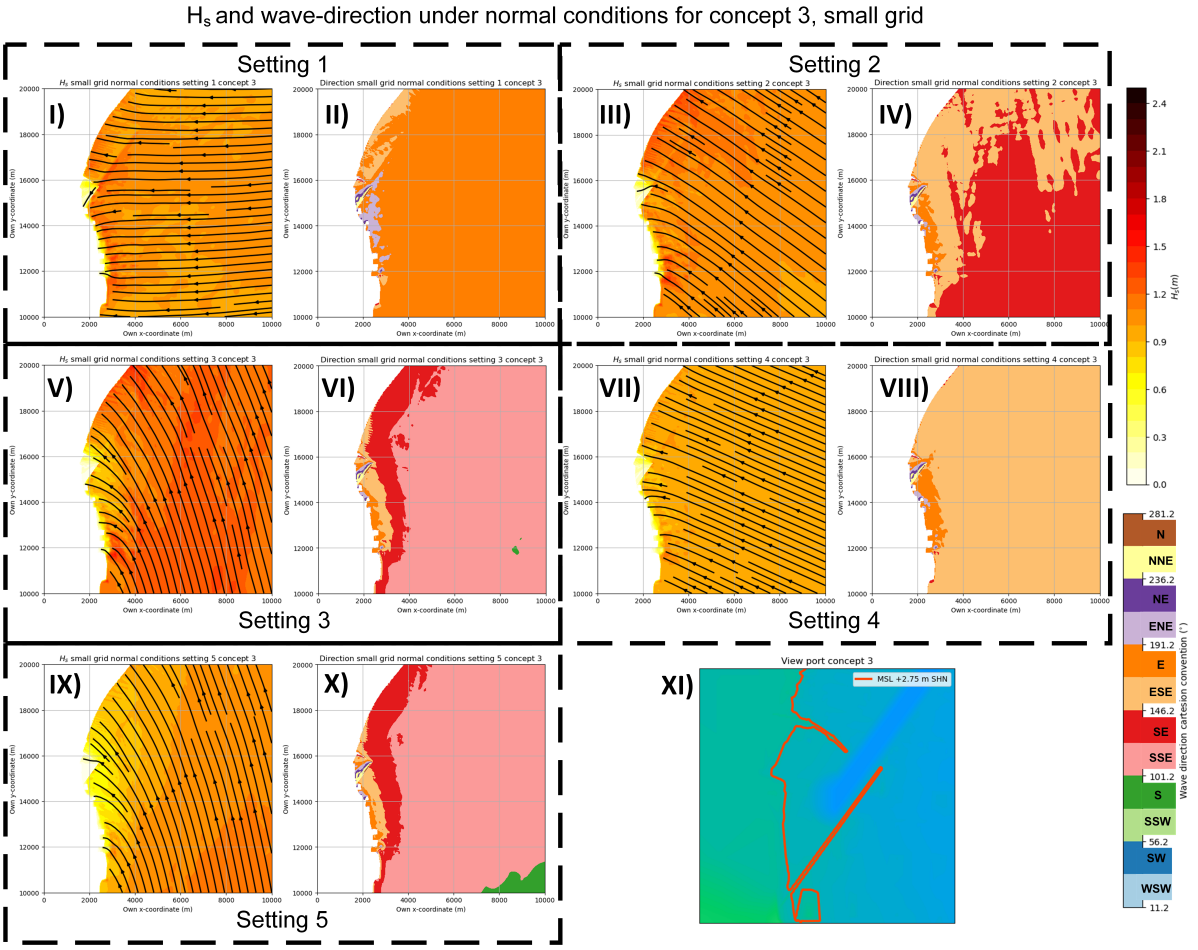


Figure K.4: Wave transformation results, H_s and wave direction under normal conditions for concept 3 small grid. I) H_s small grid offshore setting 1; II) Wave direction small grid offshore setting 1; III) H_s small grid offshore setting 2; IV) Wave direction small grid offshore setting 2; V) H_s small grid offshore setting 3; VI) Wave direction small grid offshore setting 3; VII) H_s small grid offshore setting 4; $VIII$) Wave direction small grid offshore setting 4; IX) H_s small grid offshore setting 5; X) Wave direction small grid offshore setting 5; XI) Schematic of port for concept 3

K.2. Longshore sediment transport

This section presents the outcomes for the alongshore sediment transport volumes, illustrated in Figure K.5, and derived as outlined in Section 5.4. Detailed interpretation of this figure, in the reference scenario, can be found in Subsection 5.5.2. Briefly, the rewritten CERC formulation (Equation 5.2) was applied to calculate the bulk alongshore sediment volumes (Q_s) for each 200-meter section along the coast. This process was repeated for each normal offshore condition (Table 5.1), with the overall sediment transport calculated based on the frequency of occurrence for each condition (depicted by the black line). Negative Q_s values denote southward transport, while positive values indicate transport to the north. The cross-sections used for calculating sediment transport gradients are also displayed, with results discussed in Subsection 7.2.2.

As only the bathymetry near the port varies between scenarios, noticeable differences in sediment transport patterns occur only between coordinates 14000, and 16000.

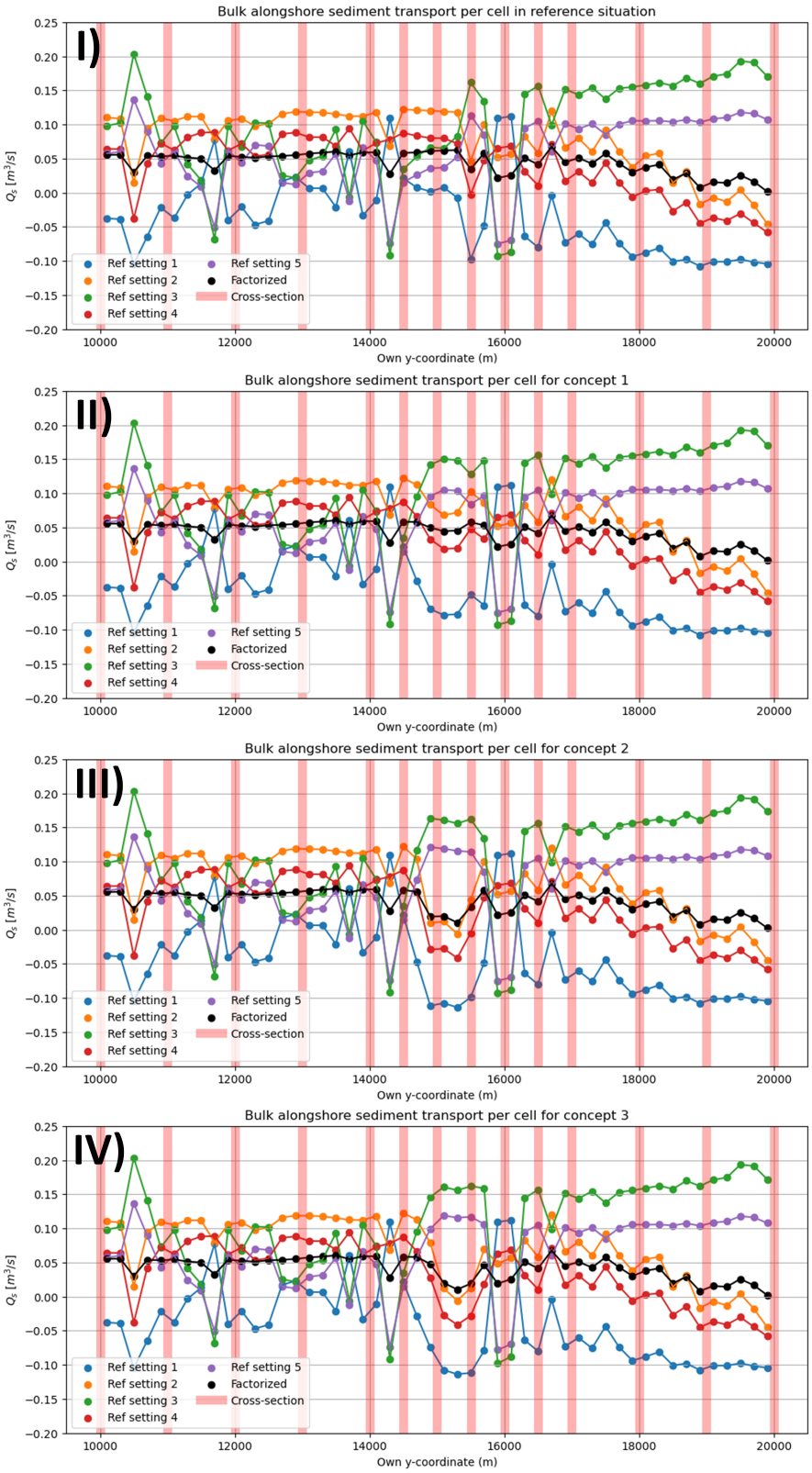


Figure K.5: Bulk alongshore sediment volumes for each segment in all settings for all designs and the reference. Added with the calculated factorized sediment volume according to the frequency of retrieved normal conditions. I) Reference situation; II) Concept 1; III) Concept 2; IV) Concept 3

L

Results extreme conditions

This appendix presents the outcomes of model simulations performed under extreme offshore conditions. The first section outlines the wave transformations for each extreme setting, while the following section presents the wave height results near the port for concept 3, including the parameters required at this location. Both sections provide supplementary insight to the findings discussed in Section 7.3.

L.1. Wave transformations

The following section illustrates the wave transformation results under extreme offshore conditions, displaying both wave heights and directions in Figure L.1. Each setting varies solely by offshore wave direction and applies the parameters specified in Table 5.2. Results are provided for both the larger coarse grid (30 by 30 km) and the smaller fine grid (10 by 10 km).

The wave transformation settings are presented as follows: SSW offshore direction setting (top left), S offshore direction setting (top right), SSE offshore direction setting (bottom left), and SE offshore direction setting (bottom right). The wave height scale in these figures extends up to 9 meters, differentiating it from the scales used in the wave transformations for normal conditions, presented in section K.1. However, the simplified wave directions are categorized in colour similarly, for consistency.

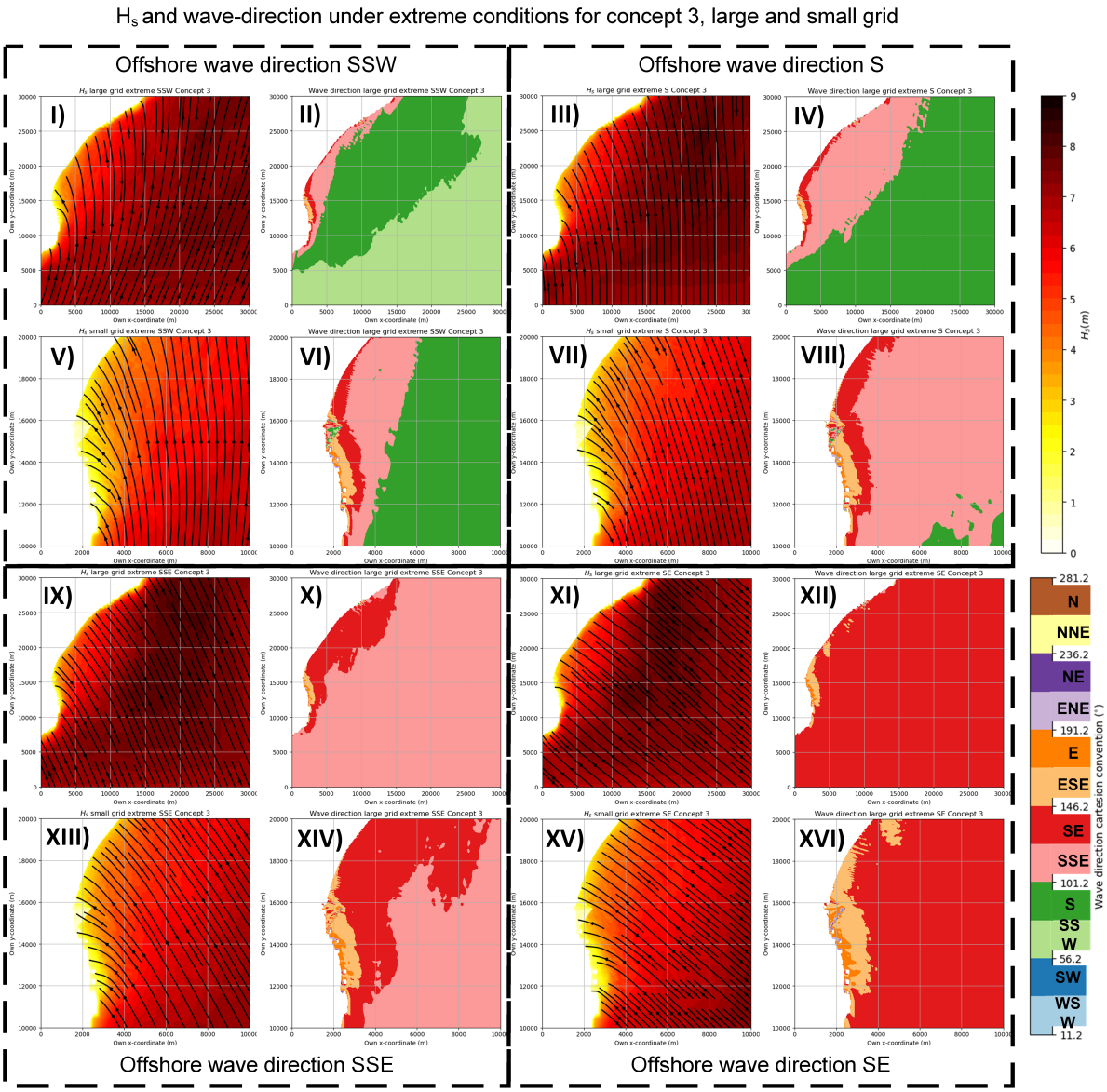


Figure L.1: Wave transformation results, H_s and wave direction under extreme conditions for concept 3 small and large grid. I) H_s large grid SSW offshore conditions; II) Wave direction large grid SSW offshore conditions; III) H_s large grid S offshore conditions; IV) Wave direction large grid S offshore conditions; V) H_s small grid SSW offshore conditions; VI) Wave direction small grid SSW offshore conditions; VII) H_s small grid S offshore conditions; $VIII$) Wave direction small grid S offshore conditions; IX) H_s large grid SSE offshore conditions; X) Wave direction large grid SSE offshore conditions; XI) H_s large grid SE offshore conditions; XII) Wave direction large grid SE offshore conditions; $XIII$) H_s small grid SSE offshore conditions; XIV) Wave direction small grid SSE offshore conditions; XV) H_s small grid SE offshore conditions; XVI) Wave direction small grid SE offshore conditions

L.2. Near port wave height results

Figure L.2 presents the wave transformation results near the port under extreme offshore conditions. The bottom right section of the figure highlights the highest wave height observed in front of the breakwater for concept 3. This maximum corresponds with an offshore wave direction of southeast, establishing the normative extreme conditions for a 100-year return period. The pink cross in this figure represents the toe position, located at the offshore limit of the breakwater. This point serves as the location where the most extreme forces impact the structure, with its dimensions calculated based on the parameters at this location.

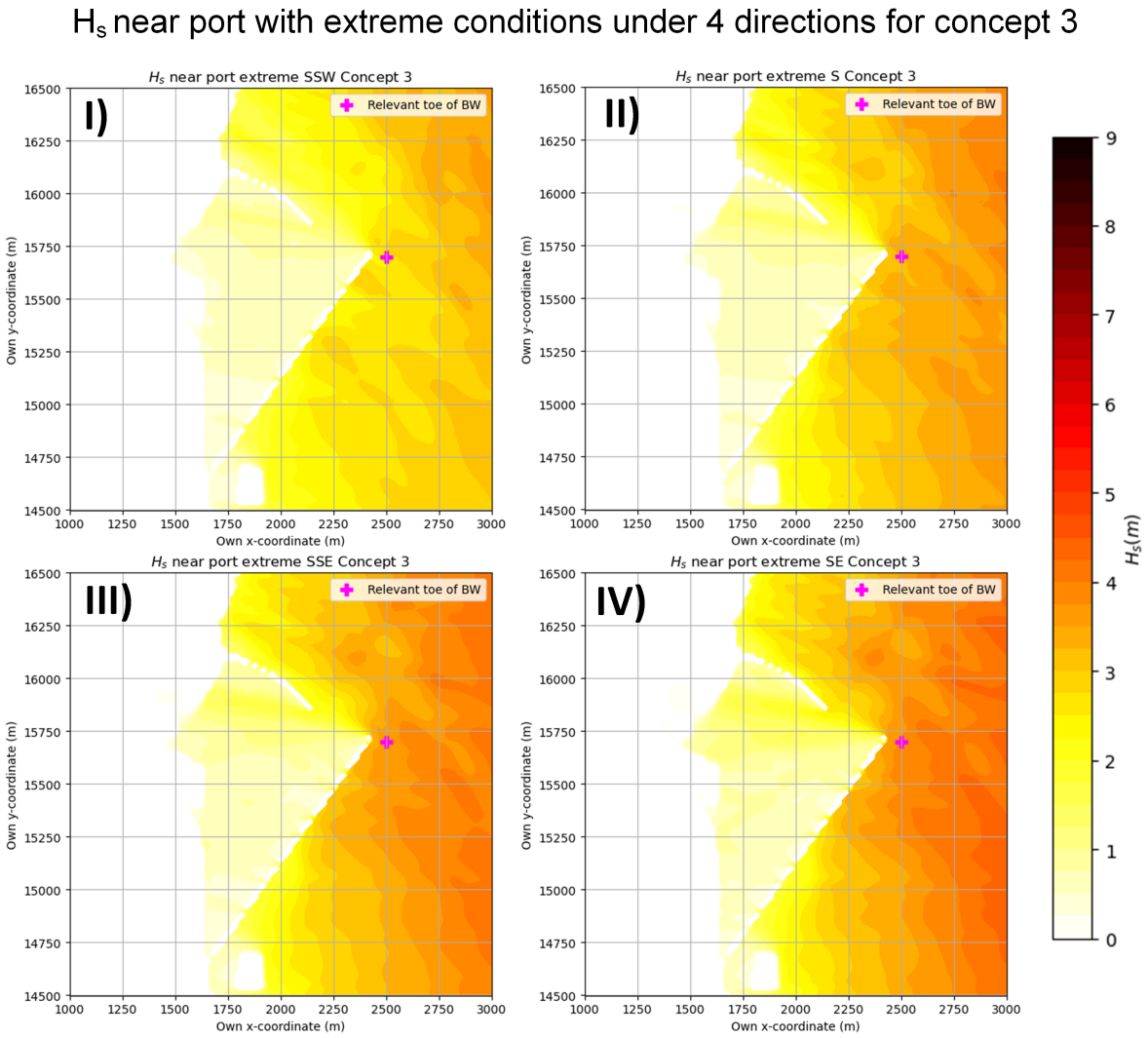


Figure L.2: H_s near port for concept 3 under 4 extreme conditions. I) SSW offshore conditions; II) S offshore conditions; III) SSE offshore conditions; IV) SE offshore conditions

The hydrodynamic parameters at the toe position, as indicated in Figure L.2, are summarized in Table L.1. These data further clarify that setting 4, with the SE offshore wave direction, is the most critical for design.

Table L.1: Results extreme conditions from four offshore directions for concept 3, parameters at the toe

Setting	**Offshore direction**	H_s [m]	T_p [s]	T_{m01} [s]	**Direction [°N]**	**Wave set-up** [m]	**Water depth** [m]
1	SSW	2.87	11.64	6.68	138.4	0.031	8.651
2	S	3.47	11.64	7.41	133.2	0.054	8.674
3	SSE	3.81	11.64	7.91	125.2	0.091	8.711
4	SE	3.98	11.64	8.21	117.2	0.126	8.746

M

Dimensions of Accropodes

This appendix provides a brief overview of the dimensions of both the original Accropode I [41] and the Accropode II units [1]. Table M.1 provides the volume, height, and thickness, needed in Subsection 8.2.1.

Table M.1: Dimensions of both the original Accropode I [41] and the Accropode II units [1].

Armour type	**Volume** $[\mathrm{m}^3]$	**Height** $[\mathrm{m}]$	**Armour thickness** $[\mathrm{m}]$
Accropode I	1.0	1.43	1.29
	2.0	1.81	1.63
	3.0	2.07	1.86
Accropode II	1.0	1.51	1.36
	2.0	1.90	1.71
	3.0	2.17	1.96

Additionally, a thickness check of the Accropodes should be conducted. If the thickness check suffices, using Equation M.1, the Accropode I units can be used in combination with the Accropode II units in the same construction. This check has to be repeated three times, each for a different Accropode volume. Table M.2 shows the results of these checks, confirming that the Accropodes I and the Accropodes II can be used in the same construction.

$$|t_{Acc1} - t_{Acc2}| \leq \frac{1}{6} H_{Acc2} \tag{M.1}$$

Where:

t_{Acc1} : Armour thickness of Accropode I $[\mathrm{m}]$;
t_{Acc2} : Armour thickness of Accropode II $[\mathrm{m}]$;
H_{Acc2} : Height of Accropode II $[\mathrm{m}]$;

Table M.2: Thickness checks

Volume $[\mathrm{m}^3]$	**Equation result**	**Suffices**
1.0	$0.07 \leq 0.25$	Yes
2.0	$0.08 \leq 0.29$	Yes
3.0	$0.10 \leq 0.33$	Yes

N

Supplementary conceptual designs

This appendix provides a detailed explanation of the design choices made in conceptual design 1 and conceptual design 2. This information is an addition to Subsection 6.2.1.

N.1. Conceptual design 1

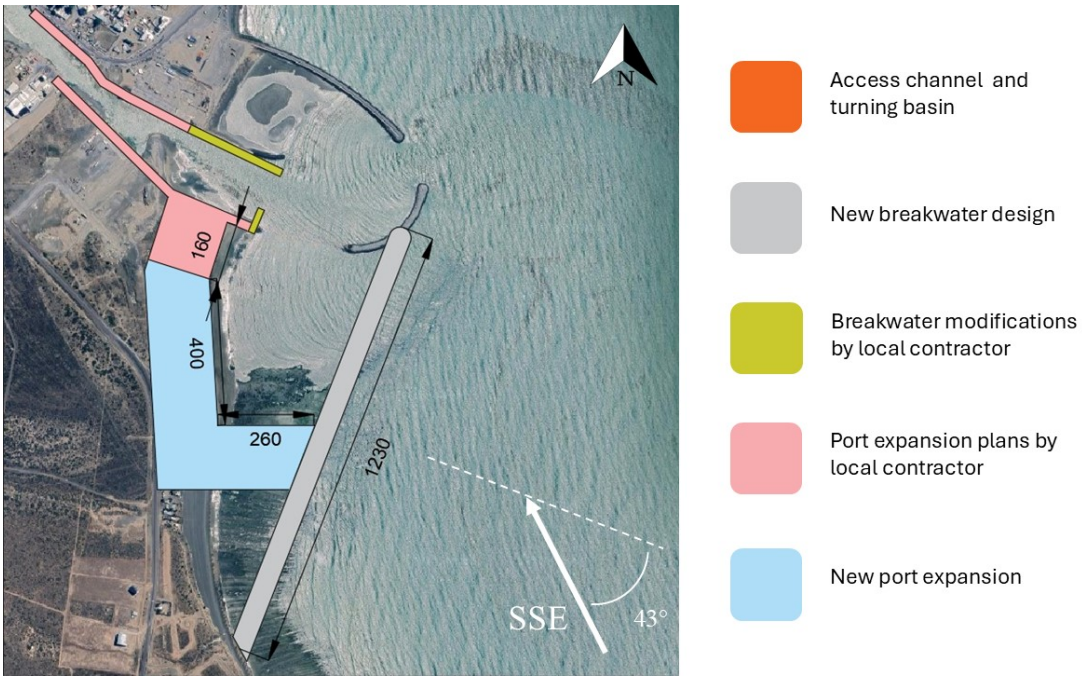


Figure N.1: Schematic drawing of conceptual design 1

The first conceptual design is developed with a focus on achieving the optimal breakwater orientation in alignment with longshore sediment transport theory. The design aims to keep the existing breakwater lay-out of the harbour by extending the most seaward part of the new southern breakwater to create a new breakwater. The orientation of the new breakwater is set such that the angle between its shore normal and the dominant wave direction matches the optimal angle of 43° for longshore sediment transport. Figure N.1 shows the schematic visualization of conceptual design 1.

Considering this orientation, the position breakwater in the ocean can differ, as the extension of the new southern breakwater is not a requirement of the design. Positioning the breakwater farther west, relative to Figure N.1, would reduce available space between the breakwater and the shore, limiting

opportunities for port operations. Conversely, aligning the breakwater further east, relative to Figure N.1, would significantly increase the length of the breakwater. Furthermore, this alignment would require construction in deeper waters, missing the use of the restinga as its foundation. Such a scenario would lead to excessive material use, resulting in the design being environmentally unsustainable. The final alignment of the breakwater in conceptual design 1 ensures that the restinga provides support to the over the width and along the length of the breakwater. This orientation safes material use and therefore enhances the sustainability of the design.

The large extension of the breakwater in the design does not result in the need for a new access channel. Instead, the design includes an opening in the existing old southern breakwater to function as the entrance to the newly created harbour basin. Given that the old southern breakwater requires renovation or reconstruction in the near future due to its current condition (Section 3.2), partial removal can be considered a viable option for future developments. However, the condition of the old southern breakwater prevents the reuse of its armour units.

No modifications are proposed to the dimensions of the existing access channel. Therefore, no access channel is illustrated in Figure N.1. As a result, the conceptual design does not accommodate a safe entrance for all future vessel sizes, given that the current dimensions are insufficient. Firstly, any adjustments to the dimensions of access channel, while maintaining its orientation, result in modifications to both the new northern breakwater and the old southern breakwater. Specifically, widening the access channel by shortening the new southern breakwater, would allow nearshore refracting waves to directly enter the inner harbour, which could cause damage to docked vessels. Secondly, dredging a wider or additional access channel would be disadvantageous for longshore coastal sediment transportation.

Table N.1 presents the design criteria and their presence or absence in the design respectively as a *pro* or *con* of the concept design.

Table N.1: Pros and cons of concept design 1

Pros	Cons
Waves coming from the dominant direction (SSE) cannot enter the harbour directly.	The new breakwater design does not incorporate reused material of the existing breakwaters.
The angle of the breakwater orientation relative to the dominant wave direction is 43°.	The access channel is not of sufficient width and length to provide a safe entrance for vessels expected in Phase I and Phase II.
The angle between the access channel and the dominant wave direction (SSE) is between 30° and 90°.	The harbour basin does not have adequate width and length to accommodate a turning basin for the vessels expected in Phase I and Phase II.
The design only incorporates one access channel.	
The restinga fully supports the crest width along at least half of the length of the breakwater.	
The new breakwater design incorporates parts of the existing breakwaters.	

To conclude, this conceptual design focuses on optimizing the coastal sediment transport by implementing an optimal breakwater orientation of 43° with respect to waves from the dominant SSE direction. This breakwater orientation is expected to improve northward sediment transport, which theoretically leads to a bypass of sediment over the port. If effective, this would reduce the erosion in Playa Unión. However, due to the limited space for future port expansion and given the uncertainty regarding permits to modify the existing breakwater configuration, the design remains unfeasible to construct.

N.2. Conceptual design 2

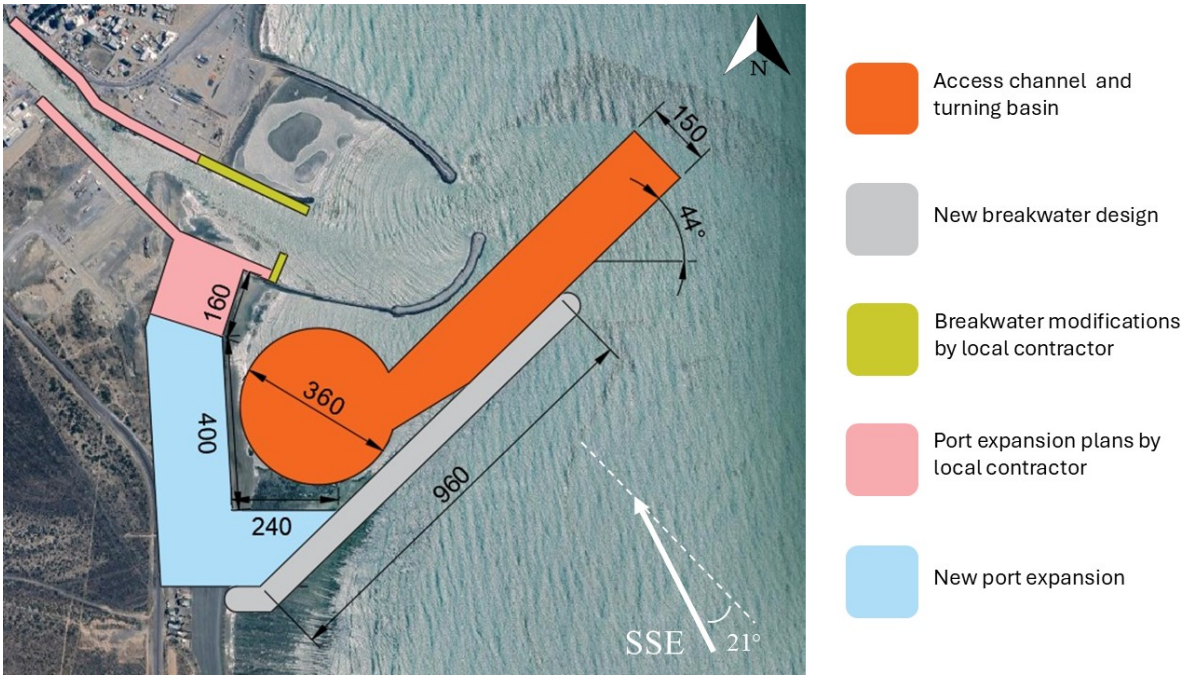


Figure N.2: Schematic drawing of concept design 2

The second conceptual design is developed with a focus on the feasibility of construction. Given the uncertainty regarding permits of the local government to modify the existing breakwater configuration, this design serves as a practical alternative in cases where a separate harbour access is required. The design aims to keep the entire existing breakwater lay-out and expand the harbour by adding a separate access channel to the new harbour basin. The new breakwater is positioned along the edges of the restinga to use the elevated soil layer as a foundation, reducing the need for extensive substructure materials. The structure is then aligned to ensure adequate distance to the southern breakwater, allowing for sufficient width in the access channel to safely accommodate for future vessel sizes.

The following states a detailed explanation of the design choices made for the breakwater orientation. At first, the length of the breakwater is not extended to prevent interference with the existing access channel. It is also not shortened, as this would allow waves to penetrate directly into the new harbor basin. Positioning the breakwater farther west could increase available space for the harbor basin, yet this option was dismissed since it would extend the breakwater beyond the restinga. Constructing the breakwater outside of the restinga would result in excessive material use, making the design environmentally unsustainable. Similarly, a breakwater alignment parallel to the shore is avoided for the same reason.

Regarding the access channel, its orientation is not reccommended, according to PIANC guidelines [60]. The angle between the access channel and the dominant wave direction (SSE) falls outside the optimal range of 30° to 90°, creating unsafe entry conditions for vessels of all sizes. However, this problem is difficult to solve, as it is constrained on both sides by the new southern breakwater and the restinga. As a result, limited adjustments can be made to the orientation of the access channel.

Table N.2 presents the design criteria and their presence or absence in the design respectively as a *pro* or *con* of the concept design.

Table N.2: Pros and cons of conceptual design 2

Pros	Cons
Waves coming from the dominant direction (SSE) cannot enter the harbour directly.	The new breakwater design does not incorporate reused material of the existing breakwaters.
The restinga fully supports the crest width along at least half of the length of the breakwater.	The angle of the breakwater orientation relative to the dominant wave direction is 21°.
The access channel is of sufficient width and length to provide a safe entrance for vessels expected in Phase I and Phase II.	The angle between the access channel and the dominant wave direction (SSE) is not between 30° and 90°.
The new breakwater design incorporates parts of the existing breakwaters.	The design incorporates two access channels.
The harbour basin does have adequate width and length to accommodate a turning basin for the vessels expected in Phase I	The harbour basin does not have adequate width and length to accommodate a turning basin for the vessels expected in Phase II.

In conclusion, this breakwater design prioritizes feasibility of construction. Given the uncertainties regarding the removal of the old southern breakwater, the design serves as a practical alternative when a separate harbour access is required. Additionally, the new harbour basin accommodates entry and docking for future vessel sizes. However, wave conditions are not optimal due to the orientation of the access channel. Ultimately, the presence of an additional access channel in combination with a suboptimal breakwater orientation, result in a negative impact on longshore sediment transport.

O

Accroberm II toe unit

In this appendix the position and specific placement of the Accroberm II toe unit is made visible. These figures provide supplementary visualizations to Chapter 8.

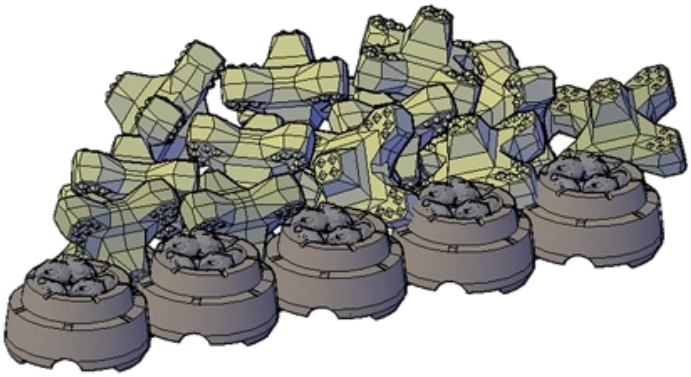


Figure O.1: Accroberm II toe unit placement [1].

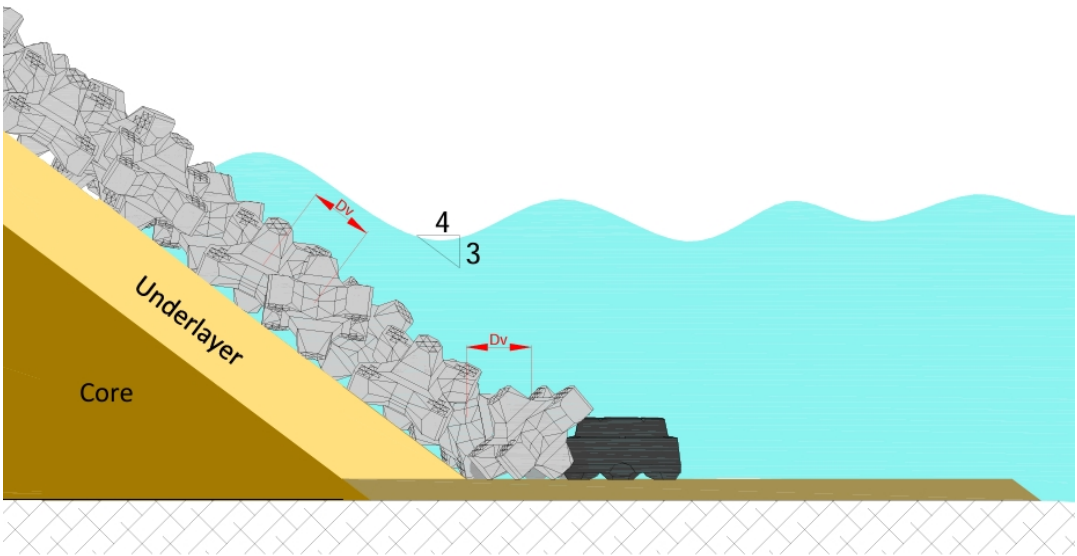


Figure O.2: Accroberm II unit in toe berm position [1].

P

Mix design proportions

In Table P.1 and Table P.2 are the mix design proportions of respectively the initial and the proposed cement mixtures.

Table P.1: Initial cement mixture proportions

		Initial cement mixture		
Components	Material	Density [$\mathrm{kg/m^3}$]	Weight [kg]	Volume [$\mathrm{m^3}$]
Water	Potable water	1000	160	0.16
Cement	CPP 40, Com. Riv.	3050	380	0.12
Fine aggregate	Sand, Chubut river	2570	740	0.29
Coarse aggregate	Pebble, Chubut river	2650	1095	0.41
Plasticizer	Sikament 90E, Sika	1180	1.33	11.3 $\cdot 10^{-4}$
Concrete	Fresh	2408	2376	0.99
Concrete	Dry	2288	-	-

Table P.2: Proposed cement mixture proportions

		Proposed cement mixture		
Components	Material	Density [$\mathrm{kg/m^3}$]	Weight [kg]	Volume [$\mathrm{m^3}$]
Water	Potable water	1000	157.5	0.16
Cement	CPP 40, Com. Riv.	3050	350	0.11
Fine aggregate	Sand, Aridos Fontana	2570	804	0.31
Coarse aggregate	Porphyry quarry waste	2510	955	0.38
Plasticizer	Sikament 90E, Sika	1180	0.95	8.04 $\cdot 10^{-4}$
Air entrainer	AER, Sika	1015	0.06	0.57$\cdot 10^{-4}$
Concrete	Fresh	2345	2268	0.96
Concrete	Dry	2228	-	-

Q

Life Cycle Assessment

The LCA aims to compare the environmental impact of the current and proposed method. This appendix gives an overview of the steps done in the LCI and LCIA. The latter is further monetized by means of shadow costs per impact category and the results are discussed in Section 9.3.

Q.1. Life Cycle Inventory Analysis

The LCI provides a systematic overview of the products and processes involved in both the current and proposed methods in a simplified manner. It captures the most important inputs that differ between the two methods within the system boundaries, ensuring clarity while maintaining essential distinctions.

A compact summary of both methods is provided below, with an asterisk [*] indicating actions included in the proposed method only.

- C1 (Deconstruction):
  - Deconstruction of breakwater structure and moving Accropodes;
  - On-site sorting of Accropodes for different EoL solutions based on visual inspection and physical testing. *
- C2 (Transport):

  Transportation of Accropodes to their assigned EoL location:
  - Option 1: Reuse. Transport of units to the new southern breakwater; *
  - Option 2: Repurpose. Transport of units to artificial reefs close to Puerto Madryn, 70 km away [4]; *
  - Option 3: Recycle. Transport of units suitable for crushing into recycled concrete aggregates (RCA) in Puerto Madryn, 70 km away [73]; *
  - Option 4: Disposal. Transport to a landfill in Trelew, 25 km away [21].
- C3 (Waste processing):
  - Option 1: Reuse. Preparing Accropodes for reuse in the new breakwater; *
  - Option 2: Repurpose. Preparing and placing of Accropodes as artificial reefs.; *
  - Option 3: Recycle. Recycling of the Accropodes at a concrete recycling plant in Puerto Madryn; *
  - Option 4: Disposal. Preparing Accropodes for disposal at landfill in Trelew.
- C4 (Disposal):
  - Option 4: Disposal. Accropodes at landfill in Trelew.

- D (Benefits beyond system boundary)
  - Option 1: Reuse. Less new Accropodes have to be made which puts a lower pressure on the environment; *
  - Option 2: Repurpose. To quantify the positive impact that the use of Accropodes in marine environments generates, an EPD of the production of new concrete elements is taken and imported into the LCIA as a negative value for environmental impact; *
  - Option 3: Recycle. To quantify the positive impact RCA has, an EPD of the production of new aggregates is taken and imported into the LCIA as a negative value for environmental impact. *
- A1 (Raw material supply):

  The two cement mixtures are composed out of different materials which are obtained from different locations.
- A2 (Transport):

  Transport of raw materials to the temporary concrete manufacturing plant, which is constructed next to the new southern breakwater.
- A3 (Manufacturing):

  Mixing, casting and curing of concrete at this plant.
- A4 (Transport to the site):

  Transport of the fully hardened Accropodes to the new southern breakwater construction site.
- A5 (Construction installation):
  - Placement of the newly produced Accropodes at the breakwater;
  - Placement of the reused Accropodes at the breakwater. *

The methods are further simplified and visualised in two process trees in Figure Q.1 and Figure Q.2.

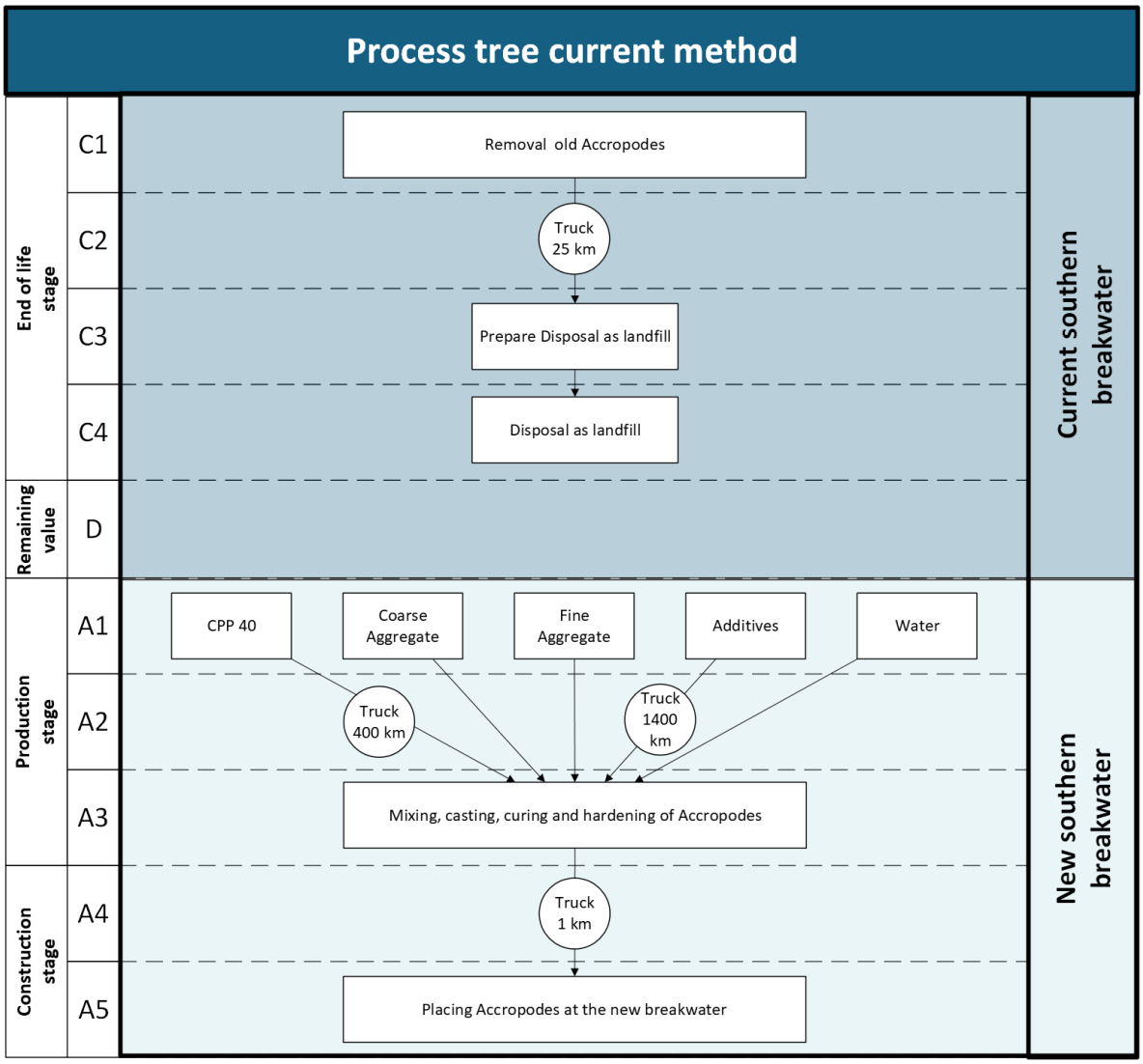


Figure Q.1: LCA process tree - current method

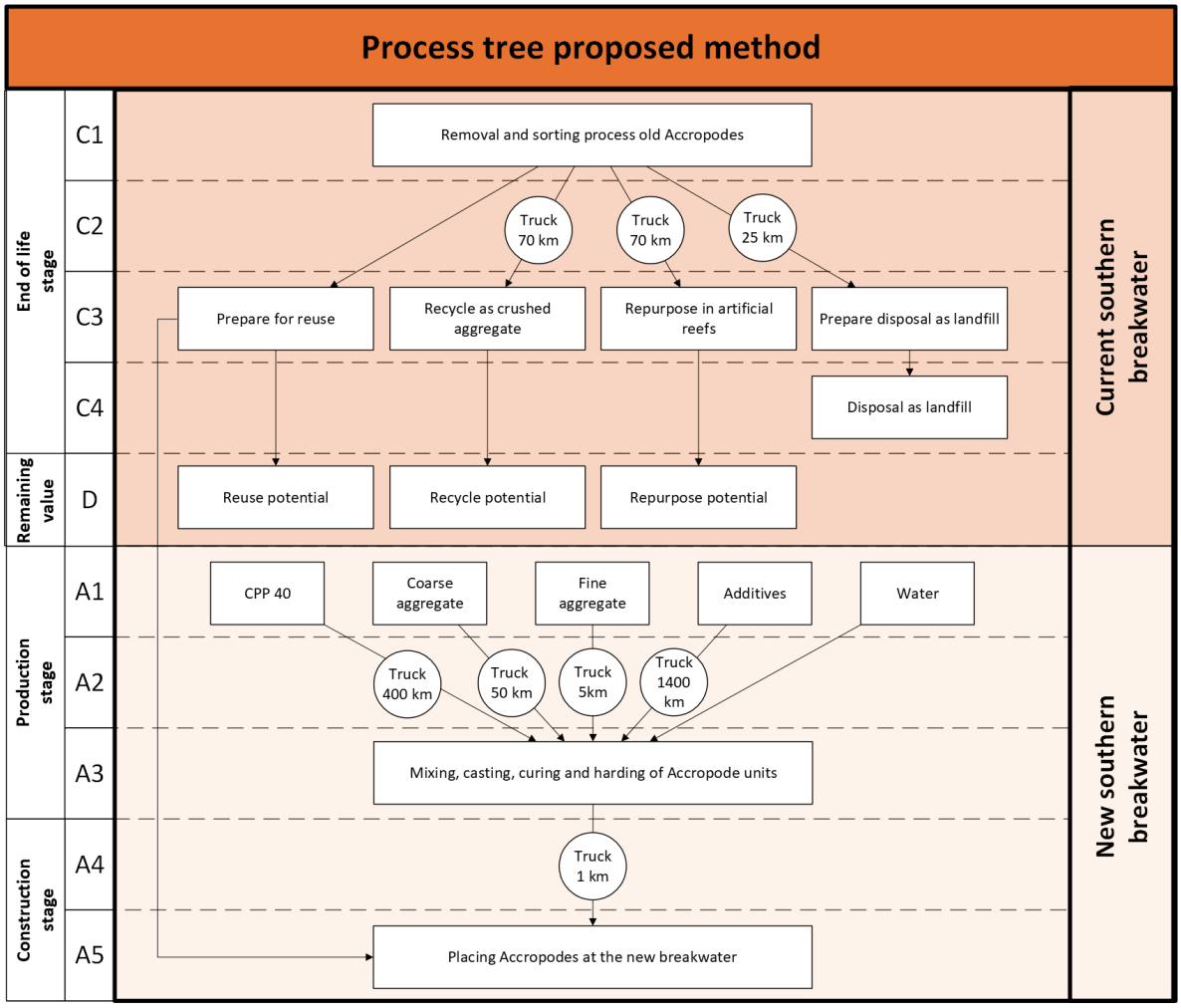


Figure Q.2: LCA process tree - proposed method

The bills of materials and processes (BoMP), given in Figure Q.3 and Figure Q.4, give a quantification of the inputs for both methods. Material weights and volume are obtained from Appendix P and Subsection 8.10.3. Only the processes related to transport are listed, including the origin, destination, distances, transport types, and associated tonne-kilometres. Other building processes, such as casting and placement, are not considered in the quantification since these are difficult to quantify and largely the same for both methods.

CURRENT METHOD							
Material	**Location of origin**	**Destination**	**Mode of transport**	**Distance [km]**	**Volume [m^3]**	**Weight [kg]**	**Transport [t*km]**
Old Accropodes	Old breakwater	Landfill	Truck > 35 t	25	9150	2,09E+07	5,23E+05
New Accropodes	Temporary construction site	New breakwater	Truck > 35 t	1	32710	7,48E+07	7,48E+04
Water, potable	Rawson	Temporary construction site	-	-	5302	5,30E+06	-
Cement, CPP	Comodora Rivadera	Temporary construction site	Truck < 35 t	400	4131	1,26E+07	5,04E+06
Fine aggregate, sand	Rawson, Chubut river south bank	Temporary construction site	-	-	9542	2,45E+07	-
Coarse aggregate, Pebble	Rawson, Chubut river south bank	Temporary construction site	-	-	13696	3,63E+07	-
Plasticizer, Sika Argentina	Buenos Aires	Temporary construction site	Truck < 35 t	1400	37	4,42E+04	6,19E+04

Figure Q.3: BoMP of the current method

PROPOSED METHOD							
Material	**Location of origin**	**Destination**	**Mode of transport**	**Distance [km]**	**Volume [m^3]**	**Weight [kg]**	**Transport [t*km]**
Old Accropodes	Old breakwater	New breakwater	-	-	2070	4,74E+06	-
		Recycled Aggregates	Truck > 35 t	70	460	1,05E+06	7,37E+04
		Artificial reefs	Truck > 35 t	70	3205	7,33E+06	5,13E+05
		Landfill, Trelew	Truck > 35 t	25	3415	7,81E+06	1,95E+05
					9150	2,09E+07	
New Accropodes	Temporary construction site	New breakwater	Truck > 35 t	1	30640	6,83E+07	6,83E+04
	Old breakwater			-	2070	4,74E+06	-
					32710	7,30E+07	
Water, potable	Rawson	Temporary construction site	-	-	4991,3	4,99E+06	-
Cement, CPP	Comodora Rivadera	Temporary construction site	Truck < 35 t	400	3517,5	1,11E+07	4,44E+06
Fine aggregate, sand	Playa Unión, Aridos Fontana	Temporary construction site	Truck > 35 t	5	9927,4	2,55E+07	1,27E+05
Coarse aggregate, porphyry waste	Puerto Madryn	Temporary construction site	Truck > 35 t	50	12056,8	3,03E+07	1,51E+06
Plasticizer, Sika Argentina	Buenos Aires	Temporary construction site	Truck < 35 t	1400	25,5	3,01E+04	4,21E+04
Air entrainer, Sika Argentina	Buenos Aires	Temporary construction site	Truck < 35 t	1400	1,8	1,84E+03	2,58E+03

Figure Q.4: BoMP of the proposed method

Q.2. Life Cycle Impact Assessment

The inputs from the LCI are linked to outputs in the LCIA. The different processes and materials are analysed in terms of their contributions to various environmental impact categories.

The BoMP serves as input for the LCIA, of which the calculations are given on the next page. The environmental impact categories and shadow costs used are in line with the regulations from NEN-EN 15804+A2 [54].

Take note of the following:

- Some processes (e.g. placing of the Accropodes) defined in the process trees are not taken into account for the LCIA calculation. This is justified by difficulty in quantification due to big uncertainties in labour needed or significant similarities in these processes for both methods.
- Substitute materials and processes, which are comparable in terms of environmental impact, are used to calculate the shadow costs. These materials and processes are given in the LCIA e.g. for heavy weight transportation by truck in Argentina a substitute process in Brazil is used: *Transport, freight, lorry >32 metric ton, EURO 5, Brasil*.
- To express remaining value of an EoL solution the environmental impact of producing a comparable product is taken. For example: recycling potential of a new aggregate is quantified by the production of a virgin aggregate from a quarry.

The results of the LCIA, in terms of shadow costs and ratio between both methods, are given in Figure Q.5. Next to presenting the different stages, it also gives insight into the elements of interest, the aggregates and EoL solutions.

		SHADOW COSTS		
STAGE	**NAME**	**Current method**	**Proposed method**	**Ratio**
C	End-of-Life	€ 41.095	€ 25.703	1,60
D	Remaining value	€ -	€ -102.419	-
A1-A3	Production	€ 1.695.584	€ 1.423.771	1,19
A4-A5	Construction	€ 1.276	€ 1.164	1,10
TOTAL		**€ 1.737.955**	**€ 1.348.218**	**1,29**

A	Aggregates	€ 123.406	€ 27.965	4,41
C / D	EoL	€ 41.095	€ -76.717	-

Figure Q.5: Total shadow costs of the LCA, monetized and quantified. The ratio between the current and the proposed method is included.

CURRENT METHOD

			Shadow prize [€/kg eq]	0,39	0,116	0,116	0,116	0,116	0,00013	1,96	3,28	0,36	1096368	147588	0,049	0,000178	32	549750	1,22	0,3	0,00033	0,00506			
			Impact category	AP	GWP - total	GWP - fossil	GWP - biogeni	GWP - luluc	ETP-fw	EP - freshwater	EP - marine	EP - terrestial	HTP-c	HTP-nc	IR	SQP	ODP	PM	POCP	ADPE	ADPF	WDP			
			Unit	Mol H+-eq.	kg CO_2-eq	kg CO_2-eq	kg CO_2-eq	kg CO_2-eq	CTUe	kg P-eq	kg N-eq	Mol N-eq.	CTUh	CTUh	kg kBq U23 5-eq	Pt/m^2.jaar	kg CFC-11 eq	kg disease incidence	kg NMVOC-eq.	kg Sb-eq	MJ net cal. val.	m^3 water, world eq. deprived			
Stage	**Material / process**	**Substitute material / process**	**Unit**	**Amount**																			**Shadow costs [€/unit]**	**Shadow costs [€]**	
C End-of-life stage																									€ 41.095
C2 (Transport)	Truck, disposal, 25 km	Transport, freight, lorry >32 metric ton, EURO 5, Brasil	t*km	5,23E+05	2,90E-04	8,58E-02	7,76E-02	2,06E-03	6,15E-03	1,13E+00	7,76E-06	1,30E-04	1,08E-03	3,58E-11	1,30E-09	6,54E-03	1,88E+00	8,04E-09	7,67E-09	3,60E-04	2,10E-07	1,21E+00	1,26E-02	1,7048E-02	€	8.922
C4 (Disposal)	Landfill disposal	Treatment of waste concrete, inert material landfill, Europe	kg	2,09E+07	4,95E-05	5,28E-03	5,27E-03	5,71E-06	4,85E-06	9,03E-02	4,82E-07	1,72E-05	1,90E-04	2,35E-12	6,11E-11	6,50E-04	2,25E-01	2,13E-09	9,72E-10	5,48E-05	1,20E-08	1,47E-01	6,74E-03	1,5368E-03	€	32.173
A1-A3 Production stage																									€ 1.695.584
A1 (Raw material suppy)	CPP 40 cement	Market for cement, pozzolana and fly ash 6-14%, Brazil	kg	1,26E+07	3,01E-03	7,63E-01	7,21E-01	3,66E-02	4,77E-03	5,36E+00	1,36E-05	8,80E-04	9,50E-03	1,02E-10	3,05E-09	1,78E-02	2,46E+00	4,86E-08	1,89E-08	2,48E-03	7,18E-07	3,55E+00	1,25E-01	1,1376E-01	€	1.432.884
	Coarse aggregate, Pebble	Sand quarry operation, extraction from river bed, Brazil	kg	3,63E+07	4,85E-05	4,73E-03	4,72E-03	1,21E-05	2,54E-06	3,86E-02	1,77E-07	2,13E-05	2,30E-04	1,83E-12	2,92E-11	2,90E-04	2,45E+00	9,91E-10	1,28E-09	6,41E-05	3,95E-09	6,45E-02	8,84E-03	2,0289E-03	€	73.640
	Fine aggregate, Pebble	Sand quarry operation, extraction from river bed, Brazil	kg	2,45E+07	4,85E-05	4,73E-03	4,72E-03	1,21E-05	2,54E-06	3,86E-02	1,77E-07	2,13E-05	2,30E-04	1,83E-12	2,92E-11	2,90E-04	2,45E+00	9,91E-10	1,28E-09	6,41E-05	3,95E-09	6,45E-02	8,84E-03	2,0289E-03	€	49.766
	Plasticizer, Sikament 90 E	Plasticizer - water reducer, Netherlands	kg	4,42E+04	7,79E-03	1,34E+00	1,34E+00	5,75E-04	1,09E-03	2,49E+01	4,83E-05	1,27E-03	1,48E-02	1,50E-09	1,68E-08	4,41E-02	3,55E+00	2,27E-07	7,09E-08	1,30E-03	1,28E-04	1,57E-02	9,76E-01	2,2351E-01	€	9.878
	Potable water	Tap Water Production, conventional treatment, Brazil	kg	5,30E+06	1,94E-06	2,20E-04	1,90E-04	2,75E-05	4,59E-06	7,62E-03	8,05E-08	2,30E-07	2,50E-06	3,10E-13	1,00E-11	1,66E-05	2,07E-03	2,11E-11	1,63E-11	6,97E-07	1,34E-08	2,31E-03	4,35E-02	2,6252E-04	€	1.392
A2 (Transport)	Truck, cement 400 km	Transport, freight, lorry 16-32 metric ton, EURO 5, Brazil	t*km	5,04E+06	4,30E-04	1,35E-01	1,22E-01	3,33E-03	9,98E-03	1,77E+00	1,27E-05	1,90E-04	1,57E-03	6,21E-11	1,91E-09	9,76E-03	2,25E+00	1,06E-08	9,58E-09	5,10E-04	4,76E-07	1,81E+00	1,91E-02	2,5102E-02	€	126.471
	Truck, additives, 1400 km	Transport, freight, lorry 16-32 metric ton, EURO 5, Brazil	t*km	6,19E+04	4,30E-04	1,35E-01	1,22E-01	3,33E-03	9,98E-03	1,77E+00	1,27E-05	1,90E-04	1,57E-03	6,21E-11	1,91E-09	9,76E-03	2,25E+00	1,06E-08	9,58E-09	5,10E-04	4,76E-07	1,81E+00	1,91E-02	2,5102E-02	€	1.553
A4-A5 Construction stage																									€ 1.276
A4 (Transportation)	Truck, new units 1 km	Transport, freight, lorry >32 metric ton, EURO 5, Brasil	t*km	7,48E+04	2,90E-04	8,58E-02	7,76E-02	2,06E-03	6,15E-03	1,13E+00	7,76E-06	1,30E-04	1,08E-03	3,58E-11	1,30E-09	6,54E-03	1,88E+00	8,04E-09	7,67E-09	3,60E-04	2,10E-07	1,21E+00	1,26E-02	1,7048E-02	€	1.276
																							Shadow costs TOTAL	**€ 1.737.955**	

Note: the cells in blue are summed, such that the leftmost cell represents all the blue ones

PROPOSED METHOD

			Shadow prize [€/kg eq]	0,39	0,116	0,116	0,116	0,116	0,00013	1,96	3,28	0,36	1096368	147588	0,049	0,000178	32	549750	1,22	0,3	0,00033	0,00506			
			Impact category	AP	GWP - total	GWP - fossil	GWP - biogeni	GWP - luluc	ETP-fw	EP - freshwater	EP - marine	EP - terrestial	HTP-c	HTP-nc	IR	SQP	ODP	PM	POCP	ADPE	ADPF	WDP			
			Unit	Mol H+-eq.	kg CO_2-eq	kg CO_2-eq	kg CO_2-eq	kg CO_2-eq	CTUe	kg P-eq	kg N-eq	Mol N-eq.	CTUh	CTUh	kg kBq U23 5-eq	Pt/m^2.jaar	kg CFC-11 eq	kg disease incidence	kg NMVOC-eq.	kg Sb-eq	MJ net cal. val.	m^3 water, world eq. deprived			
Stage	**Material / process**	**Substitute material / process**	**Unit**	**Amount**																			**Shadow costs [€/unit]**	**Shadow costs [€]**	
C End-of-life stage																									€ 25.703
C2 (Transport)	Truck, recycle, 70 km	Transport, freight, lorry >32 metric ton, EURO 5, Brasil	t*km	7,37E+04	2,90E-04	8,58E-02	7,76E-02	2,06E-03	6,15E-03	1,13E+00	7,76E-06	1,30E-04	1,08E-03	3,58E-11	1,30E-09	6,54E-03	1,88E+00	8,04E-09	7,67E-09	3,60E-04	2,10E-07	1,21E+00	1,26E-02	1,7048E-02	€	1.256
	Truck, repurpose, 70 km	Transport, freight, lorry >32 metric ton, EURO 5, Brasil	t*km	5,13E+05	2,90E-04	8,58E-02	7,76E-02	2,06E-03	6,15E-03	1,13E+00	7,76E-06	1,30E-04	1,08E-03	3,58E-11	1,30E-09	6,54E-03	1,88E+00	8,04E-09	7,67E-09	3,60E-04	2,10E-07	1,21E+00	1,26E-02	1,7048E-02	€	8.751
	Truck, disposal, 25 km	Transport, freight, lorry >32 metric ton, EURO 5, Brasil	t*km	1,95E+05	2,90E-04	8,58E-02	7,76E-02	2,06E-03	6,15E-03	1,13E+00	7,76E-06	1,30E-04	1,08E-03	3,58E-11	1,30E-09	6,54E-03	1,88E+00	8,04E-09	7,67E-09	3,60E-04	2,10E-07	1,21E+00	1,26E-02	1,7048E-02	€	3.330
C3 (Waste processing)	Recycling, cruhsing concret	Waste processing concrete, crushing, Europe	kg	1,05E+06	7,43E-06	1,64E-03	1,63E-03	9,42E-06	3,10E-07	1,77E-02	5,07E-08	4,06E-06	4,51E-05	0,00E+00	0,00E+00	6,93E-05	3,65E-03	2,00E-10	2,00E-10	9,18E-07	4,60E-09	1,14E-05	9,90E-05	3,4034E-04	€	358
C4 (Disposal)	Landfill disposal	Treatment of waste concrete, inert material landfill, Europe	kg	7,81E+06	4,95E-05	5,28E-03	5,27E-03	5,71E-06	4,85E-06	9,03E-02	4,82E-07	1,72E-05	1,90E-04	2,35E-12	6,11E-11	6,50E-04	2,25E-01	2,13E-09	9,72E-10	5,48E-05	1,20E-08	1,47E-01	6,74E-03	1,5368E-03	€	12.008
D Remaining value																									€ -102.419
	Recycling potential, eq. new	Gravel production, crushed, Brazil	kg	1,05E+06	2,00E-04	5,21E-03	4,92E-03	2,50E-04	4,42E-05	1,06E+01	5,39E-07	6,34E-05	9,70E-04	1,74E-12	8,27E-11	2,80E-04	5,43E-02	6,81E-10	2,02E-09	1,90E-04	2,82E-08	5,81E-02	3,09E-03	-4,0333E-03	€	-4.245
	Repurpose potential, eq. ne	Concrete Block Production, Brazil	kg	7,33E+06	4,10E-04	6,81E-02	6,41E-02	3,23E-03	7,30E-04	6,67E+00	2,08E-06	1,30E-04	1,54E-03	1,56E-11	4,70E-10	2,15E-03	1,14E+00	5,21E-09	4,34E-09	3,70E-04	8,96E-08	4,33E-01	1,96E-02	-1,3388E-02	€	-98.174
A1-A3 Production stage																									€ 1.423.771
A1 (Raw material suppy)	CPP 40 cement	Market for cement, pozzolana and fly ash 6-14%, Brazil	kg	1,11E+07	3,01E-03	7,63E-01	7,21E-01	3,66E-02	4,77E-03	5,36E+00	1,36E-05	8,80E-04	9,50E-03	1,02E-10	3,05E-09	1,78E-02	2,46E+00	4,86E-08	1,89E-08	2,48E-03	7,18E-07	3,55E+00	1,25E-01	1,1376E-01	€	1.261.647
	Coarse aggregate, Porphyry	Assume no environmental impact ince using waste	kg	3,03E+07	0,00E+00	0,00E+00	0,00E+00	0,00E+00	0,00E+00	0,00E+00	0,00E+00	0,00E+00	0,00E+00	0,00E+00	0,00E+00	0,00E+00	0,00E+00	0,00E+00	0,00E+00	0,00E+00	0,00E+00	0,00E+00	0,00E+00	0,0000E+00	€	-
	Fine aggregate, Aridos Font	Natural aggregate 0/4 mm, round average, Switerland	kg	2,55E+07	1,23E-05	1,71E-03				1,00E-02	3,59E-06			5,00E-13	7,50E-12	7,50E-05	6,50E-01	4,51E-10	3,20E-10	3,97E-07	7,38E-06	2,41E-02	2,25E-03	5,3049E-04	€	13.515
	Plasticizer, Sikament 90 E	Plasticizer - water reducer, Netherlands	kg	3,01E+04	7,79E-03	1,34E+00	1,34E+00	5,75E-04	1,09E-03	2,49E+01	4,83E-05	1,27E-03	1,48E-02	1,50E-09	1,68E-08	4,41E-02	3,55E+00	2,27E-07	7,09E-08	1,30E-03	1,28E-04	1,57E-02	9,76E-01	2,2351E-01	€	6.721
	Air entrainer	SikaAer-S, Sweden	kg	1,84E+03	1,83E-03	4,39E-01	4,86E-01	-8,48E-02	3,89E-02	6,50E+00	4,73E-06	2,91E-04	4,59E-03	3,75E-10	4,50E-09	1,10E-02	9,00E-02	6,74E-09	1,80E-08	1,06E-03	6,14E-07	1,21E+01	1,48E-01	7,2660E-02	€	134
	Potable water	Tap Water Production, conventional treatment, Brazil	kg	4,99E+06	1,94E-06	2,20E-04	1,90E-04	2,75E-05	4,59E-06	7,62E-03	8,05E-08	2,30E-07	2,50E-06	3,10E-13	1,00E-11	1,66E-05	2,07E-03	2,11E-11	1,63E-11	6,97E-07	1,34E-08	2,31E-03	4,35E-02	2,6252E-04	€	1.310
A2 (Transport)	Truck, cement 400 km	Transport, freight, lorry 16-32 metric ton, EURO 5, Brazil	t*km	4,44E+06	4,30E-04	1,35E-01	1,22E-01	3,33E-03	9,98E-03	1,77E+00	1,27E-05	1,90E-04	1,57E-03	6,21E-11	1,91E-09	9,76E-03	2,25E+00	1,06E-08	9,58E-09	5,10E-04	4,76E-07	1,81E+00	1,91E-02	2,5102E-02	€	111.357
	Truck, additives, 1400 km	Transport, freight, lorry 16-32 metric ton, EURO 5, Brazil	t*km	4,47E+04	4,30E-04	1,35E-01	1,22E-01	3,33E-03	9,98E-03	1,77E+00	1,27E-05	1,90E-04	1,57E-03	6,21E-11	1,91E-09	9,76E-03	2,25E+00	1,06E-08	9,58E-09	5,10E-04	4,76E-07	1,81E+00	1,91E-02	2,5102E-02	€	1.122
	Truck, course aggregates, 5	Transport, freight, lorry >32 metric ton, EURO 5, Brasil	t*km	1,51E+06	2,90E-04	8,58E-02	7,76E-02	2,06E-03	6,15E-03	1,13E+00	7,76E-06	1,30E-04	1,08E-03	3,58E-11	1,30E-09	6,54E-03	1,88E+00	8,04E-09	7,67E-09	3,60E-04	2,10E-07	1,21E+00	1,26E-02	1,7048E-02	€	25.794
	Truck, fine aggregates, 5 Km	Transport, freight, lorry >32 metric ton, EURO 5, Brasil	t*km	1,27E+05	2,90E-04	8,58E-02	7,76E-02	2,06E-03	6,15E-03	1,13E+00	7,76E-06	1,30E-04	1,08E-03	3,58E-11	1,30E-09	6,54E-03	1,88E+00	8,04E-09	7,67E-09	3,60E-04	2,10E-07	1,21E+00	1,26E-02	1,7048E-02	€	2.172
A4-A5 Construction stage																									€ 1.164
A4 (Transportation)	Truck, new units, 1 km	Transport, freight, lorry >32 metric ton, EURO 5, Brasil	t*km	6,83E+04	2,90E-04	8,58E-02	7,76E-02	2,06E-03	6,15E-03	1,13E+00	7,76E-06	1,30E-04	1,08E-03	3,58E-11	1,30E-09	6,54E-03	1,88E+00	8,04E-09	7,67E-09	3,60E-04	2,10E-07	1,21E+00	1,26E-02	1,7048E-02	€	1.164
																							Shadow costs TOTAL	**€ 1.348.218**	